معاونت برنامه ریزی و نظارت راهبردی ریاست جمهوری
دفتر فنی و تدوین معیارها و کاهش خطرپذیری زلزله

گزارش نهائی

تحلیل خطر لرزه‌ای ایران– فاز یک محدوده تهران بزرگ

Probabilistic Seismic Hazard Analysis
Phase I- Greater Tehran Regions

Final Report

(جلد ۱)

تهیه شده توسط:

یعقوب قلی‌پور ، یوسف بزرگ‌نیا، محسن رهنما، مانوئل بربریان
منوچهر قریشی، طالبیان، نظری، جعفر شجاع طاهری، علی شفیعی

گروه پژوهشی بهینه‌سازی مهندسی
پردیس دانشکده‌های فنی، دانشگاه تهران

TABLE OF CONTENTS

1. INTRODUCTION 3

1.1. PROJECT AREA 4
1.2. SCOPE OF THE RESEARCH STUDY 6
1.3. PROBABILISTIC SEISMIC HAZARD ANALYSIS – METHODOLOGY AND ELEMENTS 10
1.4. DATA SOURCES 12
1.5. QUALITY CONTROL / QUALITY ASSURANCE (QA/OC) 13

2. TECTONIC FRAMEWORK 14

2.1. THE SOUTH CASPIAN BAIN 15
2.2. THE ALBORZ SEIMOTECHTONIC PROVINCE 16
2.2.1. The Northern Alborz 17
2.2.2. The Southern Alborz (the Southern Tertiary Zone) 18
2.3. THE CENTRAL IRAN SEISMOTECTONIC PROVINCE 20
2.4. THE TEHRAN SEDIMENTATY AND BASIN RESONANCE (BASIN-INDUCED / TRANSDUCED SURFACE-WAVES) 21

3. SESMICITY – EARTHUQAKE CATALOG 24

3.1. THE PRE-INSTRUMENTAL ERA (PRE-1900) 24
3.1.1. Completeness of Historical (Pre-Instrumental) Seismic Data 24
3.1. 2. Reliability and Accuracy of the Historical Seismic Data 26
3.1.3. Macroseismic Epicentral Location and Quality Criteria 27
3.1.4. Assessment of Maximum Observed Intensity 28
3.1.5. Calculation of Equivalent Magnitude 28
3.1.6. Fault Mechanisms of the Historical Surface Ruptures 29
3.1.7. Palaeoseismology 30
3.1.8. Cocluding Remarks (Historical Seismic Database) 31
3.2. INSTRUMENTAL SEISMIC DATABAE (1900-2007) – GENERAL 32
3.2.1. Instrumental Epicenter Location 33
3.3. THE EARLY INSTRUMENTAL ERA (1900-1963) 36
3.3.1. The BASS Period of 1913-1917 39
3.3.2. The ISS Period of 1918-1963 39
3.3.3. The Local Seismic Stations 42
3.3.4. Relocations of the Early Instrumental Era Earthquakes 42
3.4. THE MODERN INSTRUMENTAL ERA (1964-2007) 43
3.4.1. The ISC Period of 1964-2004 44
3.4.2. Reappraisal of the ISS/ISC Teleseismic Data 45
3.4.3. The National Seismic Networks 46
3.4.4. The National Strong Motion Network 48
3.5. COMPARISON OF INSTRUMENTAL AND MACROSEISMIC EPICENTERS, AND QUALITY CRITERIA OF THE TELESEISMIC DATA 48
3.6. EARTQUAKE INTENSITY 49
3.7. FOCAL DEPTH 49
3.8. EARTQUAKE MAGNITUDE 50
3.9. SEISMIC MOMENT (MO) AND MOMENT MAGNITUDE (MW) 53
3.10. REGIONAL FREQUENCY-MAGNITUDE DISTRIBUTION (GUTENBERG-RICHTER RELATION) 54
3.11. EARTHQUAKE SOURCE PARAMETERS FROM LONG-PERIOD P/SH BODY-WAVE INVERSIONS 55
3.12. CMT SOLUTIONS 56
3.13. LOCALLY-RECORDED MICROEARTHQUAKES 58
3.14. COMPLETENESS AND RELIABILITY OF LONG-TERM DATA AT THE PROJECT AREA 59
3.15. CONCLUDING REMARKS (INSTRUMENTAL SEISMIC DATABASE; 1900-2007) 60

4. REGIONAL SEISMOTECTONIC MODEL 62

4.1. SEISMOGENIC SOURCES 63
4.1.1. Fault Source 63
4.1.2.Area Source 64

4.2.Characteristic Magnitude (M_{CHAR}) and Maximum Magnitude (M_{MAX}) of Earthquakes 64
4.3. Regression of Rupture Length and Magnitude (M_S & M_W) 65
4.4. Regression Of Fault Displacement And Magnitude 66
4.5. Slip Rates 67
4.6. Fault Parameters of the Project Area 68
4.6.1. Fault Mapping Accuracy 69
4.6.2. Primary Fault Displacement 71
4.6.3. Probability of Distributed Ruptures/Secondary Faulting And Displacements Near the Fault Zone 71
4.6.4. Blind Faults that Do Not Break the Surface 71
4.6.5. Depth of the Seismogenic Zone 72
4.6.6. Simultaneous Ruptures of Contiguous Segments ('Cascade') 72
4.7. Sesimogenic Sources in the Project Area 72
4.7.1. Uncertainties of Seismogenic Sources (Quality Criteria) 74
4.7.2. Geologic Scenarios; Gutenberg-Richter (G-R) and Characteristic Distributions 76
4.8. Concluding Remarks (Geologic Database) 79

5. GROUND MOTION ATTENUATION FUNCTIONS 83

5.1. Introduction 83
5.2. Key Features of NGA Database and Models 84
5.3. Applicability of NGA Models to Iran 86

6. SEISMIC HAZARD ANALYSIS 94

6.1. Recurrence of Earthquakes 94
6.2. Seismic Hazard Quantification – Theoretical Background 102
6.2.1. Analysis of Seismic Hazard from Fault Sources 106
6.2.2. Analysis of Seismic Hazard from Area Sources 108
6.2.3.Analysis of Seismic Hazard from Gridded Sources 110
6.2.4. Truncation of Attenuation-Function Residuals 110
6.2.5. Deaggregation of Hazard 111
6.2.6. Near Source Directivity Factors 112
6.3. Hazard Analysis Modeling of the Great Tehran Region 112
6.3.1. Seismic Hazard Analysis Modeling Assumptions 113
6.3.2. Stochastic Event Set 114
6.3.3. Probabilistic Seismic Hazard at a Site 115
6.3.4. Calculating the Probabilistic Hazard Map 115
6.3.5. Generating the Stochastic Event Set 116
6.3.6. Active Crustal Faults 116
6.3.7. Area Sources 120
6.4. Numerical Approximations – Analysis Results 126
6.4.1. Magnitude 126
6.4.2. Rupture Area 126
6.4.3. Numerical Calculation Parameters 127
6.4.4. Calculation of Event Rates 127
6.4.5. Calculating the Site Hazard Value per Event 127
6.4.6. Incorporating Uncertainty 130
6.4.7. Calculating the Hazard Exceedance Probability 130
6.4.8. Single Site Results 131
6.4.9. Hazard Map Results 141
6.5.Final active fault map and calculation of seismic parameters by Geological Survey of Iran 144

7 – RESPONSE SPECTRA 157

7.1. Shape of Smoothed Response Spectra 157

8. REFERENCES 161

9. APPENDIX A – EARTHQUAKE CATALOG 181

10. Persian Appendices 1,2,3

List of TABLE

3.1. Summary of The Existing Historical Seismic Database Sources For The Iranian Earthquakes 25

3.2. Rating Criteria Used For The Historical (Pre-Instrumental) Seismic Data For The Greater Tehran Region (34.35°N to 37.10°N & 49.80°E to 53.10°E) 27

3.3. Summary of The Existing Telesiemic Database Sources For The Iranian Earthquakes 34

3.4. Rating Criteria For The Instrumental Seismic Data (1900-2007) 49

3.5. Seismic Source Parameters From *P/SH* Body-Wave Modeling of The Earthquakes of The Greater Tehran Region (34.35°N to 37.10°N & 49.80°E to 53.10°E) 55

3.6. Best Double-Couple Harvard (HRVD) CMT Solutions of The Earthquakes of The Greater Tehran Region (34.35°N to 37.10°N & 49.80°E to 53.10°E) 57

3.7. Best Double-Couple Swiss Seismological Service (ZUR-RMT) CMT Solutions of The Earthquakes of The Greater Tehran Region (34.35°N to 37.10°N & 49.80°E to 53.10°E) 57

4.1. Rating Criteria For The Mapped Faults of The Greater Tehran Region (34.35°N to 37.10°N & 49.80°E to 53.10°E) 69

4.2. Summary of The Existing Seismogenic Databse Sources For The Iranian Earthquakes 73

4.3. Rating Criteria For The Seismogenic Sources From Geologic/Geophysical Data of The Greater Tehran Region (34.35°N to 37.10°N & 49.80°E to 53.10°E) 75

TABLE-4.4 VALUES OF CONSTANT PARAMETERS (a & b) FOR THE FAULTS OF THE GREATER TEHRAN REGION (34.35oN to 37.10oN & 49.80oE to 53.10oE)'] 77

TABLE-4.5 VALUES OF CONSTANT PARAMETERS (a & b) FOR THE SEISMOTECTONIC PROVINCES OF THE GREATER TEHRAN REGION (34.35oN to 37.10oN & 49.80oE to 53.10oE)'] 78

Table 6.1. Event counts for 0.5 Magnitude bins and 25 year bins. 97

Table 6.2 Proposed completeness periods for 0.5 Magnitude bins in the GSI catalog 101

Table 6.3. Event counts and annualized rates attributed to the background source for each Magnitude bin (up to Magnitude 6.0) 121

Table 6.4. Cumulative event rates for given minimum magnitudes using different a- and b-values determined in this study. The rates are compared to the rates given by the catalog (top line) 122

Table 6.5-1: seismic parameters for major faults in greater Tehran region 147

Table 6.5-2: evaluation of b-value for greater Tehran Rregion 150

LIST OF FIGURES

Figure 1.1 - Fault Map of the Greater Tehran Region 6

Figure 1.2 illustration of Steps in a Probabilistic Seismic Hazard Assessment 12

Figure 2.1 Fault Map of the Greater Tehran Region 22

Fig. 5.1 Distribution of recordings with magnitude and distance used in Campbell and Bozorgnia NGA model 87

Fig. 5.2 Comparison of magnitude-scaling characteristics of PGA between the NGA and CB2003 empirical ground motion models for the following event characteristics: strike-slip faulting and NEHRP BC site conditions. 87

Fig. 5.3 Comparison of magnitude-scaling characteristics of spectral accelerations at period of 1.0 sec. between the NGA and CB2003 empirical ground motion models for the following event characteristics: strike-slip faulting and NEHRP BC site conditions. 88

Fig. 5.4 Comparison of attenuation characteristics of PGA between the NGA and CB2003 empirical ground motion models for the following event characteristics: strike-slip faulting and NEHRP BC site conditions. 88

Fig. 5.5 Comparison of attenuation characteristics of spectral accelerations at period 1.0 sec. between the NGA and CB2003 empirical ground motion models for the following event characteristics: strike-slip faulting and NEHRP BC site conditions. 89

Fig. 5.6 Predicted acceleration spectra for a Strike Slip fault, M = 7.0, VS30 = 760 m/s for various distances from fault rupture 89

Fig. 5.7 Predicted acceleration spectra for a Strike Slip fault, distance 10 km, various magnitudes, VS30 = 760 m/s. 90

Fig. 5.8 Predicted displacement response spectra for a Strike Slip fault with various magnitudes, RRUP = 10 km, VS30 = 760 m/s 90

Fig. 5.9: Comparison of total aleatory standard deviations of PGA between the NGA and CB2003 empirical ground motion models. The NGA standard deviation does not account for the diminution of uncertainty due to nonlinear site effects. 91

Fig. 5.10: Comparison of total aleatory standard deviations of 1.0-second SA between the NGA and CB2003 empirical ground motion models. The NGA standard deviation does not account for the diminution of uncertainty due to nonlinear site effects as recommended in the text 91

Fig. 5.11: Ratios of various measures of horizontal components over the new geometric mean used in NGA 92

Fig. 5.12: Distribution of recorded earthquake ground motions in Iran (from Shoja-Taheri, et al., 2007) 93

Figure 6.1 Plot of earthquake epicenters (mainshock only) from the declustered catalog 97

Figure 6.2 Plot of reverse cumulative rates for Magnitude bins 5.5 and below 99

Figure 6.3 Plot of reverse cumulative rates for Magnitude bins 5.0 to 6.0 100

Figure 6.4 Plot of reverse cumulative rates for Magnitude bins 6.0 and above 100

Figure 6.5 The graphical representation of Characteristics Magnitude 104

Figure 6.6 The graphical representation of fault modeling in EZ-Frisk program 106

Figure 6.7 Fault source three definitions of distance R 108

Figure 6.8 Area source modeling in EZ-Frisk 109

Figure 6.9 Cumulative Annual rate of the region and all faults 118

Figure 6.10 Fault Geometry Map 119

Figure 6.11 Regression results using the Least-Squares and Maximum Likelihood methods 122

Figure 6.12. Plot of cumulative rates using the a- and b-values from different methods 123

Figure 6.13. Locations of the three test sites used in the study relative to Tehran 132

Figure 6.14. Map of locations of the three test sites used in the study relative to the active faults in the model 132

Figure 6.15. Hazard curves for Site 1 for each attenuation relationship used and the mean 134

Figure 6.16. Hazard curves for Site 2 for each attenuation relationship used and the mean 136

Figure 6.17. Hazard curves for Site 3 for each attenuation relationship used and the mean 140

Figure 6.18. PGA hazard map of the study region with a 475-year return period 142

Figure 6.19. PGA hazard map in the vicinity of the three test sites with a 475-year return period 142

Figure 6.20. PGA hazard map of the study region with a 1000-year return period 143

Figure 6.21. PGA hazard map of the study region with a 2500-year return period 143

Figure 6.22. Major active faults (thicker lines) and other faults in greater Tehran region 144

Figure 6.23. Referred names for major active faults in greater Tehran region 145

Figure 7.1: Simplified uniform hazard spectra for site 1 for return periods 475 and 2475 years 159

Figure 7.2: Simplified uniform hazard spectra for site 2 for return periods 475 and 2475 years 160

Figure 7.3: Simplified uniform hazard spectra for site 3 for return periods 475 and 2475 years 160

1. INTRODUCTION

Iran is one of the most seismic active countries in the world. During the last several decades several thousand people lost their lives, sever economic impacts and social damages were experianced. For example, during the 1990 Rudbar earthquake (Mw=7.3) in northwest Iran, more than 40,000 people lost their lives, more than 500,000 became homeless, nearly 100,000 buildings were destroyed, three cities and 700 villages were demolished. Iran has been host to a long series of large damaging earthquakes, many of them occurring within the 20th century. There have been roughly 126,000 deaths attributed to 14 earthquakes of magnitude ~7.0 (one 7.0 earthquake/7-yr), and 51 earthquakes of 6.0-6.9 (one/2-yr) that have occurred in Iran since 1900. During this period nine (9) cities were devastated (one city/10-yr). Review of the historical seismic data shows that almost every part of the country has been hit by major earthquakes during the last century. Zagros, Alborz and Khorasan seismic regions are among the most seismically active regions of the country.

The increasing population in the earthquake prone cities, poor construction quality and lack of building code enforcement are major reason why the vulnerability due to earthquake is also, increasing. These known facts are primary sources for the large number of victims in recent earthquakes especially in the developing countries. In addition to the recent earthquakes in Iran, other regions of the world had experienced major divesting earthquakes, which had significant social and economic impacts. The 1976 great Tangshan China (Mw = 7.8) with number of casualty ranages form official figure of 242,000 to informal figure of more than 650,000 is among deadliest earthquake which occurred during the last three decades. Among other earthquakes, the 1985 Mexico City magnitude 8.0 earthquake caused more than 9,500 deaths, the 1988 Aremina magnitude 6.9 results more than 25,000 fatilities, the 1995 Kobe Japan (Mw = 6.8) caused 6,434 death, the 1999 Izmit Turkey (Mw = 7.8) reported official fatility number is 17,127, the 1999 Chi-Chi Taiwan (Mw = 7.3) caused 2416 catulity, the 2001 Gujarat India magnitude 7.7 caused more than 20,000 cautlaity and finally the 2005 Muzaffarabad Pakestan earthquake resulted more than 75,000 fautlity. The lessons learned from each of these earthquake events highlight the issues related to the poor performance of buildings and infrastructures, lack of

public knowledge about issues for living in the earthquake-prone environments, inadequate building code enforcement and finally deficiency in the building code due to lack of complete understanding of the building performance phenomenon. For instance, the poor seismic performance of the steel frame structures became known after the 1994 Northridge earthquake where many steel frame structures performed poorly. After this event significant amount of research performed to better understand issues that caused the poor performance of the steel structures. The finding of many researchers leads to implement more restricted design requirements for designing the steel frame structures in the 1997 UBC building code. Additinally, these earthquakes provide informative and valaubale information related to the source mechanism, directivity, soil and near field effects on the characteristics of ground motions which are very critical for seismology and earthquake engineering disciplines. This information can be incorporated into seismic hazard analysis modeling, development of attaneuation functions, selection of appropriate ground motions and finally development of design spectra for different retrun periods.

Major earthquakes in Iran have motivated Iranian earth scientists and engineers to map and study the seismogenic faults, estimate the seismic-fault hazard, and enhance the existing building codes. The study of earthquake ground motions and associated earthquake hazard and risks plays an important role in the sustainable development of countries like Iran, where devastating earthquakes have occurred repeatedly.

1.1. Project Area

The region considered in this project, is the area in a radius of 150 km from the center of the mega-city of Tehran (35.70^{o}N-51.41^{o}E). It covers a quadrangle limited by 34.35^{o}N to 37.10^{o}N and 49.80^{o}E to 53.10^{o}E, a total area of approximately 90,000 km2 [see the Figure1.1 Fault Map of the Greater Tehran Region (34.35^{o}N to 37.10^{o}N & 49.80^{o}E to 53.10^{o}E)']. It covers the northern Central Iranian depression in the south, the central part of the Alborz Mountains in the north, and the southern part of the South Caspian Basin to the farthest north. In the delineation of the seismic sources, consideration is given to regional tectonics, structural trends, and seismic history of the project area.

The mega-capital city of Tehran, as well as cities such as Qazvin, Karaj, Ray, Qom, Saveh, Ramsar, Tonekabon [Shahsavar], Chalus, Naushahr, Amol, Babol [Barforush], Babolsar, Sari, Qa'emshahr

[Shahi], Firuzkuh, and Garmsar, together with towns of Hashtgerd, Salafchegan, Damavand, Tafresh, Varamin, Nur, Pol-e-Sefid, Baladeh, and many more, are located in the project area.

As mentioned earthquakes are one of the most costly natural hazards in Iran, and almost 70 million Iranians in different provinces face significant risk from earthquakes (Berberian, 2005). The mega-capital city of Tehran, the center of the project area, has a rapid and significant unplanned growth since the 1960s and has become Iran's largest city with an official population of 7 million. The property market has increased substantially in the city, and the construction industry has become one of the key elements in its economy. The housing market has been subject to less state control than other markets in the Iranian economy. Although the Iranian Codes for Seismic Resistant Design of Buildings implemented in 1969, 1988, the codes have not been enforced in the new buildings, and they do not require the existing buildings to be retrofitted and upgraded. Therefore, the codes have no regulations specifying the disclosure of earthquake resistance information during transactions (Khalili-Araghi, 1988; UPAR, 1992; Willis and Asgary, 1997). After the 1991 Mangil earthquake due to people awareness about the earthquake issues and government requirements the building code enforcement in Tehran and major cities somehow improved. The 2nd addition of the Iranian seismic code "standard 2800' became effective in 1999, and recently the 3rd addition has been published in 2007. The city of Tehran has not experienced a damaging earthquake since 1830, but it has been located in an active seismic zone with evidence of historical destructive earthquakes and high probability of occurrence of a future large-magnitude earthquake (Berberian, 1981, 1995, 2005; Berberian et al., 1985; 1986; Berberian and Yeats, 1999, 2001; JICA, 2000). The extent of destruction and the probable death toll in the poorly constructed and unprepared institutions of the mega-city of Tehran, covering an area of close to 900 km2, hugging numerous active faults, with a population of greater than 7 million living in 1.5 million housing units composed of 48% old and traditional buildings, and aging infrastructure, subjected to strong ground motion, will definitely be disastrous.

Like many urban areas in the developing countries, earthquake risks have increased significantly in Iranian cities especially in Tehran since the last major earthquake in the region, which took place in 1830 (Io~IX, Ms~7.1) near Tehran (Berberian et al., 1985). Until possibly the early 1960's, the rate of investment in large urban and industrial developments in Iran was minimal at best. Although during the first 60 years of the 20th century, earthquakes had taken a toll of more than 24,750 lives, damage in economic terms had remained relatively low (Berberian, 2005). However, with the massive

investments of the last four decades in new urban and industrial centers, future earthquakes in Iran are likely to result in serious economic loss. There has been a 3.5-fold increase in the Iranian population since 1956, and a two-fold increase since 1976 (SCI, 2004). The population growth has concentrated in the mega-city of Tehran and the large provincial capital cities throughout the country.

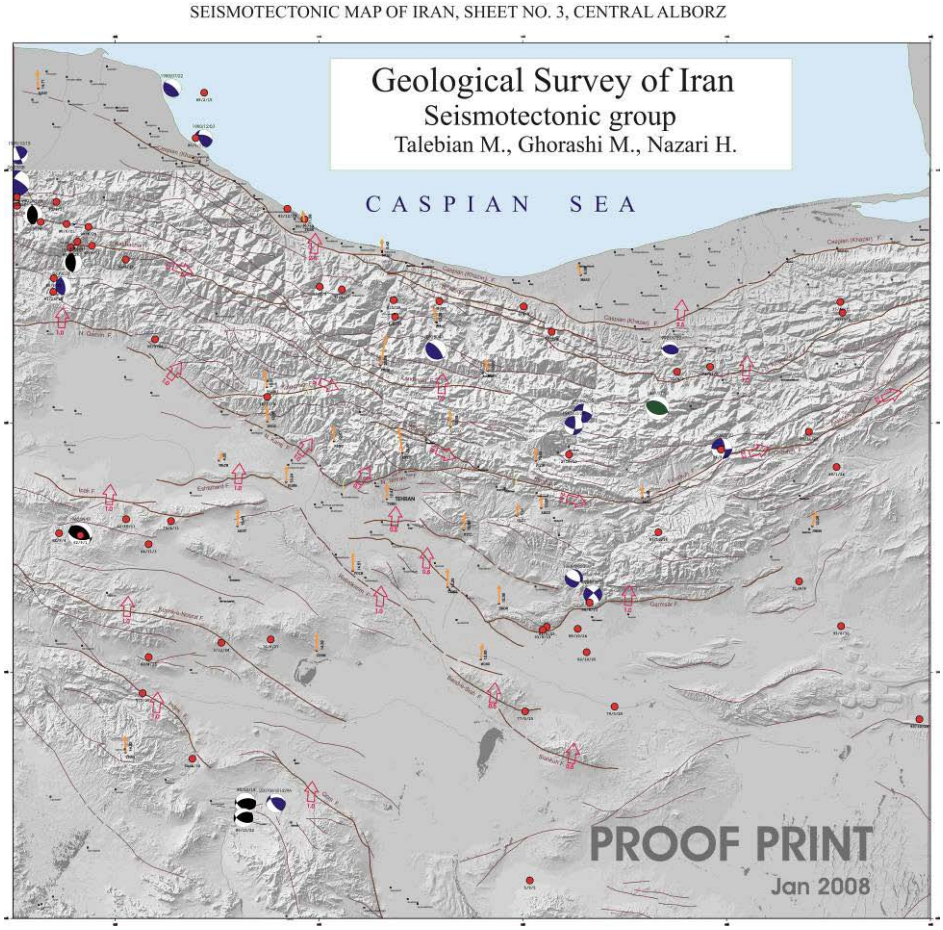

Figure 1.1 Fault Map of the Greater Tehran Region

1.2. Scope of the Research Study

The general approach to seismic hazard evaluation is usually directed towards reducing the uncertainties at various stages of the research process by collecting a sufficient amount of reliable and relevant data. There is generally a trade-off between the effort needed to compile a detailed, reliable, and relevant database, and the degree of uncertainty that should be taken into consideration at each step of the process. In this study, the available surface/subsurface geophysical, geological, seismological, geotechnical, geodetic, and hydro geological characteristics of the project area is

evaluated. Accordingly, comprehensive, homogeneous, and integrated databases including all relevant information are created prior to developing seismic hazard analysis. The databases for the project area, to the extent possible, or at a minimum, will be sufficiently complete for characterizing the major seismotectonic features and important seismic sources. The databases will, therefore, be sufficient enough to determine the strong ground motion and earthquake-fault displacement hazards at the project area.

The overall goal of this project is critically review, update, and development of improved dataset for estimating fault rupture hazard, conditional probabilities of earthquake occurrence on various faults and/or fault segments, estimating earthquake recurrence times and magnitudes from geologic data, and implementing them in the fault rupture hazard maps and regional risk analysis. We have revised and updated the fault parameters and earthquake catalogue of the area under investigation to be included in the risk analyses. Estimates of seismic hazard depend on knowledge of (i) potential seismic sources based on the faults characteristics, historical earthquake data, and GPS measurements, (ii) estimation of the ground motion parameters, (iii) seismic wave paths, and (iv) local site conditions. This report contributes to an improved understanding of the first two factors.

Despite limited available data and lack of detailed large-scale fault maps, we tried to follow as much as possible the original guidelines employed by the Geological Survey of Californian (http://consrv.ca.gov.CGS/rghm/psha) for the probabilistic seismic hazard assessment for the State of California, as well as the Southern California Earthquake Center (http://www.scec.org) Working Group on the Probabilities of Future Large Earthquakes in Southern California (Jackson et al., 1995). The utilized data are cited in the References Section at the end of the text. Integration of seismologic and geologic databases in this study has led to a much better, though still far from complete, understanding of the relationships between faults and earthquakes in space and time used in seismic hazard analysis. Hopefully, it will provide a basis for evaluating long-term earthquake potential in the study area, and will be reviewed and revised regularly every five years.

Hazard analysis requires characteristics of the seismic sources that can be expected to affect a selected place in terms of location, magnitude, and frequency of occurrence of earthquakes. Earthquake ground motions will vary throughout the region, depending upon the magnitude of

earthquake, the distance of the site from the causative fault, and the types of materials underlying the site. In summary the objectives of this study were to:

- A review of available published data relating to the regional seismicity to compile a comprehensive earthquake catalog of the region
- Review of the existing published fault geometry and fault mechanism information and incorporate the latest research performed by the Geological Survey of Iran (GSI) to prepare the Iranian fault map and database
- The faults slip rates information and the GPS measurement data, which is used to estimate the relative motion of the two sides of fault is used by GSI to develop the sesmsicty rates for the faults in the region
- Evaluation of the NGA attenulation functions using the Irainin recorded ground motions to verify its applicability for use in the hazard analysis of the project area
- Perform probailistics hazard analysis based on the orginal guidelines employed by the USGS for the development of the porbabilistics seismic hazard map
- Estimation of the PGA and spectra acceleration for the entire project area for 75, 475, 1000 and 2475 years return periods.

Seismic hazard analysis is required for the design of all critical and essential structures in order to estimate expected level of ground shaking at the site. The expected PGA of site can be evaluated using the probabilistic or deterministic approach. A deterministic seismic hazard evaluation (DSHA) is based on the postulated occurrence of an earthquake of a specified size occurring at a specified location. The DSHA provides a framework for evaluation of worst-case ground motion. However, this methodology provides no information on the likelihood of occurrence of the controlling earthquake and where it may occurs, and the level of shaking that might be expected during a finite period of time (such as the useful lifetime of a particular structure or facility). As an alternative to this procedure the use of probabilistic concepts has allowed uncertainties in the size, location, rate of recurrence of earthquakes, and the variation of ground motion characteristic with earthquake size and location to be explicitly considered in the evaluation of seismic hazards. Probabilistic seismic hazard analysis (PSHA) provides a framework in which these uncertainties can be identified, quantified, and combined in a rational manner to provide a more complete picture of the seismic hazard. Obviously the accuracy of evaluated ground motion parameters at site is

strongly depends on the reliability of data in which the analysis is based on. For better understanding the concepts of PSHA a detailed discussion of the methodology and some of the terminology is presented in the following section.

1.3. Probabilistic Seismic Hazard Analysis – Methodology and Elements

The PSHA computes the likelihood of occurrence of potential seismic events, the intensity of ground shaking those events would produce at the sites being analyzed. The hazard analysis is covering the following three hazard related components:

- Seismic sources that describe the location of potential seismic events, the maximum size event the source is capable of producing, and event recurrence parameters. The probability distribution of potential rupture locations within the source must also be characterized. Probability distributions are assigned to each source zone, implying that earthquakes are equally likely to occur at any point within the source zone.

- The ground motion produced at the site by earthquakes of any possible size occurring at any possible point in each source zone must be evaluated with the use of appropriate ground motion attenuation models. The use of several ground motion attenuation functions reduces the level of uncertainty associated with characteristics of the faults in the region and other seismic hazard analysis parameters. Modern ground motion attenuation models correlate the ground motion parameters with magnitude, site-to-source distance, local soil condition, and fault mechanism.

- Once the first two steps of the seismic hazard have developed, they will be combined to quantify the seismic hazard at a site, and to estimate the probability that the ground motion parameter will be exceeded during a specified time period. Soils information data is used to consider the effects of soil condition on the estimated PGA and acceleration response spectra.

Each of these three components is schematically described in the following sections. Figure 1.2 on the following page shows the interaction of the components of hazard analysis. The detiled discussion about the methodology and seismic hazard analysis program used to perform the seismic hazard analysis of the project area is discussed in Section 6.0

1.3.1. Seismic Source Locations and Maximum Magnitudes

Seismic sources are geographically designated regions, which have experienced, or expected to have, seismic activities and serve as potential sources of earthquakes in the future. Seismic source boundaries are delineated based on homogeneity of seismic activity as well as geophysical features. This homogeneity requirement applies to the rate of occurrence of earthquakes, the magnitude distribution (small events vs. moderate or large events) and the largest event that source is capable of generating (based on geophysical and geological considerations).

For each seismic source, it is assumed that past earthquake activity is a reliable predictor of future activity. The past earthquake history associated with a source is therefore the main element in determining future activity, however, in some cases where the seismicity data is limited other measures such as fault slip rates information, the GPS measurement, fault trenching are commonly used to define the faults seismic rates.

Usually, seismic sources are represented by line/plane or area sources. Line or plane sources are typically earthquake faults, which can be defined either through visual evidence of a fault trace or through geophysical evidence of a fault. More often, the geometry of line sources are defined by one or more line segments. The coordinates of each segment are defined by the latitude and longitude of the beginning and end of the segment. A line source is defined as the projection of the fault on the ground surface with a depth representative of depths at which earthquakes are typically generated. Plane sources, typically utilized when the fault plane is dipping at an angle relative to the earth's surface, are geometrically defined by the plane boundary coordinates.

Area sources are defined as geographical areas in which earthquake activity has shown signs of homogeneity over time. Typically, area sources are not defined based upon visual or geophysical evidence of earthquake faults, but rather on historical seismic activity and broad seismotechtonic characteristics within the area. In this study the area sources are geometrically defined as a quadrangle and defined as the projection of the seismic source on the ground surface with a depth representative of depths at which earthquakes are typically generated. For computational purposes, area sources are modeled by a series of line sources of uniform seismicity distributed evenly within the area source. The total seismicity rate allocated to the line sources is equal to the seismicity rate of the entire area source.

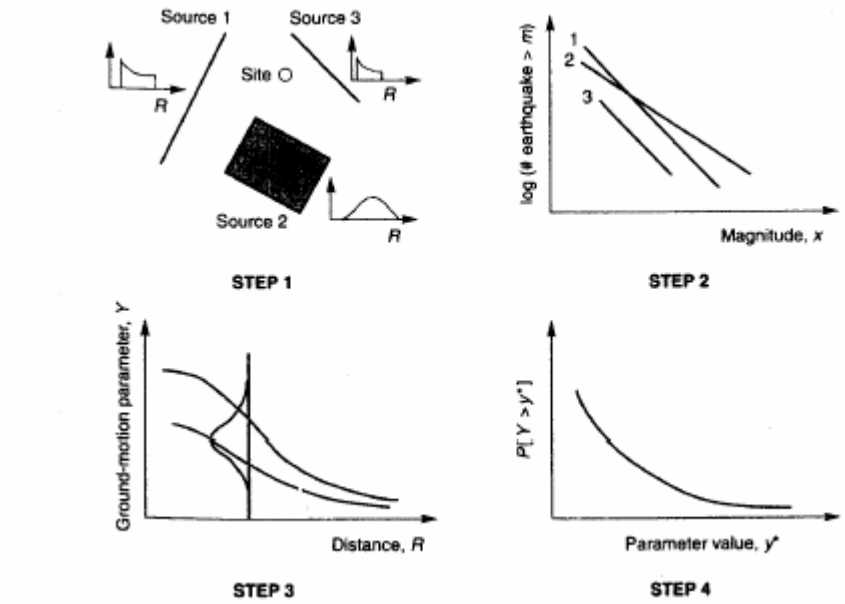

Figure 1.2 llustration of Steps in a Probabilistic Seismic Hazard Assessment

1.4. Data Sources

Gathering and interpreting data have been a critical effort for every task in this project. The effort to supplement that data with the most recent data is ongoing. The key resources from which data have been supplied for various efforts in the project is given in following. A detailed list of the references is presented at the end of this report.

1.4.1. Earthquake Data Bases

The seismological investigations conducted for the original seismic basis evaluation of the site were based on incomplete and heterogeneous seismic data compiled from different sources with unknown magnitude of errors in epicenters, hypocenters, and magnitudes.

The seismicity/seismotectonic analysis in this Report is based on records from the International Seismological Summary (ISS)/International Seismological Center (ISC) in England, the National Geographic Data Center (NGDC/NOAA) in Boulder, Colorado, the National Oceanic and Aeronautic Administration (NOAA) Earthquake Research Center listings, Berberian (1995), and personal files. Earthquakes from historical to 2007 were considered in this report.

An extensive amount of effort and time was required to combine the databases to eliminate duplicate records after reconciling differences, as well as sorting out aftershocks. The clean earthquake catalog has been developed for this study.

1.4.2. Seismic Techtonic and Fault Data

Most of the published seismotectonic maps and reports that contain data in a scale such as that can be used with acceptable precision has been utilized. At the site regional scale, the existing geological and active fault maps released by the Geological Survey of Iran (GSI) and the latest publications by the present authors were used.

1.4.3. Litterature Searches

Extensive data gathering efforts took place for documented research on regional seismicity parameters and seismotectonic characteristics. The reference list at the end of this report details numerous papers that were researched in an effort to incorporate the most comprehensive possible set of data, which includes seismicity, seismic techtonic, ground motions and hazard analysis modeling.

1.5. Quality Control / Quality Assurance (QA/OC)

The most complete estimates of seismic hazard will only result from an integration of historical, seismological, geological, and geodetic observations. A QA/QC program has been established and implemented to cover all the data collection and data processing activities, analyses and evaluations that are within the scope-of-work of the project. It is clear that the most sophisticated methods will not yield good models if the database is poor or insufficient. It is therefore important to incorporating the uncertainties in seismic source characterization and our evolving understanding of the earthquake process. Limitations associated with each category of input data are discussed in the appropriate Sections in this report.

2. TECTONIC FRAMEWORK

The tectonic framework physically links the geologic, geodetic, and seismological data on earthquake sources presented in this report. It constrains geodetic models of crustal deformation, where earthquakes are likely to occur, and what their mechanisms are likely to be. Earthquakes and crustal deformation result from plate tectonic processes. These processes have been going on for hundreds of millions of years. They involve movements of large plates of lithosphere with different types of plate boundaries.

Shortcomings such as: (i) complicated geologic structures of the country in different seismotectonic provinces, (ii) insufficient seismic data available for seismicity study along individual seismic sources, (iii) incompleteness and inhomogeneity of seismicity in time and space are present in seismic risk study of Iran mainly due to factors such as (a) lack of uniform distribution of seismographic stations, and (b) lack of reported earthquakes of all magnitudes (only large-magnitude earthquakes were reported prior to 1950, and the pre-1964 low- to medium-magnitude earthquakes have large magnitude of location and foci errors). We will return to these issues later in the text.

In order to overcome these shortcomings in the project area, seismotectonic provinces are delineated and seismicity parameters (such as *b*-values, annual mean occurrence rate, M_{max}, etc.) are evaluated. Due to the aforementioned factors, the numbers of earthquakes in each seismotectonic province are, therefore, at great variance, and, there are many seismic sources within each province, where the number of earthquakes are nil or too few to allow a satisfactory statistical analysis. Where enough data are available, potential seismic parameters are evaluated along each seismic source within its respected province.

Since earthquakes are phenomena accompanying tectonic processes, knowledge of the tectonic situation and particularly the trends of recent tectonic movements are of great importance. For this reason, the study of seismotectonic provinces has been included here and a short review of the major structural zones has been given separately. Our approach requires that seismic history and source databases created, and seismotectonic provinces of the project area be defined from analysis of available geologic, tectonic, and seismotectonic information. The complicated geologic-structural development of the Iranian plateau, which is a tectonically active part of the Alpine-Himalayan tectonic belt, has produced a complex arrangement of structural provinces (Berberian and King, 1981; Berberian et al., 1981; Berberian, 1981, 1983, 1989). Structural province subdivisions primarily are based on similar styles and trends of tectonic deformation. The project area mainly covers three seismotectonic provinces of (i) the South Caspian Basin in the north (the Caspian Coastal Plain in the project area), (ii) the Alborz to its south, and (iii) the Central Iran in the south [see the attached 'Fault Map of the Greater Tehran Region [34.35^{o}N to 37.10^{o}N & 49.80^{o}E to 53.10^{o}E)'].

2.1. The South Caspian Bain

This is a tectonic depression to the north of the Khazar active reverse fault (Berberian, 1981, 1983), in which the Caspian Sea forms a deep midland basin [see the attached 'Fault Map of the Greater Tehran Region [34.35^{o}N to 37.10^{o}N & 49.80^{o}E to 53.10^{o}E)']. The Basin is situated in the northern part of the Alpine-Himalayan orogenic belt, and is surrounded in the south by arcuate active fold-thrust belt of the Alborz Mountains. The downward motion of the Depression seems to be linked with the uplifting of the surrounding region along the Khazar reverse fault, and appears to have started early in the Cenozoic Era, with intense phases of activity in Neogene and Pleistocene times (Berberian, 1983; Jackson et al., 2002).

The lack of earthquakes within the South Caspian Basin itself indicates that it behaves as a rigid block, though its sedimentary cover is deformed by numerous folds that are decoupled from its rigid basement by over pressured mud. The South Caspian Basin contains a sedimentary sequence almost 20 km thick above a relatively high-velocity basement that is thinner within the Basin than on its margins. The basement beneath the Basin could be either unusually thick oceanic crust or thinned, but relatively high-velocity, continental crust (Jackson et al., 2002).

No earthquakes deeper than 30 km can be confirmed in the Kopeh Dagh, Alborz, and Talesh, which bound the NE, S, and W sides of the South Caspian Basin. In contrast, earthquakes occur to depths of at least 80 km on the Apsheron-Balkhan sill, which bounds the northern side of the South Caspian Basin and where no earthquakes can be confirmed that are shallower than 30 km. Hence, Jackson et al. (2002) interpreted these deeper earthquakes to indicate the onset of subduction of the South Caspian Basin beneath the central Caspian, a process that appears occurring aseismically at shallow levels. Although oblique shortening is partitioned into pure strike-slip and pure thrust in many areas, conjugate right-lateral and left-lateral components in the Kopeh Dagh and eastern Alborz suggest that the South Caspian Basin has a westward component of motion relative to both Eurasia and Iran. This motion enhances westward underthrusting of the South Caspian Basin beneath the Talesh Mountains, the northwestern extension of the Alborz. Jackson et al. (2002) estimated the present motions of the South Caspian Basin to be ~13-17 mm/yr to the SW relative to Iran (a maximum value) and ~8-10 mm/yr to the NW or NNW relative to Eurasia. They suspected that these motions are all relatively recent, and may have begun only in the Pliocene (3-5 Ma).

Recent global positioning system (GPS) data analyses indicated that the South Caspian Basin presently moves N-NW and has a northward and westward velocity of 6.1 (in a 330^{o} direction) and 2.6 mm/yr respectively (Nilforoushan et al., 2003, Vernant et al., 2004a, b).

2.2. The Alborz Seimotechtonic Province

The Alborz is a narrow mountainous area of approximately 100 km wide curving along the South Caspian Sea. The mean elevation of the Alborz drops from +3,000 m amsl in the inner belt to -28 m at the Caspian Sea shoreline in the north, and to approximately +1500 m at northern central Iran in northern city of Tehran. The structural trend of the Alborz changes from $N110^{o}E$ in the western Alborz to $N80^{o}E$ in the eastern Alborz, and a marked hinge occurs near longitude $52.50^{o}E$. It is characterized with range-parallel tight-folds, thrusts and strike-slip faults [see the attached 'Fault Map of the Greater Tehran Region ($34.35^{o}N$ to $37.10^{o}N$ & $49.80^{o}E$ to $53.10^{o}E$)'].

Along the Alborz Mountains in north Iran, the Bouguer gravity ranges between –100 and –120 mgal, and the crustal thickness is less than 35 km. Apparently, the Mountains have no expression in the regional gravity field and are isostatically overcompensated. Thus, it must be considered as a rootless

mountain being built up by overthrusted nappes of allochthonous masses (Dehghani and Makris, 1983).

The southern margin of the Alborz is formed by steep south-directed thrusts, which partly over-ride Pleistocene deposits (along the North Tehran Thrust). Faulting and steep thrusting is found in the central part, but northwards the structures fade towards the north, and tectonics decrease towards the South Caspian Basin. Thus, the Alborz Mountains seismotectonic province can be divided into the Northern (north of the Mosha fault) and the Southern (south of the Mosha fault) Alborz.

The structure of the Central Alborz Mountains is characterized from north to south by four steps caused, respectively, by the upthrusts of the Kandevan, the Mosha, and the North Tehran faults, by means of which the Precambrian rocks of the Kahar Formation drops from the height of Kahar Mt. (4015 m) NW of Tehran to unknown depths below the northern Central Iranian Kavir plain. First occurs an uppermost step consisting of the gently folded Paleozoic Central Zone, followed by a second step, which is characterized by strongly folded sediments of Tertiary Zone to the north, and by the more rigid complex of the Southern Paleozoic/Mesozoic Zone farther south; then occurs a vast, intensely folded step of the South Alborz (or the Southern Tertiary Zone). Still farther south there is a final step, which leads from the southern flank of the Alborz Mountains to the Kavir plain (Assereto, 1966; Berberian 1976).

2.2.1. The Northern Alborz

The Northern Alborz (the ranges north of the Mosha fault) includes the following zones:

- The Coastal Tertiary Foothill Zone
- The Coastal Mesozoic Range
- The Paleozoic Central Range
- The Tertiary Central Zone
- The Southern Paleozoic/Mesozoic Zone.

The complex fold-fault zone of (i) the Paleozoic Central Range, (ii) the Tertiary Central zone, and (iii) the Southern Paleozoic/Mesozoic Zone of the Northern Alborz is named *'High-Alborz'*. The Paleozoic-Mesozoic and Tertiary Formations of the High-Alborz upthrust southwards along the Mosha

fault over the Border Folds of the Southern Alborz, and thrust northwards along the North Alborz fault on the Northern Paleozoic/Mesozoic Border Zone.

a. The Coastal Tertiary Foothill Zone
This is a normally folded belt of the Caspian Neogene molasses along the southern margin of the Khazar fault.

b. The Coastal Mesozoic Range
A normally folded belt of mainly Mesozoic rocks along the northern margin of the North Alborz fault is called the Coastal Mesozoic Range.

c. The Paleozoic Central Zone
The Kandevan upthrust puts into contact two regions with rather different structural styles. A gentle fold style and vertical block faulting characterize the Paleozoic Central Range to the north of the Kandevan thrust.

d. The Tertiary Central Zone
This zone, which is situated to the south of the Kandevan thrust, is characterized by more plastic fold style with isoclinal folds and overthrusts. To the south of this zone, there is a predominance of the thick plastic sediments of the Eocene Karaj Formation, with tectonic style characterized by isoclinal, east-west trending folds, which are overturned to the south and in some places faulted. The Garmabdar thrust forms the southern limit of the Zone. The Garmabdar thrust dips north at a low angle, and has carried the strongly folded sediments of the Tertiary Central Zone across the more competent Formations of the Southern Paleozoic/Mesozoic zone.

e. The Southern Paleozoic/Mesozoic Zone
This is a zone between the Garmabdar thrust in the north and the Mosha fault in the south. The zone is characterized by more competent Formations with rather simple tectonic framework, consisting essentially of more or less dislocated, north-dipping monoclines.

2.2.2. The Southern Alborz (the Southern Tertiary Zone)

The Mosha fault has carried Infracambrian and Paleozoic sediments of the Southern Paleozoic/Mesozoic Zone across intensely folded Formations of the Southern Alborz (the Southern Tertiary Zone). Tectonic style of this zone essentially consists of southward overturned folds, and, locally, of upthrusts with north-dipping fault planes. All the fold axes are parallel to the trace of the Mosha fault to which they are genetically connected. The Southern Alborz consists of mainly Eocene clastic and tuffaceous rocks of the Karaj Formation.

Recent global positioning system (GPS) data analyses indicated that north-south shortening across the Alborz occurs at 5±2 mm/yr, with a left-lateral shear of the overall belt at a rate of 4±2 mm/yr (Vernant et al., 2004). Coupled with the N-S convergence of Central Iran, the southwestward motion of the South Caspian Basin with respect to Central Iran leads to a NNE-SSW transpressional regime in the Alborz accommodating the differential motion between Central Iran and the South Caspian (Jackson et al., 2002). Recently, Ritz et al. (2006) proposed that the internal domain of the central Alborz is not affected by a transpressional regime but by an active and young (Middle Pleistocene) transtension with a WNW-ESE extensional axis. It apparently postdates an earlier N-S compression and may have been initiated when the South Caspian Basin started moving. Accordingly, the transtension started between 1 and 1.5 Ma, which appears to be contemporaneous with the Damavand volcanic activity (1.8 Ma to 7 ka; Davidson et al., 2004).

The Alborz shows strong tectonic activity with several historic and few post-1900 earthquakes (Berberian, 1981, 1983, 1995; Berberian et al, 1983, 1985, 1996; Ambraseys and Melville. 1982; Priestley et al., 1991; Berberian et al., 1992; Berberian and Yeats, 1999, 2001; Jackson et al., 2002). However, occurance of few post-1970 moderate- to large-magnitude instrumental events has prevented to determine the details of the most Alborz fault parameters at depth. Little is known about the seismic activity of the longitudinal faults of the Alborz Mountains. However, length-magnitude relationships suggest that magnitudes of M_s>7.0 are possible along most of these major faults, and effects of such events upon the vibratory motions of the Sites and the resulting earthquake hazard should be investigated.

As with the Central Iran seismotectonic province (see below), earthquakes of Alborz Mountains seem to be quite limited in number and yet large destructive events have occurred. Either strong earthquakes separated by long periods of quiescence characterize this province, or the smaller events have not been detected due to insufficient seismographic stations. Due to the incomplete nature of the seismicity data, a statistical evaluation of earthquakes would possibly be meaningless.

Since the Alborz seems to be rootless, it is likely that many important earthquake-generating faults are present in the basement rocks, although they do not necessarily have surface expressions. As

mentioned, there are, however, a number of important surface seismogenic faults in the region, which will be discussed later.

2.3. The Central Iran Seismotectonic Province

This province is located to the south of the Alborz and forms a range-and-basin system with lower altitude than the Alborz, with active mountain-bordering thrust and some long strike-slip faults. Usually the Alborz is thrust from the north upon the Central Iran. The northern Central Iran trend in the vicinity of the Alborz approximately follows the trend of the Alborz. The Central Iran seismotectonic province has a complex geologic and tectonic history (Berberian and King, 1981).

Recent GPS data analysis indicates that the MOBA station located south of the Pishva fault in the northern Central Iran (35.10^{o}N-51.85^{o}E, in the project area), has northward and eastward velocities of 11.6 and 2.8 mm/yr, respectively (Vernant et al., 2004).

Selected areas of Central Iran show strong tectonic activity with surface deformation during both the historic and present time. In general, active faults in Central Iran are parallel to regional structures and are related to the overall northeasterly-directed compressional stresses. The seismicity of the province is characterized by infrequent but large-magnitude earthquakes (Berberian, 1981, 1995, 2005; Ambraseys and Melville, 1982; Berberian et al, 1983, 1985, 1996; Berberian and Yeats, 1999, 2001).

The earlier study of Hedayati et al. (1976) utilized a mircroearthquake survey to show a 31-km crustal thickness below the Tehran region. By analyzing teleseismic *P*-waveform receiver function, Doloei and Roberts (2003) estimated three main uppermost crustal structures in the Tehran region: (i) the upper crust with a *P*-wave velocity of 4.0 to 5.8 km/s and a 14-km thickness; (ii) the middle crust with a positive *P*-wave velocity gradient from 6.0 to 6.4 km/s down to ~30 km depth; and (iii) a *P*-wave velocity gradient from 6.4 to 7.5 km/s characterizing the lower crust with Moho at 46 $\pm$2 km. A low-velocity mantle, with velocity gradient gradually increasing with depth down to ~60 km depth, has been revealed beneath the Tehran region (Doloei and Roberts, 2003).

2.4. The Tehran Sedimentaty and Basin Resonance (Basin-induced / Transduced Surface-Waves)

Basin-induced surface waves are surface waves generated at edges of a sedimentary basin, such as Tehran, or at a strong lateral discontinuity inside the basin by incident *body (S* or *P)* waves. Their amplitude and waveforms depends on the basin structure along the ray path from the edge (or the discontinuity) to the site. If the site lies in the central part of a large sedimentary basin (such as the cities of Tehran and Qazvin in the project area), the basin-induced surface waves appear much later than the direct and reverberated S-waves. Surface waves transduced at edges of a basin or at a strong lateral discontinuity inside the basin from incident surface waves is called "basin-transduced surface waves". They are distinguished from "basin-induced surface waves" because of the difference in incident waves. These surface waves can be observed if the earthquake source is shallow and distant. At the edge of a basin refraction and mode conversion of both *Love* and *Rayleigh waves* and transformation among them can be seen.

Very little is known about the depth and the nature of the bedrock underneath the Tehran basin. The limited available information is based on a few indirect observations and old geophysical data (Tchalenko et al., 1974). A gravity survey carried out in 1957 (SAGP, 1958) suggests that the bedrocks exposed in the area southeast of Tehran (from Bibishahrbanu Mt. in the south to Qasr-e-Firuzeh in the north) continue under city of Tehran. Immediately to the north and south of these two limits, the gravity measurements can be taken to indicate deep troughs, with computed bedrock depths increasing from 585 m at Tehran Pars (in the east) to 77 m at Abbasabad (in central north), and from 770 m near Shahr Ray (in the south) to 1020 m at Mehrabad (in the west) (Fookes and Knill, 1968).

The thickness of the Quaternary "B" alluvial Formation (Berberian et al., 1985) as computed from electric resistivity measurements increases appreciably in a region corresponding approximately to a buried bedrock (CGG, 1965; MWP, 1968); and piezometric water-table levels measured in many wells and Qantas in and around the city of Tehran show distinct cascades in the regions of the E-W and NW-SE troughs (Knill and Jones, 1968; MWP, 1970; Tchalenko et al., 1974). Major cascading of the groundwater level in the Tehran Basin has been documented along the Niavaran, the Sorkheh Hessar, the North Ray, the South Ray, and the Kahrizak faults (Engalenc, 1968; Tchalenko et al., 1974; Rezaeian, 1998, 1999) where the faults act as barriers to groundwater flow from the north to

the south. On the ground surface, the southern limit of the Pliocene-Pleistocene "A" alluvial Formation outcrops and the location of the TV, the Tarasht, and the Shahrdad faults (Berberian et al., 1985) are approximately in the alignment with a western extension of the Sorkheh Hesar fault zone with groundwater cascading. The North Ray thrust fault seems impermeable at depth, but semi-permeable and/or more permeable near the surface. The regional groundwater surface measurements reveal that the North Ray thrust fault acts as a subsurface dam up to a certain elevation, above which the water on the hanging-wall of the fault spills over the top of its footwall aquifer (Rezaeian, 1998, 1999). The North Tehran thrust also behaves as a barrier and obstructs the recharge of the aquifer of the Tehran basin by the groundwater flow to the south, with numerous springs, seepages, and active travertine deposits along the fault trace.

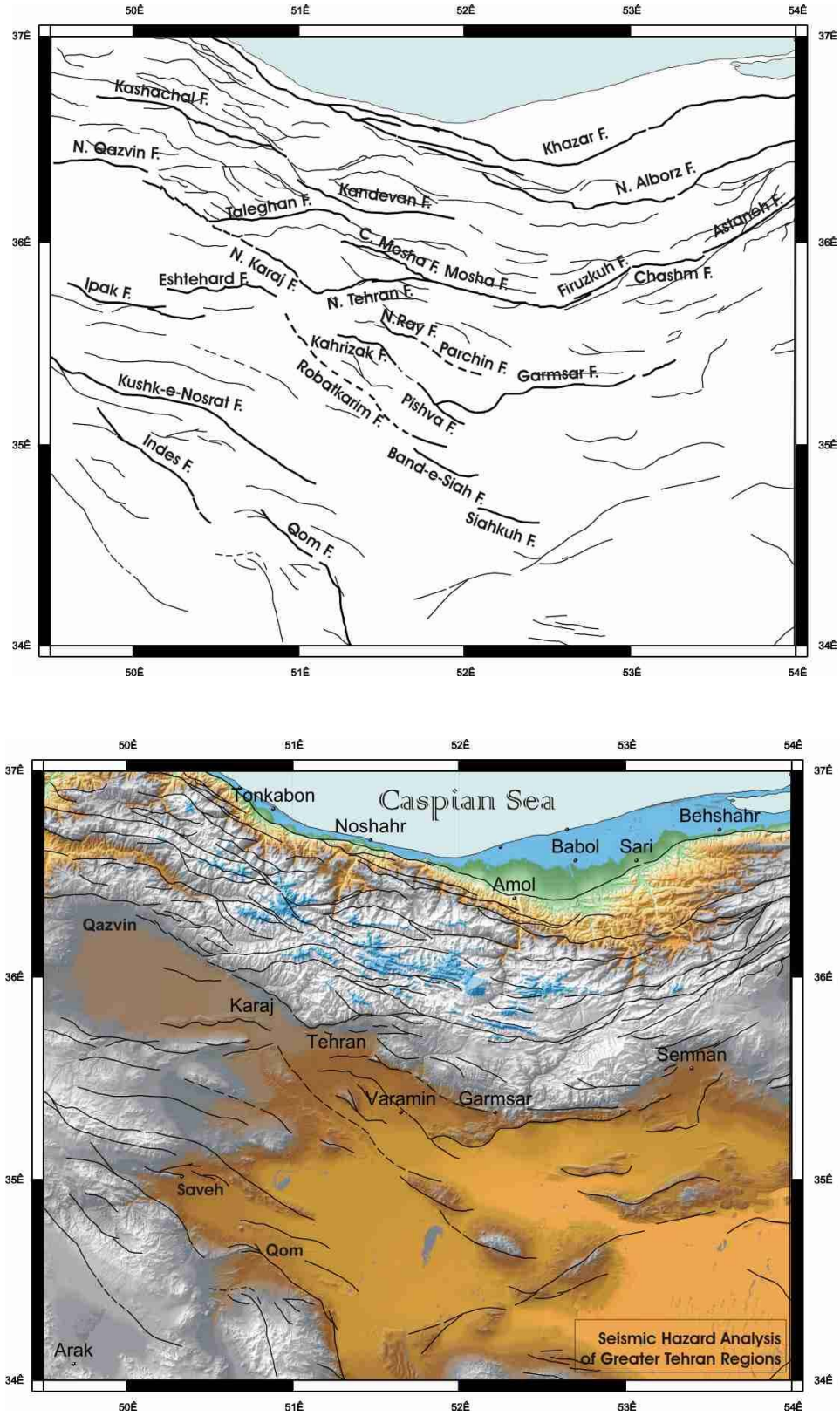

Figure 2.1 Fault Map of the Greater Tehran Region

3. SESMICITY – EARTHUQAKE CATALOG

The earthquake catalog of Iran comprises of the historical or pre-instrumnetal perior to 1900, and instrumental period. The instrumental era includes early instrumental (1900-1963) and modern instrumental ear post 1963 to present. The detilas and quality/limitation of data for each time period are discussed in the folloing setions.

3.1. The Pre-Instrumental Era (Pre-1900)

The locations of previous earthquakes provide a reasonable indicator of future events, and in order to forecast earthquake activity, we need to determine the past history of fault activities. The completeness and accuracy of available information on earthquakes have evolved with time. Since the large-magnitude earthquakes with long recurrence periods are rare events, it is important to expand the seismic catalogues as far as possible back in time.

In this Chapter, we use the currently available local and regional databases and catalogues to go back as far as possible into historical times, critically review and summarize the pre-instrumental seismic data in the project area, and create a new version of the historical earthquake catalogue for the project area [see the attached 'Macroseismic and Teleseismic Database (AD 855 through 2007) of the Greater Tehran Region (34.35^{o}N to 37.10^{o}N & 49.80^{o}E to 53.10^{o}E)'].

3.1.1. Completeness of Historical (Pre-Instrumental) Seismic Data

The assessment of completeness of the information contained in the historical seismic catalogue, particularly in terms of macroseismic epicenter, intensity, equivalent magnitude, etc., together with the teleseismic data are fundamental to a properly conducted seismic hazard evaluation. In general the pre-instrumental Iranian earthquake catalogues are incomplete for:

(i) Small- to medium-magnitude earthquakes,

(ii) Large-magnitude earthquake in rural, sparsely populated, and remote areas, and

(iii) For all earthquakes during the time of, and decades/centuries after, the international conflicts, invasions, and decades of hardships [i.e. invasions of Tiglath-III (737-735 B.C.), Sargon-II (714 B.C.), the Scythians (653 B.C.), Ashur Banipal (640 B.C.), Alexander-III of Macedonia (336-330 B.C.), Arabs (AD 636-642), Ghuzz Turks (1153), Mongol Hordes (1218-1334), Hulagu Mongol (1256), Tamurlane (1381-1388), Afghans (1722), and many more].

Major historical seismic data sources are summarized in Table-3.1.

Table - 3.1

SUMMARY OF THE EXISTING HISTORICAL SEISMIC DATABASE SOURCES FOR THE IRANIAN EARTHQUAKES

Catalogue	Time Range	Magnitude	Intensity	Remarks
Wilson (1930)	550-October 1930			Highly inaccurate
Sieberg (1932)	856-1930			Highly inaccurate
Ambraseys (1968)	856-1898			North Central Iran; contains inaccuracies
Karnik (1971)	1826-1900			Mainly European, w/some NW Iran
Nabavi (1972, 1977)	4th century B.C.-1900			Includes duplicates, errors, & dubious events.
Ambraseys (1974)	4th century B.C.-1900			North Central Iran; contains some errors
Berberian (1976)				Contains inaccuracies
Berberian (1977)				Contains inaccuracies
Alsinawi & Ghalib(1975)	1260 B.C.-1873			Iraq & western Iran; contains inaccuracies
Kondorskaya & Shebalin (1977, 1982)	2,000 B.C.-1977	~M_s	~I	Azarbaijan & N. Khorassan.
Melville (1978)	644-1696	Magnitude class (I:>7.5; II: 6.5-7.4; & III:<6.5)		
Poirier & Taher (1980)	528-1760		~I	w/some Iranian eqs; sore errors
Ambraseys & Melville (1982)	3rd mill. B.C.-1900	~M_s	~i	
Alsinawi & Issa (1985)				Iraq & western Iran
Alsinawi (1988)	1606 B.C.-1905		~I	Iraq & western Iran
Berberian (1995)	Prehistoric-1900	~M_s	~I	
Guidoboni & Traina (1995)				Greater Armenia
Berberian (1997)	2,000 B.C.-1992	~ M_s	~I	NW Iran, Armenia, Caucasus
NEIC: Significant Worldwide Earthquakes	2150 B.C.-1994			Includes high rates of errors.
Babayan (2006)	600 B.C.-2003	M	~I	NW Iran, Armenia

Notes:

~: Equivalent.
i: Simplified intensity scale (1 through 5) devised by Ambraseys & Melville (1982) describing earthquake effects on the Iranian traditional adobe buildings.
I: Intensity Scale (mostly Modified Mercalli Intensity Scale).

3.1. 2. Reliability and Accuracy of the Historical Seismic Data

The question of how historical records are retrieved, interpreted, assembled, and how their reliability is evaluated, is of primary concern for the quality and homogeneity of a historic catalogue. Most earthquake catalogues covering the Iranian earthquakes are not complete or homogeneously compiled in terms of epicentral locations and magnitude for the period before the mid-1970s. Seismotectonic studies in which earthquake locations must be associated with active faults and seismicity or seismic hazard maps, require knowledge of the unambiguous epicentral location and magnitude of past earthquakes. Regional seismic moment-surface wave magnitude [log (M_o)-M_s] and frequency-magnitude (G-R) relationships in studies of seismotectonics, and the derivation of regional predictive attenuation laws for engineering purposes, are sensitive to errors in M_s and to completeness of information, particularly for large-magnitude earthquakes (Abercrombie, 1994; Ambraseys and Melville, 1982; Ambraseys and Sarma, 1999; Ambraseys, 2001).

Normally the secondary sources do not provide a proper basis for hazard assessment. The data they contain need thorough revision and reinterpretation. During the 'Collection, process and Retrieval Phase' of the preliminary database, and after the initial processing of macroseismic data on prehistoric, historical and modern earthquakes, it became clear that most of the earthquake catalogues and reports concerning the Iranian earthquakes have many shortcomings. The secondary sources include many errors in date, location, and are contaminated with duplications, erroneous and dubious events.

Due to insufficient macroseismic data, the exact location of the epicentral area of the Caspian Gates earthquake of AD 743 is not known. The event has been located in SE Tehran in Iran (Ambraseys and Melville, 1982) and also in Derbent [Darband] in Dagestan (Guidoboni et al., 1994). Surprisingly, Nazari (2005) locates this event on the 'Rey' fault [the South Ray fault of Berberian et al., 1985] with a meizoseismal area of 1.5X1.0 km. Nazari (2005) also locates the 3$^{th\ (?)}$ Cent. [sic; 312-281 **B.C.** (M_s~7.6)], 793 [fictitious event], 853 [fictitious event], 855-856 (M_s~7.1), 864.01, 1177.05 (M_s~7.2), 1384 [fictitious event], and 1895 earthquakes on the same fault, which has a maximum length of ~20 km. Nazari (2005) also introduces a fictitious earthquake with an epicenter at ENE quarter of the city of Tehran on AD 898 for which there is no historic data. Furthermore, Nazari (2005) shows two

epicenters 42 km apart for the 1177.07 earthquake, one at Ray in the SE, and the second one at Karaj in the NW.

3.1.3. Macroseismic Epicentral Location and Quality Criteria

Like other procedures of data analysis, the macroseismic estimate of the epicenter is subject to uncertainty. Generally, epicenters of historical earthquakes have been given as macroseismic epicenters, centers of isoseismal maps (center of the area mostly affected by the earthquake), under an implicit assumption that focal depths were shallow. Excluding epicenters in sparsely populated areas and offshore regions, the macroseismic epicenters can be assessed with an error of ~10 km depending on the available data and the magnitude of the event. It is clear that the 'point of initial break' can be hardly known from 'macroseismic data'. For large-magnitude earthquakes with long rupture length, the macroseismic epicenter loses its meaning as a reference point. In such cases, estimation of source regions, fault planes, and/or asperity distributions if possible, is more meaningful.

The macroseismic epicentral data have been graded according to the quality and quantity of the macroseismic information. The quality ratings range from 'A' (most reliable) to 'E' (least reliable) and 'F' (unknown association) as summarized in Table 3.2.

TABLE-3.2

RATING CRITERIA USED FOR THE HISTORICAL (PRE-INSTRUMENTAL) SEISMIC DATA FOR THE GREATER TEHRAN REGION (34.35^{o}N to 37.10^{o}N & 49.80^{o}E to 53.10^{o}E)'].

Q: RATING CLASS	DESCRIPTION
A (Good)	• Existence of good isoseismal maps or sufficient information describing the meizoseismal region to help define its limits, derived from detailed field studies. • This may include evidence of surface faulting, or significant changes in the water supply and other factors deduced from written sources or field studies, or both.
B (Moderate)	• Evidence from locality or district where the intensity was maximum, with indications of places or areas affected at lower intensities that help assess the limits of the meizoseismal region.
C (Poor)	• Locations are based only on the evidence of high intensity shaking reported at one locality or town, and also for locations calculated only from lower intensity isoseismals, from radii or perceptibility or from a combination of the two. • Indirect evidence, such as abandonment of sites, may also help assess the location of the epicentral region.
D (Very poor)	• The shock was felt locally. • It may indicate the approximate location of a small shock, or the occurrence of a large

	magnitude event some distance away, for which data are still incomplete.
E (No confidence)	• A very approximate location of events that were probably large but for which there is insufficient details.
F (Unknown association)	• Association with earthquake is unknown.

There are only five historic seismic data with rating class "A" in the project area [see the attached 'Macroseismic and Teleseismic Database (AD 855 through 2007) of the Greater Tehran Region (34.35^{o}N to 37.10^{o}N & 49.80^{o}E to 53.10^{o}E)'].

3.1.4. Assessment of Maximum Observed Intensity

The distribution of intensity may be used for the assessment of the equivalent magnitude of historical earthquakes, constraining the dimensions of the seismic sources, and identification of subcrustal events. It is important to distinguish between damage caused by dynamic or inertia earthquake loading, and damage caused by secondary, quasi-static after-effects such as foundation spreading, liquefaction, landslides, rockfalls, and aftershock sequences. For most historical earthquakes for which macroseismic data is available, it is possible to assess the extent of the epicentral area and the associated maximum observed intensity, which may be considered to be the 'epicentral intensity' (I_o) if observed at a number of localities.

It is now well known that in any destructive historical or modern earthquake in rural areas and towns in the Middle East, the epicentral intensity saturates at intensity of about VII-VIII MSK (Medvedev-Sponheuer-Karnik intensity scale), at which all local type of constructions [adobe (A), rubble masonry (R), stone masonry (S), etc.] are destroyed or damaged beyond repair and any town or village would thus appear equally, but no more, devastated at higher intensities (Ambraseys and Tchalenko, 1969; Tchalenko and Ambraseys, 1973; Ambraseys, 2001). Therefore, any attempt to assess intensities larger than about VII in the Iranian rural areas, towns and traditional buildings in cities becomes a subjective judgment.

3.1.5. Calculation of Equivalent Magnitude

Correlation of epicentral intensity with magnitude, which is still used in hazard analyses, is very weak and usually is not suitable for practical applications. At present, in principle, magnitudes of historical earthquakes in Iran are equivalent of M_s magnitudes as defined by their reported felt area (or radii of perceptibility) assigned by Ambraseys and Melville (1982). The equivalent magnitudes

were estimated based on the radius of perceptibility [*r'*; mean epicentral distance in km at which the shock was felt with intensity IV+] using about 300 shallow depth twentieth-century Iranian earthquakes, expressed by:

$M_s = -0.67+2.87 \log (r')$.

The expression was expanded by including epicentral intensity and was well fitted for the 262 twentieth-century earthquakes in the form of:

$M_s = -0.74+1.98 \log (r') +0.28(I_o)$.

Finally based on 511 data-point M_s versus I_o for 79-year shallow earthquakes of the twentieth-century the best fit was expressed by:

$M_s = 0.77(I_o)-0.07$.

It should be emphasized that truly great earthquakes of M>8.0 are not easy to identify from historic seismic data. This is due to the fact that it is not always possible to establish reliably the simultaneity of their destructive effects at distances of hundreds of kilometers without running the risk of amalgamating several events into a single great earthquake.

3.1.6. Fault Mechanisms of the Historical Surface Ruptures

It is difficult to associate the historic earthquakes with a probable fault mechanism of thrust/reverse, normal, or strike-slip, since the historical sources are rarely explicit enough to be unequivocal. In this study, our judgment is based on our knowledge of the regional tectonics and the style of the faulting in the meizoseismal areas of the earthquakes. For example the Tabriz earthquake of 1780.01.08 (I_o~IX, M_s~7.7) [outside the project area] was reported with only 4-10 m of vertical displacement along a minimum 42 km of surface rupture (Berberian 1995a; Berberian and Yeats, 1999), and we do not expect any measurement of strike-slip displacement in the eighteenth century along the North Tabriz fault which we are aware of its dominant right-lateral strike-slip mechanism. Furthermore, the Mosha fault in northeast Tehran [in the project area] was reactivated during the 1665 (I_o~VIII, M_s~6.5) and 1830 (I_o~IX, M_s~7.1) earthquakes (Berberian et al., 1985; Berberian and

Yeats, 1999), but no recorded evidence of ground deformation has survived in historic data despite its fresh recent fault features of left-lateral reverse displacement.

On the other hand there are relatively little reports on the historic thrust/reverse surface ruptures associates with large-magnitude earthquakes. This is probably due to the fact that (i) reverse faults may fail to break the surface and they may produce surface folding and uplift, and (ii) shallow dip thrust faults rarely break the ground surface and noticed by the historic sources. Some modern large-magnitude earthquakes in the Zagros (Berberian, 1976, 1981, 1995b) and the Caucasus (Triep et al., 1995) were not associated with surface fault ruptures due to decoupling of the Zagros top sedimentary cover from the Precambrian basement along the Hormoz Salt decollement in the former case.

3.1.7. Palaeoseismology

Palaeoseismological trench study is not an established technique in Iran. The following is a summary of a few case studies conducted in the project area.

3.1.7.1. The South Eshtehard Fault

A preliminary palaeoseismologic trench study across the South Eshtehard fault, claimed to be the eastern continuation of the Ipak fault (Bolurchi, 1997), with no dating or proper detail logging resulted in speculating three events at 9,000, 4,000, and 900 BP, with 25-30 cm vertical slip for each event. Bolurchi (1997) further claimed a recurrence interval of 1,000 years (for which there is no supporting dating available), a slip-rate of 0.5 mm/yr, and characteristic earthquakes of M=5.5-6.0 for the South Eshtehard fault with a 3 m vertical and 2 m left-lateral displacement.

3.1.7.2. The Kahrizak Thrust

An attempt to study palaeoseismology of the Kahrizak fault south of Tehran (De Martini et al., 1998) failed to construct its seismic history. Despite myriad uncertainties and lack of any dating, the authors claimed that the last earthquake occurred between 5,000 and 800 years ago with a maximum slip of ~10 m, a minimum Holocene vertical slip rate of ~1 mm/yr versus a horizontal slip rate of ~3.5 mm/yr, a maximum of ~3,000 years for average recurrence time, and an expected M_w 7.0 to 7.4 (De Martini et al., 1998).

3.1.7.3. The Mosha Fault

Preliminary palaeoseismologic study across the Mosha fault near the Tar Lake, east of Tehran indicated a minimum of left-lateral component of 2 $\pm$0.1 mm/yr for the Holocene period (Ritz et al., 2003). By assuming a characteristic coseismic average displacement (using Wells and Coppersmith's functions of 1994) comprised between 0.35 m (M_w6.5, 1665 event), and 1.2 m (M_w 7.1, 1830 event), and taking the moment magnitudes attributed to these two earthquakes, Ritz et al. (2003) estimated mean maximum recurrence intervals along this portion of the Mosha fault of 160 and 620 yrs [see the attached 'Macroseismic and Teleseismic Database (AD 855 through 2007) of the Greater Tehran Region (34.35^{o}N to 37.10^{o}N & 49.80^{o}E to 53.10^{o}E)', and the 'Fault Map of the Greater Tehran Region (34.35^{o}N to 37.10^{o}N & 49.80^{o}E to 53.10^{o}E)'].

3.1.7.4. The North Tehran Thrust

Paleoseismological investigation across the North Tehran Thrust (Nazari et al., 2007) showed a 3 m fault scarp affecting Upper Pleistocene and Holocene deposits along a N115^{o}E trending, 30^{o}N-dipping fault plane. Eight surface rupturing events within the past 3,000 yrs were dated by optically simulated luminescence ages. The two last events involved 2.35 m of total reverse displacement along the fault during the last 8,000 yrs (0.77 m for the latest event and 1.58 m for the penultimate). The eight events have magnitudes M_w >6.5 and the mean return period is estimated 3,175-4,075 yrs. The average slip rate along the North Tehran thrust is estimated 0.3 $\pm$0.05 mm/yr (Nazari et al., 2007) [see the attached 'Macroseismic and Teleseismic Database (AD 855 through 2007) of the Greater Tehran Region (34.35^{o}N to 37.10^{o}N & 49.80^{o}E to 53.10^{o}E)', and the 'Fault Map of the Greater Tehran Region (34.35^{o}N to 37.10^{o}N & 49.80^{o}E to 53.10^{o}E)'].

3.1.8. Cocluding Remarks (Historical Seismic Database)

Summary of the reviewed incomplete historic seismic data of the project area presented in the 'Macroseismic and Teleseismic Database (AD 855 through 2007) indicates seismic activity along the North Tehran, the Mosha, the Maydanak, the North Qazvin, the Larzanak, the Alamutrud, the Khazar, and the Eshtehard faults during pre-instrumental period [see the attached 'Macroseismic and Teleseismic Database (AD 855 through 2007) of the Greater Tehran Region (34.35^{o}N to 37.10^{o}N & 49.80^{o}E to 53.10^{o}E)', and the 'Fault Map of the Greater Tehran Region (34.35^{o}N to

37.10°N & 49.80°E to 53.10°E)'] Reactivati on of the Mosha fault in 1830.03.27 (I_o~IX, M_s~7.1) damaged the city of Tehran located approximately 28 km SW of the fault (see the attached 'Fault Map of the Greater Tehran Region (34.35°N to 37.10°N & 49.80°E to 53.10°E)'].

3.2. Instrumental Seismic Databae (1900-2007) – General

A reliable earthquake catalogue containing accurate epicentral locations, focal depths, and earthquake magnitudes are of utmost importance in order to determine various parameters needed for seismic risk assessment. Uncertainties in the derivation of scaling laws depend on how well dependent variables are known. Teleseismic locations are known to have larger uncertainties compared with those from local networks; and parameters such as epicenters and focal depths based on teleseismic arrival times alone lack precision in areas such as the Middle East, especially for the early instrumental period. Since development of predictive relationships of ground motions for engineering purposes requires reliable instrumental epicenter and magnitude data, it is important to assess the reliability and completeness of internationally recorded seismic data.

No single earthquake catalogue lists all the events in the Middle East particularly the ones of lower magnitude. There are also frequent discrepancies in the epicenter location, magnitude, focal depth, and origin time. Examination of the instrumental seismic data for the period of 1903 to 1960 has revealed deficiencies in determination of epicenters and hypocenters in the Middle East (Ambraseys 1978; Berberian 1979). Many instrumentally determined epicenters fall at a considerable distance from the area of maximum ground deformation and damage. The distance is commonly much greater than the estimated/reported location errors.

The mean error in the instrumental and relocated epicenters of the medium- to large-magnitude Iranian earthquakes range from 500 km (in 1903) to 200 km (1918), 100-40 km (1940), and 30 km (1963) which is not acceptable for detailed seismotectonic and seismic risk studies (see Berberian 1979 for discussion). Due to considerable location error in the instrumental and relocated epicenters and lack of adequate micro-earthquake survey, it is impossible to locate the activity of most faults in the Middle East from the data supplied by national and international seismic agencies (Berberian 1976; 1979; 1981; 1983).

As mentioned above, teleseismically recorded earthquakes in Iran cannot be correlated to a particular fault. Routine teleseismic locations are usually in error due to (i) inadequate station coverage, (ii) systematic and random reading errors (poor timing), and (iii) bias due to differences between the real Earth and the earth model used in the location. Reappraisal and refinement of epicentral locations of early instrumental data is impractical since there is no reliable input data. Therefore, many of the existing regional and global parametric instrumental catalogues do not fulfill the condition of transparency.

In this study we have collected and analyzed the reliability and completeness of the instrumental earthquake (teleseismic) data from different worldwide instrumental catalogues maintained by various organizations (such as USCGS, USGS, NEIC, NEIS, ISS, ISC, HRVD, MOS, BCIS, EMSC, NDI, UPP, etc). All the existing catalogues within 150 km radii of central Tehran were utilized for independent evaluation of telesiesmic data. The evaluated data suffered from incompleteness, duplication, and large magnitude of epicentral and hypocentral location errors. Large amount of effort and time was required to evaluate different datasets, eliminating duplicate records after reconciling differences, and sorting out aftershocks. Elimination of redundancies reduced the number of events at the project area.

It became clear that the seismic history within the entire project area is non-uniform and incomplete below certain magnitude thresholds, different for various portions of the project area at different time periods, with variation of clustering in certain areas. While the main reason for such a variation in teleseismic data is variable regional seismographic station coverage, procedural changes in calculating magnitudes have often assigned widely different magnitudes to teleseismic data. At the end of the process, the best available teleseismic data for the project area were selected and a new teleseismic database was created for the project. In the final catalogue, intensity data as well as macroseismic epicenter (ME) from felt reports have been added to the teleseismic data [see the attached 'Macroseismic and Teleseismic Database (AD 855 through 2007) of the Greater Tehran Region (34.35^{o}N to 37.10^{o}N & 49.80^{o}E to 53.10^{o}E)'].

3.2.1. Instrumental Epicenter Location

The distribution of international and national seismological stations and lack of national catalogue of earthquakes has limited the study of seismicity and seismotectonics to the catalogue of

earthquakes published by international agencies. Unfortunately, threshold magnitude of reporting of about 3.5 and poor location and depth accuracy has been obstacles for realistic and quantitative assessments of seismicity in Iran. Initial instrumental epicentral locations of the Iranian earthquakes come from various international agencies (Table IV.1), which show large magnitude of location errors with systematic shifting of telesiesmic epicenter to the north or northwest of their macroseismic epicenters (Ambraseys, 1978, 2001; Berberian, 1979; Ambraseys and Melville, 1982). Locations and magnitudes given by others such as Moinfar et al. (1994) and GSHAP (2000) are nothing more than recompilation of earlier determinations of locations and magnitudes, without refinement or relocation. Ambraseys and Melville (1982) and Ambraseys (2001) reappraised epicentral locations and surface-wave magnitudes of some M_s>6 shallow Iranian earthquakes. The time spans of all these databases, which are used in most seismicity studies, are fairly short comparing to the return period of large-magnitude earthquakes. Major teleseismic data sources are summarized in Table-3.3.

Table - 3.3

SUMMARY OF THE EXISTING TELESEISMIC DATABASE SOURCES FOR THE IRANIAN EARTHQUAKES

Catalogue	Time Range	Magnitude	Intensity	M_o	CMT	Remarks
1- International Data Sources:						
BASS	1913-1917					Gross location errors. Succeeded by ISS
ISS	1918-1963					Large Location errors. Succeeded by ISC
ISC	1964-2004	*Mb, M_s, M_w*				
USCGS	1928-1960	*mb*				Succeeded by NEIS
NEIS (EDR)	1964-1985	*mb*, M_s since mid 1968				Succeeded by NEIC
NEIC (PDE)	1985-2007	*Mb, M_s, M_w*			X	
SSK (1962)	1912-1959					
MOS	1926-2007	*mb, M_s*				
Kondorskaya & Shebalin (1977, 1982)	1900-1977					Azarbaijan & N. Khorassan.
Karnik (1968, 1996)	1902-1955					NW Iran, Europe
STR	1920-1952					Succeeded by BCIS
BCIS	1952-1972	*Mb, M_s*				Succeeded by EMSC
EMSC	1972-2007					
CSEM	1977?					
LNN	1932-					
HFS	1973?					
JSA	1945-1956					
QUE	1952-					
SHL	1952-					
PEK						

NAO	1979?	*mb*				
BJI	1988?	*mb*, M_s, *mB*, M_{sz}				
LAO	1973?					
UNK (unknown source)						
EIDC	1995-2007	*mb*, M_s, M_L				
HARV	1980-2007				X	
IDC	2002-2007	*mb*, M_s, M_L				
ZUR-RMT	2002-2007	M_w			X	
KISR	2002-2007	M_L				
SNSN	2002-2007					
NNC	2003-2007					
BGS	2004-2007					
DUSS	2004-2007					
IGIL	2004-2007					
DHMR	2004-2007	*mb*				
2- National Data Sources:						
IGTU (TEH)	1996-2007	M_n				
IIEES (THR)	2002-2007	M_L				
3- Relocations:						
Nowroozi (1971)	1950-1965					
Nowroozi (1976)	1903-1950					
Nabavi (1972)	1913-1950					
McKenzie (1972)	1948-1960					
Dewey & Grantz (1973)	1962-1972					
Quitmeyer & Jacob (1979)						
EHB (Engdahl, et al., 1998)	1964-1997					
Engdahl & Villasenor (2002)	1900-1999	M_s, M_w, *mB*				
Engdahl et al. (2004, 2006)	1909-2004	M_s, M_w				Improved locations & focal depths*
4- Reappraisals:						
Gutenberg & Richter (1956)	1941-1949	M_{GR}				
Rothe (1967)	1953-1965	*mb*				
Abe (1981)	1904-1980	M_s, *mb*				
Ambraseys & Melville (1982)	1900-1979	M_s	i			Epicenters & M_s
Riad & Meyers (1985)	1903-1983	*Mb*, M_s, M_L	MMI			Calculated values for M & I
Pacheco & Sykes (1992)	1900-1989	M_s		X		
Ambraseys (2001)	1902-1999	M_s				Epicenters & M_s
5- Recompilations:						
Moinfar et al. (1994)	3rd mill. B.C.-1992.09.27					Agglomeration of heterogeneous sources w/different errors & different magnitude scales.
GSHAP (2000)						Agglomeration of heterogeneous sources w/different errors & different magnitude scales.

Notes on Table 3.3:

*: Claimed/estimated uncertainties in epicenters are on order of 10-15 km owing to Earth's lateral heterogeneity and uneven station distribution. Uncertainties of reviewed focal depth estimates are on the order of 10 km, as compared to about 4 km for the depth estimates derived from long-period *P* and *SH* body-waveform inversion.

CMT: Centroid moment tensor.

i: Simplified intensity scale (1 through 5) devised by Ambraseys & Melville (1982) describing earthquake effects on the Iranian traditional adobe buildings.
mB: Broad-band body-wave magnitude.
Mb: Body-wave magnitude.
M_L: Local Magnitude.
M_n: Local magnitude using Nuttli's formula (1973).
M_s: Surface-wave magnitude.
M_w: Moment magnitude.
M_o: Seismic moment.
MMI: Modified Mercalli Intensity.

The early instrumental epicenter locations for Iran, which often are in gross error, should be used in caution and only in the absence of better relocations or macroseismic data. In this study, whenever possible, macroseismic epicenters from field studies and technical reports were used to correct the early instrumental epicenters with large errors in epicentral locations. Macroseismic epicenters are by far the most reliable data for the association of earthquakes with seismic sources and for the calculations of the magnitudes of early earthquakes.

Only recently have there been individual attempts to acquire better depth estimates of the Iranian medium- to large-magnitude earthquakes by long-period *P* and *SH* body-waveform modeling, and improved locations (Engdahl et al., 1998, 2004, 2006). Although the installation of the National Broadband Network and some regional telemetry networks commenced in the mid-1990's (IGTU; TEH), and national seismographic bulletins were reported since 2000 (IIEES; THR), the magnitude of location errors and focal depths of the reported events are still unknown, and there have been no concerted efforts towards preparation of a national seismic catalogue for Iran. Therefore, seismicity and seismotectonic studies still rely heavily on information provided by international monitoring system.

3.3. The Early Instrumental Era (1900-1963)

Seismicity for the Early Instrumental Period of 1900 to 1963 is still poorly understood, even for basic parameters such as earthquake locations. In some cases, this is the result of inherent limitations in the distribution, response characteristics, and timing of the instruments. However, locations for most of the pre-1964 earthquakes are poorly determined.

Instrumental seismology began in 1898 with the first seismogram recording in Jena, Germany, from a distant earthquake in Japan (Von Rebeur-Paschwitz, 1889). The first half of the twentieth century

witnessed the notable expansion of a worldwide system of seismological observatories equipped with a variety of seismographs, including mechanical and early electromagnetic instruments, capable of recording the three components of short- and long-period seismic waves. Beginning in the 1960s, the deployment of the World-Wide Standardized Seismographic Network (WWSSN), a 120-station global network of high-quality, well-calibrated electromagnetic instruments, meant that most existing older mechanical instruments were discontinued. In an important concurrent development, pendulum clocks that had to be corrected for large linear drift rates were replaced by crystal clocks that were normally accurate to within a few tenths of a second. These improvements, combined with easy access to seismograms, provided the basis for great advances in seismology and played a key role in the plate tectonics revolution in earth sciences. As a result, global seismology studies naturally focused on WWSSN data, generally ignoring the seismicity recorded prior to 1964 (Villasenor et al., 1997).

The most valuable global relocation study of the pre-1964 seismicity is Gutenberg and Richter's (1954) *Seismicity of the Earth* in which they determined 4,000 earthquake locations and magnitudes for events between 1904 and 1952. This classic work, although restricted to large-magnitude earthquakes, is still the obligatory starting point for any global or regional study of pre-1964 seismicity.

Two catalogues serve as primary sources for the period 1900 to 1963, the Bulletin of the International Seismological Summary (ISS) and their predecessors (which include the data used by Gutenberg and Richter), and the Bureau Central International de Seismologie (BCIS), providing earthquake locations and arrival times of seismic phases. Regardless of the source, the catalogued locations of the pre-1964 earthquakes are generally too unreliable to be used in any quantitative application, such as seismic hazard assessment, or in the detailed study of the tectonics of seismically active regions (Ambraseys, 1978; Berberian, 1979).

Major reasons for the poor quality of the locations determined for the pre-1964 earthquakes were the primitive computational techniques and Earth models available at the time the earthquakes occurred and the locations that were produced. Since our knowledge of Earth structure is derived primarily from earthquake data, the earliest Earth models (derived from the pre-1964 data) were rudimentary at best. The earliest of these models, the Zoppritz-Turner Tables, used by the ISS from 1913 to 1929, were inaccurate and incomplete, valid only for shallow-focus earthquakes. Deep earthquakes had to be accounted for with ad hoc corrections.

This situation greatly improved with the introduction of the Jeffreys-Bullen (J-B) Tables (Jeffreys and Bullen 1940), which provided a complete, remarkably accurate representation of *P*, *S*, and other later-arriving phases. These Tables are still used by the ISC (the successor of the ISS) and the NEIC for routine teleseismic location, and even in modern relocation studies, although improved, more suitable travel-time tables have recently been developed (e.g. Kennett and Engdahl 1991; Morelli and Dziewonski 1993; Kennett et al., 1995).

Similarly, earthquake location procedures have improved with time. For instance, new earthquakes reported to the ISS were commonly assigned epicenters coincident with those determined for previously reported events in the same region. A new epicenter was only adopted if the phase data appeared significantly incompatible with any pre-existing locations. The ISS bulletins reported approximately 75% of the earthquakes simply as shallow, with a 'normal' depth of 33 km (33N). A so-called 'abnormal' focal depth was calculated only if the phase data were clearly incompatible with a shallow-focus solution. Finally, only *P*-wave arrival times were used to calculate a location, even though the Bulletin listed other later-arriving phases. Thus, constraints on the focal depths are almost nonexistent (Villasenor et al., 1997).

Rothe's 'The Seismicity of the Earth 1953-1965' (Rothe 1967) intended to be a continuation of Gutenberg and Richter's work contains magnitudes of 90 earthquakes in Iran for that period. These were calculated not from amplitude-period data, but from the average of weighted individual station magnitudes or from semi-empirical formulate. Most magnitudes shown in Rothe's work as *M* are in fact broadband m-estimates, particularly of the smaller events and they must be used with caution. Peronaci's catalogue (1958, 1959) contains only six magnitudes calculated from amplitude data of the station in Rome; the remaining 60 magnitudes are from Gutenberg and Richter, Strasbourg, and Upsala.

The first part of the instrumental era, which is taken as 1900 to 1963, is therefore, divided into two Periods of the BAAS (1900 to 1917) and the ISS (1918 to 1963).

3.3.1. The BASS Period of 1913-1917

For the period 1913 to 1917, with limited number of seismographic stations operating mainly in Europe, the British Association for the Advancement of Science (BASS; the forerunner of the ISC) reported nine epicenters of large-magnitude earthquakes in Iran, for which macroseismic information was used to determine the approximate position and time of origin of the event, whenever it was available. When local observations in epicentral regions were not available, epicenters are in gross errors, and some of these early events have more than 300 km location errors. These early instrumental locations were based on observations reported mainly from undampped seismographs, often with uncertain timing, and in a period when knowledge of seismic velocities and travel times was very poor. These factors often resulted in epicentral locations with gross error, which need correction (Ambraseys, 1978; Berberian, 1979; Ambraseys and Melville, 1982). During this period the Qeshm earthquake of 1902.06.09 (M_s 6.4), the Turshiz earthquake of 1903.09.25 (M_s 5.9), the Silakhor earthquake of 1909.01.23 (M_s 7.4) and the Ravar earthquake of 1911.04.18 (M_s6.2) [all outside of the project area], were only recorded by 9, 7, 16, and 19 seismographic stations reporting trace amplitudes.

3.3.2. The ISS Period of 1918-1963

For half a century (1913-1963), the International Seismological Summary (ISS) provided the only global seismicity catalogue that approaches comprehensiveness. Other sources, such as the Bureau Central International Sismologique (BCIS), covered more restricted time periods and/or geographic regions (for example, BCIS coverage extends back only to 1952 and within Delta ~50^o of Central Europe). The ISS evolved from its predecessor, the British Association for the Advancement of Science (BAAS), which published circulars of time and amplitude data for the global network of Milne Seismographs for the time period 1899-1913. Formal ISS bulletins began in 1918 as a consequence of an International Union of Geodesy and Geophysics (IUGG) resolution in 1922. Epicenters of the early time period (~1913-1917) were adopted from BAAS bulletins.

No magnitudes are computed or provided for the ISS data; the only size indications are the number of recording stations and their distance and the notation of registered ‘long’ waves at particular stations. In the early years station distribution and accurate timing were major problems and epicentral accuracy suffered accordingly. Focal depths, if computed at all, are quite uncertain.

Despite these deficiencies, the ISS represents a unique and irreplaceable record of seismicity for half of the Twentieth Century. It is the primary data source for subsequent studies, the most important being the massive study of Gutenberg and Richter (1954) and more recent work (e.g., Abe 1981, 1984; Pacheco and Sykes 1992), which is concerned mainly with correction factors for the Gutenberg-Richter magnitude (M_{GR}) to make it equivalent to modern teleseismic M_s. The Gutenberg-Richter catalogue was extended through 1965 and some earlier events added by Duda (1965) and Rothe (1969). Since 1952, the Bureau Central International Sismologique (BCIS) has circulated a bulletin giving rapid determination of events located within a radius of 5000 km from the center of Europe, covering Iran.

During the period 1918-1963, International Seismological Summary (ISS) reported 528 epicenters in Iran of which 239 (45%) were epicenters adopted or accepted from other sources without revision. Those calculated used routine determinations including least-square procedure, which was carried out by hand up to 1957. ISS also adopted old locations for new sets of arrivals from the same neighborhood without calculation, particularly for successive shocks. There are two dropping periods in the number of the reported events by ISS; (i) the first one during the World War II (1939-1945), and (ii) the second one during 1952-1963. The latter was the result of decision of reporting earthquake of magnitude 6.0 or over. The ISS epicentral locations vary in accuracy, and the early epicenters before 1940s must be used with great caution (Ambraseys, 1978; Berberian, 1979; Ambraseys and Melville, 1982).

The instrumental data for earthquakes in Iran, particularly prior to 1937, when adequate travel-time tables became available, are found too crude to allow significant refinements of ISS locations. This is because the early arrival data are generally of such poor accuracy and azimuthal distribution that the epicenter can be resolved only to the average limits given by the input data. The resolution of the focal depth is even worse. Inaccuracies of onset times and the lack of near stations cannot permit valid depth determinations. There simply is no way to rectify the systematic errors involved in assuming, for instance, a standard Earth model in a thrust region of Iran or constant velocities along all paths. With stations to one side, high apparent consistency is possible but the precision in locating an epicenter will be low. Not only was this a major difficulty with ISS locations of Iranian earthquakes, but also still is in any attempt to define ISS determinations. The fact that the bulk of stations reporting arrival times

were confined within a narrow segment to the northwest of the country causes errors in travel times to turn into systematic location errors (Ambraseys and Melville, 1982).

For the period prior to 1963 the number of earthquakes in Iran for which magnitudes is reliably known is very small. No magnitudes are available for events before 1909, and for the period up to 1963, Gutenberg and Richter (1954) have assigned magnitudes to only half the events of magnitude greater than or equal to 6.0. For almost all smaller shocks, magnitudes remain unknown. For the period 1931 to 1948 Gutenberg and Richter (1954) assigned magnitudes to almost all the earthquakes greater than 6.0, but only to very few below this value. In the '*Seismicity of Earth'*, they assigned magnitudes to 63 earthquakes in Iran for the period 1909 to 1948. Of these, 29 are of class d (5.3<M<5.9), 24 are class c (6.0<6.9), nine of class b (7.0<M<7.7), and one of class a (M>7.8). Four events are of intermediate depth. Magnitudes estimated by individual stations in the period 1949-1960 are quite numerous but very heterogeneous. The magnitudes of about 50 earthquakes in Iran calculated during that period are either non-homogeneous or it is not clear by which method they were derived. In fact, for the whole period up to 1962, we have an agglomeration of magnitudes estimated at different times by different scales, often by a combination of scales, or by scales that are not specified. Of every four earthquakes in Iran in that period, the magnitude of three is not known, while every three known magnitudes, two at least are of questionable quality (Ambraseys and Melville 1982). No magnitude estimates were made by the ISS up to 1963.

Since 1952 the Bureau Central International Seismologique (BCIS) has circulated a bulletin giving rapid determination of events located within a radius of 5,000 km from the center of Europe, which covers Iran. The United States Coast and Geodetic Survey (USCGS) and the Institue of Physics of the Earth, Moscow (MOS) also released preliminary estimates of epicenters as soon as sufficient information became accumulated to ensure a reasonable degree of accuracy.

During this time period (i) the number, and (ii) distribution of seismological stations [which remained ill distributed less than 60^{o} but confined within the northwest quadrant], and (iii) the quality of the input data [such as arrival time, magnitude, etc.], were not adequate to allow accurate epicentral location and focal depth determination of the Iranian earthquakes. Therefore, it is clear that the low accuracy of instrumental locations calculated by BAAS, ISS, BCIS, USCGS, MOS, Gutenberg and Richter (1965) and many more, as well as the later re-locations with different

procedures made by Gutenberg and Richter (1965), Rothe (1969), Nowroozi (1971, 1976), Nabavi (1972), Quitmeyer and Jacob (1979), and Engdahl et al. (1998) is common for this period. It is clear that the procedures used to recalculate the epicentral positions of earthquakes in the mentioned period cannot overcome uncertainties of location arising from poor data and azimuthal distribution of seismographic stations, occasionally resulting in gross mislocations (Ambraseys, 1978, 2001; Berberian, 1979; Ambraseys and Melville, 1982).

3.3.3. The Local Seismic Stations

Before 1963, the only two seismic stations, in Tehran (TEH) and Shiraz (SHI), which began to operate in 1958 and 1959 respectively, did not publish amplitude-period data. Nor did the secondary station at Sefidrud report such data. Tehran and Tabriz began to determine magnitudes of near earthquakes after 1971.

3.3.4. Relocations of the Early Instrumental Era Earthquakes

i- Nabavi (1972):

A relocation of the earthquakes that occurred before 1951 in Iran was computed in the Institute of Geological Sciences (IGS), Edinburgh (Nabavi 1972). Out of 824 earthquakes that are known to have occurred in Iran during the first half of the century, 451 were tested using the program by Lilwall and Douglas (1970). About one third of the events tested were rejected as very inconsistent without further investigation. The remaining 292 events, of magnitude between 4.8 and 7.4 were relocated for a fixed focal depth of 33 km; inaccuracies of arrival times could not possibly permit valid depth determination. The relocated epicenters of Nabavi (1972) were found to have locations somewhat different from those computed originally by ISS, with an average shift for all magnitudes of about 70 km. However, it is interesting to note that the changes of average distance from their corresponding macroseismic locations were found to be negligible which remained significant at some 60 km (Ambraseys 1978). This observation led to a further effort to resolve the earthquake locations of a number of well-recorded events for which there was sufficient macroseismic information. By comparing readings from stations that had observed events in the same region over a decade or two, and by rejecting readings from stations with large travel-time residuals, the results from the remaining stations confirm the difficulty of improving on ISS locations. Simply, instrumental data for earthquakes in Iran, particularly before the mid-1930's, were found to be too crude to allow significant refinements of ISS locations. Excluding adapted epicenters, which were not after all computed, ISS-calculated locations do have an

accuracy, which although by modern standards is low, is nevertheless comparable with that of the input data, particularly after 1937 when adequate travel-time tables became available. Occasional gross mislocations of epicenters by ISS, even of well-observed events, are not so much due to lack of adequate routine calculation methods, as to the crudeness of the data reported from different stations distributed around the country in the most unfavorable pattern (Ambraseys and Melville, 1982).

ii- Nowroozi (1976):

Nowroozi (1976) re-examined the location of 131 events that occurred in 1903-1950. Of these, 24 occurred outside Iran, 26 were adopted without calculation and five are unidentified. The remaining 76 events, which represent 9% of the number of known earthquakes in Iran during the first half of the century, were relocated and also assigned focal depths using the method by Bolt (1960). The earthquake of 1945.05.11, which had a magnitude of 4.7, was assigned a focal depth of 149 km by Nowroozi (1971, 1976). This event caused concentrated damage within a very small area near Tehran and was hardly felt in the capital. The earthquake of 1948.06.30 with a magnitude of 5.0 caused similar surface effects and was assigned a depth of 114 km by Nowroozi (1971, 1976).

3.4. The Modern Instrumental Era (1964-2007)

The Modern Instrumental Era is the time span covered by the International Seismological Centre (ISC, 1964-2007) and the Preliminary Determination of Epicenters (PDE; U.S. Geological Survey, 1964-2007). Standard magnitude (m_b and/or M_s) are assigned by these agencies for all major events that are recorded teleseismically, i.e., geocentric distance Delta>20^o, representing approximately ray paths that enter the lower mantle. Originally, only the short-period *mb* was reported (USCGS from 1963, ISC from 1964); calculation of M_s, for example was not begun by the USGS until 1968, and M_s was not adopted by the ISC until 1978 (and not with depth restrictions on its calculation until mid-1981).

In a significant analytical advance, routine centroid-moment tensor (CMT) determinations of earthquake faulting mechanisms have been computed for nearly all earthquakes of m_b>5.5 or M_s>5.0 for 1977 to the present (e.g., Dziewonski et al., 1981; Dziewonski and Woodhouse 1983; Harvard University 1977-2007). As part of the inversion, the static seismic moment M_o is determined for the best double-couple solution; hence, moment magnitude ***M*** (Hanks and Kanamori 1979) is available for all CMT events. This capability essentially divides the Modern Instrumental Era into two sub-eras: (i)

'1964-1976 for standardized global locations and magnitudes', and (ii) '1977-2007 for those capabilities plus CMT solutions for larger events'.

3.4.1. The ISC Period of 1964-2004

The seismicity of the Modern Instrumental Era is most completely reported by the International Seismological Centre (ISC). The ISC Bulletin (ISC, 1964-2004) has a lag time of about two years. Although other organizations, such as the U.S. Geological Survey (NEIS/SEIC), Moscow (MOS) and Beijing (PEK/BJI) seismological centers, are more timely and report locations and magnitude globally, they utilize fewer stations and report fewer events than does the ISC.

The beginning of the Modern Instrumental Era is marked by a dramatic, order-of-magnitude increase in reported and calculated events in 1963-1964. Between 1964 and 1987 a further increase by a factor of 3-4 has occurred. The difference between number of events with ISC-calculated hypocenters and total number arises from publication of contributed solutions for smaller events from local and regional agencies. The difference between total calculated hypocenters and total with m_b or M_s calculated arises because many events are too small or do not satisfy the ISC restriction criteria for magnitude computation.

Earthquake size estimation in the Modern Era depends mainly on the teleseismic m_b and M_s magnitudes provided by ISC or occasionally by other agencies mentioned above. Only 25-50% on the total reported ISC events are assigned an m_b value. In addition, M_s -begun only in 1978 by ISC- is calculated for only 4-10% of all reported events. It is clear from this that even in the Modern Era a major problem for a comprehensive global seismicity data base will be uniform magnitude assignment, i.e., a single size descriptor for each earthquake. The size descriptor of choice is moment magnitude $\boldsymbol{M}$. $\boldsymbol{M}$= M_w, where $\boldsymbol{M}$ is moment magnitude as defined by Hanks and Kanamori (1979) and M_w is moment magnitude as originally defined by Kanamori (1977). Since $\boldsymbol{M}$ is recovered directly from seismic moment M_o, the Harvard CMT catalogue constitutes an important subset of events for which M_o, hence $\boldsymbol{M}$, is directly determined from seismic waveform data of the Global Digital Seismic Network (GDSN).

3.4.2. Reappraisal of the ISS/ISC Teleseismic Data

Engdahl et al. (1998; EBH) relocated the large part of the ISC catalogue from 1964 through June 1997 by using improved velocity model and also including the arrival times of additional phases, particularly teleseismic depth phases to supplement the direct *P* arrival times in the location procedure. It was claimed that the relocations resulted in a better location than that of the ISC.

Ambraseys (2001) reappraised locations and surface-wave magnitudes (M_s) of 91 Iranian earthquakes with M_s>6.0 between period of 1902 through 1999. By analyzing the ISS data, Ambraseys (2001) found that the ISS data are shifted towards the NNE of their macroseismic epicenters with an overall standard deviation in azimuth larger than that from the ISS data set [Berberian et al. (1992) also found that the ISS epicenter locations are generally shifted towards NE of the USCGS/NEIS teleseimic data; see Figure 3, p. 1732, in Berberian et al., 1992 which covers the northwestern portion of the project area]. The difference between instrumental and macroseismic locations is only significant if they are greater than the radius of the epicentral of maximum observed intensity; i.e., the smaller events having smaller radii are more suitable for such a comparison than large-magnitude earthquakes with large epicentral region.

Engdahl and Bergman (2001) determined highly accurate relative locations for a number of teleseismically well-recorded earthquake clusters in Iran using a multiple event location method. Engdahl and Villasenor (2002) produced a relocated twentieth century catalogue of global seismicity with uniform computer-determined hypocenters whenever possible utilizing a modern Earth model (ak 135) and location algorithm of Engdahl et al., (1998). For the 1900-1963 period they selected magnitude cut-off value of 6.5 (although the resulting catalogue is complete only to magnitude 7.0). For 1964-1999 period their magnitude cut-off is 5.5, and the catalogue is complete at this magnitude threshold.

Later, Engdahl et al. (2006) relocated and reassessed more than 2000 Iranian teleseismic data reported by ISS/ISC for the period of 1923-2004, using an advanced technique for 1-D earthquake location. They claimed that (i) uncertainties in their relocated epicenters are on the order of 10-15 km in Iran, owing to the Earth's lateral heterogeneity and uneven station distribution; and (ii) uncertainties of the focal depth estimates are on the order of 10 km, as compared to about 4 km for long-period *P* and *SH* body-waveform inversions [see the attached 'Macroseismic and Teleseismic

Database (AD 855 through 2007) of the Greater Tehran Region (34.35°N to 37.10°N & 49.80°E to 53.10°E)'].

3.4.3. The National Seismic Networks

The Iranian networks of seismographic stations were usually functioning during the twentieth century without publishing the seismic parameters. The seismographic station in Tehran (TEH), the first to be installed in the country, came into operation in 1958 and was followed a year later by the station in Shiraz (SHI). In 1962 a secondary station was set up at Sefid Rud dam site (SEE, WRI) and soon after in 1964-5, the station in Tabriz (TAB), Mashhad (MHI), and Kermanshah (KER) came into operation. Shiraz (SHI), Tabriz (TAB) and Mashhad (MHI) being equipped with instruments of the World-Wide Standardized Seismograph network (WWSSN).

In 1971 the Ferdowsi Mashhad University (MUI) began to expand its regional network with subordinate stations (KHI, KHB, MUI, SHD, TGI, & ZRG) equipped with MEQ-600/800 recorders. A little later, the Atomic Energy Organization of Iran (AEOI) began to operate local networks of MEQ-800 recorders. In 1975, six instruments were deployed in the region of Bushehr within a radius of 37 km from 29.10°N-51.10°E (H1, R2, A3, A3b, K4, K4b, G6, and G6b). In August 1976, another network of seven recorders was installed in the Esfahan region within a radius of 42 km from 32.60°N-51.70°E (N1 through N7). Early in 1977, another network of five recorders began to operate around Tehran, deployed 30 km around Amirabad.

In 1976 a permanent, long-period array was established in the region of Saveh, southwest of Tehran, consisting of seven stations deployed around 34.45°N-50.73°E (ILPA). At least two other networks were in operation prior to 1978 in the Qasr-e-Firuzeh Royal Hunting Park, in southeast Tehran, and along the southern Caspian shore in northern Iran. Both these U.S. based networks were operating secretly and their data are not available to the Iranians. The networks were destroyed during the Islamic revolution of 1979.

In 1984, AEOI began to operate a local network of a telemetry seismographic array in Tabriz (DND, NTB, HRS, SRB, SND, AZS, & SHB). The network was shutdown a few weeks prior to the Spidak, Armenia earthquake of 1988.12.07 (M_s 6.8). The seismographs were shipped to and stored at AEOI

Tehran office! Moreover, during the 1990.06.20 Rudbar earthquake of M_w 7.3, the Sefid Rud dam site stations (SEE & WRI) which were set up in 1962, were out of order.

At present there are two regional permanent seismic networks in Iran operated by the Institute of Geophysics, Tehran University (IGTU; TEH), and the International Institute of Earthquake Engineering and Seismology (IIEES; THR), Tehran. IGTU operates more than 40 short-period digital seismological stations, distributed into eight seismic networks. Management is within the National Centre of Seismic Networks.

i- The Iranian Long-Period Array (ILPA; 7 stations)

ILPA has operated since 1976 and is comprised of seven short period and long period borehole sensors located within a 30-km-diameter circle equipped with long-period seismometers located in the area southwest of Tehran and northeast of Saveh. It transmits continuous data to a central recording station in Tehran. Available data consists of three years of long period and 17 months of short period recordings (Akasheh et al., 1976).

Located earthquakes using the ILPA network and the Tehran (TEH) and Kermanshah (KER) seismographic stations during the period of March 1976 through December 1978 (Akasheh and Berckemer, 1983) showed a scattered seismicity. Since no listing was published with the report, it is difficult to locate the sources of errors and illustrate the quality of the data. Akasheh and Berckemer (1983) claimed that their data shows that the North Tehran and the Mosha faults do not show any significant activity, but the Ipak and the South Parandak faults show activity. The authors also mentioned that the scattered seismicity coincides with areas where the geological character changes. Composite focal mechanisms (no polarity readings presented) showed unreliable results with four normal faulting (one along the North Tehran thrust), and two north-south thrust faulting in a region with predominant NW-SE structures (Akasheh and Berckemer, 1983). This is due to the fact that the authors used reported polarity readings of short- and long-period data. It is known that short period data are sensitive to detailed behavior of the source and the velocity structure at the source and at the receiver sites and, therefore, do not generally provide a reliable focal mechanism solution.

ii- The Tehran Seismic Telemetry Network (12 stations)

The network is comprised of a Canadian Nanometrics Acquisition System of 12-telemetry, short-period stations, installed in 1996. Each station consists of a short-period, three-component seismometer that is digitally telemetered to the central station that stores the earthquake records on a computer disk using a trigger mode. A continuous telemetry system allows a common clock that is synchronized with a GPS receiver and reduces time uncertainties. Telemetry delay times are corrected to reduce time picking errors. However, incorrect phase readings have caused large scatter in arrival times. The recording is done on a triggering basis (Ghods and Sobouti, 2005).

iii- The Azarbaijan Telemetry Seismic Network (8 stations)

The network consists of eight short period seismographs connected to central recording station via telemetry. The recording is done on a triggering basis.

iv- The Broadband Network (11 stations)

This network consists of 11 broadband seismic stations of Guralp (CMG3T) sensors and Guralp 25 bit data loggers. The seismographs record continuously at the station sites. Selected time windows, on request of the analyzing seismologists, are sent to the IIEES central recording station in Tehran via satellite (VSAT).

3.4.4. The National Strong Motion Network

Since 1973 the Strong Motion Network of Iran (SMNI) started its activities in the organizational framework of the Plan and Budget Organization of Government of Iran under management of A.A. Moinfar. In 1981 the strong motion network operation was transferred to the Building and Housing Research Center (BHRC) of the Ministry of Housing and Urban Development. Initially, the SMNI consisted of about 300 analogue SMA-1 accelerographs. From 1992 to 2001, the number of accelerographs of the network increased to 957 digital SSA-2 and 97 SMA-1 Kinemetrics recorder analogue units (http://www.bhrc.gov.ir).

3.5. Comparison of Instrumental and Macroseismic Epicenters, and Quality Criteria of the Teleseismic Data

With the large location errors of instrumental epicenters, especially for the period prior to 1964, the best method for improving or confirming instrumental epicenters of the Iranian earthquakes is to attempt to find correlations with macroseismic (non-instrumental) data from first-hand field studies

with defined meizoseismal (epicentral) region (the region of intense shaking in the near-field of an earthquake within the isoseismal of highest intensity). It should be noted that the earthquake epicenter is not in the center of the meizoseismal region, and the meizoseismal region in turn may depend on population distribution. Nonetheless, the macroseismic epicenters are not liable to gross misallocations that are present in the early Iranian instrumental locations discussed above. Ambraseys (1978) and Berberian (1979) calculated considerable shifts of the instrumental epicenter locations from the corresponding macroseismic epicenters of the moderate-sized Iranian earthquakes with restricted damage zones assessed from field studies.

The instrumental data have been graded according to the quantity of the information. The quality ratings range from 'A' (most reliable) to 'E' (least reliable) and are assigned on the epicentral uncertainties and on the network configuration (azimuthal gap), respectively [see the attached 'Macroseismic and Teleseismic Database (AD 855 through 2007) of the Greater Tehran region (34.35^{o}N to 37.10^{o}N & 49.80^{o}E to 53.10^{o}E)'].

TABLE-3.4

RATING CRITERIA FOR THE INSTRUMENTAL SEISMIC DATA (1900-2007)

Q: RATING CLASS	EPICENTRAL LOCATION ERROR (in km)
A	<5
B	5-10
C	10-20
D	20-30
E	>30

3.6. Eartquake Intensity

Intensity data of the well-studied events from the published and unpublished sources have been included in the project database [see the attached 'Macroseismic and Teleseismic Database (AD 855 through 2007) of the Greater Tehran Region (34.35^{o}N to 37.10^{o}N & 49.80^{o}E to 53.10^{o}E)']

3.7. Focal Depth

In principal, the hypocenter of an earthquake marks the onset of earthquake rupture, and it could lie anywhere within the aftershock distribution zone. The location method routinely employed by the

international agencies such as ISS/ISC and USGS/NEIS/NEIC, which is based on the arrival times of teleseismic *P* waves alone, suffer from a trade-off between origin time and depth, which can cause errors in focal depth of several tens of kilometers. Furthermore, the effects of lateral heterogeneity and station coverage for earthquakes in Iran usually result in ISC depths that are significantly overestimated (Engdahl et al., 2006). Therefore, focal depths of the Iranian teleseismic data are often not determined with sufficient accuracy for many geological, tectonic, and seismic-hazard purposes.

By the early 1980s, synthetic seismogram techniques for modeling *P* and *SH* body waveforms allowed depths to be estimated typically to $\pm$4 km for earthquakes larger than about M_s 5.5. In this study whenever such studies available, the centroid depth is used [See the attached 'Macroseismic and Teleseismic Database (AD 855 through 2007) of the Greater Tehran Region (34.35^{o}N to 37.10^{o}N & 49.80^{o}E to 53.10^{o}E)']. Since October 1985, NEIC has been routinely determining a broad-band depth; either from inversion of differential times of depth phases identified on broad-band waveforms, or by modeling of *P* and transversely polarized *S* waves, for most earthquakes of magnitude >M_w 5.5.

The relocations by Engdahl et al. (1998) and Engdahl and Villasenor (2002) for focal depth of earthquakes seem to be better than those routinely calculated by ISC and NEIC. However, comparison with centroid depths obtained by waveform modeling shows that the errors are still large. Engdahl et al. (2006) claimed that their relocated and reassessed Iranian earthquakes have uncertainties of focal depth estimates on the order of 10 km [See the attached 'Macroseismic and Teleseismic Database (AD 855 through 2007) of the Greater Tehran Region (34.35^{o}N to 37.10^{o}N & 49.80^{o}E to 53.10^{o}E)'].

3.8. Eartquake Magnitude

The importance of knowing the quality and completeness of earthquake epicenters and magnitudes in teleseismic parametric catalogues is obvious. Complete magnitude estimates are important for the derivation of reliable regional seismic moment-surface wave magnitude [log (M_o)-M_s] relationships, which are needed to estimate seismic moments before the mid-1970s. They are equally important for the derivation of long-term frequency-magnitude relationships, which are needed to estimate the

total moment release and tectonic motion in continental regions, the rate of which is known from GPS measurements, and for the assessment of aseismic creep. These relationships are sensitive to errors in M_s and degree of incompleteness of the record, particularly for larger earthquakes.

The use of non-uniform and incomplete magnitude estimates may cause a potentially serious distortion in magnitude-frequency recurrence relationships that are important in assessing seismic hazard. The contribution to this distortion from the low-magnitude range should not be under-estimated, particularly for regions of apparent low seismicity where recurrence formulate are usually computed on the basis of low to intermediate magnitude earthquakes. In addition, the use of non-uniform magnitudes is likely to lead to erroneous conclusions about the coherence between *Ms* and *mb*.

Reliable magnitudes are essential for the derivation of recurrence relations, particularly at large magnitudes where recurrence curves steep. They are also important for the scaling of ground motion and for placing constraints on the bounds of rupture zones. A cause for the concern is the reliability of magnitudes reported in different parametric catalogues, particularly for events before the advent of the magnitude scale in the 1950s.

For the period prior to 1962, an agglomeration of heterogeneous magnitudes was estimated at different times by different magnitude scales, often by combination of scales, or by scales that are not specified. Gutenberg and Richter (1956) calculated the weighted mean of M_s and M_B and specified as M (Later Assigned as M_{GR}) for their magnitude catalogues of the 1941-1949 earthquakes. According to Geller and Kanamori (1977) and Abe (1981), who work examined Gutenberg's worksheets, M in the G-R catalogue (M_{GR}) is almost equal to M_s for shallow earthquakes (h<40 km) (Utsu, 2002).

Rothe's catalogue of 1953-1965 (1969) contains magnitudes of 90 earthquakes in Iran, which were not calculated from amplitude-period data, but from average of weighted individual station magnitude estimates or from semi-empirical formulae. Most magnitudes shown in Rothe (1969) as M [surface-wave magnitude; later assigned as M_R] are in fact broadband m-estimates [body-wave magnitudes]. Peronaci's catalogue (1958, 1959) contains six magnitudes calculated from amplitude data of the station at Rome; the remaining 60 magnitude assessments are from Gutenberg and Richter, Strasbourg, and Uppsala (Ambraseys and Melville, 1982).

No magnitude estimates were made by the ISS up to 1963. Starting with 1964, the ISC began to report body-wave magnitudes (*mb*) like the USCGS [*mb*(PDE)]. On the average *mb*(PDE) is about 0.05 higher than *mb*(ISC). This difference persists from 1966 to 1997. In the earliest two years (1964-1965) the average difference is about 0.1 (Utsu, 2002). The difference between published body-wave, *m,* magnitude of USCGS and MOS values are mainly due to the different response of the WWSSN (short period) and MOS (medium period) instruments and also because of USCGS reading amplitudes within the first 5 seconds as compared to within 20 seconds read by MOS. The *Q*-values of Gutenberg and Richter are based on amplitudes from medium period instruments, so MOS procedure is closer to the original M_B (Ambraseys and Melville, 1982). According to Lienkaemper (1984), M_s calculated by the Prague formula, which is used for Preliminary Determination of Epicenters (PDE; USGS), is directly comparable to M_{GR} of Gutenberg and Richter (1954). M_S computed by Abe (1981), Gutenberg (1945), and Richter (1958) differ systematically from M_s of PDE and M_{GR} (Lienkaemper, 1984). There is no systematic difference between the M_s(PDE) and M_s(ISC) since 1976 for earthquakes of M_s less than 7.3. However, *M_s(PDE)* is larger than M_s(ISC) by about 0.1 on the average for M_s(PDE) larger than 7.4 (Utsu, 2002).

Tehran and Tabriz stations began to determine local magnitudes of near earthquakes after 1971 (Adams, 1977). Since 1966 IGTU (TEH) and 2001 IIEES (THR) began reporting the Iranian earthquake local magnitudes (M_L). IGTU has been using the Nuttli's formula (M_n; Nuttli, 1973) [See the attached 'Macroseismic and Teleseismic Database (AD 855 through 2007) of the Greater Tehran Region (34.35^{o}N to 37.10^{o}N & 49.80^{o}E to 53.10^{o}E)'].

Traditional magnitude scales are limited by both the frequency response of the earth and the response of the recording seismograph. There are several problems associated with using M_s to analyze source parameter relationships (Wells and Coppersmith, 1994). Because M_s is a measure of seismic wave amplitude at a specific period of 18 to 22 seconds, it measures only the energy released at this period. Although M_s values generally are very stable between nearby stations, significant variations in M_s may occur between distant stations. These variations are related to azimuth, station distance, instrument sensitivity, and crustal structure (Panza et al., 1989). Furthermore, for very large earthquakes (>8.0), the periods at which M_s is measured become saturated and no longer record large-scale faulting characteristics (Hanks and Kanamori, 1979).

A similar problem with saturation of measured seismic waves occurs for scales such as local (M_L) or Richter magnitude (M_{GR}) and body-wave magnitude (m_b). The latter (m_b) is known to saturate at M~6.0 underestimating the size of larger earthquakes. For small earthquakes (M_s >5.5), 20-second surface wave amplitudes are too small to be recorded by many seismographs (Kanamori, 1983). Use of longer period measures of magnitudes, such as M_s or M_w, is preferred.

In this study, whenever available, we reported both M_s and M_w for the earthquakes in the project area [see the attached 'Macroseismic and Teleseismic Database (AD 855 through 2007) of the Greater Tehran Region (34.35^{o}N to 37.10^{o}N & 49.80^{o}E to 53.10^{o}E)].

3.9. Seismic Moment (Mo) and Moment Magnitude (Mw)

Seismic moment (M_o) is a physical meaningful link between earthquake size and fault rupture parameter, and is expressed by:

M_o=μ D A

Where μ is the 'shear modulus' [usually taken as 3 X 10^{11} dyne/cm^2 for crustal faults (Hanks and Kanamori, 1979)]; D is the 'average displacement' across the fault surface [a range of 0.2 X d_{max} to 0.8 X d_{max} can be adopted from the epicentral relation proposed by Wells and Coppersmith, 1994]; and A is the 'area of the fault surface' that ruptured or expected to rupture [for Iran in general a fault width of 15 km (that is the average thickness of the seismogenic layer), and a surface rupture length can be used for calculating the area of the fault surface]. In turn seismic moment (M_o) is directly related to moment magnitude (M_w), which is computed using the scalar seismic moment (M_o) [e.g., M_w=2/3*log M_o-10.7; Hanks and Kanamori, 1979].

Seismic moment (M_o) is considered a more accurate measure of the size of an earthquake than are traditional magnitude scales such as M_s and m_b because it is a direct measure of the amount of radiated energy, rather than a measure of the response of a seismograph to an earthquake (Hanks and Wyss, 1972). It is computed from the source spectra of body and surface waves (Hanks et al., 1975; Kanamori and Anderson, 1975) or is derived from a moment tensor solution (Dziewonski et

al., 1981). Furthermore, there is a larger variability in the value of M_s than of M_o measure at different stations. For any earthquakes, M_s values from stations at different azimuths may differ by as much as 1.5 magnitude units, whereas M_o values rarely differ by more than a factor of ten, which is equivalent to a variability of 0.7 in M_w values. Thus, M_w is considered a more reliable measure of the energy released during an earthquake (Kanamori, 1977; Hanks and Kanamori, 1979). M_w is proportional to 1.5 times the base 10 logarithm of M_o. When available this is the preferred magnitude scale, because it does not saturate for very large or great earthquakes [see the attached 'Macroseismic and Teleseismic Database (AD 855 through 2007) of the Greater Tehran Region (34.35^{o}N to 37.10^{o}N & 49.80^{o}E to 53.10^{o}E)'].

3.10. Regional Frequency-Magnitude Distribution (Gutenberg-Richter Relation)

The annual cumulative rate (N) of occurrence of earthquakes of magnitude equal to or greater than *M* for a homogeneous region or a single fault zone is usually expressed by:

$$\text{Log (N)} = a - bM$$

in which *a* is a measure of the level of seismic activity and *b* is the rate at which events occur within a given magnitude range. Estimated *b*-values (coefficient in the frequency-magnitude relation) for most seismic zones fall between 0.6 and 1.1. Mean return period (T) is usually defined as the expected time interval for occurrence of one earthquake with magnitude greater than or equal to *M:*

$$\text{T} = 1/\text{N}; \text{ hence, } \text{T} = 10^{-a+bM}$$

Frequency-magnitude relations calculated with different magnitude scales differ. They also differ when calculated in terms of M_s or moment magnitude (M_w). The reason for this is that because of scaling, M_s is not related linearly to log (M_o), and smaller events contribute proportionally more moment than large ones. The use of non-uniform and incomplete magnitude estimates may cause a potentially serious distortion in magnitude-frequency recurrence relationships that are important in assessing seismic hazard. The contribution to this distortion from the low-magnitude range should not be under-estimated, particularly for regions of apparent low seismicity where recurrence formulae are usually computed on the basis of low to intermediate magnitude earthquakes.

The selected teleseismic dataset was subjected to least-squares method for fitting an exponential magnitude-frequency (Gutenberg-Richter) law for establishing a Gutenberg-Richter recurrence relation for the project area. With the scarcity of reported events in certain magnitude ranges, we used the cumulative frequencies exceeding given magnitude levels in this study (see also Section V.7.2).

3.11. Earthquake Source Parameters from Long-Period P/Sh Body-Wave Inversions

The Seismograms used for long-period *P* and *SH* body-wave modeling are narrower in bandwidth than the broad-band records used by NEIC, but contain higher frequencies than those used in the routine Harvard Centroid Moment Tensor (CMT) determinations, and are sensitive to depth for shallow earthquakes. The method looks at the *P*, *pP*, and *sP* arrivals in the *P* waveforms and the *S* and *sS* arrivals in the *SH* waveforms (Nabelek, 1984; McCaffrey and Nabelek, 1987; Molnar and Lyon-Caen, 1989; Taymaz et al., 1991). Uncertainties of centroid depths (an averaged center of the rupture surface) obtained from long-period *P* and *SH* body-waveform modeling for earthquakes >M_w 5.4 is usually on the order of $\pm$4 km. Source parameters of the project earthquakes from *P* and *SH* body-wave modeling are set forth in Table 3.5 as well as the attached 'Macroseismic and Teleseismic Database (AD 855 through 2007) of the Greater Tehran Region (34.35°N to 37.10°N & 49.80°E to 53.10°E)'.

TABLE-3.5

SEISMIC SOURCE PARAMETERS FROM *P/SH* BODY-WAVE MODELING OF THE EARTHQUAKES OF THE GREATER TEHRAN REGION (34.35°N to 37.10°N & 49.80°E to 53.10°E)'].

Date (Region)	Time	*mb*	M_s	M_w	M_o (10^{18} Nm)	Nodal Plane-1 Strike-dip-rake	Nodal Plane-2 Strike-dip-rake	Z (km)	Ref.
1962.09.01 (Bo'in Zahra)	19:20	6.9	7.1	6.98	36.7	311-42-113	101-52-070	10	P&,1994
1980.12.19	01:16	5.5	5.8	6.2	1.4	115-41-120		14±8	P&, 1994
1980.12.22	12:51	5.4	5.2	5.7	0.28	113-56-125		15±5	P&, 1994
1990.01.20	01:27	5.5	5.8	5.9	1.02	075-80-015		13	J&, 2002
1990.06.21 (Rudbar af)	09:02	5.8 5.8 5.59	5.3	5.8 5.8 5.59	0.51 0.40	026-69-087 023-64-092 170-28-081	 001-62-095	17 08 10	B&, 1992 G&, 1995 J&, 2002
1991.11.28	17:19	5.6	5.0	5.66	0.38	185-44-101	350-47-080	08	J&, 2002
2004.05.28 (Baladeh)	12:38	6.2	6.4	6.3	3.1	110-34-76		22	T&, 2007

Notes:
af: Aftershock.
mb: Body-wave magnitude.

M_o: Seismic Moment (in units of 10^{18} Nm) from body-wave modeling.
M_w: Moment magnitude.
Ref: Reference of the earthquake source parameters from body-wave modeling on each line (B&, 1992: Berberian et al., 1992; J&, 2002: Gao et al., 1995; Jackson et al., 2002; P&, 1991: Priestley et al., 1991; P&, 1994: Priestley et al., 1991); T&, 2007: Tatar et al., 2007.
Z: Centroid depth (in km).

3.12. CMT Solutions

Centroid Moment Tensor (CMT) inversion of the Iranian earthquakes at teleseismic distances are automatically computed by Harvard, USGS/NEIC, and the Swiss Seismological Service, Zurich (Zur-RMT) for earthquakes of M_w >5.5 (Table IV.1). These solutions have been determined with long-period body and mantle waveform data using a moment tensor inversion method (Dziewonski et al., 1981; Dziewonski & Woodhouse 1983; Ekstrom, 1989). The waveforms used are usually low-pass filtered at 45s, and thereby lose sensitivity to depth for shallow crustal events. Hypocentral parameters are obtained by adding perturbations resulting from the inversion to parameters reported by the NEIC. If the depth is not perturbed during the inversion, it is fixed to be consistent with the waveform matching of reconstructed broadband body waves. Occasionally, a 'geophysicist' depth is applied, especially in continental regions where both the NEIC and CMT give dubious depths. In the absence of such detailed examination, default depths are 15 km (later became 12 km), and 33 km (10 km from 1981 to 1985). The CMT data set provides an extremely valuable resource of focal mechanism data, but centroid depths lack the resolution. Although automatic determination of moderate earthquakes is becoming more and more a routine process, the uncertainties concerning epicentral location, focal depth, and nodal planes make the results not very useful for seismotectonic investigations in association of earthquakes with known faults.

Source parameters of the project area earthquakes for the best double-couple Harvard and Zurich CMT solutions are set forth as Tables 3.6 and 3.7 as well as the attached 'Macroseismic and Teleseismic Database (AD 855 through 2007) of the Greater Tehran Region (34.35^{o}N to 37.10^{o}N & 49.80^{o}E to 53.10^{o}E)'.

TABLE-3.6

BEST DOUBLE-COUPLE HARVARD (HRVD) CMT SOLUTIONS OF THE EARTHQUAKES OF THE GREATER TEHRAN REGION (34.35°N to 37.10°N & 49.80°E to 53.10°E)'].

Date (region)	Time	*mb*	M_s	M_w	M_o (10^{18} Nm)	Nodal Plane-1 Strike;dip;rake	Nodal Plane-2 Strike;dip;rake	Z (km)
1980.12.19	01:16	5.4	5.8	6.2	2.1	135; 45; 157	242; 74; 47	15f
1980.12.22	12:51	4.4	5.2	5.7	0.46	241; 52; 42	122 ;59 ;133	15f
1983.03.25	11:57	5.1	4.9	5.4	0.17	280; 68; 005	188; 86; 157	33f
1983.03.26	04:07	5.4	4.9	5.3	0.12	104; 61; 017	005; 75; 149	10
1988.08.22	21:23	5.0	5.0	5.3	0.09	317; 75; -175	225; 85; -015	15f
1988.08.23	05:30	5.0	4.8	5.1	0.065	348; 31; -041	114; 69; -115	16f
1990.01.20	01:27	5.5	5.8	5.9	1.0	357; 66; 172	090; 82; 024	33f
1990.06.21	09:02	5.8	5.3	5.8	0.49	204; 26; 121	068; 351; 068	15f
1990.06.24	09:45	5.1	4.8	5.3	0.12	234; 69; 163	137; 74; -021	15f
1991.11.28	17:20	5.6	5.0	5.6	0.32	219; 36; 130	354; 63; 65	15f
1992.09.22	14:05	5.1	4.3	5.0	0.043	268; 44; 075	108; 47; 104	33f
1995.10.15	06:56	4.9	4.0	5.1	0.066	065; 49; 178	157; 88; 041	15f
2002.04.19	13:46	5.2	4.6	5.2	0.077	183; 26; 103	349; 64; 84	18
2004.05.28	12:38	6.2	6.3	6.3	3.6	119; 24; 72	319; 67; 98	22

Notes:
mb: Body-wave magnitude.
M_o: Seismic Moment (in units of 10^{18} Nm) from body-wave modeling.
M_s: Surface-wave magnitude.
M_w: Moment magnitude.
Z: Centroid depth (in km).

TABLE-3.7

BEST DOUBLE-COUPLE SWISS SEISMOLOGICAL SERVICE (ZUR-RMT) CMT SOLUTIONS OF THE EARTHQUAKES OF THE GREATER TEHRAN REGION (34.35°N to 37.10°N & 49.80°E to 53.10°E)'].

Date (region)	Time	*mb*	M_s	M_w	M_o (10^{18} Nm)	Nodal Plane-1 Strike;dip;rake	Nodal Plane-2 Strike;dip;rake	Z (km)
2002.04.08	18:30	4.8	4.1	5.1	0.048	296; 49; 78	134; 42; 104	15F
2002.04.19	13:46	5.2	4.6	5.2	0.075	1; 47; 94	176; 43; 86	19
2003.06.21	15:00	4.5	3.6	4.5	0.007	116; 80; 155	211; 66; 11	6
2003.12.24	03:49	4.6	3.8	4.9	0.0024	304; 46; 97	114; 45; 83	10
2004.05.28	12:38	6.2	6.3	6.5	5.2	320; 53; 102	120; 39; 74	14
2004.05.28	19:47	5.4	4.1	4.7	0.0011	318; 68; 124	76; 40; 35	10
2004.05.29	09:23	4.8	4.6	5.2	0.0067	311; 81; 88	185; 3; 145	14
2005.03.25	12:48	4.7	4.4	4.5	0.006	11-; 53; 107	264; 40; 69	

Notes:
af: Aftershock.
mb: Body-wave magnitude.
M_o: Seismic Moment (in units of 10^{18} Nm) from body-wave modeling.
M_s: Surface-wave magnitude.
M_w: Moment magnitude.
Z: Centroid depth (in km).

3.13. Locally-Recorded Microearthquakes

Microearthquakes are not usually related to individual active faults and are often representative of response of a brittle pre-fractured crust to regional stress field. Therefore, mechanism related to these earthquakes is not usually associated with the finite slip on major faults. Thus, the slip vectors associated with their focal mechanisms could be randomly distributed, but their *P* and *T* axes should be consistent. However, microearthquakes can refine the thickness of the local seismogenic layer.

3.13.1. Tehran Region (1976)

Within the project area, a short microearthquake survey comprised of a dozen of temporary network in late 1974 in the Tehran region (Brander et al., 1976) with complementing the two permanent regional networks, recorded 37 events in the southern Alborz. Since the timing accuracy was only about 0.25s, and the temporary station locations were not accurate, the locations as well as the composite focal mechanisms were not reliable, although the authors proposed seismic activity associated with the Mosha fault. Composite focal mechanism solutions for the Mosha fault indicated a left-lateral strike-slip faulting with slight reverse motion dipping steeply NNE (see Figure 7 in Hedayati et al., 1976); whereas their proposed 'Ray Lineation' focal mechanism solution shows two well-defined planes with normal mechanism (see Figure 9 in Hedayati et al., 1976). The cumulative number versus magnitude relation was also obtained from the 1974 study of 198 well-recorded events. The *b*-value of -0.79 (Long=4.374-0.787m_b) agreed well with the value of -0.86 (Long=5.135-0.856 m_b) determined from the 30 USCGS records of the 1961 to 1973 teleseismic data. The seismic intensity risk curve calculated for the area showed that the city of Tehran can expect ground movement of intensity VII every 12 years, and intensity IX every 350 years (Hedayati et al., 1976).

3.13.2. Rudbar Area (1998)

Microearthquake survey in the 1990 Rudbar-Tarom earthquake region of the northwestern Alborz (NW of the project area) during June-July 1998 utilizing 30 portable seismographic stations (Tatar, 2001) showed seismic activity in a zone of ~ 80 km X 20 km with earthquake concentrations at 4-16 km depths with thrust and left-lateral focal mechanisms.

3.13.3. Tehran Region (1999 & 2000)

Microearthquakes recorded by a temporary network of 19-21 portable seismological stations, installed for several weeks in 1999 and 2000 around the city of Tehran (Ashtari et al., 2005) indicated little seismic activity along the western segment of the Mosha fault (northwest of Tehran), whereas, the eastern segment of the Mosha fault, as well as the Garmsar fault showed active seismicity. The seismic activity is mainly concentrated up to 20 km depth with few activities extended up to 30 km depth. A northward deepening of seismicity associated with the Mosha and the Garmsar faults are shown by the relocated events using the double difference method (Ashtari et al., 2005).

3.13.4. Baladeh Earthquake Aftershocks (2004)

The well-recorded aftershocks of the 2004.05.28 (M_w 6.2) Baladeh earthquake in the central Alborz (2004.05.29-2004.07.19) were confined in space to a region about 40 km along strike and 20 km across strike (Tatar et al., 2007). The hypocenters were confined to depth range 10-35 km, and there was a complete lack of high-quality earthquake depths shallower than 10 km (possibly aseismic). Although the aftershock distribution were relatively dispersed and definitely not confined to a single plane, they showed a zone dipping SSW, possibly along the dip direction of the Khazar thrust, with thrust and strike-slip aftershock fault-plane solutions (Tatar et al., 2007).

3.14. Completeness and Reliability of Long-Term Data at the Project Area

No formal method can be devised to test the completeness of long-term teleseismic data other than by testing their implications. Formal statistical tests are as valid as the distributional assumptions on which they are based. Seismic activity is both regional and long-term dependent, which renders particularly problematic the assessment of hazard from short-term observations. The true, long-term nature of the frequency-magnitude distribution is hampered not only because the 20th century record is too short but also because test areas may be too small to disclose the repeat time of large earthquakes as the shape of the frequency-magnitude distribution from short-term observations cannot be defined at large magnitudes. The implication is that large earthquakes in a test area are less frequent, when predicted from the long-term dataset than from the usual 100-year instrumental period, making the notion of recurrence time, in its usual definition questionable, and the

characteristic model an artifact of incompleteness of data in space and time. Incomplete data and clustered seismicity is the principal reason why statistics from short-term data alone cannot quickly answer the question of data completeness for seismic hazard evaluation.

In general, the teleseismic data are incomplete for (i) small-magnitude earthquakes owing to the threshold of the recording sensitivity, and for (ii) large-magnitude earthquakes owing to their long-recurrence periods and the comparatively short period of coverage of the telesiesmic catalogues. Therefore, it is unlikely that all small- and some moderate-magnitude earthquakes in the early part of the twentieth century in Iran have been recorded. However, it is probable that most medium- to large-magnitude earthquakes have been recorded. It is, therefore, reasonable to assume that the available twentieth century Iranian seismic data is almost complete only for medium- to large-magnitude earthquakes [see the attached 'Macroseismic and Teleseismic Database (AD 855 through 2007) of the Greater Tehran Region (34.35^{o}N to 37.10^{o}N & 49.80^{o}E to 53.10^{o}E)'].

3.15. Concluding Remarks (Instrumental Seismic Database; 1900-2007)

For The early period of instrumental seismic data mislocation of instrumental epicenters is the norm, while for earthquakes before the 1940s macroseismic locations are more reliable but they must be used with caution. For the later period location accuracy is not better than 30 km, but improves to about 10-15 km for more recent earthquakes. However, bearing in mind that, earthquakes with magnitudes greater than M_s 6.6 will have ruptured faults 30 km to more than 100 km in length, the epicenter indicates nothing more than the general location of the event. Without knowledge of the causative fault, these epicenters with large magnitude of epicentral and hypocentral errors are of little use for design purposes.

The completeness and accuracy of the homogenized data imply a significant improvement compared with the various international databases. By crosschecking data from various catalogues and using data from specific studies, we eliminated the erroneous entries and selected the 'best' and/or 'preferable' available telesiesmic data with the larger number of recorded stations for inclusion in our homogenized database covering a longer time span. The advantage of the attached 'Macroseismic and Teleseismic Database (AD 855 through 2007) of the Greater Tehran Region

(34.35°N to 37.10°N & 49.80°E to 53.10°E)' over the various existing catalogues used in different studies and projects is significant, due to:

- Inclusion of macroseismic data of the well field-studied events,
- Improved epicentral, focal depth, and centroid depth data,
- Harmonized magnitudes (M_s, M_w, & *mb*),
- Better coverage in time,
- Inclusion of accurate intensity of the events,
- Assignment of the causative faults of the events,
- Inclusion of reported national teleseismic data (regularly since 2000),
- Highlighting the dependent events (foreshocks & aftershocks) for the process of declustering when needed,
- Inclusion of radius of meizoseismal (epicentral) & radius of perceptibility,
- Inclusion of coseismic rupture areas, aftershock depth zones, & seismic moment (when available), and
- Quality ranking of the events (wherever possible).

Nonetheless, the earthquake catalogue of the project area only includes about 200 earthquakes since 1900, of which (i) only three events with magnitude greater than *M* 6.0 (or on average about one *M*>6.0/36yr), and (ii) nine events with magnitude between 5.5 and 6.0 (or on average about one 6.0<*M*>5.5/12yr) were recorded in the project area. This clearly shows the limitations and difficulties in comparing the rates of medium- to large-magnitude earthquakes in an active region with numerous major active faults with long recurrence periods for large-magnitude earthquakes, with a short-term catalogue which has such a small size and coverage.

The study also indicated that the Garmsar, Pishva, Mosha, Baijan, Firuzkuh, Ipak, Qom, Rudbar, Kushk-e-Nosrat, Alamutrud, Taleqan, Siahkuh, Sarajeh, and Khazar faults were reactivated during the instrumental period.

In section 6.1.1 detailed discussion regarding the data completeness process is presented to develop the seismicity rates for the background and faults sources.

4. REGIONAL SEISMOTECTONIC MODEL

Forecasting future fault activity depends on developing and using information on the past behavior of the faults. Earthquake geology, especially seismotectonics, plays a fundamental role (i) to assess the past history of earthquakes in regions of active tectonics, and (ii) in estimating the location, size, amount of displacement, and expected recurrence time of future earthquake, and, hence, seismic hazard analyses. This active approach is much better than relying solely on generally short and incomplete historical and teleseismic records of the earthquakes. For example, whereas geologic and geomorphologic study shows the North Tehran thrust (Berberian et al., 1985) and the North Qazvin thrust (Berberian et al., 1983) to be clearly active [see the attached 'Fault Map of the Greater Tehran Region (34.35^{o}N to 37.10^{o}N & 49.80^{o}E to 53.10^{o}E)'], the faults are virtually devoid of seismic activity at least since 1900 [see the attached 'Macroseismic and Teleseismic Database (AD 855 through 2007) of the Greater Tehran region (34.35^{o}N to 37.10^{o}N & 49.80^{o}E to 53.10^{o}E)'], even down to microearthquake level (Ashtari et al., 2005). Similar observations along the San Andreas Fault (Allen et al., 1965) provided the impetus to incorporate geological observations of fault slip rate and recurrence time into seismic hazard analysis.

The obvious link between the geologic/seismologic database and any calculated model for deriving hazard levels is a regional seismotectonic model, which should be on a coherent merging of the regional databases. In this study all the seismotectonic data have been taken into account and a sound geologic database has been created for construction of a reliable seismotectonic model. The standard procedure is to integrate the elements of the seismological and geophysical database in order to construct a coherent seismotectonic model consisting of a discrete set of seismogenic structures. The identified seismogenic structures may not explain all the observed earthquake activity. This is because (i) seismogenic structures may exist without 'easily recognized' surface or subsurface manifestations (such as blind faults), (ii) diffuse seismicity not attributable to specific

identifiable structures using the available database, and (iii) because of the time scales involved (long recurrence intervals of earthquakes with respect to the short period seismological data set).
In this chapter we first review few major topics and then address the newly created geologic database for the project area.

4.1. Seismogenic Sources

The need to identify seismogenic structures and their slip rates is ultimately due to their significance for determining the strong ground motion and the earthquake surface-faulting hazard. The identification of seismogenic structures is made on the basis of geological, geophysical, and seismological data providing direct or indirect evidence that these structures have been the source of earthquakes under current tectonic conditions. The correlation of historical and instrumental recordings of earthquakes with geological and geophysical features is particularly important in identifying seismogenic structures. A lack of correlation does not necessarily indicate that a structure is not seismogenic.

The seismic sources can be divided into two categories: *'fault sources'* and *'area sources'*.

4.1.1. Fault Source

Displacement along a fault releases energy in the form of earthquake (sudden release of elastic energy) and in lesser extent in some cases in aseismic creep form. The amount of energy available to a fault is determined by considering the slip-rate of the fault, fault area (fault length X down-dip width), maximum magnitude, and rigidity of the displaced media. These factors are combined to calculate the seismic moment release on a given fault. The total seismic energy release for a fault source is sometimes partitioned between two different recurrence models, the 'characteristic' and 'truncated Gutenberg-Richter' magnitude-frequency distributions. These models incorporate our knowledge of the range of magnitudes and relative frequency of different magnitudes for a particular fault.

The fault sources can either be visible at the surface where their behavior can be quantified (surface faults), or be considered 'blind' with low-angle dip that do not cut the ground surface ('blind thrust'). It is difficult for the latter case to assess directly segmentation, magnitude distribution,

recurrence intervals, characteristic displacement, and slip rate. However, blind faults do have surface expression in the form of overlying folds that are known to grow during large-magnitude earthquakes (Stein and Yeats, 1989). Quantitative approaches have been developed that to relate fold shape and growth rate to fault geometry and slip rate (Suppe, 1983; Suppe et al., 1992). Kinematic and geometric modeling of active axial surfaces in fault-bend folds, based on shallow seismic reflection profiles and borehole stratigraphic data, allow the location, geometry, and cumulative slip of underlying blind thrust faults to be inferred (Davies et al., 1989; Shaw, 1993; Shaw and Suppe, 1994a, b).

Blind thrust faults have demonstrated their importance in regional hazard. The 1987.10.01 M_s 5.7 Whittier Narrows, and the 1994.01.17 M_w 6.7 Northridge [BSSA, 1996, 86(1)] earthquakes in California, as well as the Sefidabeh earthquakes of 1994.02.23 (M_w6.1), 1994.02.24 (M_w 6.2) and 1994.02.28 (M_w 5.5) in southeast Iran (Berberian et al., 2000) occurred on blind thrust faults that did not rupture to the surface. There is considerable uncertainty about their extent, geometry at depth, and the nature of the postulated regional detachment into which they might root. At present, there is no direct data on recurrence intervals or characteristic displacements for individual blind thrust segments.

4.1.2.Area Source

If earthquake locations cannot be clearly assigned to a particular fault, an *'area source'* or a *'grided seismicity approach'* is recommended. Earthquake recurrence in the area source is based on models that consider the historic occurrence of earthquakes in the area and calculate magnitude-frequency distribution for each area source. A Gaussian smoothing process is applied to the historical background seismicity to distribute the earthquake potential through a grid of points that covers the area source (Cao et al. (1996; Peterson et al., 2000). The source area can be considered as the *'background seismicity'* in the modeling.

4.2.Characteristic Magnitude (M_{char}) and Maximum Magnitude (M_{max}) of Earthquakes

Characteristic magnitude is the magnitude assigned to a fault from observed magnitude-length relations. Maximum magnitude is the highest magnitude that a fault or fault segment is likely to suffer, and plays an important role in earthquake hazard estimates (Jackson et al., 1995; Ward,

1997). This is because that seismic hazard estimates depend on the upper magnitude limit adopted for each seismotectonic source zone. The common practice method has been relating earthquake size to the length of an independent fault segment, but the Landers earthquake of 1992.06.28 M_w 7.3 [BSSA, 1994, 84(3)] in California, together with the 1981.07.28 M_w 7.0 Sirch (Berberian et al., 1984, 2001), the 1990.06.20 M_w 7.3 Rudbar (Berberian et al., 1992), and the 1997.05.10 M_w 7.1 Zirkuh Qa'enat (Berberian et al., 1999) earthquakes in Iran, demonstrated that several fault segments can break in a single earthquake rupture. Therefore, it is vital to understand better the relationship between fault geometry and earthquake size, and more generally what limits the size of large earthquakes.

Computer modeling of rupture on faults of various strengths and configurations (Ward, 1997) recommended M_{max}, the maximum likely earthquake on a fault, be set about 0.2 to 0.3 units higher than M_{char}, to account for limitations in historical seismic catalogue, potential multi-fault segment failure, and slip amplifications that may occur in multi-fault ruptures.

4.3. Regression of Rupture Length and Magnitude (M_s & M_w)

A considerable number of relationships between magnitude, rupture length, surface displacements and mechanism, using a variety of data sets, have been derived for different parts of the world (see for example, Wells and Coppersmith, 1994). Anderson et al. (1996) introduced a regression for moment magnitude (M_w) as a function of surface rupture length (L) and fault slip-rate (S) which reduces the uncertainty in estimating the potential size of future earthquakes on mapped faults as compared to the standard regressions of M_w on L that are commonly used in seismic hazard analysis. The least-squares regression for a data set of 43 earthquakes occurring on worldwide faults for which slip rates are reported showed:

$$M_w = 5.12 + 1.16 \log L - 0.20 \log S,$$

where, M_w is earthquake moment magnitude, L is fault length in km, and S is fault slip- rate in mm/yr. The results of the regression indicated that faults with slower slip-rates tend to fail in earthquakes with higher static stress drop (Anderson et al., 1996).

Ambraseys and Jackson (1998) by using 62 eastern Mediterranean twentieth century earthquakes with well-determined surface-wave magnitudes (M_s) from instrumental data and reasonably reliable rupture lengths from field observations obtained a predictive relationship between magnitude and fault length expressed by:

M_s= 5.27+1.04 log (L) and

Log (L) = 0.9615M_s - 5.067,

where L is in km.

The equation is almost identical to that derived by Wells and Coppersmith (1994) from a global data set, out of which 127 are associated with surface ruptures, and 117 with calculated surface ruptures; as follows:

M_w=5.08+1.16 log (L) for all data regardless of mechanism;

M_w=5.00+1.22 log (L) for reverse slip events; and

M_w=5.16+1.12 log (L) for strike-slip faulting.

In this report maximum moment magnitude (M_{wmax}) was calculated from rupture length-M_w regression derived by Wells and Coppersmith (1994) [see the attached 'Fault Map of the Greater Tehran Region (34.35^{o}N to 37.10^{o}N & 49.80^{o}E to 53.10^{o}E)'].

4.4. Regression Of Fault Displacement And Magnitude

Based on 58 eastern Mediterranean earthquake cases with horizontal and vertical maximum surface displacements, Ambraseys and Jackson (1998) presented the following relation between surface-wave magnitude and resultant displacement:

M_s= 5.21 + 0.78 log(R),

where R is resultant displacement in cm regardless of mechanism. The authors found that the resultant displacement R is about 5.0 ($\pm$4.0) X $10^{-5}L$, regardless of mechanism, and a number close to compilations by Scholz (1982) and Scholz et al., (1986). However, the size of the sample is insufficient and the scatter too large to allow a better estimates.

In this study we calculated the average characteristic displacement using equation derived by Wells and Coppersmith (1994) [see the attached 'Fault Map of the Greater Tehran Region (34.35^{o}N to 37.10^{o}N & 49.80^{o}E to 53.10^{o}E)'].

4.5. Slip Rates

Reid (1910) demonstrated that earthquake is the result of a sudden release of slowly accumulating elastic stress. In this regard, geological estimates of fault slip rate are a direct measure of that long-term rate of strain accumulation along active faults. By dividing the measures of coseismic offset expected along faults by estimates of fault slip rate along the respective fault, one is able to begin estimating the long-term recurrence rate of major earthquakes along active faults. Slip rates can be estimated from (i) geological observation, (ii) geodetic data, and (iii) empirical equations [such as $U^g = M^g_o/\mu LW$; where U^g is the slip rate, M^g_o is the seismic moment rate, μ is the rigidity modulus (3 X 10^{11} dyne/cm^2), and L and W are the fault length and width; Stirling and Wesnousky, 1997).

As mentioned, slip-rates reflect the rate of strain energy release on a fault, which can be expressed as seismic moment. Hence, they can be used to estimate earthquake recurrence on individual faults in probabilistic seismic hazard analysis. Slip-rate measurements along active faults could vary from long- to short-terms.

1- The *'long-term slip-rate'* of the superficial faults, which is a method of roughly estimating potential displacement on a fault, is determined geologically based on total displacement of geological units divided by the age of the unit [mostly through palaeoseismological trench investigation (~10,000 yrs); balanced section modeling (very long slip-rates ~10^6yr), etc.]. The potential slip is equal to long-term rate multiplied by the elapsed time since the last displacement minus any tectonic creep in the interval [for example the long-term slip rate of the northern San

Andreas fault is about 3 cm/yr (Herd 1979). It had no surface displacement between 1981 and 1906, at which time the potential slip was about 3 X 75 = 225 cm].

2- The *'short-term slip-rate*' of the superficial fault is determined geodetically [global positioning system -GPS- satellite data; ~10 yrs] or seismologically [using the seismic moment of the earthquakes that have occurred during historic (~2,000 yrs) or instrumental periods (M_o= shear modulus X average fault slip X area of the fault that has slipped)]. It should be noted that the latter is strongly influenced by the level of seismicity during the short period of study and does not definitely reflect the long-term slip-rate. The GPS network is not designed to derive individual fault slip-rates, and the GPS rate may represent a longer-term deformation of the crust. Except for the creeping segments of the faults, faults that rupture during large-magnitude earthquakes remain locked by friction between earthquakes; even though the crustal blocks separated by the faults continue to be deformed by tectonic force. A consequence is that much of the differential strain occurs near the faults bounding the blocks. Therefore, geodetic measurements can reveal regions where locked faults are accumulating strain, even though those faults may not be exposed at the surface. Geodetic and seismic data are potentially very important in assessing regional seismic hazard. A wider geodetic coverage at increased resolution, as well as a better understanding of the relationship between geodetic strain, active faults, and historic seismicity, will help a better assessment of seismic hazard.

Recent slip-rates along most of the Iranian faults are unknown, and independent observations of finite offsets and onset of motion along the active Iranian faults are lacking. Summary of slip-rate estimates along some of the Iranian faults are set forth in the attached 'Fault Map of the Greater Tehran Region (34.35^{o}N to 37.10^{o}N & 49.80^{o}E to 53.10^{o}E)'. Some of the estimates are uncertain because both the ages and the offsets are questionable.

For this project the Gegology Survey of Iran (GSI) use the recent GPS data to develop the fault rates. Dr. Talebian and Dr. Ghorishi lead this study and the GPS data used to develop the seismic rates for the faults. The result of their study will be published in the GIS publication.

4.6. Fault Parameters of the Project Area

Although the identification and mapping of active faults in Iran have a long history (e.g. Berberian, 1976, 1977, 1981) data on the Iranian faults are very poor, and hence, the regional seismotectonics

are poorly understood. Furthermore, in the face of poor epicentral locations and lack of slip measurements in the field, it is very difficult to accurately associate earthquakes with the known surface faults.

4.6.1. Fault Mapping Accuracy

Structural complexities, accurate age of the surface Quaternary deposits, geomorphic expression, mapping experience, and scale of the maps are some of the factors influencing the mapping accuracy. We, therefore, assign the following mapping accuracy category for the faults in the project area (Table 4.1). Mapped faults with rating class "A" are not known in Iran and majority of the intermediate-scale maps which should automatically be categorized in rating class "B" have their peculiar setbacks, which disqualifies them belonging to this rating class. Hence, majority of the faults can be rated as class "C" (see the following discussion).

TABLE-4.1

RATING CRITERIA FOR THE MAPPED FAULTS OF THE GREATER TEHRAN REGION (34.35^{o}N to 37.10^{o}N & 49.80^{o}E to 53.10^{o}E)'].

Q: RATING CLASS	DESCRIPTION
A	Accurately-located with fine details and great accuracy on a large-scale map (1:25,000 & larger).
B	Well-located on an intermediate-scale map (1:50,000 & 1:100,000).
C	Approximately located showing only generalized detail on a small-scale map (1:250,000 and smaller).
D	Inferred.

Unfortunately, the available Iranian geological maps prepared by the Geological Survey of Iran (GSI) on scale of 1:250,000 and recently on scale of 1:100,000 do not include any topographic contour lines. Almost all the Quaternary alluvial deposits have not yet been dated, and mechanism of majority of the faults is not clear on these maps. Therefore, it is impossible to calculate or even estimate or guess the fault dip and in most cases the dip-direction. The fault map accuracy is unknown because of lack of contour lines, and it is impossible to guess the recency of the fault movement due to lack of any dating. Another set back with these maps are errors in the exact coordinates, especially with the 1:250,000 series maps. We, therefore, should assume inherent errors in the exact fault locations and their length shown on both sets of the maps (1:250,000 & 1:100,000). The uncertainty in the location of the fault is estimated to be at least 1 to 2 kilometers.

Majority of the faults on the existing geological maps are shown with vertical dips, and if dip-directions are added to the faults on some maps and cross-sections, they are almost speculative and unrealistic in the cross sections [see for example the cross sections on the 1:100,000 scale Geological Map of Harsin (Shahidi and Nazari, 1996)]. The North Alborz reverse fault on a single 1:100,000 scale geological map of Pol-e-Sefid dips towards south on the western half of the map (Vahdati, 2005) and along the longitude 53.15N the dip of the fault abruptly changes to the north (Ajari, Qarib, and Sa'idi, 2005; Alavi, 1996). The Khazar thrust dipping south (Berberian, 1981, 1983) is mapped dipping northeast with normal mechanism on two cross-sections on the Geological Map of Ramsar on 1:100,000 scale (Baharfirouzi et al., n.d; ca. 2004-2006).

In some cases the important earthquake fault has not been mapped [see the 1:100,000 scale Geological Map of Rudbar (Nazari and Salamati, 1998), where the 1990.06.20 (M_w 7.3) Rudbar earthquake surface rupture of 80 km long has been totally ignored and not mapped few years after the event]. Group of maps are densely crisscrossed by secondary transverse faults with centimeter/millimeter intervals cutting and interacting with the major longitudinal faults [see the 1:100,000 Geological Map of Sari (Khabbaz-nia and Sadeghi, 2003); and the 1:100,000 Geological Map of Surian (Oveisi, n.d.)]. The issue of drawing numerous imaginary crisscrossing faults is a major problem on all existing geological maps of Iran.

The Astaneh left-lateral strike-slip active fault (Berberian et al., 1995, 2002) is mapped as a right-lateral fault (Alavi, 1996). Numerous N-S and NNW-SSE trending faults shown in the Tehran basin, mainly along the riverbeds (Amini and Emami, 1992; Feghhi, 1999; Abbassi and Shabanian, 1999, 2006; Abbassi, 2004), are speculative and have no morphotectonic and/or seismotectonic supporting data. Feghhi's (1999) assertion regarding active normal faults in the Tehran basin cannot be backed so far by the existing data.

Purkermani and Soleymani (1998) and Soleymani and Zare (1999) introduced two 'seismic faults' in the Tehran-Karaj basin; the 'Mahdasht-Karaj' and the 'Soltanabad' faults. These newly introduced 'seismic faults' have no surface manifestations and cannot be supported by scientific data. Their Mahdasht-Karaj fault, with a trend of N85^{o}E and an alleged length of >80 km, should truncate the eastern segments of the active Ipak and the Eshtehard faults, for which there is no evidence. Soleymani and Zare's (1999) Soltanabad seismic fault is apparently located at a depth of

about 250 km below ground surface and has a length of >50 km. Purkermani and Soleymani (1998) and Soleymani and Zare (1999) speculated that the Soltanabad fault was the seismic source of the 1177 earthquake of M_s 7.2. Surprisingly, the newly introduced fault trend has to truncate the Dotuyeh anticline as well as the western segment of the Kahrizak thrust, for which there is no morphotectonic or seismotectonic evidence.

We put forth these comments to show the limitations of the existing fault data on the available 1:100,000 scale maps and individual reports as our input data source, and in hope of (i) stimulating further and possibly better work to resolve these fundamental shortcomings, and (ii) establishing a QA/QC process for the geological maps of Iran by the Geological Survey prior to approval and publication of their intermediate-scale maps.

4.6.2. Primary Fault Displacement

No data in this category is available from the existing geological maps of the project area. Available fault displacement information from individual reports are set fort in the attached 'Fault Map of the Greater Tehran Region (34.35^{o}N to 37.10^{o}N & 49.80^{o}E to 53.10^{o}E)'.

4.6.3. Probability of Distributed Ruptures/Secondary Faulting And Displacements Near the Fault Zone

Numerous lesser or secondary faults that are individually not as hazardous, but pose a significant aggregated danger, are present along the major fault zones (Berberian et al., 1983, 1985) but they are not mapped in detail on the available geological maps on scales of 1:100,000 and 1:250,000 (Geol. Surv. Iran).

4.6.4. Blind Faults that Do Not Break the Surface

No study on the blind faults is conducted in the project area. Available data on a few cases are set forth in the attached 'Fault Map of the Greater Tehran Region (34.35^{o}N to 37.10^{o}N & 49.80^{o}E to 53.10^{o}E)'.

4.6.5. Depth of the Seismogenic Zone

When possible, the depth of the seismogenic rupture zone was obtained from (i) long-period body-wave modeling of the early part of the *P* and *SH* waveforms [see IV.8 and Table IV.3], (ii) aftershock and/or microearthquake sequence recorded by local reliable portable seismographic network [see Section IV.10], and (iii) hypocentral locations of well located, relocated, reassessed earthquakes surrounding the major faults [see the attached (i) 'Macroseismic and Teleseismic Database (AD 855 through 2007) of the Greater Tehran Region (34.35^{o}N to 37.10^{o}N & 49.80^{o}E to 53.10^{o}E)', and (ii) the 'Fault Map of the Greater Tehran Region (34.35^{o}N to 37.10^{o}N & 49.80^{o}E to 53.10^{o}E)']. Excluding the case of the Khazar thrust case, it seems that 15 km seismogenic zone is a reliable estimate for the project area.

4.6.6. Simultaneous Ruptures of Contiguous Segments ('Cascade')

Like the Sirch/Golbaf earthquake of 1981.07.28 M_w 7.0 (Berberian et al., 1984, 2001), the Rudbar earthquake of 1990.06.20 M_w 7.3 (Berberian et al., 1992), the Zirkuh Qa'enat earthquake of 1997.05.10 M_w 7.1 (Berberian et al., 1999), the 1857.01.09 M 7.9 Fort Tejon (Sieh, 1978) earthquake on the San Andreas fault, and the Landers earthquake of 1992.06.28 M_w 7.3 [BSSA, 1994, 84(3)] in CA., many past earthquakes have ruptured more than one segment in a single event. To explain the long-term slip rate, it makes no difference whether these events are treated as cascades or as separate earthquakes on individual segments. However, for seismic hazard estimates there is a difference. If individual segments always rupture independently, then there will be more earthquakes per unit time. Thus, the frequency with which one segment triggers another becomes important. Due to lack of basic data, no valid segment boundary could be utilized in this study.

4.7. Sesimogenic Sources in the Project Area

Several major fault systems accommodate slip and significantly contribute to the earthquake hazard in the Iranian plateau. Most earthquakes in the Iranian continental lithosphere occur in the upper crust (~15 km); with the crustal shortening produced by the Arabian-Eurasian continental collision accommodated entirely by thickening, uplifting, and distributed deformation. We conducted a comprehensive survey of the available geological maps of the project area, as well as the published and unpublished reports on the subject throughout literature searches.

Along the Alborz and the Central Iran seismotectonic provinces (Sections II.2 & II.3) seismicity occur primarily in the upper crust, but some infrequent events occur in the mid-crust of the Alborz, where the South Caspian basin underthrusts the Alborz along the Khazar fault [see the attached 'Fault Map of the Greater Tehran region (34.35^{o}N to 37.10^{o}N & 49.80^{o}E to 53.10^{o}E)'].

The seismic sources that could pose risk to the Tehran region in the project area [see the attached 'Fault Map of the Greater Tehran region (34.35^{o}N to 37.10^{o}N & 49.80^{o}E to 53.10^{o}E)'] can be, therefore, put into two categories:

(i) Shallow earthquakes associated with surface and/or blind faults (reverse and strike-slip) in the north Central Iran and the southern Albortz (Berberian et al., 1983, 1985, 2002; Berberian 2005), and

(ii) Slightly deeper earthquakes associated with the deeper extend of the Khazar thrust allowing slip further to the south (Tatar et al., 2007).

The latter case may increase the vulnerability of the high-rise building in the mega-city of Tehran to the long-period ground shaking, which is less attenuated than short period.

Many faults with Late Quaternary offsets are distributed in the Tehran region with presence of some blind thrusts detected from the hydrogeological and geomorphologic investigations discussed earlier in Section II.4 [see also the attached 'Fault Map of the Greater Tehran region (34.35^{o}N to 37.10^{o}N & 49.80^{o}E to 53.10^{o}E)'].

The existing seismotectonic source databases for the Iranian earthquakes are set forth as Table 4.2.

Table – 4.2

SUMMARY OF THE EXISTING SEISMOGEINC DATABASE SOURCES FOR THE IRANIAN EARTHQUAKES

Catalogue	Time Range	Magnitude	Intensity	Remarks
Berberian (1979)				Khorasan & Kopeh Dagh
Berberian (1981)				
Berberian et al. (1983)			X	Qaazvin Quadrangle
Berberian et al. (1985)			X	Tehran Quadrangle
Berberian et al. (1996)			X	Semnan Quadrangle
Berberian (1995a)	Prehistoric through 1900			
Berberian (1995b)	Historic & modern		X	Zagros
Berberian (1997)	2,000 B.C.-1992	M_s	X	NW Iran, Armenian, & Caucasus

Ambraseys & Jackson (1998)	280 B.C.-AD 1994	M_s	X	24 collective events in Central & NW Iran
Berberian & Yeats (1999)	743-1997	M_s	X	Selective major sources
Berberian & Yeats (2001)	2,000 B.C.-AD 1997	M_s	X	Selective major sources

4.7.1. Uncertainties of Seismogenic Sources (Quality Criteria)

Inaccurate association of earthquake locations to specific faults causes false risk assessment and hazardous seismic hazard maps. Safa'i (1995) claimed that the Kalarz fault of 30 km long, which is located approximately 13 km north of the Garmsar thrust (Berberian et al., 1995), was the seismic source of the Garmsar earthquakes of 1988.08.23 (M_s 5.0), 1982.10.25 (m_b 4.6), 1945.05.11 (M 4.7), and AD 743 (M_s 7.2). Safa'i's (1995) assertion cannot be backed by scientific data and it is not clear how a fault of 30 km long has the capability of creating an M_s 7.2 earthquake in 743. It should be reiterated that due to lack of macroseismic data, it is not clear that the event took place in the area to the southeast of Tehran (Iran) or in Derbent (Dagestan).

In a bizarre analysis, Ashoori (1994, 2002) claimed that the salt dome tectonics was also responsible for the AD 743 Caspian Gates earthquake; the meizoseismal area of which is still not known (SE of Tehran in Iran or Derbent in Dagestan in SW Russia?). Ashoori (1994, 2002) further declares "the Sorkheh Kalut, the Rameh, and the Ghalibaf faults were the sources of the 1955 August (M_s 4.7) and probably the 1964.11.24 (M_s 4.1) earthquakes". Ashoori (1994, 2002) also asserted that the "Garmsar and the Ejdeha Mt. faults, together with salt dome tectonites and the masses of salt at the NW of Garmsar were responsible for the occurrence of the 1953.09.22 (M_s 4.0) earthquake". Ashoori (1994, 2002) furthermore stated that the "Rud-e-Shur and the Ejdeha Mt. faults were both responsible for the occurrence of the 1988.08.22 (m_b 4.5) earthquake; and the earthquake swarm of the September-October 1988 were associated with activation of the five active faults of the Kuh-e-Gugerd, Gachab, Garmsar, Rud-e-Shur, and Ejdeha. Finally Ashoori (1994, 2002) claimed that the Gachab and the Kuh-e-Gugerd faults were reactivated during the 1973.06.30 M_L 3.7 earthquake; and that the Sorkhesar fault was the source of the 1954.09.02 (M_s 4.8, m_b 4.5) earthquake. These strange assertions

Nazari (2004) showed the damaged areas of the AD 743 and the 1895 earthquakes along the 'Rey' fault [the 1895 event to its western end and the 743 event to its eastern end with a distance of 4 km

in between the macroseismic epicenters of the two earthquakes]. His 'Rey' fault coincides with the 'South Ray' fault of Berberian et al., (1985), and there is no scientific data for his assertion regarding the meizoseismal areas of the mentioned earthquakes along the fault.

As mentioned in Section 4.6.1, we address some of the existing problems with the published data and emphasized the importance of the data retrieval, analyses, and QA/QC processes prior to establishment of a proper database for the seismic hazard evaluation of the project area. Wherever possible, the following rating criteria have been assigned for the seismogenic sources.

TABLE-4.3

RATING CRITERIA FOR THE SEISMOGENIC SOURCES FROM GEOLOGIC/GEOPHYSICAL DATA OF THE GREATER TEHRAN REGION (34.35°N to 37.10°N & 49.80°E to 53.10°E)'].

Q: RATING CLASS	DESCRIPTION
A (Good)	• Well-constrained sources with combined instrumental, historical, and geologic/geomorphic evidence. • Surface faulting explicitly deduced from field investigation • The source parameters of Class "A" sources are constrained by seismological or geodetic evidence that allows a finer resolution than that granted by surface geology data alone. • Source azimuth uncertainty: <10°
B (Moderate)	• Sources with satisfactory instrumental/historical/palaeoseismological and geologic/geomorphic evidence. • Class "B" typically includes the sources of earthquakes that occurred in the pre-instrumental era. • The source parameterization is jointly constrained by the extent of the historical rupture and by the occurrence of significant geologic features such as the size and extend of a basin, the intersection with known tectonic lineaments, the rupture terminations of Class "A" sources, etc. • Source azimuth uncertainty: 10°-24°.
C (Poor)	• Sources with limited or no historical evidence, or possess satisfactory historical but limited/debatable geologic/geomorphic evidence. In need of authentication. • The source must be on-land and associated with clearly identified large-scale features belonging to known regional trends. • This class and the following Class "D" also include sources for which there is epistemic uncertainty as to their existence as active features and to their potential as seismogenic sources. • Source azimuth uncertainty: 25°-49°.
D (Very poor)	• Sources with limited or no historical constraints. • Unlike the previous class, the source may be offshore and its location constrained only by reflection seismology data or other large-scale observations used to pinpoint regional trends of homogeneous tectonic deformation. • Source azimuth uncertainty: >50°.
E (Unknown Association)	• Source azimuth unknown. • Exact locations of fault break not known.

It is clear that there are few data in the project area, which can be categorized under rating classes of "A" and /or "B".

4.7.2. Geologic Scenarios; Gutenberg-Richter (G-R) and Characteristic Distributions

The fault energy budget is usually demonstrated by: slip-rate, fault area, M_{max}, and the crustal rigidity. These factors are combined to calculate the seismic moment/energy release on a fault (M_o). The total seismic energy release for fault sources are usually estimated based on (i) the 'characteristic' and/or (ii) the 'truncated G-R' magnitude-frequency distribution models (the characteristics of a fault or of a region affect both '*a'* and '*b'* coefficients in the latter). Regional earthquake statistics are known to satisfy the Gutenberg-Richter distribution, but the question whether seismicity of individual faults satisfies the relation remains a source of discussion (Wesnousky et al., 1983; Wesnousky, 1994). This is because that the time period of the historic earthquake catalogue is generally less than the expected return period of the large-magnitude earthquakes on the faults, and in the case of the Iranian earthquakes, the pre-1964 events are inhomogeneous and have large magnitude of location errors.

In the general absence of fault-specific seismicity data, it has commonly been assumed that the exponential recurrence model of G-R is an appropriate to individual faults as it is to regions. However, the fault study has shown that the exponential recurrence model is not appropriate for expressing earthquake recurrence on individual faults. The evaluation of geologic recurrence rests on the ability to recognize past events, date the interval between events (recurrence interval), and evaluate the size of each event. By combining the recurrence intervals for large-magnitude earthquakes developed from geologic data with the recurrence for limited period of recorded smaller-magnitude events developed from seismicity data, a characteristic earthquake recurrence is derived with a nonlinear *b*-value; the lower *b*-value reflects a recurrence curve anchored at the large-magnitude events and having relatively fewer moderate-magnitude earthquakes than would be expected for the higher *b*-values of the teleseismic data (Schwartz and Coppersmith, 1984, 1986).

It has been shown that the earthquake frequency distribution particularly to a single fault does not satisfy the Gutenberg-Richter relation. The relation is only satisfied when (i) seismicity from multiple sources is considered, or (ii) the seismicity associated with an individual fault that satisfies the Gutenberg-Richter relation is not evenly distributed in time throughout the seismic cycle of the

fault. Thus, the observation that broad region of seismicity satisfy the Gutenberg-Richter relation appears to be a consequence of combining the seismicity from multiple faults that are in various temporal positions within respective seismic cycle. In general it is known that seismic slip on faults takes place cyclically during earthquakes of characteristic size. The size and repeat time of the characteristic event are a function of the fault length and slip rate, respectively. A consequence is that the primary factor responsible for the earthquake frequency distribution in regional seismicity studies is the relative distribution of fault lengths and slip-rates (Wesnousky et al., 1983; Wesnousky, 1994, 2000).

To construct geologically realistic earthquake scenario based on available data, we used the location, extent, and dip of seismogenic faults, together with the depth of the base of the seismogenic zone as determined from the base of deepest seismicity, to determine fault plane area. We then used the regression equations to determine the moment magnitude and average displacement of postulated earthquakes on each fault [see the attached 'Fault Map of the Greater Tehran region (34.35^{o}N to 37.10^{o}N & 49.80^{o}E to 53.10^{o}E]. The recurrence interval for a particular earthquake is then the average slip estimate for each fault or fault segment divided by the geologically determined slip rate of the fault.

In this study, we have only been able to construct Gutenberg-Richter exponential recurrence model for only four individual faults located in the Alborz (Mosha, Firuzkuh, Khazar, & Rudbar), and two individual faults located in the Central Iran (Ipak & Garmsar) seismotectonic provinces. This is due to the short-term seismic history which cannot reflect the long-term seismicity along the faults with large recurrence periods [see the attached 'G-R Recurrence Models For Individual Faults and Seismotectonic Provinces of the Greater Tehran region (34.35^{o}N to 37.10^{o}N & 49.80^{o}E to 53.10^{o}E)'].

TABLE-4.4
VALUES OF CONSTANT PARAMETERS (*a* & *b*) FOR THE FAULTS OF THE GREATER TEHRAN REGION (34.35^{o}N to 37.10^{o}N & 49.80^{o}E to 53.10^{o}E)']

FAULT (Province)	*A*	*b*	R^2	M_{max} (M_w)
Firuzkuh (Al.)	2.7676	0.469	0.9798	6.9
Garmsar (CI.)	3.8274	0.6876	0.6933	7.5
Ipak (CI.)	2.7231	0.399	0.9531	7.3
Khazar (Al.)	3.3018	0.4976	0.9633	7.6
Mosha (Al.)	1.4923	0.1983	0.95	7.6
Rudbar (Al.)	3.2779	0.4611*	0.8141	7.6

Notes:

Al: Alborz.
CI: Central Iran.
*: Niazi and Bozorgnia (1992) calculated a much larger *b*-value of 0.97 for the mainshock-aftershocks sequence of the 1990 event in the 36°-28°N and 48°-51°E quadrangle, using *mb*.

We, therefore, divided the projected area into two main seismotectonic provinces of the Alborz in the north, and the Central Iran in the south (see the attached 'Fault Map of the Greater Tehran region (34.35°N to 37.10°N & 49.80°E to 53.10°E)', and constructed Gutenberg-Richter exponential recurrence models for each of them individually, and a separate model for the whole region [see the attached 'G-R Recurrence Models For Individual Faults and Seismotectonic Provinces of the Greater Tehran region (34.35°N to 37.10°N & 49.80°E to 53.10°E)']. The values of the coefficients *a* and *b* of the log-linear frequency-magnitude relation for the two seismotectonic provinces based on the project area seismic area is set forth in Table V.5. Also included are the data from earlier publications. It should be noted that neither the province boundaries, nor the seismic data are identical in the referenced studies (Table 4.5). Both provinces are capable of generating earthquakes of magnitude M_w 7.6 (see the Geologic Database: Fault Parameters Table & Table 4.4).

TABLE-4.5

VALUES OF CONSTANT PARAMETERS (*a & b*) FOR THE SEISMOTECTONIC PROVINCES OF THE GREATER TEHRAN REGION (34.35°N to 37.10°N & 49.80°E to 53.10°E)']

Province	*a*	*B*	R^2	References
Alborz	4.2744	0.5939	0.9643	This Study (2007) [confined to the outbounds of the project area]*
Central Iran	3.5304	0.502	0.9127	
Alborz	3.6935# 1.8490#	0.7776# 0.9494#		Nowroozi & Ahmadi (1986)
Central Iran	2.4947	0.6192		
West Alborz		0.85^		Niazi and Bozorgnia (1992)

Notes:
a & *b*: Constants in Gutenburg-Richter frequency-magnitude distribution (*a* = measure of the level of seismic activity; *b* = rate at which event occur within a given magnitude range).
R^2: Coefficient of determination of a linear regression.
*: 34.35°N to 37.10°N & 49.80°E to 53.10°E.
#: Estimations based on two databases (Nowroozi & Ahmadi, 1986).
^: 1900-1990 events in the 36°-28°N and 48°-51°E quadrangle, using *mb*.

Despite all the efforts carried out in this study, the earthquake rates have large uncertainties due to (i) the limited number of entries in the catalogue, and (ii) the process of assigning the earthquakes to faults are uncertain because of large magnitude of location errors.

4.8. Concluding Remarks (Geologic Database)

Active faults in Iran pose a serious hazard for a large percentage of the population, and destruction of poor constructions during earthquakes often have caused deaths of tens of thousands of people (Berberian, 1981, 2005). Very little is known of slip-rates (ratio between fault displacement and the elapsed time) of the active faults in Iran, and the average recurrence intervals between the large-magnitude earthquakes are not established. The information is critical for seismic hazard assessment of the country. Analysis of large-magnitude historical earthquakes has shown that the recurrence period is several thousand years long (Ambraseys and Melville, 1981; Berberian and Yeats, 1999, 2001), and the historic data is short to reveal the recurrence periods especially on thrust faults (Berberian, 2005).

In order to determine the average recurrence interval, we need to determine the slip-rate of individual faults over timescales of several thousands years. Data on slip-rates are very poor in Iran, since most of the faults are poorly constrained because they have not been studied sufficiently.

We reviewed the original sources of slip-rates whenever available for constraints on the direction, amount, and timing of displacement. Slip-rates are considered well constrained if the direction, amount, and timing of displacement have been demonstrated. Moderately constrained slip-rates generally have significant uncertainty for one of these components. Poorly constrained slip-rates have either significant uncertainty with respect to both amount and timing of displacement or else the reported slip rate is a long-term average rate [see the attached 'Geologic Database: Fault Parameters of the Greater Tehran Region (34.35^{o}N to 37.10^{o}N & 49.80^{o}E to 53.10^{o}E)'].

In this study we have analyzed and delineated the existing data from different sources and incorporated the final fault parameters of the major faults of the project area. Our geologic database includes 128 major faults (including few blind thrusts) located in two seismotectonic provinces of the Alborz in the north and the Central Iran in the south [see the attached 'Geologic Database: Fault Parameters of the Greater Tehran Region (34.35^{o}N to 37.10^{o}N & 49.80^{o}E to 53.10^{o}E)']. A new 'Fault Map of the Project Area' and a 'Geologic Database' have been prepared for this study. The documents can be utilized as a base data for further study and modifications. Unfortunately, data on the slip-rates, fault segmentation, creeping segments, and blind faults are almost missing for the Iranian faults, and we felt there were insufficient studies to warrant specific information regarding

the mentioned vital issues. We hope that our preliminary parameters will be modified, as more data will gradually become available in the future.

We have created the first geologic database incorporating the required fault parameters. The attached 'Geologic Database: Fault Parameters of the Greater Tehran Region (34.35^{o}N to 37.10^{o}N & 49.80^{o}E to 53.10^{o}E)' shows the faults that were incorporated into the source model of the project area, and the attached 'Fault Map of the Greater Tehran Region (34.35^{o}N to 37.10^{o}N & 49.80^{o}E to 53.10^{o}E)' indicates the associated length, slip- rate (if available), quality of slip-rate (rank), maximum magnitude (moment magnitude), characteristic earthquake rate and recurrence interval for the maximum magnitude, down-dip width of seismogenic zone, the top and bottom of the rupture surface, as well as the rake, dip, and azimuth of the rupture surface, the endpoints of the faults, and comments and references regarding the basis for these parameter values.

In addition to fault and seismological studies, geodetic, magnetic, geophysical, and earthquake source mechanism data provide insights constraining the stress and strain rates on the faults. These strain measurements are not available in general, and if available in certain cases, have not been incorporated explicitly in this study because of lack of uniform spatial coverage and availability. This strain data, however, could provide independent constraints on the slip rate information independent of the geological data. All these data, values, and quality assessments will be updated as new geologic and seismic investigation are completed and become available.

Geologic data, which can be obtained from individual faults for using in the evaluation of seismic hazard, are summarized below [see also the attached 'Geologic Database: Fault Parameters of the Greater Tehran Region (34.35^{o}N to 37.10^{o}N & 49.80^{o}E to 53.10^{o}E)']. Also, the summary of fault rates and detailed discussion about the modeling assumptions is presented in the section 6 hazard analysis.

- All faults are treated as unsegmented, and their accuracy is based on the accuracy of the published geological maps (GSI, 1980-2007), and the inherent uncertainties may cause an uncertainty in the characteristic magnitude, characteristic displacement, and hence, uncertainties in the slip-rate, magnitude-frequency distribution, and in the seismic hazard estimation.

- Although blind thrust faults are postulated to underlie the Tehran basin, only one such fault has been documented in the basin.
- Fault length, azimuth, dip, rake, mechanism, and slip-rate have been documented.
- For unknown fault dips we recommended the following dips: 35^o for thrust, 45^o for reverse (high-angle), and 90^o for strike-slip faults.
- Maximum characteristic magnitude ($M_{w\max}$) was calculated from fault length-M_w regression derived by Wells & Coppersmith (1994) for all fault types (mechanisms) rather than the relation for individual fault types. The relations for individual fault types were derived from a small number of faults and may overestimate the magnitude. Fault area was not used to calculate $M_{w\max}$ since there is insufficient seismic data to adequately define the width of the faults.
- Average characteristic displacements were obtained using formula presented by Wells & Coppersmith (1994).
- Last earthquake on each fault (if known) with its magnitude, centroid depth and slip-vector have been included.
- Recurrence period (if available) is added on the database.
- Depth of seismogenic layer (if available) is also included.
- Fault width is determined by seismogenic depth divided by the sine of the fault dip.
- Coordinates of both ends of the faults (and in the middle in case of a major bend along the fault line) are added to the database.
- Following the south California source model, we could only assign three class "A" sources [faults with constrained slip-rates, reported historic or palaeoseismic evidence regarding the recurrence rate for large earthquakes, and date of the last large-magnitude earthquake]. These faults are the North Tehran, the Mosha and the Firuzkuh faults (the latter does not have palaeoseismic data) in the Alborz seismotectonic province. The rest of the faults in the project area lack well-defined estimates of slip-rates.
- About 80.5% of the project area faults have a maximum characteristic magnitude between 6.5 and 7.2 corresponding to faults with approximate lengths between 18 and 70 km, with characteristic displacements ranging from 0.5 to 1.5 m.
- Approximately 12.5% of the project area faults have a maximum characteristic magnitude >7.2 and characteristic displacements >1.5m.

- Almost 7% of the project area faults have a maximum characteristic magnitude <6.5 and characteristic displacements <0.5m.
- Except for 11 faults out of a total of 128 faults in the project area (the Alamutrud, Baijan, Eshtehard, Firuzkuh, Garmsar, Ipak, Khazar, Mosha, North Qazvin, North Tehran, and Taleqan faults), most of the faults in the project area have not experienced any large-magnitude earthquakes during the available recorded historic time. This is partially due to the fact that our short historic catalogue cannot reflect long-term seismic rates of the geological faults.
- The short distance between condensed major faults in the project area, as well as the interaction of the thrust faults with the range-parallel strike-slip faults at depth, would require sympathetic faulting during complex rupturing and triggered events.

5. GROUND MOTION ATTENUATION FUNCTIONS

5.1. Introduction

An important element of a seismic hazard analysis is Ground Motion Prediction Equations (GMPEs) or "attenuation" models. In this research project several GMPEs are used. Three of these are the latest models developed very recently: the Next Generation of Ground Motion Attenuation ("NGA") models. Three NGA models used are as follows:

- Campbell-Bozorgnia NGA model (2007, 2008),
- Boore-Atkinson NGA model (2007),
- Chiou-Youngs NGA model (2007)

Four GMPEs previously developed are also used, as follows:

- Abrahamson-Silva (1997)
- Boore, Joyner & Fumal (1997)
- Campbell-Bozorgnia (2003)
- Sadigh, et al. (1997)

By using such variety of GMPEs in the probabilistic seismic hazard analysis (PSHA), model-to-model variability of GMPEs, i.e., epistemic uncertainty is also implicitly included. Otherwise, an epistemic uncertainty should be additionally incorporated in the PSHA. The previous attenuation models listed above have been well studied by various researchers; thus, their characteristics are not elaborated in this chapter. However, due to major new developments in the recent NGA models, some key features of the NGA database and models are summarized below.

5.2. Key Features of NGA Database and Models

The NGA database is one of the largest databases of uniformly processed strong-motions recorded in shallow crustal earthquakes in active tectonic regions. The database includes recorded ground motions in 173 worldwide earthquakes. Data recorded in earthquakes from the 1935 Helena, Montana earthquake through the 2002 Denali (magnitude 7.9) are included in the NGA database. Major worldwide earthquakes such as the Chi-Chi (Taiwan), Tabas and Manjil (Iran), Kobe (Japan), Kocaeli (Turkey), among others, are part of the database. Besides the processed recorded ground motions, the database also includes major metadata about earthquakes and recording stations, such as: source characteristics of the earthquakes, various distance measures, local soil conditions, among others. The NGA database includes 3551 three-component recordings.

The NGA ground motion modelers selected a subset of the larger NGA data, to develop their GMPEs (Power, *et al*, 2008). The key features of the NGA models are as follows:

- GMPEs for ground motion parameters of peak ground acceleration, velocity, and displacement (PGA, PGV, PGD), and 5%-damped elastic response spectral accelerations in the period range of 0s (PGA) to 10s.
- Average horizontal motion.
- Shallow crustal earthquakes (strike slip, reverse, and normal earthquakes).
- Moment magnitude range of 5.0 to 8.5.
- Distance range of 0 to 200 km.
- Soil site classification scheme based on shear-wave velocity at the top 30 meters of the soil.

As an example, selected results of GMPE developed by Campbell and Bozorgnia, CB (2007, 2008) are presented here. The database used to develop the model by CB (2007, 2008) contains 1561 recordings from 64 earthquakes. The distribution of the recordings with respect to magnitude and distance is shown in Figure 5.1

Figure 5.2 shows magnitude scaling of the predicted PGA by CB (2007, 2008) model for “rock” with the soil shear-wave velocity of 760 m/sec. The results of the older model of CB

2003 are also plotted for comparison. The magnitude scaling for spectral ordinates at period 1.0 sec is plotted in Figure 5.3. The difference between the CB2003 and NGA results are pronounced at larger magnitudes and close distances.

Attenuation, i.e., distance scaling, for PGA and for spectral ordinate at period 1.0 sec are plotted in Figures 5.4 and 5.5 respectively. Again, the difference between CB2003 results and those of NGA are most at large magnitudes and short distances.

Figure 5.6 shows complete predicted response spectra for a strike-slip fault with magnitude 7.0, and for various distances from the source. As shown, the NGA spectra can be predicted up to a period of 10 sec; as this is a major improvement of the new models. By increasing the distance, the peak of the spectrum is shifted to a longer period. This is due to a faster attenuation of shorter period waves with respect to long-period motions. Figure 5.7 shows the predicted response spectra for a distance of 10km for various magnitudes on a strike-slip fault. Displacement spectra are plotted in Figure 5.8 (in a linear-log scale). The behavior of the predicted spectra at long-period was checked against theoretical constraints (Campbell and Bozorgnia, 2007).

An important element of a GMPE is modeling of aleatory uncertainty. This uncertainty is generally a function of structural period, among other parameters. The aleatory uncertainties for PGA and 1.0 sec spectral ordinate are plotted in Figures 5.9 and 5.10. The estimated uncertainty in CB2003 is also shown in these figures. It is evident that the new NGA uncertainty is higher at larger magnitudes, and lower at lower magnitudes, than that in CB2003. Both median and aleatory uncertainty of GMPEs are incorporated in PSHA.

It should be noted that the NGA models predict a new geometric mean of two horizontal components (Boore, *et al.*, 2006). If the user is interested in estimating other measures of horizontal motions (e.g., maximum of the two horizontal components), the results of the NGA GMPEs should be multiplied by one of the scaling factors presented in Figure 5.11.

More details, and comparisons, of the NGA models can be found in Campbell and Bozorgnia (2007, 2008), Power, *et al.*(2008), Abrahamson, *et al.*(2008).

5.3. Applicability of NGA Models to Iran

Shoja-Taheri, *et al.* (2007) carried out a comprehensive study on comparison of the three NGA listed previously with the strong-motion data recorded in Iran. There are important strong ground motions recorded in Iran, including ground motions recorded in the 1978 Tabas and 1990 Manjil earthquakes, among others. However, the number of near-source recordings, especially for larger earthquakes, is very limited. For example, for magnitudes greater than 7.0 and distances less than 30 km, the Iranian strong- motion data have a total of only 4 recordings (see Figure 5.12, from Shoja-Taheri, *et al.*, 2007). Having such a limited number of recordings in near-source areas of large earthquakes, cannot constraint any attenuation model developed based on only the Iranian data, especially in near-source areas of large earthquakes (Bozorgnia and Campbell, 2007). Therefore, international data recorded in a similar tectonic environment are needed to be added to the local data. This is what has been developed in the NGA database. In the NGA database (which also includes data recorded in the Tabas and Manjl earthquakes) there are 112 recordings (3 components each) for magnitudes greater than 7.0 and distances less than 30 km. This is over 30 times more data than those recorded in Iran.

Regarding the comparison of NGA models and the recorded strong-motion data in Iran, Shoja-Taheri, *et al.* (2007) concluded that "Investigation of distribution of earthquake data recorded in Iran with the three NGA relations, with respect of residuals and their RMS, shows that the three NGA models are generally compatible with the recorded ground motion in Iran." Complete report by Shoja-Taheri *et al.*(2007) is attached.

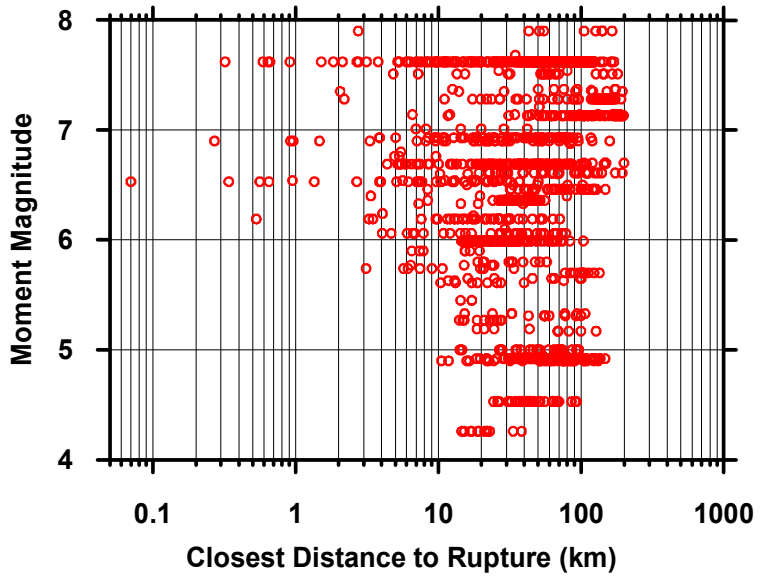

Fig. 5.1 Distribution of recordings with magnitude and distance used in Campbell and Bozorgnia NGA model

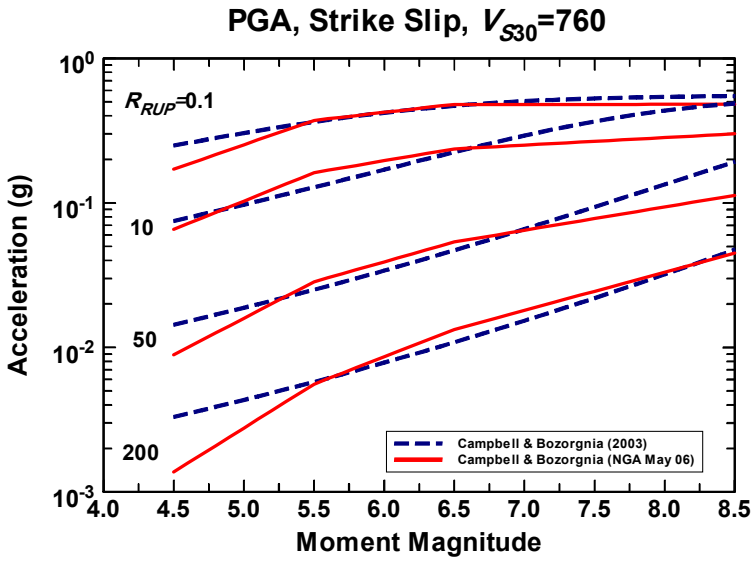

Fig. 5.2 Comparison of magnitude-scaling characteristics of PGA between the NGA and CB2003 empirical ground motion models for the following event characteristics: strike-slip faulting and NEHRP BC site conditions.

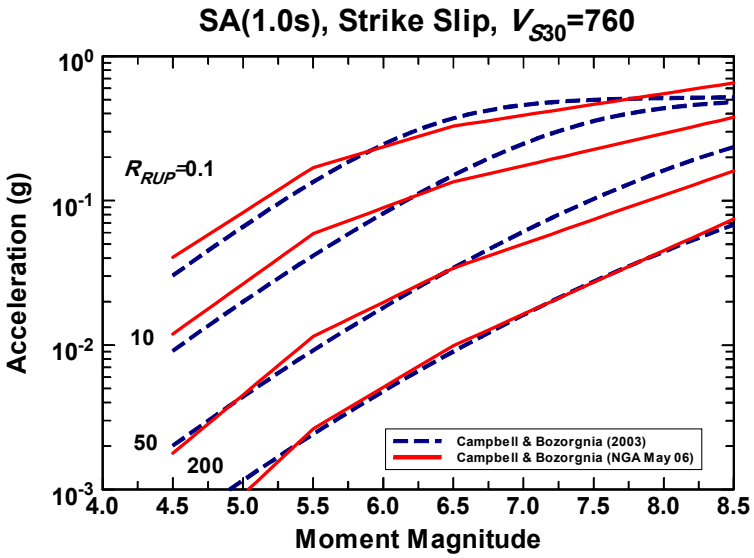

Fig. 5.3 Comparison of magnitude-scaling characteristics of spectral accelerations at period of 1.0 sec. between the NGA and CB2003 empirical ground motion models for the following event characteristics: strike-slip faulting and NEHRP BC site conditions.

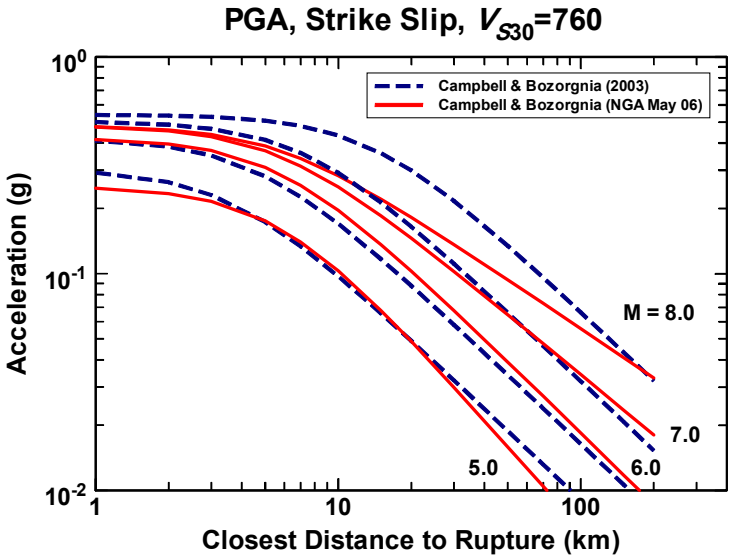

Fig. 5.4 Comparison of attenuation characteristics of PGA between the NGA and CB2003 empirical ground motion models for the following event characteristics: strike-slip faulting and NEHRP BC site conditions.

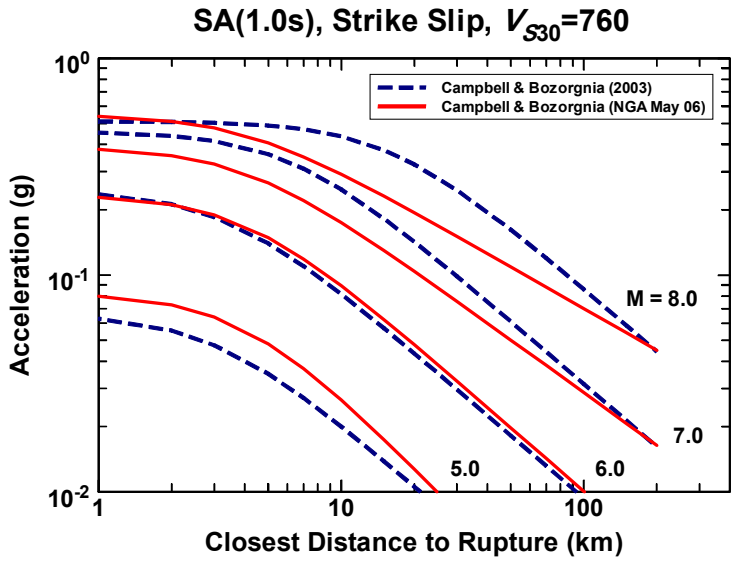

Fig. 5.5 Comparison of attenuation characteristics of spectral accelerations at period 1.0 sec. between the NGA and CB2003 empirical ground motion models for the following event characteristics: strike-slip faulting and NEHRP BC site conditions.

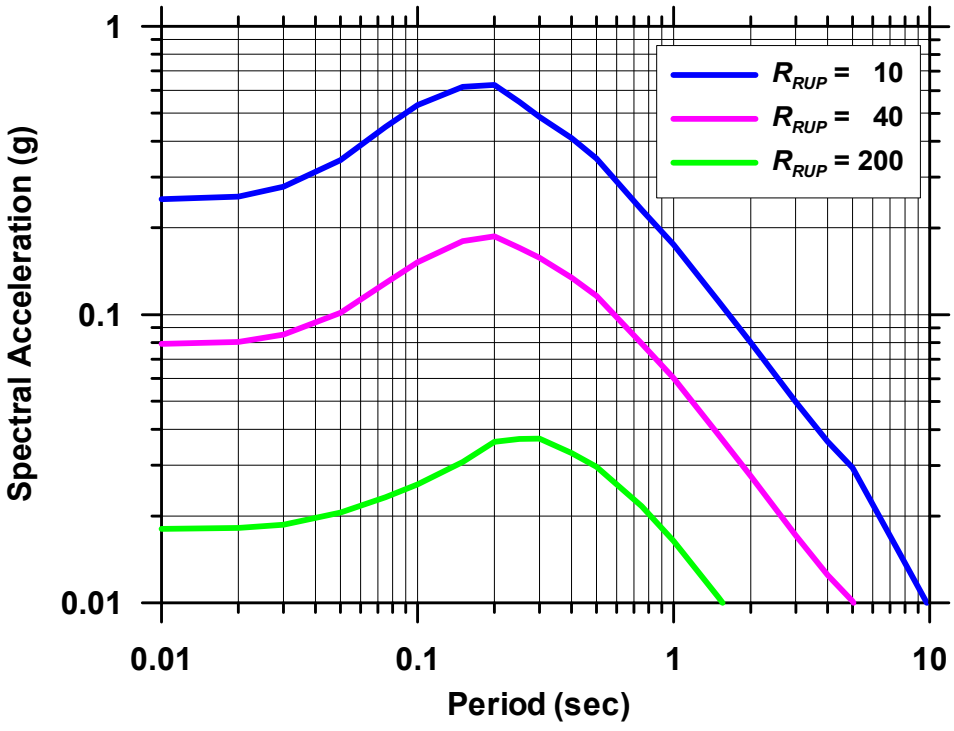

Fig. 5.6 Predicted acceleration spectra for a Strike Slip fault, M = 7.0, VS30 = 760 m/s for various distances from fault rupture

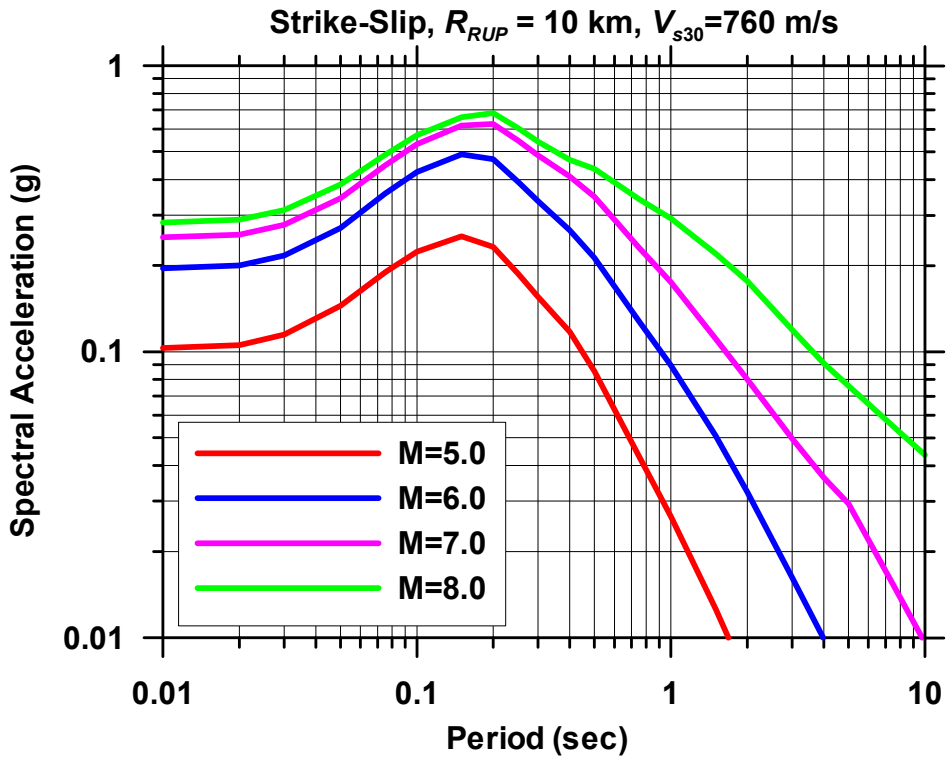

Fig. 5.7 Predicted acceleration spectra for a Strike Slip fault, distance 10 km, various magnitudes, VS30 = 760 m/s.

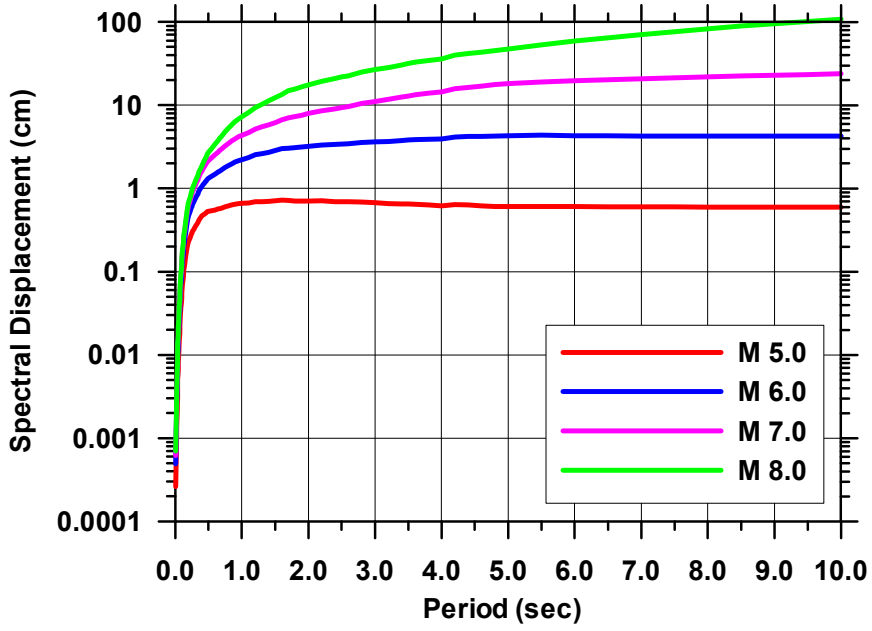

Fig. 5.8 Predicted displacement response spectra for a Strike Slip fault with various magnitudes, RRUP = 10 km, VS30 = 760 m/s

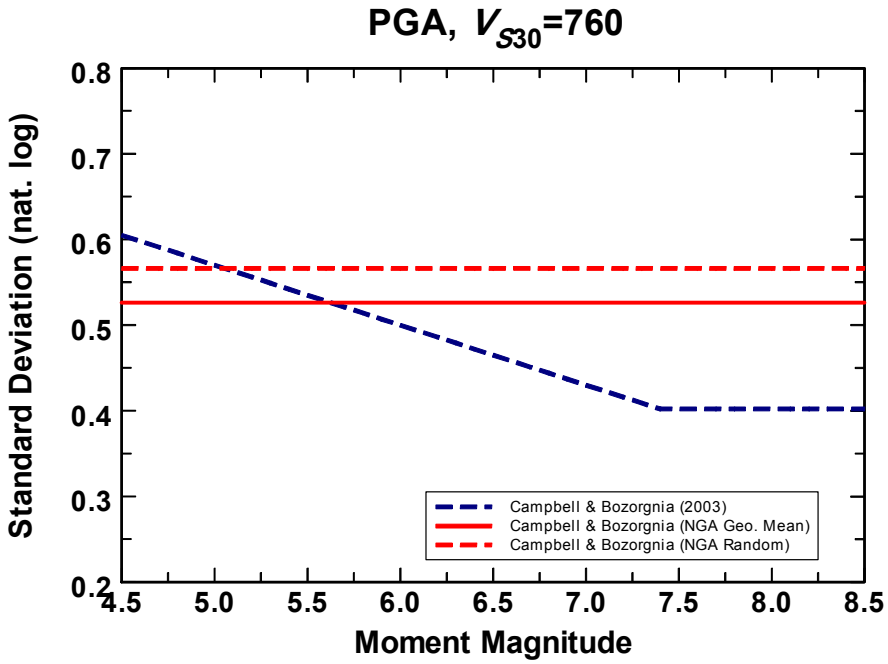

Fig. 5.9: Comparison of total aleatory standard deviations of PGA between the NGA and CB2003 empirical ground motion models. The NGA standard deviation does not account for the diminution of uncertainty due to nonlinear site effects.

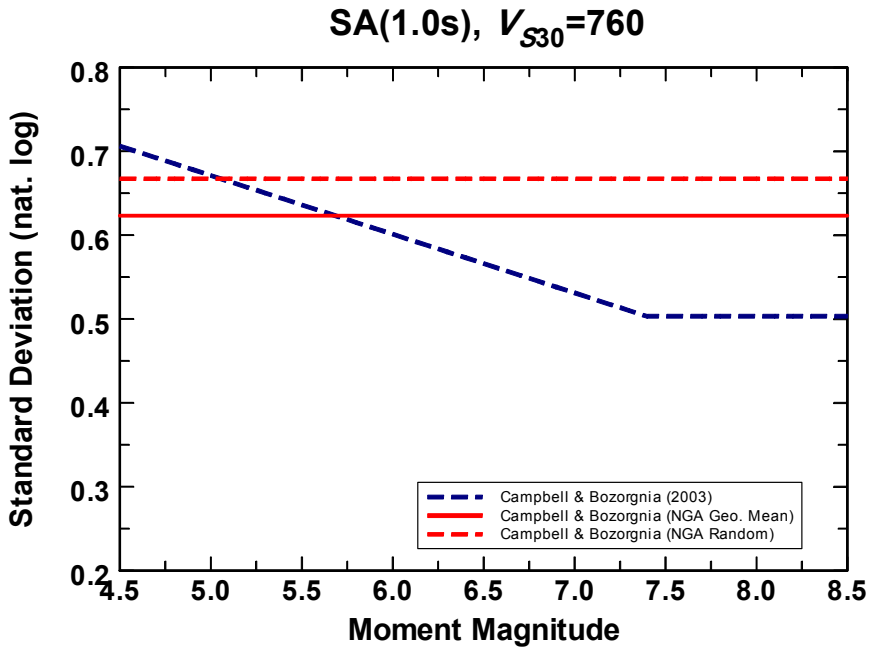

Fig. 5.10: Comparison of total aleatory standard deviations of 1.0-second SA between the NGA and CB2003 empirical ground motion models. The NGA standard deviation does not account for the diminution of uncertainty due to nonlinear site effects as recommended in the text

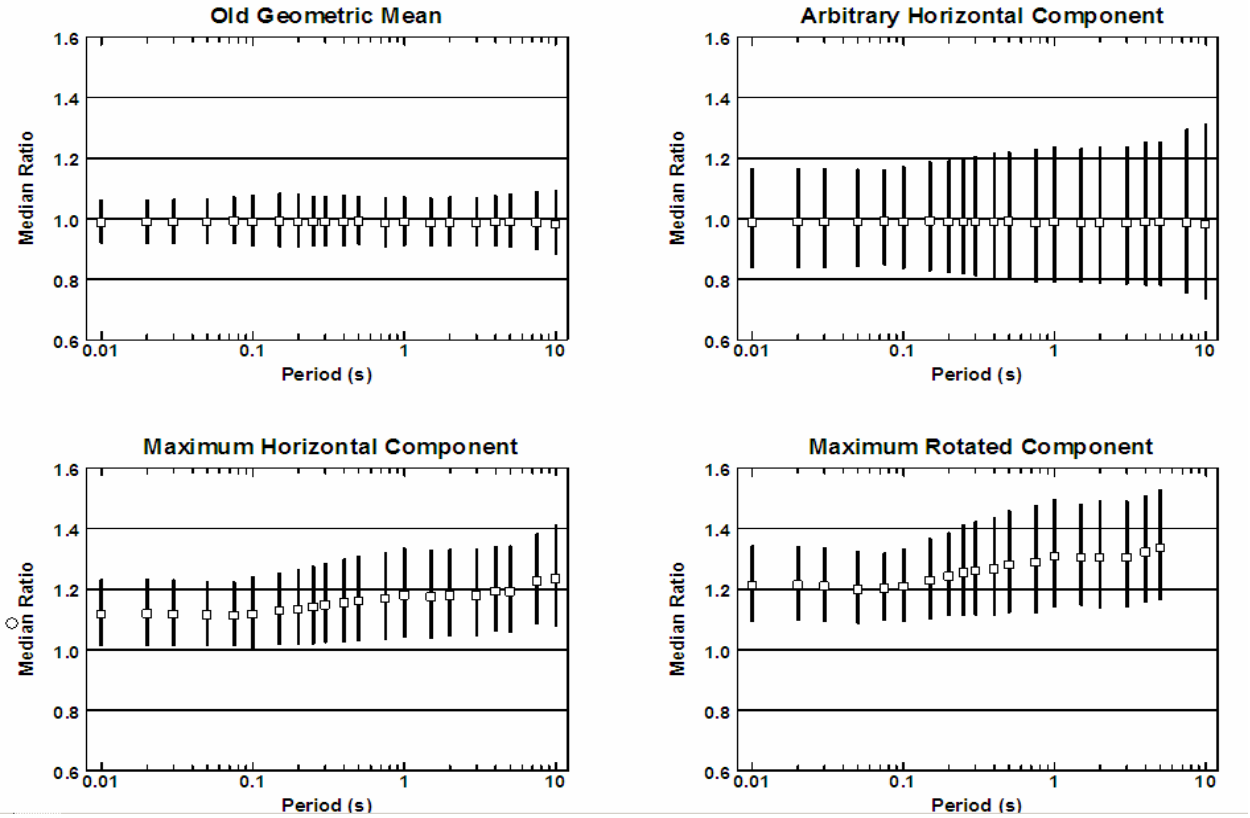

Fig. 5.11: Ratios of various measures of horizontal components over the new geometric mean used in NGA

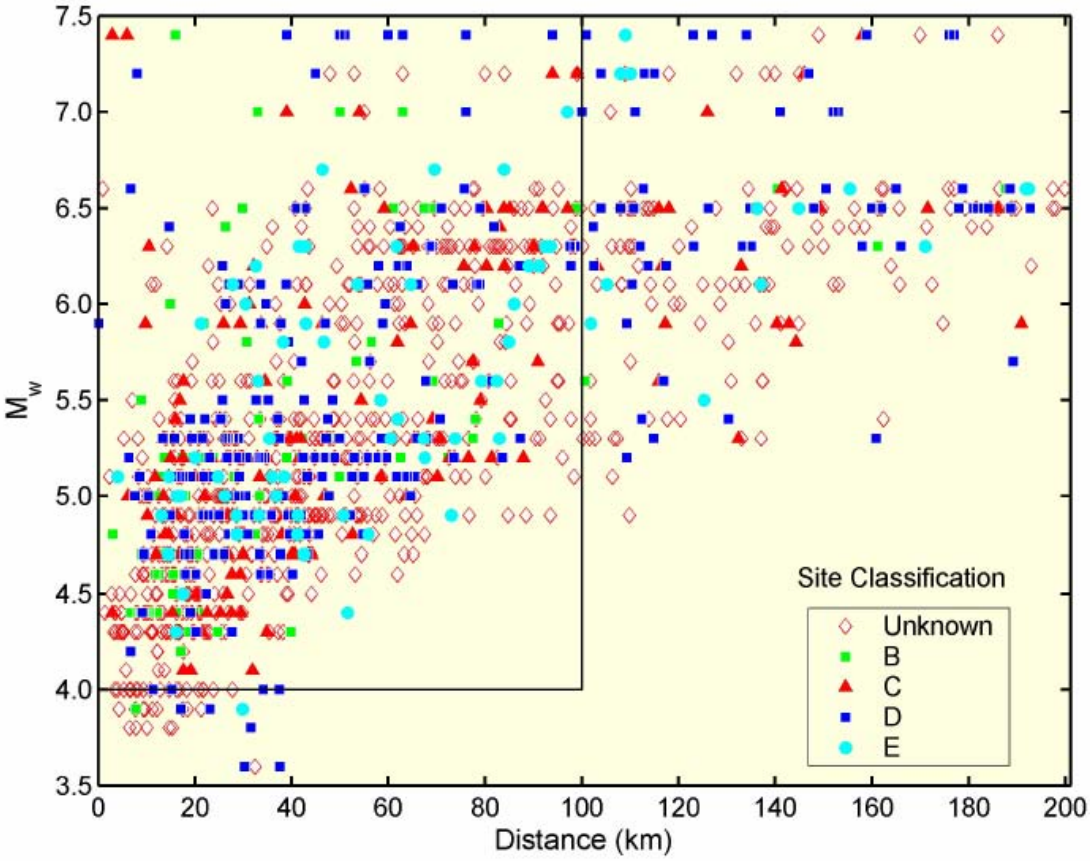

Fig. 5.12: Distribution of recorded earthquake ground motions in Iran (from Shoja-Taheri, et al., 2007)

6. SEISMIC HAZARD ANALYSIS

The purpose of this part of the seismic hazard assessment is to develop a model for seismic hazard analysis. The development is based on a multi-disciplinary collaboration among earth scientists and earthquake engineers to identify the location of tectonic structures that are capable of generating seismic events. Based on the availability of data on faults locations and their association with historic or paleo-seismicity, the earth scientist uses different modeling techniques to develop a seismic source model. These techniques include fault-specific source model, area sources and background sources. A fault-specific seismic source is used to model an identifiable active fault or system of faults. In the previous sections, the seismic sources of the siting area were identified based on the comprehensive research performed by Dr. Berberian and Geology Survey of Iran lead by Dr. Ghorishi, Dr. Talebian and Dr. Nazari. The following sections provide theoretical background for seismic hazard analysis, as well as detailed discussion about the modeling assumptions to develop the seismic hazard map of the region.

6.1. Recurrence of Earthquakes

The seismicity of a source is described by the mean rate of occurrence of events greater than given magnitude. Once earthquakes are stored according to the sources identified it is necessary to develop a statistical relationship between the frequency of occurrence of earthquakes and range of possible Richter magnitudes. The recurrence of earthquake events is described by the Gutenberg-Richter relationship.

Recurrence relationship for each area or fault is obtained by fitting a regression line through all earthquake data with $M \geq 3.0$. The number of events, N(M), occurring above a magnitude M are given by the following equation:

$$LnN(M) = \alpha + \beta M$$

or

$$LogN(M) = a + bM$$

where M = Richter magnitude, a and b or αand β are regression constants evaluated for each regression line. α is a measure of number of events above magnitude zero for a given source. β is the measure of the seismic severity for a given source.

The available earthquake data are used to develop recurrence relationships for seismic sources. In this study seismic sources of the region are divided into area sources, which are primary background seismicity to account for the effects of unknown faults, their seismic rates are defined using earthquake catalog. Additionally major faults, which are modeled by line source (e.g., North Tehran, Mosha, North and South Ray, Parchin and Kahrizaic faults, etc.) their rates were developed based on the slip rate using GPS data that is developed by Dr. Talebian from GIS.

These recurrence models are based on the selected historical and the 20th Century records specially post 1964 data with some modification to the rates based on the length of the faults to account for the uncertainty. Additionally, in order to minimize the errors involve in the evaluation of recurrence parameters we adapted statistical approach (completeness method) to assess the seismic rates for the background seismicity. The earthquake catalog was processed to remove duplicates, aftershocks and foreshocks as indentified in the earthquake catalog develop by Dr. Berberian and GSI. The declustered catalog is then analyzed for completeness of the magnitude bins. Details of the process are given in following section.

6.1.1. Earthquake Catalog Processing and Completeness Analysis

Historical catalogs include events from a long time ago. But other events that occurred in the past may not be detected or recorded because of the technical capabilities at that time (making it difficult to detect smaller magnitude events) and population density in the epicentral region (making it not possible to record even large earthquakes.)

The purpose of the completeness analysis is to determine the period of time where events of given magnitudes are assumed to be all recorded.

6.1.1.1. Completemess Analysis Methodology

The completeness analysis is based on the assumption that the event rate within a study region for a given magnitude bin is constant thru time. This is measured by counting the recorded events in the catalog for selected year bins. The rate of the magnitude bin is equal to the number of events divided by the width of the year bin.

Checking if the event rates are constant can be performed by plotting the calculated event rates per year bins over time. However, it is easier visually to check if the rates are constant by looking at the slope of the cumulative rates. If the rates are constant over time, then the slope of the cumulative rates should be linear. Since in the most recent years most of the events up to the smallest magnitudes are recorded, then calculating the reverse cumulative rates from the most recent year bins to the older bins would result in a constant slope until the period where the events are not completely recorded. The year where the first change in slope (from the latest year) occurs is a candidate for the limit of completeness. Ideally, the analysis is repeated using different magnitude and year bins to confirm or fine-tune the most likely limit for completeness.

6.1.1.2. Catalog Declustering

The catalog needs to be declustered (aftershocks and foreshocks removed) because the assumption of constant event rates and the log-linear relationship between rates and magnitudes are based on main shocks only. Therefore, the first step is to clean up the catalog by removing duplicates, foreshocks, and aftershocks.

The final declustered catalog has 120 events from 850 to 2005 and the numbers of events for different magnitude bins at 25-year windows are given below.

Table 6.1. Event counts for 0.5 Magnitude bins and 25 year bins.

Count of Mag	Mag									
Year	3.5-4	4-4.5	4.5-5	5-5.5	5.5-6	6-6.5	6.5-7	7-7.5	7.5-8	Grand Total
850-874					1			1		2
950-974									1	1
1100-1124							1			1
1175-1199								1		1
1300-1324							1			1
1475-1499								1		1
1600-1624									1	1
1650-1674							1			1
1800-1824					1		1			2
1825-1849							1			1
1850-1874						1				1
1875-1899					1					1
1900-1924			1		1					2
1925-1949			1	2	2					5
1950-1974	1	5	15	1	4		1	1		28
1975-1999		16	23	3	1	2				45
2000-2024	1	16	5	2	1	1				26
Grand Total	2	37	45	8	12	4	6	4	2	120

Note:
Some year bins are not displayed because there are no events recorded for some year bins.

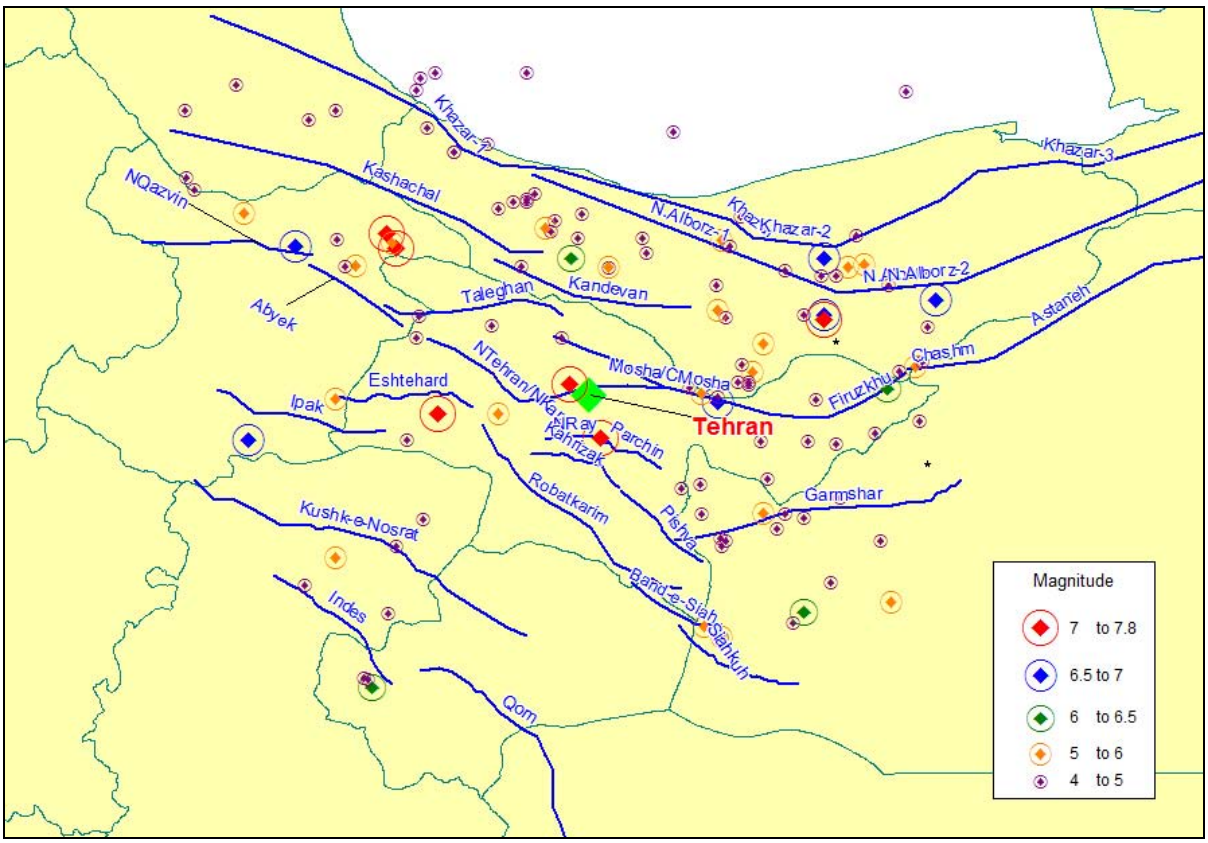

Figure 6.1 Plot of earthquake epicenters (mainshock only) from the declustered catalog

The choices of the width of the magnitude and year bins are dependent on the magnitude being considered. Smaller magnitudes are expected to be complete only during recent times, so the year bins should be small enough to capture the year where the slope changes. For large magnitudes, the events occur infrequently so that many year bins would not have events. Because of this, it is necessary to try different year bin widths to analyze different magnitude bins. It is also sometimes useful to smooth the rate plots a bit by overlapping the year bins.

The events in the catalog were counted using 10-year bins for 0.5 magnitude bins. The results shown below use a time step of 5-years, giving a 5-year overlap between the 10-year bins.

The figure below shows the plot of the reverse cumulative rates (actually cumulative event counts but since the year bins are uniform the slopes will apply to the annual rates as well) for the lower magnitude bins. A good example of the methodology is to look at the reverse cumulative rates for the M4.5 bin (M4.25 to M4.75) in Figure 6.2; the slope is relatively constant from the last (right-most) bin up to about the 1965 bin. The same process is used for the other magnitude bins as well.

Note that the event rates for the Magnitude 4.0 bin do not exhibit any trend. This implies that the completeness limit for this Magnitude is very short. Indeed, the event rate for Magnitude bin goes below the rate for Magnitude 4.5 earlier than 1975.

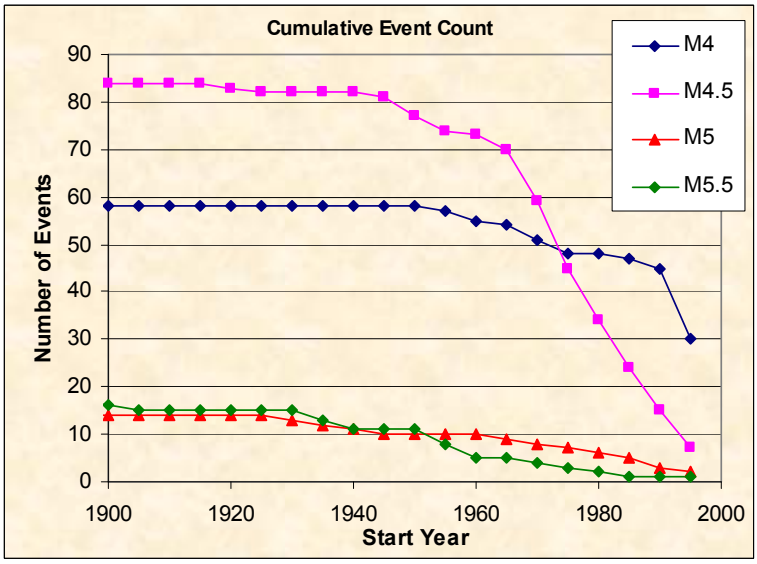

Figure 6.2 Plot of reverse cumulative rates for Magnitude bins 5.5 and below

The cumulative rates for Magnitude bins 5.0 and 5.5 are also given in Figure 6.3 to show the slopes in a different scale. The slope of the cumulative rates for the periods 1925 to 1945 is close to the trend established in the years 1960 to 2000, suggesting that that in the period between 1925 to 1945, magnitude 5.0 events are completely recorded, except for the quiet period from 1945 to 1960. The event rates for Magnitude 6.0 are difficult to analyze. It seems that there are not Magnitude 6.0 events recorded from 1870 to 1970 (a period of 100 years). Since the completeness years for larger events are usually longer than smaller magnitudes, the completeness period for Magnitude 6.0 is set equal to Magnitudes 5.0 and 5.5.

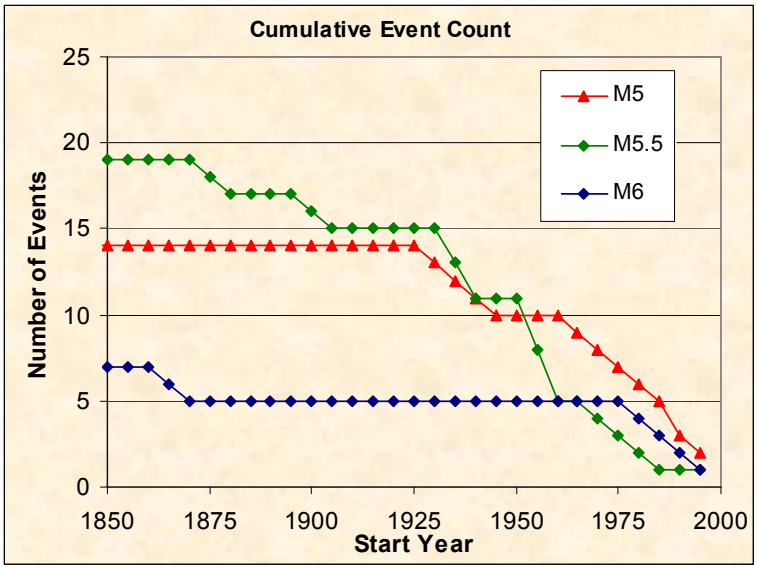

Figure 6.3 Plot of reverse cumulative rates for Magnitude bins 5.0 to 6.0

Figure 6.4 shows the cumulative rates for the largest magnitude bins (up to 8.0, although there are no Magnitude 8.0 and above events are recorded in the catalog). The cumulative event rate for Magnitude 6.5 has an overall straight-line trend during the period 1600 to 2000. The completeness periods for Magnitude 7.0 and above are assumed to be at least equal to the beginning of the catalog (i.e., year 600). However, because of the long return periods for these large events, it is possible that the average return period may be longer than the total catalog period, which can lead to an over-estimation of the annual rates for these magnitudes.

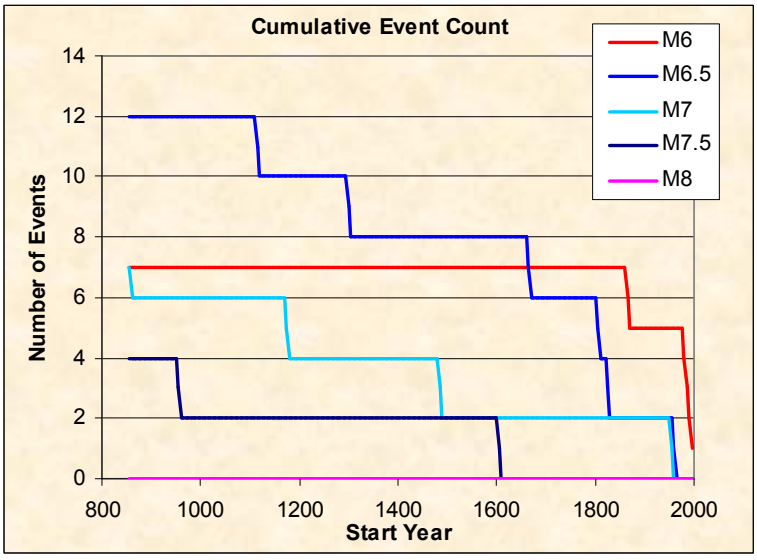

Figure 6.4 Plot of reverse cumulative rates for Magnitude bins 6.0 and above

Based on these observations, the final completeness table proposed for this catalog is given in Table 6.2 below. The annual rates for magnitude bins for 5.0 and 6.0 may be underestimated because of possible missing events in the catalog, while the rates for Magnitude 7.5 and above may be overestimated because the catalog may not be long enough to capture the recurrence trends for the very large magnitudes.

Table 6.2 Proposed completeness periods for 0.5 Magnitude bins in the GSI catalog

Magnitude	Start year	Comments	No. of Years
4.0	1990		16
4.5	1965		41
5.0	1930	With "missing" events during 1945 to 1960	76
5.5	1930		76
6.0	**1930**	"Missing" events during 1870 to 1970	76
6.5	1600		406
7.0	855		1151
7.5	before 855		1151+
8.0	no events		1151+
8.5	no events		1151+

6.2. Seismic Hazard Quantification – Theoretical Background

In most seismic hazard analyses, the recurrence of earthquake is assumed to follow a Poisson distribution even when the physical earthquake generating mechanism or a distinct occurrence pattern indicates that a time-dependent model would be more appropriate. The Poisson model formulation requires the small number of parameters to be estimated, and the ease with which hazard due to several sources can be combined.

With the assumption that earthquake occurrences form a Poisson process with mean rate of occurrence independent of magnitude, probability distribution on the number of occurrences is obtained for a given period of time and for a given source. The annual rate of occurrence of earthquake events is

$$\lambda = N'(M) = \frac{N(M)}{T}$$

where

$$N(M) = e^{a-\beta M}$$

Poisson process assumes earthquakes occur independently in time and uniformly in space and rate of earthquake events remains constant with time. Let X(t) be the number of events in time t, then [X(t); t>0] forms a Poisson process provided that

$$P[X(t) = n, t] = \frac{e^{-\lambda}(\lambda t)^n}{n!} \qquad \text{for } l > 0,\ n=0,1,2,\ ...$$

Therefore, the probability of at least one event of M≥m in future time t is defined as

$$P[X(t) \geq 0] = 1 - P[X(t) = 0] = 1 - e^{\lambda t}$$

The kernel of the seismic hazard assessment is the estimation of the frequency of exceeding ground motion at a site due to earthquake that occur in a single seismic source. The seismic hazard at a site (i.e., the annual frequency) for an individual seismic source is calculated according to:

$$v(A > a^*)_i = v_i \int_r \int_{m_o}^{m_{\max}} P(A > a^* | m,r) f_M(m)_i f_R(r)_i \, dm dr$$

where a^* is a specified level of ground motion, M is earthquake magnitude and R is the source to site distance. The probability density function on earthquake magnitude, $f_M(m)_i$, is generally defined by a doubly-truncated exponential density function. In some cases an alternative density function is used. For example, a characteristic earthquake model is used for certain type of faults. The lower-bound magnitude, m_o, defines the smallest size event that is considered in the analysis and m_{max} is the maximum magnitude that a seismic source can generate. The occurrence of earthquakes in seismic source *i* above the lower-bound magnitude, m_o, is defined by v_i, the seismic activity rate.

The term $P(A>a^* \mid m,r)$ is the ground attenuation model that defines the probability that a ground motion level a^* will be exceeded for an earthquake of magnitude *m* that occurs a distance *r* from the site. Based on the geometry of the seismic source as it relates to the site location, the probability that earthquakes occur at distance *r* from the site is defined by the probability density function, $f_R(r)_i$.

The integration in the above is performed over the range of distance at which earthquakes occur in a seismic source and the range of magnitude up to $M_{max.}$

When multiple seismic source (e.g., faults) in the vicinity of a site are active (i.e., generate earthquake above the lower-bound magnitude), the total or composite frequency with high levels of ground motion are exceeded is the likelihood that any one source generates ground motions that exceed these levels. The total seismic hazard at the site is obtained by summing the contribution from all the active seismic sources:

$$v(A > a^*) = \sum_i v(A > a^*)_i$$

where *i* is the index on the active seismic sources in the vicinity of the site.

For the hazard analysis the professional version of the program EZ-FRISK program utilized to compute the hazard analysis of this study. The EZ-FRISK program calculates seismic hazard using the standard methodology for seismic hazard analysis mentioned above.

Seismic sources may be either faults or area sources; the specification of source geometries and the calculation of the probability density functions on magnitude are performed differently for these two types of sources. For fault sources, the common form for calculating P[A > a|m, r] is as follows:

$$\ln A = C_1 + C_2 M + C_3 \ln R + C_4 R + \varepsilon; \qquad \varepsilon \approx N(0, \sigma_\varepsilon^2)$$

in which R is some measure of distance to the earthquake rupture (see the next section for common definitions of R). For area sources, the general form for calculating P[A > a|m, r] is:

$$\ln A = C_1 + C_2 M + C_3 \ln(R + RZEROA) + C_4 R + \varepsilon; \qquad \varepsilon \approx N(0, \sigma_\varepsilon^2)$$

in which *R* is focal distance (assuming a point source), which is computed from the horizontal distance and the source depth *h*. In the above two equations, *C*1, *C*2, *C*3, *C*4, *RZEROA* and ε are constants and independent of *M* and *R*. Either of the above two equations can be transformed into

$$P[A > a|m,r] = \Phi^*\left(\frac{\ln a - \overline{\ln A(m,r)}}{\sigma_\varepsilon}\right)$$

in which ϕ is the normal complementary cumulative distribution function and lnA(*m,r*) is the value of ln A obtained from the above E=equations by setting ε = 0. The introduction of truncation in the distribution of ε is described below. Common, recently-published attenuation equations are programmed into the software, so that the user can easily select an attenuation equation appropriate for analysis of the site. The distribution of magnitude is generally assumed to be doubly truncated exponential, i.e.,

$$f_{M_i}(m) = k_i \beta_i \exp[\beta_i (m = M_{oi})], \qquad M_{oi} \le m \le M_{\max i}$$

n which *ki* = (1-exp[*bi* (*m* - *Moi*)])-1 is a normalizing constant, *Moi* is the threshold magnitude defined earlier, and *M*max*i* is the largest magnitude that may occur in the source. An alternative to the exponential magnitude distribution is the characteristic model proposed by Youngs and Coppersmith (1985), which is described by the equation:

$$\begin{aligned} f_{M_i}(m) &= k_i' \exp(-\beta_i (m = M_{oi})), && M_{oi} \le m \le M_{\max i} - 3/2, \\ &= k_i' \exp(-\beta_i ((M_{\max i} - 3/2) - M_{oi})), && M_{\max i} - 1/2 \le m \le M_{\max i} \end{aligned}$$

in which *ki*' is a normalizing constant. The characteristic model can only be used with fault sources.

The distribution of distance is determined by the dimensions of the source and its distance and orientation relative to the site. If the size of the rupture is considered in the calculation of distance, the distribution of distance depends on magnitude. The graphical representation of characteristics magnitudes is shown in Figure 6.5.

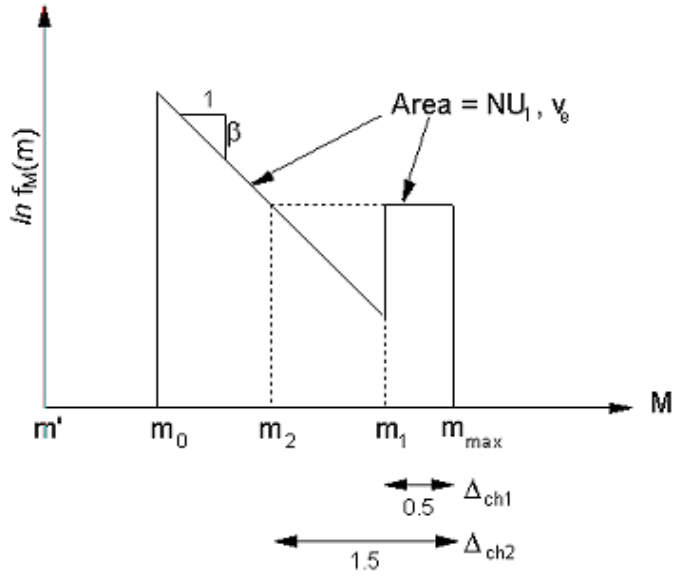

Figure 6.5 The graphical representation of Characteristics Magnitude

6.2.1. Analysis of Seismic Hazard from Fault Sources

EZ-FRISK uses a three-dimensional representation of the geometry of a fault source. A fault is characterized by its surface trace and its vertical cross section.

The surface trace of the fault is represented by connected straight-line segments between fault points [XF(1),YF(1)], [XF(2),YF(2)], [XF(3),YF(3)], ... [XF(NPTS),YF(NPTS)], which are input by the user. The vertical cross sections are characterized by two dip angles and three depths. These depths specify the minimum depth of energy release, the depth where the dip angle changes, and the depth of maximum energy release. In this representation of fault geometry, the fault cross section is not allowed to vary along the length of the fault; portions of the fault surface between plane segments are modeled as surfaces of revolution. Figure 6.6 shows the representation of fault modeling in EZ-Frisk program.

Note: The epicentral distance integration increment used at a particular distance from the source varies linearly between the minimum and maximum values, but is not allowed to decrease below the minimum value.

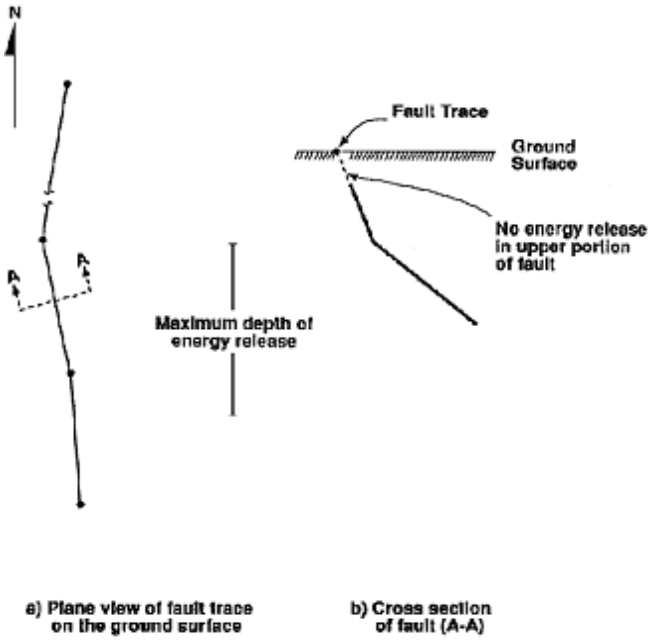

Figure 6.6 The graphical representation of fault modeling in EZ-Frisk program

In the calculation of distance, EZ-FRISK explicitly considers the finite dimensions of the rupture and the dependence of rupture size on earthquake magnitude. The depth and horizontal location of the earthquake rupture are assumed to be uniformly distributed. Rupture length *LR* and width *WR* are assumed to vary with magnitude according to the expression:

$$\log_{10} L_R = \log_{10} W_R = AL + BL + \delta, \qquad \delta \approx N(0, SIGL^2)$$

Coefficients *AL* and *BL* are usually obtained from regression analyses of magnitude on rupture size; SIGL represents the scatter observed in these analyses. If, for a specific value of □, the value of L_R given in the above equation is larger than the fault length, L_R is made equal to the fault length. Similarly, if W_R is larger than the fault width, W_R is made equal to the fault width.

The calculations of horizontal and vertical locations of the rupture have been decoupled for the sake of simplicity. A consequence of this decoupling is that, when the rupture extends between two segments of a dipping fault, the rupture length at a depth is different from *LR*, where *LR* represents the rupture length as measured at the surface. This difference is generally small because the strike of the fault changes little between segments.
For fault sources, three definitions of distance R are available to the analyst, as follows:

- *R*0: the shortest distance to the rupture.
- *R*1: based on the shortest distance to the horizontal projection of the rupture:

*R*1 = *R*horizontal

- *R*2: based on the shortest distance to the surface expression of the rupture (i.e., the shortest distance to the ruptured portion of the fault trace, if rupture extends to the surface); may include a fixed "depth" term RZEROF; i.e.,

*R*2 = *R*to. surf. Expression

Note: *R*1 is identical to *R*2 for a vertical fault. Figure 6.7 shows a graphical interpretation of these definitions:

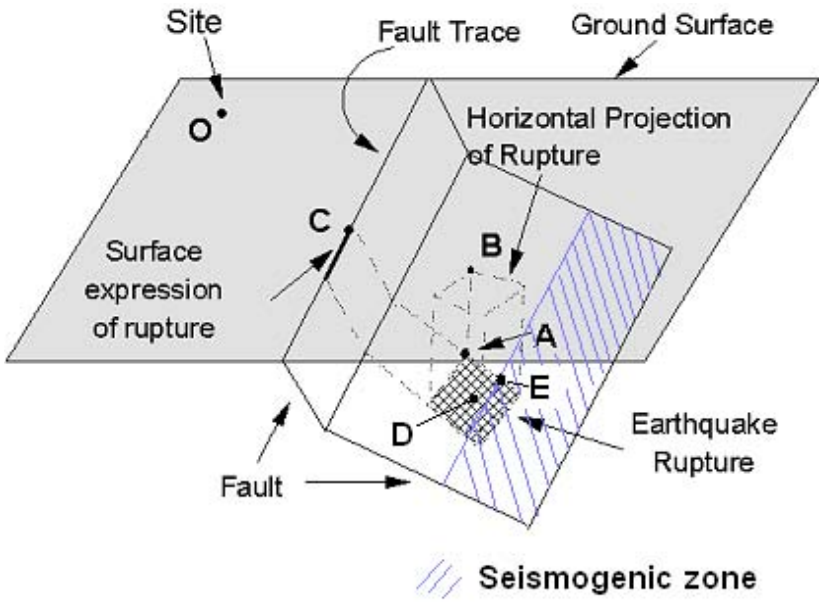

Figure 6.7 Fault source three definitions of distance R

The most common definition of distance is *R*0, but other definitions may be used in order to be consistent with the distance used in the specific attenuation function. With the above definitions, the sequence of seismic hazard calculations in EZ-FRISK for fault sources can be represented by a modified form of standard hazard equation.

$$H_j(a) = \nu_j \int_m f_{M_j}(m) \int_l f_{L_R}(l) \int_r P[A > a | m, r] f_{R_j | M_j, L_R}(r; m, l) dr\, dl\, dm$$

The integrals over *m* and *l* in Equation 10 are performed numerically in EZ-FRISK. The integration over *r* is represented by two numerical integrations over horizontal and vertical locations of the rupture.

6.2.2. Analysis of Seismic Hazard from Area Sources

An area source (or seismic zone) is characterized by a polygon in the horizontal plane, with a depth range. Dimensions of the polygon are specified by the user through the input of coordinates [X(1),Y(1)], [X(2),Y(2)], [X(3),Y(3)], ... [X(NPTS),Y(NPTS)]. Earthquake locations are assumed to be uniformly distributed in space inside the polygon. The various distance metrics are calculated

from the earthquake to the site by presuming that the rupture profile is vertical, that the top of the rupture is uniformly distributed with depth, and that the rupture may be modeled as a point source or as having finite length, depending on parameter values. The orientation of the rupture with respect to the site is modeled by using a finite set rupture azimuths. If the only on rupture azimuth is used, it will directed at the site. If multiple rupture azimuths are used, they will be uniformly distributed. Figure 6.8 shows the graphical representation of the area geometry.

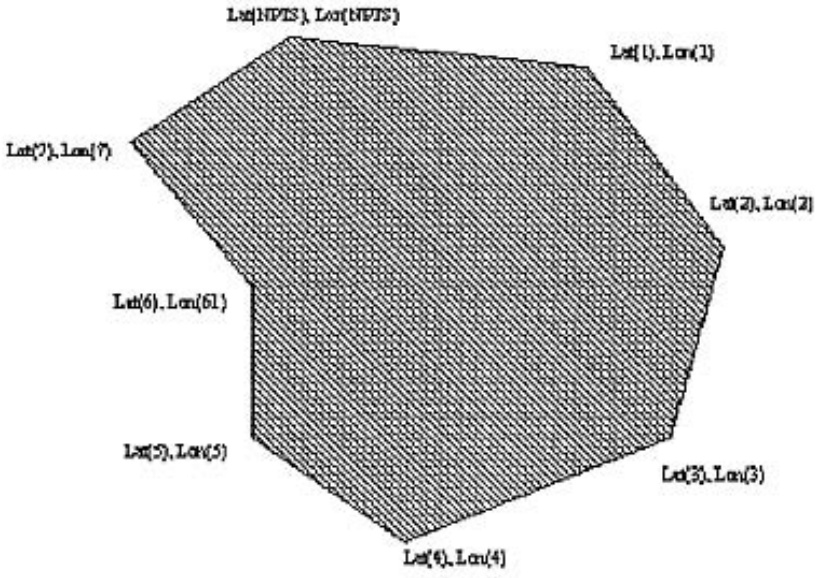

Figure 6.8 Area source modeling in EZ-Frisk

The calculation of hazard for source *j* may be represented by the following modified form of the standard hazard Equation:

$$H_j(a) = \nu_j \int_{\rho} \frac{arc_j(\rho)}{Area_j} \left[\int_{m} P[A > a | m, r(\rho)] f_{M_j}(m) dm \right] d\rho$$

in which ρ is horizontal distance from the site, *arcj* (ρ) is the length of the intersection between the source polygon and a circle with center at the site and radius ρ, and

$$Area_j = \int_{\rho} arc_j(\rho) d\rho$$

is the area of the area source.

6.2.3.Analysis of Seismic Hazard from Gridded Sources

Gridded seismic sources are primarily used to model the variable seismicity background sources used by the USGS. This source is used to represent seismicity that is not associated with known faults. Our goal is to reproduce USGS results, while retaining the flexibility to choose alternative attenuation equations as desired by the analyst.

These sources are modeled by a set of points located on an evenly spaced grid. Typically the grid spacing is 0.1 degrees of latitude and longitude, but other values are also used. The rate of events per cell is allowed to vary with each grid point. In addition, the maximum magnitude is lowered if a grid point lies near a known fault. The hypocenter of each event is presumed to be located at the grid point. The rupture profile is presumed to be vertical. The orientation of the rupture with respect to the site is represented by a random rupture azimuth. Although the USGS uses only a single azimuth for the events of a particular magnitude, EZ-FRISK uses a variable number of azimuths depending on the rupture length and distance between the site and the grid point. This reduces the variability of background hazard caused by a randomly oriented rupture pointing directly at a particular site, without excessively slowing the background hazard calculations.

6.2.4. Truncation of Attenuation-Function Residuals

You may specify truncation of the attenuation-function residuals so that, given M and R, the log ground-motion amplitude may not exceed a certain amplitude $\ln(a\text{trun})$, as follows:

- No truncation: $\ln(a\text{trun}) = 4$.
- Truncation at a fixed amplitude: $\ln(a\text{trun}) = const.$
- Truncation at a number of standard deviations above the untruncated median amplitude: $\ln(a\text{trun}) = \ln A(m,r) + const.\ \sigma\varepsilon$.
- Truncation at a constant times the untruncated median acceleration: $\ln(a\text{trun}) = \ln A(m,r) + \ln(const.)$, or, equivalently,

If truncation is desired by the user, the variable *const.* in the above equations must be specified. In this case the general annual frequency equation transforms to:

$$P[A > a \mid m, r] = \frac{1}{1 - K\Phi}[\Phi^*(\frac{\ln a - \overline{\ln A(m,r)}}{\sigma_\varepsilon}) - K_\Phi] \quad a \le a_{trun}$$

in which

$$K_\Phi = \Phi^*(\frac{\ln a_{trun} - \overline{\ln A(m,r)}}{\sigma_\varepsilon})$$

6.2.5. Deaggregation of Hazard

For a specified spectral period and ground motion amplitude, the seismic hazard can be *deaggregated* to show the contribution to the annual frequency of exceedence by magnitude (*M)*, distance(*R)*, and the deviation parameter in the attenuation equation (ε). If a ground motion of amplitude *a* occurs at the site of interest, certain magnitudes, distances, and ε values are more likely to have caused that amplitude than others, and the deaggregation shows these relative contributions. The deaggregation is useful in identifying which sources contribute to hazard, i.e. whether the following items contribute significantly: earthquakes near the maximum magnitude on a fault, rare ground motions (high ε values), and other sensitivities. The deaggregation of hazard can also be used to construct "design earthquakes" that replicate the uniform hazard spectrum for any chosen return period.

In general, deaggregating the hazard at high amplitudes indicates that large *M*, small *R*, and large ε contribute most to hazard (these indications are reversed for low amplitudes of shaking). Low frequencies of shaking are usually associated with larger *M* and larger *R* than high frequencies. Attenuation equations that show lower dependence on *M* (or magnitude saturation at high amplitudes) generally show more contribution from lower magnitudes than those with high dependence on *M* (or no magnitude saturation). Finally, magnitude-dependent ε terms on attenuation equations (where ε decreases with increasing *M*) tend to shift the contribution to lower magnitude values. EZ-FRISK allows deaggregation by *M*, *R*, and ε, as well as *M*-*R*, through plots and printed reports.

6.2.6. Near Source Directivity Factors

The near-source directivity implemented in EZ-FRISK is based on research done by Paul Somerville and Norm Abrahamson. In their research, they found that amplitudes of ground motion increase for spectral periods of 0.5 seconds and greater for sites near fault ruptures. They also found that amplitudes are greater in the perpendicular direction from the fault than those in the parallel direction.

EZ-FRISK first generates a rupture along the fault and then calculates the ground motion for equally-spaced hypocentral locations within the rupture. These equally-spaced locations are determined by dividing the rupture length by the integration increment and then adding one to get the number of hypocenters. The actual integration increment is then determined by dividing the rupture length by the number of hypocenters, thereby always either maintaining the desired integration increment or possibly reducing it a little. This particular option can significantly increase the runtime if the interval spacing is small relative to the fault length.

6.3. Hazard Analysis Modeling of the Great Tehran Region

This section summarizes the procedures and methods used in calculating the seismic hazard of the Great Tehran region. It includes the functions of the seismic hazard program used, the parameters entered into the program and the procedures followed by the program to calculate the hazard maps. Computer programs that calculate probabilistic seismic hazard invariably use numerical methods to discretize continuous probability distributions and integrals. This is primarily to convert complex theoretical calculations into steps that can be tackled by computer algorithms.

Common numerical methods in seismic hazard analysis and methods specifically used by the computer programs are briefly discussed. The data, parameters and options used in this particular study are also described.

A brief summary of the EZ-Frisk program functionality that is used to perform the hazard analysis is provided for reference using the program technical guide. The procedures described in the program guide are geared towards the calculation of seismic hazard at a given site. The values to

create the hazard maps are generated by repeated hazard analyses for a dense grid of points that comprise the area of the hazard map.

Seismic hazard analysis calculates the earthquake hazard at a site under certain assumptions specified by the user. These assumptions involve identifying where earthquakes will occur, what their characteristics will be, and what the associated ground motions will be. EZ-FRISK™ performs both probabilistic and deterministic seismic hazard calculations:

- Probabilistic Calculations - The results of the program's probabilistic calculations are annual frequencies of exceedence of various ground motion levels at the site of interest. EZ-FRISK™ also calculates the mean and distributions of magnitude, distance, and epsilon causing exceedence of a specified ground motion level.

- Deterministic Calculations - The program's deterministic calculations estimate ground motions (for the mean and specified fractiles of the ground motion dispersion) corresponding to the largest magnitude occurring on each seismic source at its closest approach to the site of interest.

Seismic hazard analysis with EZ-FRISK™ is driven by databases of ground motion equations and seismic sources.

6.3.1. Seismic Hazard Analysis Modeling Assumptions

The input to a typical seismic hazard analysis can be broken down into two main components, the seismic source model and the ground motion attenuation model. The final output of the seismic source model is a set of stochastic events that represent possible earthquakes. Each event in the stochastic event set is defined by the magnitude and the geometry (3-dimensional in space) of the rupture and the type of rupture. The discretization results in a number of possible locations for an earthquake with the same magnitude. These possible locations can be considered as independent events and are assigned an annual probability of occurrence based on their magnitude and the number of probable fault geometries assumed for the source.

The output of the ground motion model is the estimate of ground motion at a given site due to each event in the stochastic event set. The ground motion at a site is primarily a function of the magnitude and distance of the site from the event rupture. There are other parameters that can

affect the hazard such as the type of faulting, the depth, etc. However, the main dependencies are on earthquake magnitude and distance.

The hazard at a site, therefore, can be formulated as a convolution of effects of the magnitude and distance, together with their probability distributions. Most computer programs that calculate the hazard discretize the probabilistic distribution of the magnitude of events for each source and the probable fault rupture geometry for each magnitude.

The hazard maps generated in this project are based on a uniform site condition with Vs30 = 150, 225, 525, 760 and 1070 m/s.

6.3.2. Stochastic Event Set

The stochastic event set is generated from a model of seismic sources that are expected to generate events in the future. Each seismic source is assigned parameters that define how big and how often earthquakes are generated by the source. These sources are commonly active faults, subduction zones, area sources, deep intraslab zones, etc. Generating stochastic event sets from each source type is similar. The steps given below apply to a generic seismic source and are repeated for all seismic sources in the model.

Each source is expected to generate events having a range of magnitude. The distribution of the probability of the event magnitude is given by the recurrence model. The recurrence model used in this analysis is a variation of the Gutenberg-Richter relationship, also called the exponential or log-linear relationship. For each magnitude generated by the source, the rate of recurrence is calculated from the recurrence model assumed for the source.

For the largest magnitude, the source typically will rupture its whole area. However, for smaller magnitudes, the rupture dimension and location may change within the confines of the source dimension. The distribution of how big the rupture is for a given magnitude is typically defined by a mean and standard deviation. To consider the uncertainty, a number of possible values are sampled from the distribution. The conditional probability of each sample is calculated from the assumed distribution and the type of sampling methodology used.

The actual location of the rupture within the source dimension is numerically integrated by moving the rupture incrementally across the source. The conditional probability of each location is usually considered uniformly distributed.

In summary, the stochastic event set from a seismic source is composed of the magnitude bins multiplied by the number of event dimension samples, and multiplied by the number of locations considered for each event dimension. The rate of each event in the stochastic set is determined by the total rate multiplied by the sum of conditional probabilities of the variations in dimensions and locations.

6.3.3. Probabilistic Seismic Hazard at a Site

The hazard caused by a single stochastic event is normally estimated by attenuation relationships that give the mean and standard deviation of the ground motion value estimate for the site. The attenuation relationships are mostly dependent on the magnitude and distance of the site from the event rupture. However, other parameters can affect the attenuation relationships applicable, such as:

1. Tectonic Structure: Shallow Crustal, Subduction Interface, Deep Intraslab, etc.
2. Rupture Mechanism: Strike-slip, Reverse, Extensional, etc.
3. Site condition (although hazard maps are typically calculated for a standard site condition)
4. Site in hanging wall or footwall

The probability of exceedance for a given site is then the sum of all exceedance probabilities for all events in the stochastic event set.

The plot of the exceedance probabilities for several hazard values is called the hazard curve. This curve can be used to determine the hazard value for a given probability of exceedance.

6.3.4. Calculating the Probabilistic Hazard Map

The hazard map is then generated by calculating the hazard for many sites on a grid that comprises the map. A hazard map is usually generated for a single level of exceedance probability.

6.3.5. Generating the Stochastic Event Set

For this study the sources are modeled by faults and area sources.

1. Faults – sources that are predominantly linear (length > down-dip width) and may be dipping at a specified angle. The coordinates of the surface projection of the top edge are specified and the rupture plane is derived from these coordinates, the dipping angle and the depth of the top edge. These sources can be crustal faults, subduction, or deep intraslab. The faults option is used to represent the active crustal faults around Tehran as defined by the Geological Survey of Iran (GSI).

2. Area sources – sources that are flat (uniform depth) and may have irregular shapes. The rate of seismicity within each area source is assumed to be uniform. The area sources option is used to represent the background seismicity of the region. The characteristics of the background seismicity is defined by GSI, Dr. Berberian and authors given in the Section 6.3.7

6.3.6. Active Crustal Faults

The source parameters for the active crustal faults are as follows:

6.3.6.1 Max and Min Magnitude

These specify the range of magnitudes of the stochastic events generated by the given source:

- The maximum magnitude generated by each fault is based on the fault parameter table given by GSI. For the sources where the maximum magnitude is given by more than one estimate, the larger one is used in the analysis.
- The minimum magnitude for the faults is Mw 6.1. Earthquakes that have magnitudes Mw 6.0 and below are assumed to be generated by the background sources.
- Events in the stochastic event set in the analysis are generated in 0.1 magnitude bin increments.

6.3.6.2 Fault Rupture Type

This characterizes the rupture mechanism followed by each fault. This is necessary because the ground motion values generated by the same magnitude and distance usually differs depending on the type of rupture mechanism. For example, reverse-thrust earthquakes normally give higher ground motion values than strike-slip earthquakes.

- The fault rupture type for each fault is specified in the fault parameter Table 6.1 given by GSI (Dr. Talebian & Dr. Ghorishi) and Dr. Berberian. The fault rupture type entered in the program is the closest match between the type specified by GSI and the fault rupture types that are accepted by the program.

- The program accepts the following fault rupture types:
    a. Strike-slip
    b. Normal
    c. Normal-Oblique
    d. Strike Slip
    e. Reverse-Oblique
    f. Reverse
    g. Subduction

6.3.6.3. Magnitude Recurrence Relationship (a- and b-values)

These parameters affect the annual cumulative rates of occurrence of the stochastic events. The b-value gives the relativity of rates between smaller and larger magnitudes. The cumulative rates for events with magnitudes between the minimum and maximum magnitude are entered into the program. The program also uses the beta-value which can be directly calculated from the b-value: beta = b-value * LN(10)

- The b-value for the faults is assumed to be equal to 0.85 based on the fault characteristics and earthquake catalog data. The regional constant b-value is used for all the faults with in region.

- Based on the GPS data, and using regional constant b-value, the a-values for each fault are given in the fault parameter table given by GSI based on the research performed by Dr. Talebian. The program does not use the a-value as an input, but uses the cumulative rate above the minimum magnitude. This cumulative rate can be calculated using the a- and b-values assigned to each fault. Figure 6.9 shows the cumulative rate for all the 26 faults in the regions. The top curve represents the sum of all the rates for the region, which is distributed between each fault based on their characteristics.

- The magnitude recurrence relationship used in this analysis is the Guttenberg-Richter magnitude recurrence model (or sometimes called log-linear magnitude recurrence model) that is truncated.

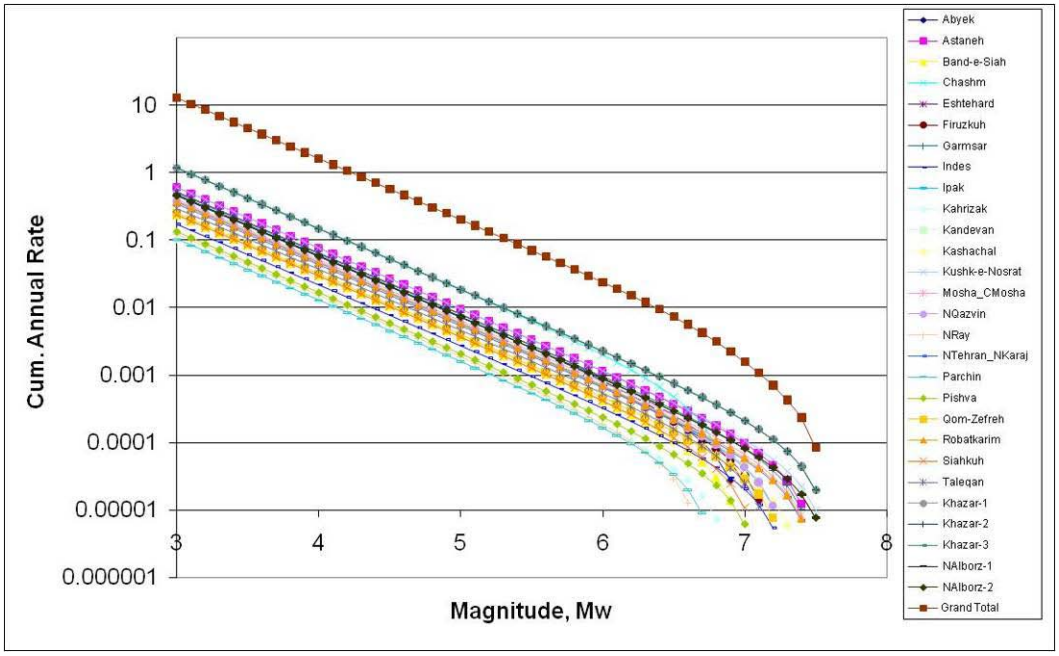

Figure 6.9 Cumulative Annual rate of the region and all faults

6.3.6.4 Fault Coordinates of the Top Edge

These coordinates locate the surface projection of the top edge of the fault.

- Fault coordinates are based on the files given by GSI and Dr. Berberian

- Complex fault systems are simply represented by single line segments. A map of the simplified fault segments used in the analysis overlaying the original fault traces along the fault zones is given in Figure 6.10
- The coordinates of the top edge of the faults are sorted such that the dipping angles as entered into the program are between 0.0 and 90.0 degrees.
- The dipping angle is based on fault information given by GSI/Dr. Talebian & Dr. Berberian as shown in the Table 6.1

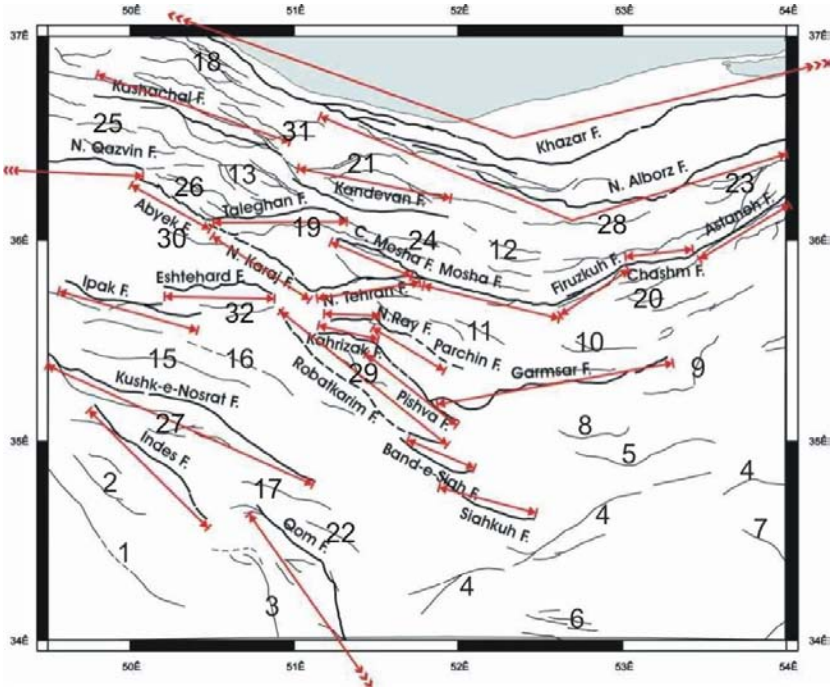

Figure 6.10 Fault Geometry Map

6.3.6.5 Fault Rupture

Mean and Standard deviation of the length/width/area of the fault rupture dependent on the magnitude based on the following assumptions

- The relationship between the faults' rupture area and magnitude is assumed to be the same one used by the USGS in the U.S. National Seismic Hazard maps release in 2002 for the Western U.S. region.

- The rupture area is modeled by the equation:

$$\log_{10}(\text{rupture area}) = -3.29 + 0.91M_w \text{ with sigma} = 0.24$$

Table 6.1. Fault parameters for crustal faults used in the analysis

Fault Name	Fault Type	Mmin	Mmax	Rate**	Dip Dir.
Khazar*	Reverse	6.1	7.60	0.06161	35S
NAlborz*	Reverse	6.1	7.60	0.01772	50S
Kashachal	Strike Slip	6.1	7.40	0.00414	80-90N
Kandevan	Reverse	6.1	7.30	0.00672	50N
NQazvin	Reverse	6.1	7.30	0.00627	35-70N
Abyek	Reverse	6.1	7.00	0.00642	45N
Taleqan	Normal Oblique	6.1	7.20	0.00444	55S
Mosha_CMosha	Strike Slip	6.1	7.50	0.00720	60-70N
Firuzkuh	Normal Oblique	6.1	7.20	0.00572	70S
Chashm	Reverse	6.1	6.90	0.01505	45N
Astaneh	Strike Slip	6.1	7.50	0.01090	90
NTehran_NKaraj	Reverse Oblique	6.1	7.50	0.00613	35-70N
Ipak	Reverse	6.1	7.30	0.00613	52S
Eshtehard	Reverse	6.1	7.10	0.00720	45N
Robatkarim	Reverse Oblique	6.1	7.50	0.00657	60N
Band-e-Siah	Reverse	6.1	7.00	0.00314	45N
Siahkuh	Reverse	6.1	7.10	0.00329	45N
NRay	Reverse	6.1	6.70	0.00137	45N
Parchin	Reverse	6.1	6.80	0.00131	45N
Kahrizak	Reverse	6.1	6.90	0.00131	45N
Pishva	Reverse Oblique	6.1	7.10	0.00185	45NE
Garmsar	Reverse	6.1	7.50	0.00907	45N
Kushk-e-Nosrat	Reverse	6.1	7.60	0.00950	45N
Indes	Reverse	6.1	7.30	0.00704	45N
Qom-Zefreh	Reverse Oblique	6.1	7.30	0.00657	45N
Khazar-1	Reverse	6.1	7.60	0.02054	35S
Khazar-2	Reverse	6.1	7.60	0.02054	35S
Khazar-3	Reverse	6.1	7.60	0.02054	35S
NAlborz-1	Reverse	6.1	7.60	0.00886	50S
NAlborz-2	Reverse	6.1	7.60	0.00886	50S

* Note that the Khazar and N. Alborz faults are sub-divided into two or three sub-faults which are modeled as independent sources. The rates for each sub-section are assumed to be uniform for each fault zone.
** The rate is given in annual probabilities of occurrence of a Magnitude at or above the minimum Magnitude.

6.3.7. Area Sources

Background seismicity around the Tehran Region is represented in the analysis as events modeled by an area source. Only one area source is defined so that the background seismicity within the source region is assumed to be uniform. The following parameters are used in the analysis as input to the seismic hazard calculation program:

The parameters of the background seismicity around the Tehran region are evelauated based on the several detailed discussion with Dr. Talebian. Two independent approaches were investigated to assess the background seismicity rates. The basis for Dr. Talebian's estimates is estimates of the crustal rates of deformation assumed to be released by the background events. This section compares the resulting event rates to those determined from the processing of the catalog.

6.3.7.1 Catalog Processing Summary

The catalog provided by GSI and Dr. Berberian was processed to remove duplicates, aftershocks, and foreshocks as identified in the spreadsheet. The declustered catalog is then analyzed for completeness of the magnitude bins. Details of the process are given in section 6.1.1**.** To establish baselines of event rates from the declustered catalog, events that satisfy the following criteria are considered for the background seismicity:

- Events not identified in the catalog as generated from a known fault
- Magnitudes, Mw, less than or equal to 6.0
- Events with focal depths less than 50 km
- Events not identified as aftershocks or foreshocks

The event rates for specific Magnitude bins for the background are given in the Table 6.3 below, assuming that the background catalog has the same completeness intervals as the whole catalog. The resulting "background" catalog is fitted against the Gutenberg-Richter model, using the Least Squares of Errors and Maximum Likelihood methods.

Table 6.3. Event counts and annualized rates attributed to the background source for each Magnitude bin (up to Magnitude 6.0)

Mag bin	Count	N years	Rate	Cum Rate
3.75 – 4.25	9	16	0.563	1.9476
4.25 – 4.75	46	41	1.122	1.3851
4.75 – 5.25	13	76	0.171	0.2632
5.25 – 6.75	6	76	0.079	0.0921
6.75 – 6.00	1	76	0.013	0.0132

6.11 shows the event rates for each Magnitude bin normalized against its' completeness period. Note that although the Maximum Likelihood method is the preferred approach, it is apparent that

this method significantly overestimates event rates at the larger magnitudes. It appears that the rate for the Mw 4.0 bin may be incomplete since the bin incremental rates are smaller than for bin Mw 4.50, and this is affecting the b-value calculated by the Maximum Likelihood approach. In contrast, the fit using Least Squares method gives a better fit to the event rates in the higher magnitudes.

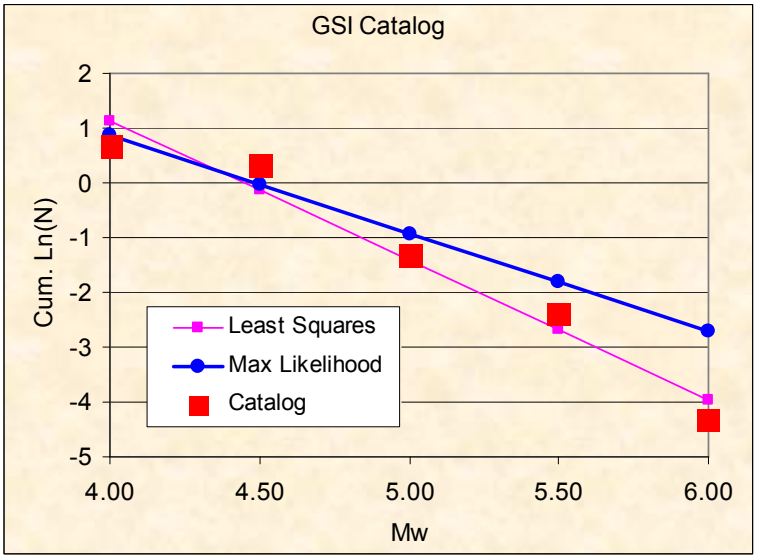

Figure 6.11 Regression results using the Least-Squares and Maximum Likelihood methods

Using the catalog based Magnitude Recurrence relationships; we calculate the cumulative event rates for specific minimum Magnitudes and compare with the parameters suggested by GSI. The table below gives the cumulative annual event rates for the different parameters:

Table 6.4. Cumulative event rates for given minimum magnitudes using different a- and b-values determined in this study. The rates are compared to the rates given by the catalog (top line)

Parameter Source	a-value	b-value	M 3.0	M 4.0	M 4.5	M 5.0	M 5.5	M 6.0
Catalog				1.948	1.385	0.263	0.092	0.013
GSI Approach	4.450	-0.850	79.433	11.220	4.217	1.585	0.596	0.224
Least-squares	4.629	-1.104	20.806	1.639	0.460	0.129	0.036	0.010
Maximum Likelihood	3.294	-0.778	9.115	1.519	0.620	0.253	0.103	0.042
Manual Calibration	4.300	-1.000	19.953	1.995	0.631	0.200	0.063	0.020
Final Model	4.000	-0.925	16.788	1.995	0.688	0.237	0.082	0.028

Table 6.3 shows that using a b-value of 0.85 and a-value of 4.45 as suggested by Dr. Talebian gives much higher event rates compared to the catalog. It should be noted that since the magnitudes considered in these comparisons are relatively low and more likely to be complete within the period of the catalog. Although it is possible that the rates determined from the catalog are not complete,

the true event rates are not expected to be very different from the rates recorded by the catalog. For example, the cumulative rate estimated by the a- and b-values suggested by Dr. Talebian for Magnitudes 4.0 to 6.0 is 11.22 events per year, while the catalog suggests a little less than 2 events per year (not counting foreshocks and aftershocks.)

As an alternative, a b-value of 1.0 is assumed for the background, given the relatively good fit of the Least-Squares method to the catalog rates. The b-value of 1.0 is also a good default value, when the b-value is unknown, especially for background seismicity. It is noted that the world-wide b-value average is very close to 1.0. Assuming a b-value of 1.0, the a-value is determined by manually adjusting the a-value so that the cumulative event rates for Mw 4.0 to 6.0 are a little bit higher than the catalog rate.

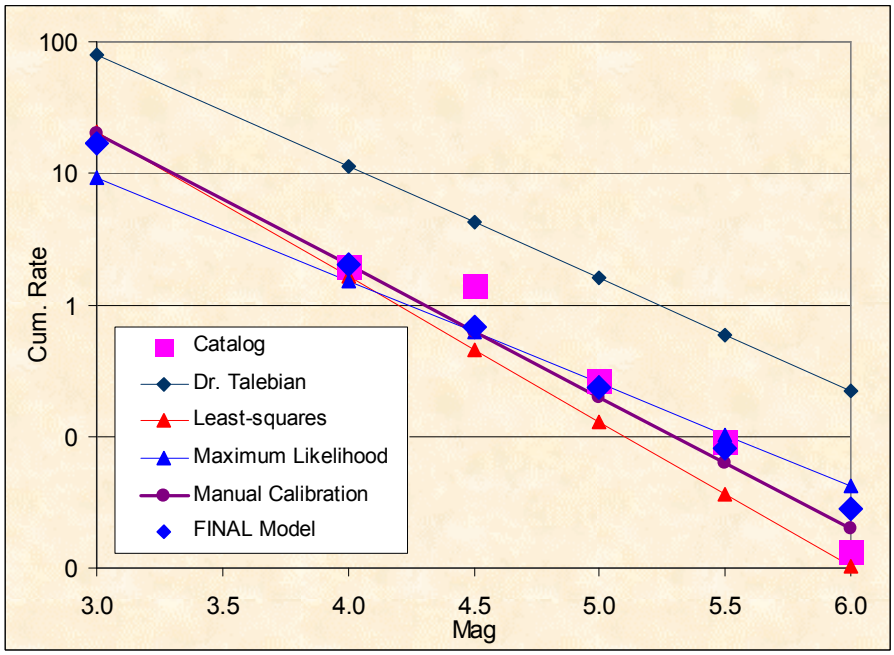

Figure 6.12. Plot of cumulative rates using the a- and b-values from different methods

Figure 6.12 above shows the relativities of the cumulative event rates determined by the different methods. It can be seen that the proposed a-value of 4.30 with a b-value of 1.0 has a good fit with the catalog rates, and gives results that are in between the rates suggested by the Least-Squares and Maximum Likelihood methods.

The final model uses a b-value as the average between 0.85 (suggested by Dr. Talebian) and 1.0 (worldwide average), equal to 0.925. This is to represent the uncertainty on the correct value of the

b-value. The a-value to use for the b-value = 0.925 is determined by using the cumulative events rates for Magnitude 4.0 (to 6.0) as a target and adjusting the a-value until the event rates for Magnitude 4.0 is very close to the target. This method sets the background rates close to the observed seismicity. As more information about the deformation of the crust in the study region is gathered, the results in this study should be reevaluated. During the development of seismic rate for faults and background seismicity the principal authors had significant amount of discussions with GSI and Dr. Talibian to finalize the rates.

6.3.7.2. Max and Min Magnitude

These specify the range of magnitudes of the stochastic events generated by the given source

- The maximum magnitude generated by the area source is Mw 6.0.
- The minimum magnitude for the faults is Mw 3.0 as proposed by GSI/Dr. Talebian and Dr. Berberian
- Events in the stochastic event set in the analysis are generated in 0.1 magnitude bin increments

6.3.7.3. Recurrence Relationship (a- and b-values)

These parameters affect the annual cumulative rates of occurrence of the stochastic events. The b-value gives the relativity of rates between smaller and larger magnitudes. The cumulative rates for events with magnitudes between the minimum and maximum magnitude are entered into the program. The program also uses the beta-value which can be directly calculated from the b-value: beta = b-value * LN(10).

The a- and b-values for the background source are based on the analysis of the catalog, GSI input as discussed in section 6.3.7.1. The b-value is fixed at -0.925 based on the analysis of the rates of events with magnitude, Mw 6.0 and below in the declustered catalog.

6.3.7.4. Background Source Coordinates

The background source used in the analysis is assumed to cover a rectangular area bound by these coordinates:

49.50, 34.00
53.50, 34.00
53.50, 37.00
49.50, 37.00

6.3.7.5. Rupture Length

The mean and standard deviation of the rupture length of the event (Magnitude-dependent function) , specified by the equation: log(rupture length in kilometers) = Al + Bl * (moment magnitude). The rupture is assumed to be horizontal and has no vertical dimension (that is, line rupture). These ruptures should also include a number of azimuths assigned in the input file. Area source ruptures assume the sigma value is 0.

- For this analysis, Al is equal to -4.0 and Bl is equal to 0.0. This effectively models the background sources as point sources.

- The number of azimuths is three (3). The long processing time required to generate the hazard maps is the main constraint for selecting a relatively low number of azimuths. Equal weight is given to each of the azimuths of the background events. However, since the background events have very short fault rupture lengths, the low number of azimuths does not have much effect.

6.3.7.6. Depth

The program is capable of uniformly distributing the events from area sources to a given range of depths. The depth increment used to distribute the event depths in the area sources is specified as an input to the program.

- The depth of the background source is assumed to be 5 km., that is, the minimum and maximum depths are entered as 5 km.
- Since the depth is constant in the analysis, the increment in the depth distribution is not used.

6.4. Numerical Approximations – Analysis Results

In calculating the seismic hazard, numerical techniques are used to simplify the calculations and avoid complicated closed form solutions. A good example of this is the discretization of the parameter distributions such that the integration over the values of the parameters is replaced by numerical integration. The seismic hazard program also considers some level of uncertainty in the models by using a kind of logic-tree approach, which uses alternatives and applies a weight to each case to represent their relative uncertainty. Whenever a numerical integration or logic-tree is used, the occurrence rate of a given event is also distributed according to the assumed probability distribution of the parameters.

6.4.1. Magnitude

The magnitude is discretized at 0.1 bins, except near the maximum magnitude where it may be at 0.01 magnitude bins. The magnitude bin defines the conditional probability of an event with a certain magnitude by using the Guttenberg-Richter magnitude recurrence relationship. All stochastic events in a source with magnitudes within a magnitude bin will contribute to the annual rate of occurrence for that bin.

6.4.2. Rupture Area

After the list of magnitudes that are generated by a source is compiled, the location of the fault rupture is considered next. For large magnitude events, especially near the maximum magnitude, the fault/source usually ruptures as a whole so that the entire occurrence rate for the magnitude is assigned to just one event. For smaller magnitudes, the rupture length, rupture width, or rupture area may be smaller than the source dimensions so that the location of the event rupture may be distributed along the source dimension. The seismic hazard program considers this by sampling against the distribution of the rupture length, rupture width, or rupture area and moving this event rupture area around the source dimension at specified intervals. The parameters used in this process are entered as numerical calculation parameters into the program.

6.4.3. Numerical Calculation Parameters

Each type of source in the program can have specific numerical calculation parameters so that they can be adjusted to provide a balance between numerical accuracy and runtime performance. In this analysis, only the faults and area source types are used. The larger magnitudes are assumed to be generated by the faults and the smaller events are generated by the area source to represent the background seismicity. The parameters used in this project are given below

- **Faults:**

Parameter	Value
Down dip integration increment	5 km
Horizontal integration increment	10 km
Number rupture length per Earthquake	1
Include near-source directivity	NO

- **Area Sources:**

Parameter	Value
Maximum inclusion distance	300 km
Vertical integration increment	3 km
Number of rupture azimuths	3
Minimum epicentral distance step	0.5 km
Maximum epicentral distance step	10 km

6.4.4. Calculation of Event Rates

The calculation of stochastic event rates is independent of the ground motion relationships. However, multiple attenuation relationships are implemented to account for epistemic uncertainty in the ground motion model using a logic-tree approach with equal weights.

6.4.5. Calculating the Site Hazard Value per Event

Assuming that all the parameters defining an event are known, the hazard in a site due to the event is estimated using attenuation relationships. Attenuation relationships are mostly dependent on the

magnitude of the event and the distance of the site to the fault rupture. Contemporary attenuation relationships consider other parameters that are found to be correlated with the observed hazard values. The common parameters include the fault rupture type, soil amplification effect, hanging wall effect, depth of focus, etc. In this analysis, the following seven attenuation relationships are used. Also, ground motion modeling section 5 discusses the NGA attenuation functions and their applicability to Iran.

1- **Name: Boore-Atkinson (2006) NGA**

Base: Boore-Atkinson 2006 NGA
Truncation Type: No Truncation
Truncation Value: 0
Magnitude Scale: Moment Magnitude
Distance Type: Horizontal Distance to Rupture

2- **Name: Campbell-Bozorgnia (2006) NGA**

Base: Campbell-Bozorgnia 2006 NGA
Truncation Type: No Truncation
Truncation Value: 0
Magnitude Scale: Moment Magnitude
Distance Type: Distance to Rupture

3 - Name: Chiou-Youngs (2006) NGA

Base: Chiou-Youngs 2006 NGA
Truncation Type: No Truncation
Truncation Value: 0
Magnitude Scale: Moment Magnitude
Distance Type: Distance to Rupture

4 - Name: Abra.-Silva (1997) Rock USGS 2002

Base: Abrahamson-Silva 1997
Truncation Type: Trunc Sigma*Value
Truncation Value: 3

Magnitude Scale: Moment Magnitude

Distance Type: Distance to Rupture

5 - Name: Boore-Joyner-Fumal (1997) USGS 2002

Base: Boore-Joyner-Fumal 1997

Truncation Type: Trunc Sigma*Value

Truncation Value: 3

Magnitude Scale: Moment Magnitude

Distance Type: Horizontal Distance to Rupture

6 - Name: Campbell-Bozorgnia (2003) USGS 2002

Base: Campbell-Bozorgnia 2003-2

Truncation Type: Trunc Sigma*Value

Truncation Value: 3

Magnitude Scale: Moment Magnitude

Distance Type: Distance To Rupture

7 - Name: Sadigh (1997) Rock USGS 2002

Base: Sadigh 1997 Rock

Truncation Type: Trunc Sigma*Value

Truncation Value: 3

Magnitude Scale: Moment Magnitude

Distance Type: Distance to Rupture

The first three attenuation relationships were used in the 2007 USGS National Seismic Hazard Maps for the Western United States. The USGS methodology includes additional epistemic uncertainty by considering a higher and lower value of the hazard relative to the median estimate. However, the computer program used in this analysis does not have the feature built in and would require substantial effort to include this feature. To compensate for the epistemic uncertainty, the last four attenuation relationships used in the previous version of the USGS Hazard Maps are also included. The results from these attenuation relationships are equally weighted.

6.4.6. Incorporating Uncertainty

Incorporating some uncertainty into the analysis are performed by sampling and/or the logic-tree approach, have been discussed throughout this document. While this section tries to explicitly identify the types of uncertainty considered in the analysis, it will not include the specific parameters used, which have been already given in previous discussions.

6.4.6.1. Epistemic Uncertainty in Ground Motion Model

The analysis uses seven attenuation relationships to account for the epistemic uncertainty of the ground motion relationship used. Attenuation relationships are matched with the fault rupture type.

6.4.6.2. Aleatory Uncertainty in Rupture Geometry

For each magnitude generated by one source, there can be several ways that the actual fault rupture can happen. This uncertainty in the actual event rupture is considered by assuming a distribution of the length, width, or area of the rupture surface for a given magnitude. The location of the event rupture is moved around the source dimension by incrementally moving the event according to the interpolation parameters set in the program.

6.4.7. Calculating the Hazard Exceedance Probability

The exceedance probability for a given site is calculated as the sum of probabilities of exceeding a given hazard value for each stochastic event in the model. This includes the branches of the logic trees generated to account for epistemic and aleatory uncertainty in the model. By calculating the exceedance probability for a range of hazard values, the hazard curve can be derived. The technical aspects of the seismic hazard analysis are given in section 6.2.

Hazard maps are usually generated for a single risk level or exceedance probability, so the hazard value corresponding to the risk of the map is extracted from the hazard curve. This process is repeated for several grid points in a region to create a map.

6.4.8. Single Site Results

The main objective of this study is to develop the seismic hazard maps for the region around Tehran. However, a hazard map can only show one parameter at a time and it is important to have a deeper view of the hazard at individual sites. This gives the users a better feel for the characteristics of the hazard in several ways.

First, we look at the influence of the largest probable events that give the biggest effects to the three sites by performing deterministic analyses. The largest magnitudes from two of the closest faults are considered. The ground motion from each of the attenuation relationships considered in this study are given as a median value and at the 84^{th} percentile level to represent the ground motion at the mean plus one standard deviation. The values for the PGA as well as response acceleration spectra, Sa, for the periods 0.2, 1.0, and 3.0 seconds are given.

Next, we look at the hazard curves for the three sites due to each of the attenuation relationships used and the mean value. The hazard curves show the level of ground motion at different annual exceedance rates (reciprocal of the return period.) The curves will show the degree of uncertainty in the hazard due to the choice of attenuation relationships. The curves given in this report is for the PGA only, but the hazard curves for other Sa periods were also calculated as part of the analyses.

Finally, the hazard values for the PGA and three Sa periods are given in tables as a function of the return period. The values for each attenuation relationship are given to enable comparison with the mean value and give an idea of the sensitivity of the hazard values to the attenuation relationships at different recurrence return periods.

For this study, we chose three sites around Tehran that may be interesting in terms of concentration of exposure and proximity to active faults. The coordinates of the sites are given below and their locations are shown in Figures 6.13 and 6.14

- Site 1 (51.45E, 35.75N)
- Site 2 (51.44E, 35.60N)
- Site 3 (51.42E, 35.64N)

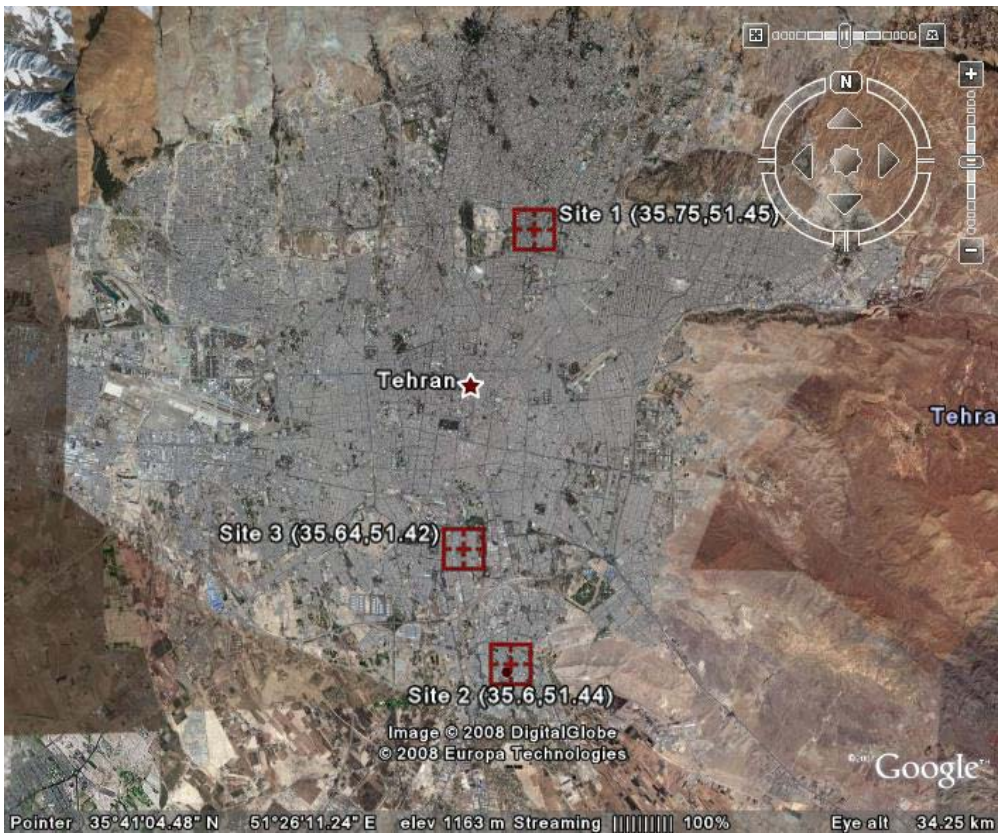

Figure 6.13. Locations of the three test sites used in the study relative to Tehran

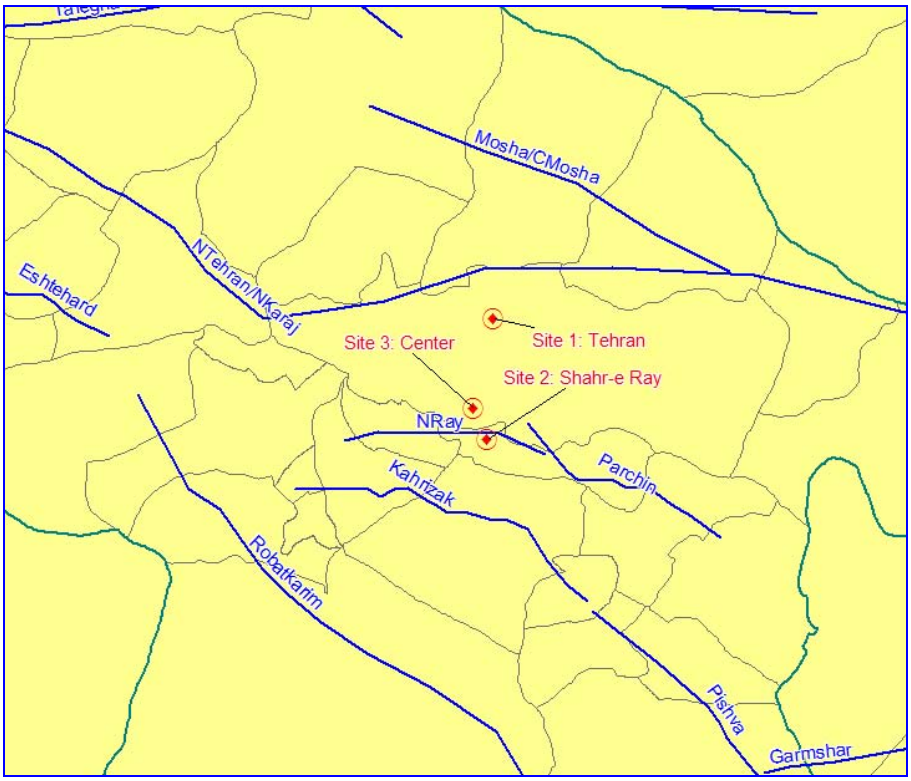

Figure 6.14. Map of locations of the three test sites used in the study relative to the active faults in the model

6.4.8.1 Site 1 Results

The results of the deterministic analyses are given in the following tables.

Source: N. Tehran/N. Karaj
Closest Distance: 6.87 km
Amplitude Units: Acceleration (g)
Magnitude: 7.50 Mw

Median	Periods, T (s)			
Attenuation Relationship	PGA	0.2	1.0	3.0
Boore-Atkinson (2006) NGA	0.350	0.852	0.298	0.106
Campbell-Bozorgnia (2006) NGA	0.387	0.970	0.353	0.121
Chiou-Youngs (2006) NGA	0.490	1.270	0.387	0.098
Abra.-Silva (1997) Rock USGS 2002	0.597	1.443	0.552	0.151
Boore-Joyner-Fumal (1997) USGS 2002	0.450	0.989	0.544	0.175
Campbell-Bozorgnia (2003) USGS 2002	0.482	0.928	0.483	0.179
Sadigh (1997) Rock USGS 2002	0.547	1.295	0.558	0.148
AVERAGE	0.472	1.107	0.454	0.140

Fractile: 0.84	Periods, T (s)			
Attenuation Relationship	PGA	0.2	1.0	3.0
Boore-Atkinson (2006) NGA	0.523	1.290	0.459	0.166
Campbell-Bozorgnia (2006) NGA	0.577	1.485	0.549	0.190
Chiou-Youngs (2006) NGA	0.731	1.932	0.595	0.153
Abra.-Silva (1997) Rock USGS 2002	0.835	2.094	0.836	0.235
Boore-Joyner-Fumal (1997) USGS 2002	0.651	1.413	0.814	0.268
Campbell-Bozorgnia (2003) USGS 2002	0.663	1.322	0.701	0.260
Sadigh (1997) Rock USGS 2002	0.743	1.801	0.818	0.217
AVERAGE	0.675	1.620	0.682	0.213

Source: N. Ray
Closest Distance: 11.13 km
Amplitude Units: Acceleration (g)
Magnitude: 6.70 Mw

Median	Periods, T (s)			
Attenuation Relationship	PGA	0.2	1.0	3.0
Boore-Atkinson (2006) NGA	0.572	1.408	0.439	0.093
Campbell-Bozorgnia (2006) NGA	0.409	1.088	0.272	0.051
Chiou-Youngs (2006) NGA	0.434	1.094	0.231	0.043
Abra.-Silva (1997) Rock USGS 2002	0.453	1.061	0.280	0.058
Boore-Joyner-Fumal (1997) USGS 2002	0.476	1.186	0.558	0.114
Campbell-Bozorgnia (2003) USGS 2002	0.405	0.912	0.302	0.056
Sadigh (1997) Rock USGS 2002	0.414	0.967	0.336	0.079
AVERAGE	0.452	1.102	0.346	0.071

Fractile: 0.84	Periods, T (s)			
Attenuation Relationship	PGA	0.2	1.0	3.0
Boore-Atkinson (2006) NGA	0.854	2.132	0.678	0.146
Campbell-Bozorgnia (2006) NGA	0.609	1.666	0.423	0.080
Chiou-Youngs (2006) NGA	0.647	1.665	0.355	0.066
Abra.-Silva (1997) Rock USGS 2002	0.648	1.569	0.430	0.090
Boore-Joyner-Fumal (1997) USGS 2002	0.689	1.694	0.836	0.174
Campbell-Bozorgnia (2003) USGS 2002	0.557	1.298	0.439	0.082
Sadigh (1997) Rock USGS 2002	0.586	1.397	0.508	0.120
AVERAGE	0.656	1.632	0.524	0.108

The hazard curves for Site 1 based on each of the attenuation relationships used and the mean are given in Figure 6.15.

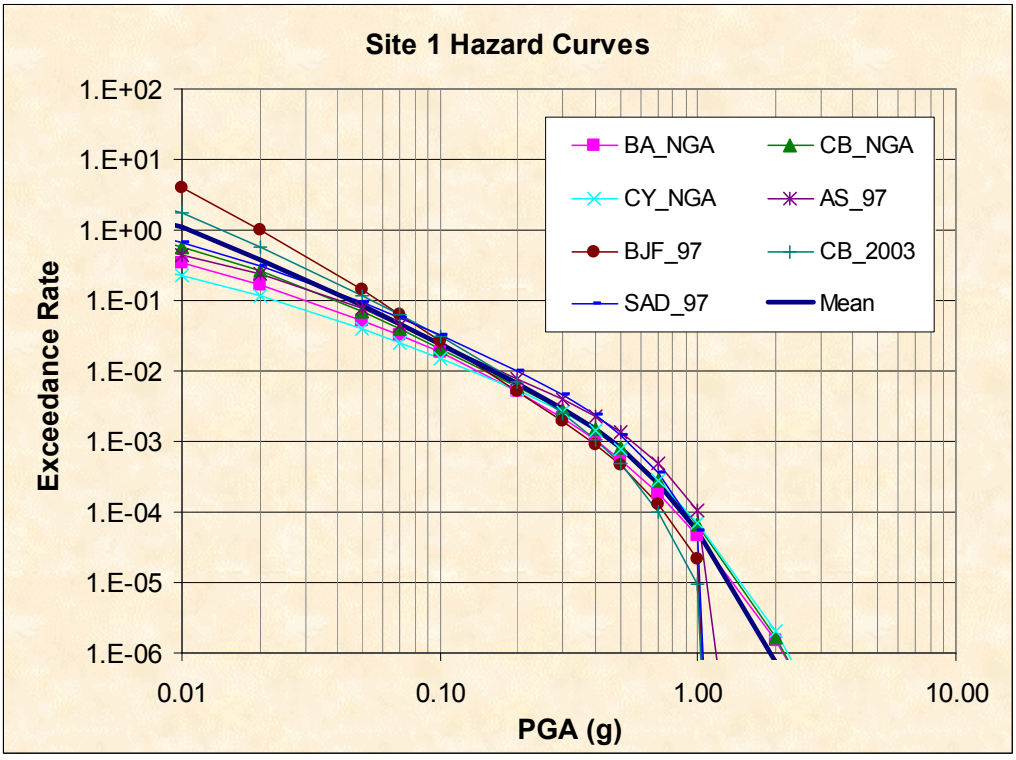

Figure 6.15. Hazard curves for Site 1 for each attenuation relationship used and the mean

The Uniform Hazard Spectra values for Site 1 for each attenuation relationship used and the mean are given in the following tables.

475-years Return Period	Spectra Period, T (s)			
Attenuation Relationship	PGA	0.2	1.0	3.0
Mean	0.347	0.834	0.259	0.069
NGA - Boore & Atkinson	0.303	0.721	0.230	0.058
NGA - Campbell & Bozorgnia	0.342	0.898	0.226	0.054
NGA - Chiou & Youngs	0.332	0.808	0.203	0.044
USGS2002 - Abrahamson & Silva	0.413	0.973	0.324	0.085
USGS2002 - Boore, Joyner & Fumal	0.292	0.734	0.234	0.081
USGS2002 - Campbell-Bozorgnia (2003)	0.320	0.772	0.255	0.066
USGS2002 - Sadigh (1997) Rock	0.414	0.946	0.315	0.077

975-years Return Period	Spectra Period, T (s)			
Attenuation Relationship	PGA	0.2	1.0	3.0
Mean	0.459	1.104	0.356	0.095
NGA - Boore & Atkinson	0.403	0.976	0.314	0.080
NGA - Campbell & Bozorgnia	0.459	1.202	0.312	0.075
NGA - Chiou & Youngs	0.453	1.112	0.287	0.064
USGS2002 - Abrahamson & Silva	0.546	1.273	0.436	0.113
USGS2002 - Boore, Joyner & Fumal	0.384	0.976	0.332	0.111
USGS2002 - Campbell-Bozorgnia (2003)	0.405	0.967	0.339	0.095
USGS2002 - Sadigh (1997) Rock	0.525	1.183	0.430	0.104

2,475-years Return Period	Spectra Period, T (s)			
Attenuation Relationship	PGA	0.2	1.0	3.0
Mean	0.613	1.488	0.507	0.134
NGA - Boore & Atkinson	0.550	1.331	0.445	0.115
NGA - Campbell & Bozorgnia	0.623	1.691	0.447	0.111
NGA - Chiou & Youngs	0.622	1.559	0.420	0.097
USGS2002 - Abrahamson & Silva	0.728	1.781	0.608	0.158
USGS2002 - Boore, Joyner & Fumal	0.517	1.246	0.493	0.157
USGS2002 - Campbell-Bozorgnia (2003)	0.518	1.184	0.464	0.138
USGS2002 - Sadigh (1997) Rock	0.674	1.542	0.595	0.140

6.4.8.2.Site 2 Results

The results of the deterministic analyses are given in the following tables.

Source: N. Ray
Closest Distance: 0.95 km
Amplitude Units: Acceleration (g)
Magnitude: 6.70 Mw

Median	Periods, T (s)			
Attenuation Relationship	PGA	0.2	1.0	3.0
Boore-Atkinson (2006) NGA	0.556	1.380	0.433	0.092
Campbell-Bozorgnia (2006) NGA	0.642	1.476	0.498	0.116
Chiou-Youngs (2006) NGA	0.683	1.780	0.526	0.120
Abra.-Silva (1997) Rock USGS 2002	1.069	2.644	0.677	0.126
Boore-Joyner-Fumal (1997) USGS 2002	0.474	1.182	0.550	0.113
Campbell-Bozorgnia (2003) USGS 2002	0.848	1.441	0.810	0.209
Sadigh (1997) Rock USGS 2002	0.933	2.160	0.673	0.147
AVERAGE	0.743	1.723	0.595	0.132

Fractile: 0.84	Periods, T (s)			
Attenuation Relationship	PGA	0.2	1.0	3.0
Boore-Atkinson (2006) NGA	0.830	2.090	0.667	0.144
Campbell-Bozorgnia (2006) NGA	0.956	2.260	0.774	0.181
Chiou-Youngs (2006) NGA	1.019	2.708	0.808	0.187
Abra.-Silva (1997) Rock USGS 2002	1.529	3.911	1.039	0.199
Boore-Joyner-Fumal (1997) USGS 2002	0.686	1.688	0.823	0.173
Campbell-Bozorgnia (2003) USGS 2002	1.167	2.052	1.177	0.303
Sadigh (1997) Rock USGS 2002	1.320	3.121	1.018	0.223
AVERAGE	1.072	2.547	0.901	0.201

Source: Parchin
Closest Distance: 5.94 km
Amplitude Units: Acceleration (g)
Magnitude: 6.80 Mw

Median	Periods, T (s)			
Attenuation Relationship	PGA	0.2	1.0	3.0
Boore-Atkinson (2006) NGA	0.333	0.840	0.276	0.061
Campbell-Bozorgnia (2006) NGA	0.397	0.999	0.279	0.074
Chiou-Youngs (2006) NGA	0.432	1.090	0.304	0.070
Abra.-Silva (1997) Rock USGS 2002	0.730	1.739	0.441	0.088
Boore-Joyner-Fumal (1997) USGS 2002	0.376	0.967	0.328	0.095
Campbell-Bozorgnia (2003) USGS 2002	0.590	1.178	0.494	0.109
Sadigh (1997) Rock USGS 2002	0.614	1.431	0.492	0.114
AVERAGE	0.496	1.178	0.373	0.087

Fractile: 0.84	Periods, T (s)			
Attenuation Relationship	PGA	0.2	1.0	3.0
Boore-Atkinson (2006) NGA	0.497	1.272	0.425	0.096
Campbell-Bozorgnia (2006) NGA	0.591	1.530	0.434	0.116
Chiou-Youngs (2006) NGA	0.644	1.660	0.467	0.109

Abra.-Silva (1997) Rock USGS 2002	1.036	2.556	0.673	0.138
Boore-Joyner-Fumal (1997) USGS 2002	0.544	1.381	0.491	0.145
Campbell-Bozorgnia (2003) USGS 2002	0.811	1.678	0.718	0.158
Sadigh (1997) Rock USGS 2002	0.862	2.053	0.739	0.172
AVERAGE	0.712	1.733	0.564	0.134

The hazard curves for Site 2 based on each of the attenuation relationships used and the mean are given in Figure 6.16.

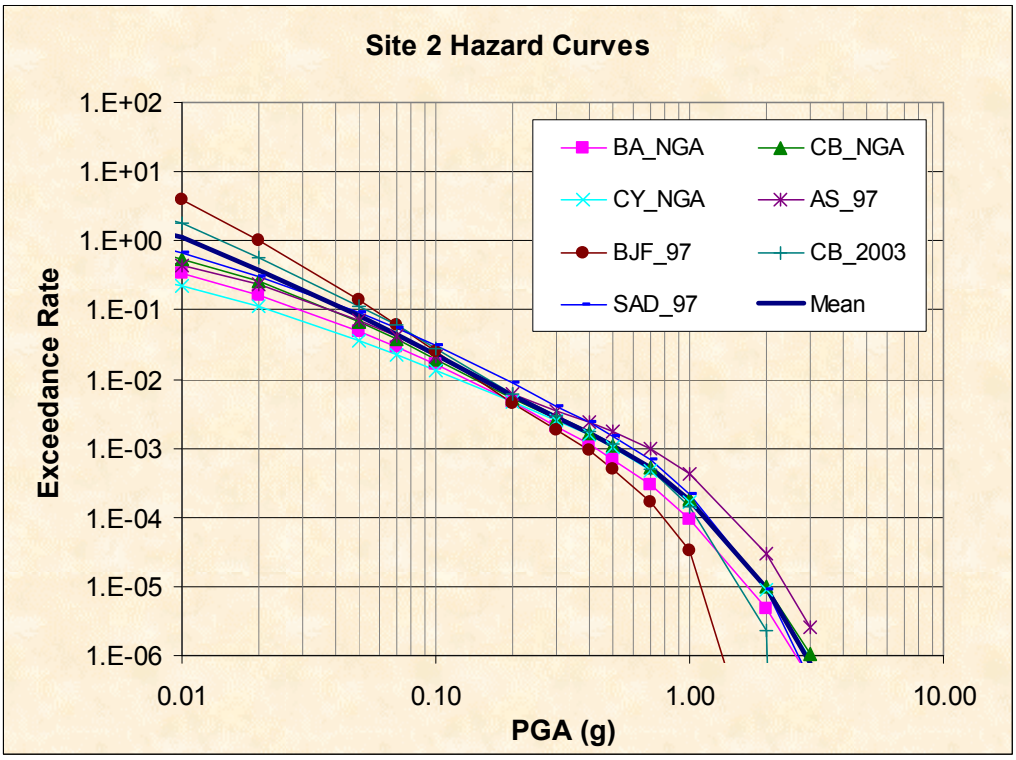

Figure 6.16. Hazard curves for Site 2 for each attenuation relationship used and the mean

The Uniform Hazard Spectra values for Site 2 for each attenuation relationship used and the mean are given in the following tables.

475-years Return Period	Spectra Period, T (s)			
Attenuation Relationship	PGA	0.2	1.0	3.0
Mean	0.353	0.836	0.255	0.065
NGA - Boore & Atkinson	0.299	0.703	0.224	0.055
NGA - Campbell & Bozorgnia	0.348	0.888	0.224	0.051
NGA - Chiou & Youngs	0.336	0.813	0.197	0.042
USGS2002 - Abrahamson & Silva	0.440	1.013	0.313	0.080
USGS2002 - Boore, Joyner & Fumal	0.281	0.689	0.226	0.074
USGS2002 - Campbell-Bozorgnia (2003)	0.360	0.834	0.270	0.064
USGS2002 - Sadigh (1997) Rock	0.423	0.952	0.299	0.073

975-years Return Period	Spectra Period, T (s)			
Attenuation Relationship	PGA	0.2	1.0	3.0
Mean	0.517	1.195	0.365	0.088
NGA - Boore & Atkinson	0.419	1.004	0.314	0.075
NGA - Campbell & Bozorgnia	0.515	1.282	0.329	0.071
NGA - Chiou & Youngs	0.502	1.205	0.298	0.061
USGS2002 - Abrahamson & Silva	0.687	1.552	0.430	0.105
USGS2002 - Boore, Joyner & Fumal	0.384	0.963	0.335	0.100
USGS2002 - Campbell-Bozorgnia (2003)	0.525	1.113	0.391	0.089
USGS2002 - Sadigh (1997) Rock	0.585	1.306	0.423	0.099

2,475-years Return Period	Spectra Period, T (s)			
Attenuation Relationship	PGA	0.2	1.0	3.0
Mean	0.760	1.806	0.547	0.125
NGA - Boore & Atkinson	0.616	1.465	0.468	0.108
NGA - Campbell & Bozorgnia	0.760	1.999	0.508	0.104
NGA - Chiou & Youngs	0.739	1.877	0.459	0.094
USGS2002 - Abrahamson & Silva	1.010	2.439	0.624	0.142
USGS2002 - Boore, Joyner & Fumal	0.535	1.282	0.521	0.136
USGS2002 - Campbell-Bozorgnia (2003)	0.744	1.506	0.591	0.131
USGS2002 - Sadigh (1997) Rock	0.823	1.943	0.616	0.136

6.4.8.3 Site 3 Results

The results of the deterministic analyses are given in the following tables.

Source: N. Ray
Closest Distance: 2.46 km
Amplitude Units: Acceleration (g)
Magnitude: 6.70 Mw

Median	Periods, T (s)			
Attenuation Relationship	PGA	0.2	1.0	3.0
Boore-Atkinson (2006) NGA	0.601	1.454	0.451	0.095
Campbell-Bozorgnia (2006) NGA	0.829	1.977	0.623	0.115
Chiou-Youngs (2006) NGA	0.866	2.281	0.537	0.102
Abra.-Silva (1997) Rock USGS 2002	0.986	2.409	0.601	0.113
Boore-Joyner-Fumal (1997) USGS 2002	0.479	1.192	0.572	0.115
Campbell-Bozorgnia (2003) USGS 2002	0.806	1.424	0.719	0.167
Sadigh (1997) Rock USGS 2002	0.809	1.877	0.596	0.132
AVERAGE	0.768	1.802	0.586	0.120

Fractile: 0.84	Periods, T (s)			
Attenuation Relationship	PGA	0.2	1.0	3.0
Boore-Atkinson (2006) NGA	0.898	2.202	0.695	0.149

Campbell-Bozorgnia (2006) NGA	1.235	3.028	0.968	0.180
Chiou-Youngs (2006) NGA	1.293	3.471	0.824	0.159
Abra.-Silva (1997) Rock USGS 2002	1.410	3.563	0.922	0.178
Boore-Joyner-Fumal (1997) USGS 2002	0.693	1.703	0.857	0.175
Campbell-Bozorgnia (2003) USGS 2002	1.108	2.027	1.045	0.242
Sadigh (1997) Rock USGS 2002	1.145	2.712	0.902	0.200
AVERAGE	1.112	2.672	0.888	0.183

Source: Parchin
Closest Distance: 7.53 km
Amplitude Units: Acceleration (g)
Magnitude: 6.80 Mw

Median	Periods, T (s)			
Attenuation Relationship	PGA	0.2	1.0	3.0
Boore-Atkinson (2006) NGA	0.300	0.745	0.243	0.054
Campbell-Bozorgnia (2006) NGA	0.347	0.892	0.240	0.064
Chiou-Youngs (2006) NGA	0.379	0.949	0.261	0.060
Abra.-Silva (1997) Rock USGS 2002	0.628	1.485	0.383	0.078
Boore-Joyner-Fumal (1997) USGS 2002	0.337	0.871	0.279	0.085
Campbell-Bozorgnia (2003) USGS 2002	0.512	1.073	0.420	0.090
Sadigh (1997) Rock USGS 2002	0.545	1.273	0.445	0.105
AVERAGE	0.435	1.041	0.324	0.077

Fractile: 0.84	Periods, T (s)			
Attenuation Relationship	PGA	0.2	1.0	3.0
Boore-Atkinson (2006) NGA	0.447	1.128	0.374	0.085
Campbell-Bozorgnia (2006) NGA	0.517	1.366	0.374	0.100
Chiou-Youngs (2006) NGA	0.565	1.445	0.401	0.093
Abra.-Silva (1997) Rock USGS 2002	0.891	2.183	0.585	0.122
Boore-Joyner-Fumal (1997) USGS 2002	0.488	1.244	0.418	0.130
Campbell-Bozorgnia (2003) USGS 2002	0.705	1.528	0.611	0.132
Sadigh (1997) Rock USGS 2002	0.766	1.826	0.668	0.157
AVERAGE	0.626	1.531	0.490	0.117

The hazard curves for Site 3 based on each of the attenuation relationships used and the mean are given in Figure 6.17.

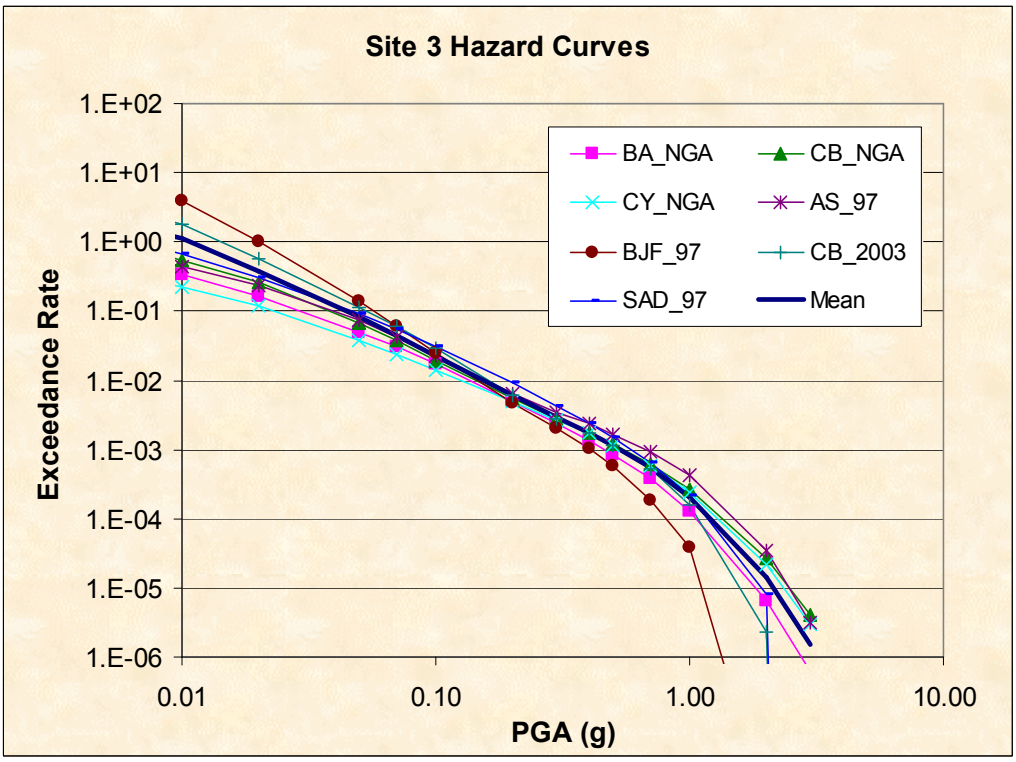

Figure 6.17. Hazard curves for Site 3 for each attenuation relationship used and the mean

The Uniform Hazard Spectra values for Site 1 for each attenuation relationship used and the mean are given in the following tables.

475-years Return Period	Spectra Period, T (s)			
Attenuation Relationship	PGA	0.2	1.0	3.0
Mean	0.361	0.858	0.264	0.067
NGA - Boore & Atkinson	0.318	0.745	0.236	0.057
NGA - Campbell & Bozorgnia	0.357	0.921	0.233	0.053
NGA - Chiou & Youngs	0.349	0.848	0.204	0.043
USGS2002 - Abrahamson & Silva	0.431	1.006	0.318	0.082
USGS2002 - Boore, Joyner & Fumal	0.292	0.718	0.243	0.077
USGS2002 - Campbell-Bozorgnia (2003)	0.356	0.833	0.274	0.066
USGS2002 - Sadigh (1997) Rock	0.423	0.956	0.305	0.074

975-years Return Period	Spectra Period, T (s)			
Attenuation Relationship	PGA	0.2	1.0	3.0
Mean	0.527	1.225	0.379	0.091
NGA - Boore & Atkinson	0.457	1.072	0.335	0.079
NGA - Campbell & Bozorgnia	0.540	1.354	0.348	0.073
NGA - Chiou & Youngs	0.530	1.288	0.309	0.063
USGS2002 - Abrahamson & Silva	0.668	1.533	0.436	0.107
USGS2002 - Boore, Joyner & Fumal	0.403	1.006	0.366	0.104
USGS2002 - Campbell-Bozorgnia (2003)	0.520	1.108	0.395	0.092

USGS2002 - Sadigh (1997) Rock	0.578	1.298	0.427	0.101

2,475-years Return Period	Spectra Period, T (s)			
Attenuation Relationship	PGA	0.2	1.0	3.0
Mean	0.785	1.874	0.568	0.127
NGA - Boore & Atkinson	0.679	1.589	0.502	0.114
NGA - Campbell & Bozorgnia	0.836	2.149	0.558	0.108
NGA - Chiou & Youngs	0.814	2.093	0.487	0.095
USGS2002 - Abrahamson & Silva	1.010	2.434	0.631	0.145
USGS2002 - Boore, Joyner & Fumal	0.556	1.324	0.562	0.141
USGS2002 - Campbell-Bozorgnia (2003)	0.754	1.506	0.593	0.129
USGS2002 - Sadigh (1997) Rock	0.813	1.909	0.614	0.137

6.4.9. Hazard Map Results

The analysis process for generating the hazard maps is the same as for the single sites. However, many of the intermediate results are not saved because the amount of data would be very large and may not be as relevant since many of the values do not change significantly across adjacent sites in a grid.

This study uses a 0.02-degree (approx. 2-km) uniformly spaced grid of points to define the hazard maps. The resolution of the analyses is dependent mostly on the amount of computer time that can be performed within the study timeline.

The hazard maps presented in this report is limited to the PGA hazard maps for the 75, 475, 1000, and 2475-year return periods. The maps assume a uniform site condition with an average shear wave velocity at the top 30 meters, Vs_{30}, to be equal to150, 225, 525, 760 and 1070 m/s. The 760 m/s site condition is the same as the one used in the USGS National Seismic Hazard Maps of the United States.

Although, only PGA hazard maps are shown in this report, the study generated the hazard map values for other Sa periods as well for the three return periods. These data are given in the hazard database files submitted as a supplement to this report. Figure 6.18 to 6.21 show the PGA hazard map for different return periods.

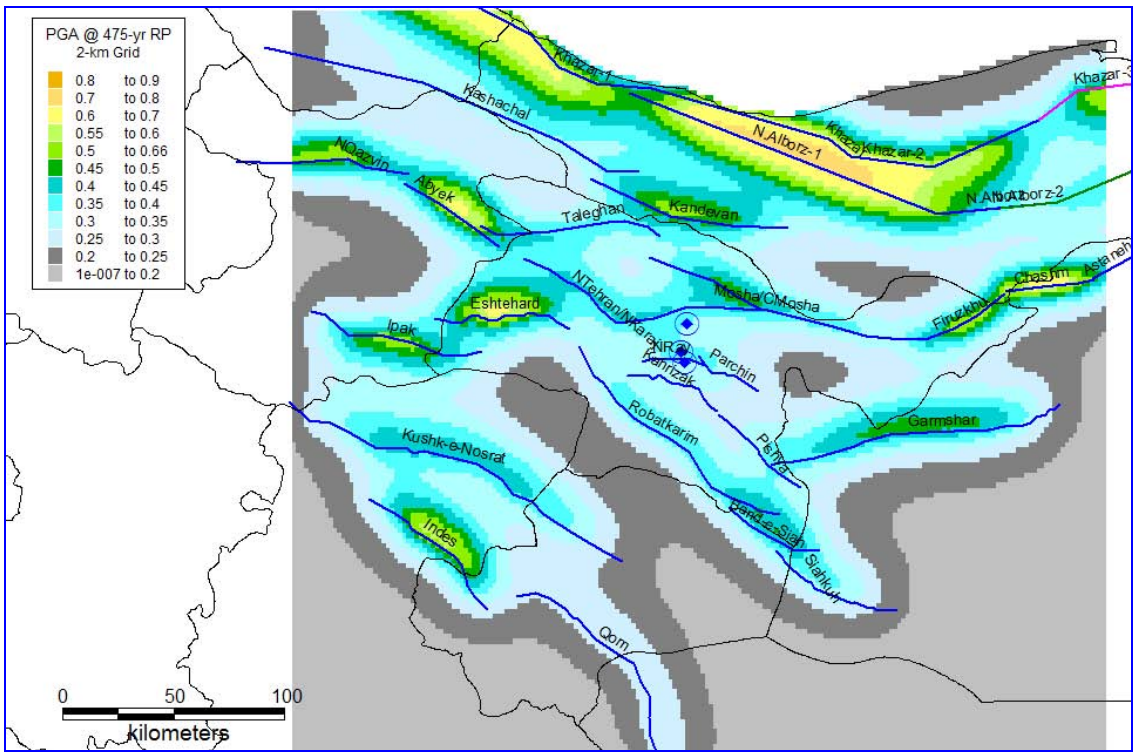

Figure 6.18. PGA hazard map of the study region with a 475-year return period

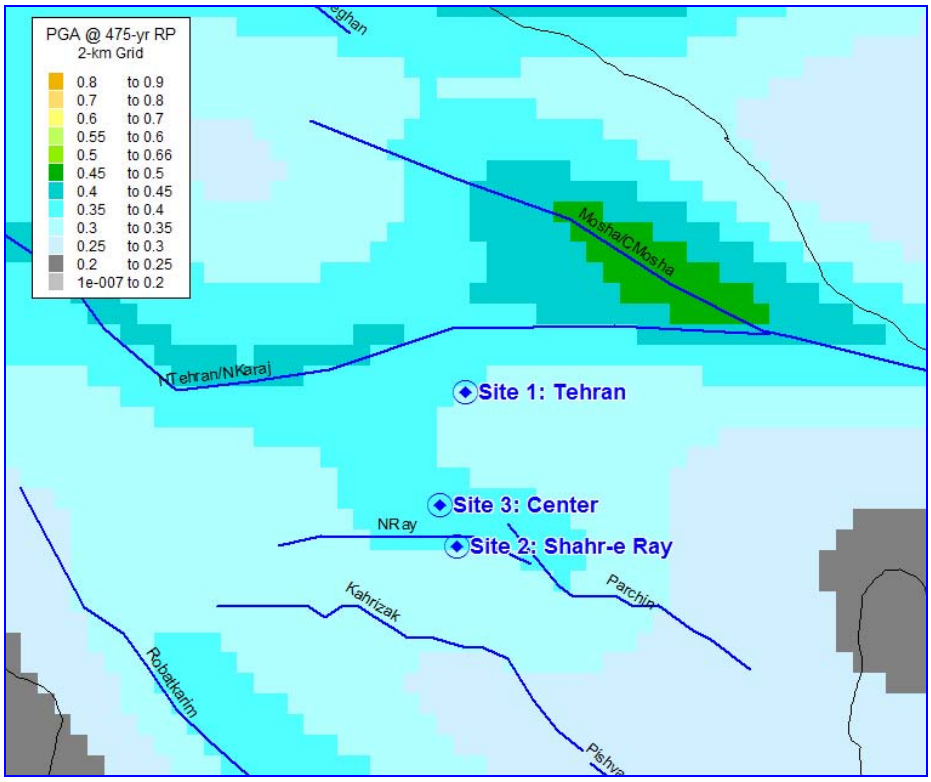

Figure 6.10. PGA hazard map in the vicinity of the three test sites with a 475-year return period

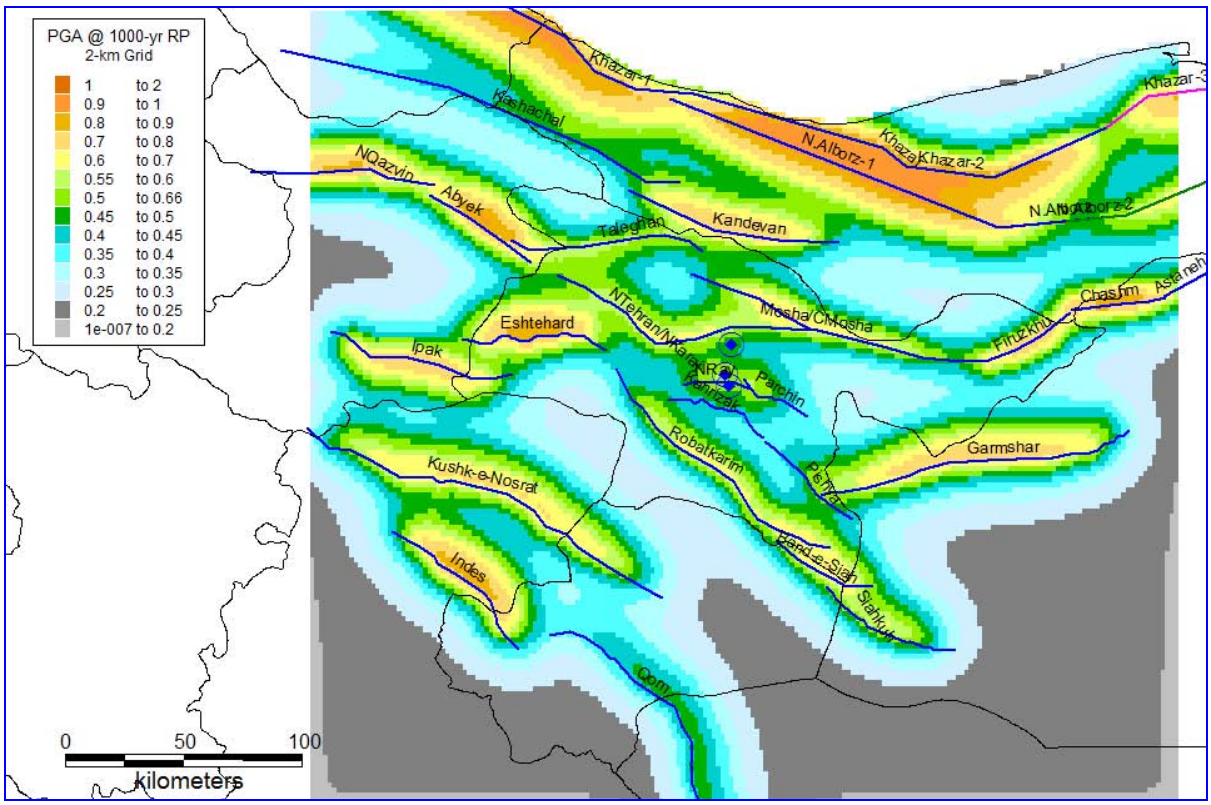

Figure 6.20. PGA hazard map of the study region with a 1000-year return period

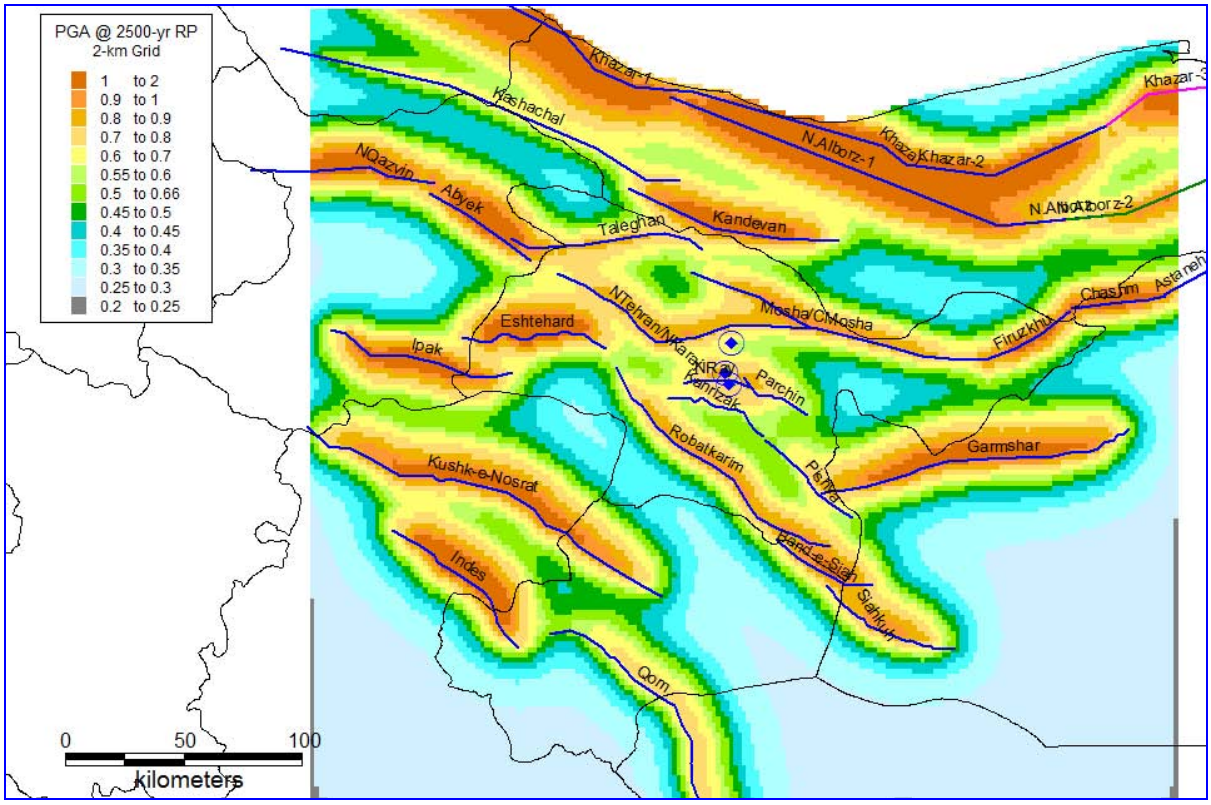

Figure 6.21. PGA hazard map of the study region with a 2475-year return period

6.5.Final active fault map and calculation of seismic parameters by Geological Survey of Iran

Fault map

The fault map is originally prepared based on 1:250,000 geological maps of the Geological Survey of Iran, and then modified using field observations and other published or unpublished data. SRTM topographic data has later been used to correct the trace of each fault. Thus in most places, especially where the fault cuts young deposits or produces a sharp escarpment, the accuracy of the fault trace should be within the resolution of SRTM data (about 90 meters).

All faults within the area of study are classified into two major groups: 1) Major active faults, for which we have some evidence about their recent activity, and thus have higher potential of causing earthquake in the future, and 2) other faults, which we do not have convincing evidence about their activity.

Evidence of activity includes both geological and seismological data. The geological data are mainly geomorphic observations and paleoseimological studies, especially when the fault activity is recorded by offset of young (Quaternary age) deposits.
The seismological data include all available information about the past (reports of historic and pre-historic earthquakes) or present-day activity of the fault (instrumental records of earthquakes).

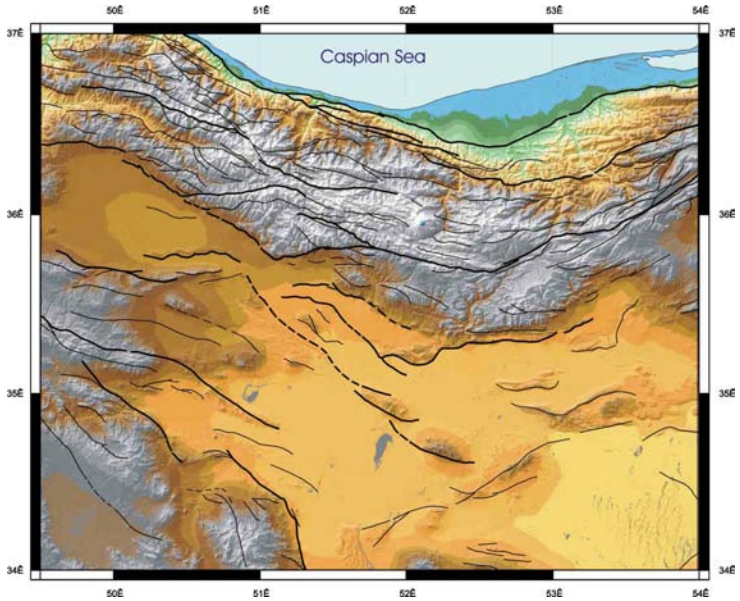

Figure 6.22. Major active faults (thicker lines) and other faults in greater Tehran region

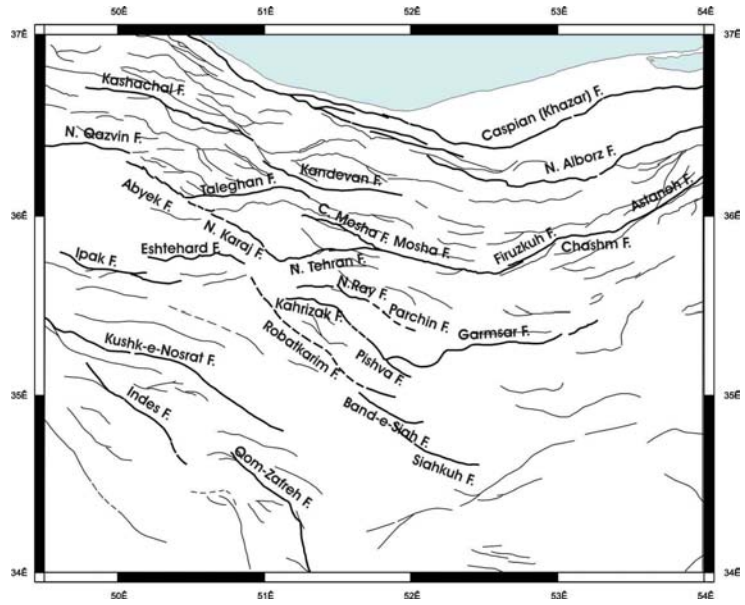

Figure 6.23. Referred names for major active faults in greater Tehran region

Crustal deformation and slip rate of faults in Greater Tehran region

Our general view about the shortening across the region of study is mainly based on recent GPS studies in Iran (Vernant et al 2004, Masson et al 2007). Vernant et al (2004) suggest an overall shortening of about 5 mm/year over a north-south distance of 100 km in the Central Alborz, equivalent to 40% of the shortening between the Central Iranian Block and Eurasia. They also suggest that the remaining shortening should occur north of the Alborz in the South Caspian basin (~6 mm/year) and south of the Alborz (~3 mm/year), possibly on the edge of the Central Iranian block. Their proposed model for internal deformation of the Alborz is transpressional. This is consistent with the activity of thrust faults to the north (North Alborz and Caspian faults) and south (North Tehran, Parchin and Pishva faults) of the Alborz; and left-lateral faults (Rudbar, Taleqan, Mosha, Firuzkuh and Astaneh faults) in the internal part of the range. Their interpretation is, however, inconsistent with results from paleoseismology and observation of active tectonics which show a transtensional movement in the internal part (Nazari, 2006 and Ritz et al., 2006).

A continuous GPS survey in central Alborz was started in 2005 to help understand and quantity the distribution of deformation in this region. Considerable time and effort has been spent in the application of recently available data (2005 to 2006) to increase the precision of velocity field within the region. Although there are some places (e.g. Mosha fault) where the results of GPS and

Paleoseismology are consistent, in most cases it is rather difficult to obtain convincing constraints on the slip rate of each individual fault. This problem arises due to the short period of measurement, the lack of sufficient stations in the internal part of the belt, possible gravitational land movements in high altitudes, and insufficient distance of some stations from active faults.
In comparison to GPS data, paleoseismology covers a longer time span and is less subject to local disturbance of deformation. This method is associated with direct measurement of slip on the fault plane and supported by several dating results of young deposits which give a more reliable rate of slip over a longer time interval. We therefore gave priority to paleoseismological data for defining both mechanism and slip rates where they were available.

During the last few years there have been more than 20 paleoseimological trenches around Tehran, most of them on the North Tehran, Taleqan, Mosha, Firuzkuh, and Astaneh faults. The Taleqan, Mosha, Firuzkuh and Astaneh faults, with mainly left-lateral strike-slip mechanism, are located in the internal part of the central Alborz, and the north Tehran fault, with principal thrust component, separates the Alborz mountains from lower lands of northern part of the central Iran along most of its length.

The Caspian (Khazar) fault is the longest active fault on the northern edge of the Alborz mountains. The latest relatively large earthquake (28 may 2004, Mw 6.2) near Tehran was possibly due to the reactivation of this fault (Tatar et al., 2007). The northern side of the Alborz is covered by dense forest, thus the surface expressions of faults are difficult to recognize. However, based on archeological studies and dating of uplifted river deposits (on the hanging wall of the fault) in a valley to the east of Amol, (Antoine et al., 2006), Nazari (2006) obtained a minimum slip rate of 2.5 mm/y for the Caspian fault. Although this is not a direct measurement of slip rate on the fault, and is associated with some assumptions, it is the only available estimation of rate which is based on ^{14}C dating.

Of course there are several other faults within the study area for which we have no direct measurement of slip rate. The available geomorphological and paleoseimological data do not amount to the total shortening calculated by GPS surveying. Thus the remaining amount of shortening should be distributed over other major active faults.

Seismic parameters of major faults

The seismic parameters for the faults in the region of study are summarized in table 6.5-1. Description and abbreviations are explained below.

Fault Names: The fault map is originally based on 1:250,000 geological maps of the Geological Survey of Iran and other available data. We thus used the same names as they are referred on the maps or reports (e.g. Berberian et al., 1985, 1993, 1996).

Fault length: This is the maximum possible length of rupture and is measured directly from the map considering other field and seismological information.

Table 6.5-1: seismic parameters for major faults in greater Tehran region

Fault Name	F. length	Mmax	M min (Mw)	Dip/Dip direction (degree)	Mechanism	Elastic Thickness (km)	Horizontal Slip Rate (mm/y)	Slip on fault (mm/y)	Mom. Accu. Rate (Nm/y)	a-value for b=0.85
Khazar	>150	**7.6**	3	35S	T	15	2-2.5	2.44-3.05	2.87E17--3.59E17	3.41-3.50
N.Alborz	>150	**7.6**	3	50S	T	15	1.0	1.55	1.36E+17	3.09
Kashachal	107	**7.4**	3	80-90N	S	15	1.0	1.00	4.83E+16	2.76
Kandevan	85	**7.3**	3	50N	T	15	1.0	1.55	7.74E+16	2.97
N.Qazvin	80	**7.3**	3	35-65N	T	15	1.0	1.55	7.28E+16	2.94
Abyek	45	**7.0**	3	45N*	T	15	1.0	1.41	4.04E+16	2.95
Taleqan	70	**7.2 (7.2)**	3	55S	S/N	15	1.0	1.00	3.84E+16	2.79
Mosha/C.Mosha	80+50	**7.5** (7.0)	3	60-70N	S	15		2.3-1.0	1.48e17-6.45e16	3.18--2.82
Firuzkuh	45	7.0 **(7.2)**	3	70S	S/N	15		2.30	4.96E+16	2.9
Chashm	40	**6.9**	3	70N*	S/T	15	2.3	2.30	4.40E+16	3.05
Astaneh	130	**7.5** (7.4)	3	90	S	15		2.50	1.46E+17	3.18
N.Tehran/N.Karaj	60+65	**7.5** (7.1)	3	35-70N	T/S	15	0.7-1.0	0.86-1.55	6.14e16-1.11e17	2.80--3.06
Ipak	77	**7.3**	3	52S	T	15	1.0	1.62	7.12E+16	2.93
Eshtehard	60	**7.1**	3	45N*	T	15	1.0	1.41	5.38E+16	3
Robatkarim	120	**7.5**	3	60N*	T/S	15	1.0	1.41	8.79E+16	2.96
Band-e-Siah	45	**7.0**	3	45N*	T	15	0.5	0.70	2.00E+16	2.64
Siahkuh	55	**7.1**	3	45N*	T	15	0.5	0.70	2.45E+16	2.66
N.Ray	25	**6.7**	3	45N*	T	15	0.3	0.35	5.56E+15	2.28
Parchin	32	**6.8**	3	45N*	T	15	0.3	0.35	7.13E+15	2.26
Kahrizak	32	**6.8**	3	45N*	T	15	0.3	0.35	7.13E+15	2.26
Pishva	62	**7.1**	3	45NE*	T/S	15	0.3	0.35	1.38E+16	2.41
Garmsar	135	**7.5**	3	45N*	T	15	1.0	1.41	1.21E+17	3.1
Kushk-e-Nosrat	165	**7.6**	3	45N*	T	15	1.0	1.41	1.48E+17	3.12
Indes	90	**7.3**	3	45N*	T	15	1.0	1.41	8.08E+16	2.99
Qom-Zefreh	85	**7.3**	3	45N*	T/S	15	1.0	1.41	7.63E+16	2.96

Mmin: This is the minimum magnitude (Mw) which used for seismic hazard evaluation and is considered to be 3.0. Earthquakes smaller than 3 account for only a very small proportion of the total moment and thus do not have much effect on the final results.

Mmax: This is calculated based on length of the active faults or directly from paleoseimological results (the larger one is used for analysis). In any case it does not exceed 7.7, which is the largest estimated magnitude (historical earthquake) for the Iranian plateau.

Dip/Dip direction: They are either known from geology or fixed to 45(starred) if they are unknown.

Mechanism: Mechanism for each fault is assigned according the available field, seismological, and geological information. The letters T and S stand for thrust and strike-slip mechanism.

Elastic thickness: assumed to be about 15 km for entire region. It is based on reliable reported depths for most earthquakes.

Down dip width of the fault: It is assumed that faults rupture the entire elastic part of the crust (down to 15 km). As all major faults in the map are longer than 25 km, this assumption is probably reasonable for all of them.

Horizontal Slip Rate: The slip rate for major faults is calculated based on combination of GPS data, paleoseismology, geomorphology and regional interpretation of geological data.

Moment accumulating rate: This is the moment (in Nm) which accumulates during one year on the fault plane and is calculated using the assigned slip rate. It is assumed that entire seismogenic layer experiences mainly seismic deformation (e.g. Masson et al., 2005).

Gutenberg-Richter's b-value: The b-value is based on observed seismicity in the central Alborz. However, due to insufficient coverage of seismic network in Iran in earlier years it is quite possible that some smaller earthquakes are not present in the available catalogues, leading to lower b-values. Thus the catalogue has been divided into two or three time domains (see table 6.5-2) with different

levels of completeness. In order to achieve a poisson distribution, a declustering has been performed to remove foreshock and aftershocks using the algorithm of Knopoff (1974). The Kijko (1989, 1982) method was then used to evaluate the Gutenberg-Richter parameters. We choose parameters coded c1 in table 6.5-2 as a preferable model for calculating b-value, where earthquakes between 1927 and 2003 are classified into two categories of pre- and post 1964 and the catalogue has been declustered.

Meanwhile, other members of the team (Dr. Rahnama and Dr. Bozorgnia) have been working independently on earthquake data. Their final proposed b-value is consistent with our results. We thus used b-value of 0.85 for further analysis.

Gutenberg-Richter's a-value: It is assumed that distribution of earthquakes follows the Gutenberg-Richter (1944) relation. This number is calculated on the basis of a simulated distribution of earthquakes on each fault, taking into account that the total moment should be equivalent to the above calculated moment.

Table 6.5-2: evaluation of b-value for greater Tehran Rregion

Code	Span of Time	Declustering	BETA	b-value	Mmin	Mmax	Mmax obs	Description
a1	-36500 to 2003	NO	2.57 +- 0.14	1.12 +- 0.06	4.2	7.65 +- 0.21**	7.40 +- 0.20	Pre-Historic : <1900 Historic : 1900*-1964 Complete : >1964
a2	-36500 to 2003	YES	2.23 +- 0.15	0.97 +- 0.06	4.2	7.65 +- 0.21**	7.40 +- 0.20	Pre-Historic : <1900 Historic : 1900*-1964 Complete : >1964
b1	743 to 2003	NO	2.57 +- 0.16	1.12 +- 0.07	4.2	7.65 +- 0.21**	7.40 +- 0.20	Historic : 743-1964 Complete : >1964
b2	743 to 2003	YES	2.42 +- 0.18	1.05 +- 0.08	4.2	7.65 +- 0.21**	7.40 +- 0.20	Historic : 743-1964 Complete : >1964
c1	1927-2003	YES	1.96 +- 0.23	0.85 +- 0.10	4.2	7.7	7.40 +- 0.20	Historic :1927-1964 Complete : >1964
c2	1927-2003	YES	1.53 +- 0.21	0.66 +- 0.09	4.2	7.7	7.40 +- 0.21	Complete :1927-1964 Complete : >1964

* Gap in Alborz data from 1900 to 1927 so catalogue begins in 1927 and ends in 1964

** Calculated Mmax

Historical and instrumental data for greater Tehran Region – Geological Survey of Iran

DATE	Ms
c.1.8 Ma	>7.0
c.38500-10000 BP	>6.5
c.4500 BP	>6.5
C.3000-2800 BP	>7.0
743	7.2
855-856	7.1
856 12 22	7.4*
0864 01 00	5.3
958 02 23	7.4
1052 00 00	6.8
1119 12 10	6.5
1127 00 00	6.8
1177 05 00	7.2
1301 00 00	6.7
1485 08 15	7.2
1486 07 03	
1495 00 00	5.9
1608 04 20	7.4
1678 02 03	6.5*
1721 07 00	
1803 00 00	>5.3*
1808 06 26	6.6*
1808 12 16	5.9
1809 00 00	6.5
1825 00 00	6.7
1830 03 27	7.1
1830 04 06	>5.3
1876 10 20	5.7
1890 02 07	>5.3
1895 00 00	>5.3

DATE	LAT	LONG	Ms	Depth	O.T	Ref.
1927/07/22	34.7	54	6.3	0	03:54:54	ISS-AMB
1927/07/22	34.7	54	4.81	0	08:37:30	ISS
1927/07/23	34.7	54	5.26	0	20:17:46	ISS
1927/07/23	34.7	54	5.26	0	22:40:18	ISS
1927/07/27	34.7	54	4.36	0	20:41:42	ISS
1927/10/31	36.5	49	4.18	0	06:23:00	ISS
1930/10/02	35.8	52.1	4.81	0	15:33:12	ISS
1930/10/07	35.8	52.1	4.63	0	20:53:06	ISS
1932/05/20	36.3	53.5	4.81	0	19:16:18	ISS

1935/03/05	36.2	53	5.08	0	10:26:37	ISS
1935/04/11	36.3	53.5	6.3	0	23:14:49	ISS-AMB
1935/04/11	36.3	53.5	4.36	0	23:59:17	ISS
1935/04/12	36.3	53.5	4.81	0	00:11:23	ISS
1935/04/12	35.8	52.8	4.81	0	00:33:44	ISS
1935/04/12	36.3	53.5	5.08	0	01:06:44	ISS
1935/04/12	36.3	53.5	5.26	0	12:44:38	ISS
1935/04/12	36.3	53.5	4.18	0	20:24:00	ISS
1935/04/12	35.9	53.5	4.81	0	22:31:48	ISS
1935/04/13	34.8	52.2	4.63	0	02:29:07	ISS
1935/04/15	36.3	53.5	4.18	0	23:04:47	ISS
1935/04/17	36.3	53.5	4.18	0	13:36:35	ISS
1937/04/07	34.8	52.1	5.08	0	18:30:59	ISS
1940/09/25	36.4	52.1	5.08	0	19:31:20	ISS
1945/05/11	34.8	52.1	4.36	0	20:17:28	ISS
1948/06/17	36.5	49	4.81	0	14:08:22	ISS
1948/06/30	36.5	49	4.81	0	19:31:39	ISS
1951/04/22	34.8	52.1	4.63	0	06:32:41	ISS
1951/11/13	36.1	52.5	4.18	0	14:01:47	ISS
1954/09/02	35.3	52	4.18	0	22:47:00	SSK
1957/03/16	34.9	52.9	5.08	0	00:43:42	ISS
1957/05/06	36.46	51.51	5.08	0	15:06:51	ISS
1957/07/02	36.21	52.72	6.8	0	00:42:22	ISS-AMB
1957/07/02	36	53	4.18	0	01:16:54	BCIS
1957/07/02	36	53	4.18	0	04:56:08	BCIS
1957/07/02	36	53	3.73	0	05:09:08	BCIS
1957/07/02	36	53	3.73	0	14:22:40	MOS
1957/07/04	36	52	3.91	0	22:43:47	MOS
1957/07/07	36	52.7	3.91	0	18:12:50	SSK
1957/07/09	36	52.7	3.91	0	09:09:11	SSK
1957/10/25	36.4	53.2	4.18	0	08:24:20	SSK
1958/01/16	34	50	4.36	0	02:04:16	BCIS
1958/06/17	36.2	53	4.18	0	16:55:01	BCIS
1958/06/25	36.24	52.83	4.81	0	01:14:01	ISS
1958/11/02	36.7	51.5	4.18	0	09:14:28	BCIS
1959/03/08	36	53	4.63	0	14:48:50	NEIC
1959/05/01	36.45	51.23	5.26	44	08:24:03	ISS
1962/09/01	35.58	49.88	7.2	29	19:20:40	ISS-AMB
1962/09/01	35.6	49.4	3.91	31	20:27:40	NEIC
1962/09/02	35.6	49.4	4.18	31	07:12:03	NEIC
1962/09/02	35.5	49.5	3.91	0	13:21:26	MOS
1962/09/04	35.6	49.7	4.81	53	13:30:14	NEIC
1962/09/06	36	49.5	3.73	0	17:04:25	MOS
1962/09/11	35.4	49.9	4.18	33	11:15:05	NEIC
1962/09/12	35.7	49	4.18	0	02:15:45	MOS
1962/09/29	36	53.3	4.18	0	19:23:22	MOS
1962/10/13	35.7	50.07	5.08	35	10:23:38	ISS
1962/12/02	35.8	50.1	4.63	0	22:21:30	NEIC
1962/12/02	35.5	50.1	3.73	0	23:36:24	NEIC

1963/05/28	35.4	49.8	4	33	10:32:47	NEIC
1964/05/15	35.76	49.86	4.18	29	01:56:08	ISC
1964/11/03	35.63	50.29	4.72	42	17:36:08	ISC
1966/10/03	35.8	53.44	4.54	14	17:05:08	ISC
1966/11/08	36.1	50.74	4.45	41	03:14:13	ISC
1967/02/03	36.7	53.7	4	37	11:17:38	ISC
1967/02/16	35.4	51.9	4.18	144	11:55:32	ISC
1967/06/23	35.5	49.6	4	38	13:15:08	ISC
1967/08/25	35.58	49.33	4.36	55	12:26:50	ISC
1967/11/10	36	53.89	4.54	5	02:50:52	ISC
1967/12/10	36.19	53.69	4.54	19	10:52:50	ISC
1968/04/26	35.09	50.16	4.81	32	02:58:24	ISC
1968/05/19	36.61	53.35	4.27	22	16:49:50	ISC
1968/07/29	36.72	53.85	4.18	14	16:03:43	ISC
1968/08/02	36.85	49.33	4.36	36	03:59:27	ISC
1968/12/12	35.8	53.49	4.54	27	18:54:47	ISC
1970/06/27	35.12	50.8	4.45	52	07:57:58	ISC
1970/10/03	36.01	51.31	3.82	78	06:57:03	ISC
1971/04/30	34.6783	50.3285	4.36	37.6	09:06:17	ISC
1971/08/09	36.2713	52.8086	4.81	11.6	02:54:35	ISC
1972/08/08	36.5144	52.7689	4.45	41.5	00:44:55	ISC
1973/09/17	36.5894	51.1898	4.36	40.2	04:06:03	ISC
1973/10/30	36.946	50.7059	3.82	47.9	15:59:31	ISC
1974/11/05	36.291	53.015	4.27	39.9	20:02:21	ISC
1975/04/11	35.6492	50.3543	4.36	59.3	14:26:46	ISC
1975/11/06	35.9986	53.1452	4.27	5.6	04:09:32	ISC
1977/05/25	34.9069	52.0641	4.9	38.9	11:01:47	ISC
1979/02/22	35.2016	52.0999	4.27	33	05:07:18	ISC
1979/03/18	36.3389	52.6467	4	33	05:19:53	ISC
1979/03/25	34.903	52.465	3.9	47.8	02:32:26	ISC
1980/12/19	34.5014	50.6728	5.8	29.2	01:16:56	ISC
1980/12/19	35.2493	52.3781	4.18	0	16:54:18	ISC
1980/12/22	34.4853	50.6718	5.2	39.5	12:51:21	ISC
1980/12/25	34.2374	50.795	4.09	33	16:13:20	ISC
1981/03/29	34.3726	50.8564	4.09	21	17:20:52	ISC
1981/08/04	36.4455	51.2687	4.36	0	18:54:00	ISC
1982/02/05	36.1265	53.678	4.18	33	23:37:12	ISC
1982/07/05	34.7403	50.9761	4.18	33	15:54:25	ISC
1982/10/25	35.1325	52.3762	4.18	43.9	16:54:52	ISC
1983/03/25	36.1322	52.3615	4.9	10	11:57:47	ISC
1983/03/26	36.057	52.2791	4.9	33	04:07:20	ISC
1983/05/29	35.2427	52.1696	4.09	39.3	17:15:40	ISC
1983/07/22	36.9783	49.2263	5	43	02:41:01	ISC
1983/12/20	36.9193	50.9108	4.45	26.2	22:21:04	ISC
1983/12/21	36.9328	51.3147	4.09	33	00:07:28	ISC
1984/09/09	35.5314	49.2774	4.27	49.5	17:55:01	ISC
1985/02/11	34.474	50.6936	4.36	61.5	09:26:47	ISC
1985/02/16	36.778	51.8447	4	33	06:57:37	ISC
1985/07/08	36.2737	53.7122	4.36	33	17:02:36	ISC
1985/10/14	35.5155	52.7022	4.3	10	15:28:31	ISC

1986/03/26	36.0107	53.6788	4.27	34.3	15:18:09	ISC
1986/09/10	36.1053	49.0681	3.91	33	19:32:26	ISC
1987/11/25	35.6724	53.0701	4.09	33	02:09:39	ISC
1988/03/01	34.4835	50.7931	4.18	15.9	01:02:03	ISC
1988/05/27	34.4121	50.2473	4.2	10	00:54:25	ISC
1988/08/22	35.3482	52.3784	5	18.4	21:23:36	ISC
1988/08/23	35.4196	52.2754	4.8	34.7	05:30:51	ISC
1988/08/23	35.3378	52.3444	4.6	16	10:58:10	ISC
1988/08/23	35.6404	52.402	3.73	10	14:56:08	ISC
1988/09/03	35.0965	52.4635	4.36	10	08:11:52	ISC
1988/10/24	35.2543	52.2958	4.4	34.2	17:01:59	ISC
1988/10/26	35.1191	52.2282	4.36	6.3	14:49:20	ISC
1988/11/12	35.4513	52.5057	3.91	33	21:00:53	ISC
1988/12/03	35.1499	52.2045	4.09	10	18:41:00	ISC
1990/01/20	35.8917	52.999	5.8	25	01:27:10	ISC
1990/01/20	35.9868	53.2911	4.27	41.6	02:15:07	ISC
1990/04/21	36.1256	53.0971	4.18	28.5	21:57:53	ISC
1990/06/20	36.9893	49.3462	7.4	18.5	21:00:11	ISC
1990/06/20	36.8142	49.7428	4.36	10	22:04:07	ISC
1990/06/20	36.9894	49.1664	5.4	10	22:23:43	ISC
1990/06/20	36.9228	49.499	5.2	32.4	22:58:54	ISC
1990/06/20	36.9621	49.4535	5.2	15	23:00:38	ISC
1990/06/20	36.8942	50.2534	5	33	23:27:47	ISC
1990/06/20	36.7469	49.8646	5.1	20	23:48:46	ISC
1990/06/21	36.6607	49.6733	4.36	10	00:52:34	ISC
1990/06/21	36.802	49.7684	4.9	34.4	02:08:55	ISC
1990/06/21	36.9302	50.2039	4	33	03:00:21	ISC
1990/06/21	36.9723	49.5523	4.54	30.5	07:50:26	ISC
1990/06/21	36.6498	49.8284	5.3	15.2	09:02:15	ISC
1990/06/21	36.9421	49.4773	4.4	40.7	12:17:32	ISC
1990/06/21	36.6116	49.7063	4.45	33	21:27:43	ISC
1990/06/21	36.7438	49.2914	4.36	53.8	21:31:13	ISC
1990/06/22	36.6159	49.4378	4.36	10	06:21:52	ISC
1990/06/22	36.9	50.0982	3.73	33	13:56:14	ISC
1990/06/24	36.8791	49.4212	4.8	38.9	09:46:01	ISC
1990/06/24	36.996	49.5925	4.27	33	19:05:25	ISC
1990/06/26	36.8902	50.0709	3.5	10	19:03:11	ISC
1990/06/27	36.9562	49.7696	3.3	41	03:56:24	ISC
1990/06/28	36.9407	49.5624	4.2	46.3	03:20:40	ISC
1990/06/28	36.6864	49.88	4.36	48	17:21:08	ISC
1990/06/29	36.6741	49.9069	4.18	46	06:25:52	ISC
1990/06/30	36.9241	50.2416	4.09	33	03:42:06	ISC
1990/07/06	36.9077	49.3005	4.5	50.9	19:34:54	ISC
1990/07/08	36.6913	50.0597	4	35.7	05:11:15	ISC
1990/07/13	36.8022	50.1048	4.36	33	13:04:12	ISC
1990/07/24	36.8416	49.8015	4	10	07:27:17	ISC
1990/08/13	36.761	49.9003	3.9	38.8	06:18:26	ISC
1990/08/20	36.8147	49.6824	4.1	56.3	12:20:14	ISC
1990/09/25	36.7736	49.8208	4.1	40.4	12:12:20	ISC
1990/10/02	36.8347	50.0123	3.82	35.4	20:19:36	ISC

1990/10/17	36.9907	49.5044	4.18	43.1	17:06:31	ISC
1990/10/22	36.9766	49.4379	4.36	58	03:50:26	ISC
1990/12/27	36.784	49.237	4.36	8.8	13:26:56	ISC
1991/01/22	35.4403	52.3225	4.18	33	12:04:25	ISC
1991/05/29	36.2317	53.2394	4.18	33.1	15:15:21	ISC
1991/08/23	35.9896	53.2735	4.5	42	22:14:21	ISC
1991/09/08	35.473	53.3543	4.09	54.1	04:20:34	ISC
1991/11/28	36.8618	49.5818	5	50.4	17:20:00	ISC
1991/12/01	36.7062	49.4059	3.19	10	11:18:24	ISC
1991/12/18	36.5837	49.712	4.27	41.9	16:42:23	ISC
1991/12/19	36.6551	49.8279	3.55	21.6	07:20:00	ISC
1991/12/24	36.0365	53.1004	3.46	38.1	07:08:29	ISC
1992/06/12	36.5885	49.9359	3.73	70.3	13:25:27	ISC
1992/09/22	36.3394	52.7185	4.3	43.5	14:05:56	ISC
1993/03/08	36.4953	51.0243	4.09	56.8	19:13:24	ISC
1993/05/12	36.7787	52.0299	4	33	09:41:19	ISC
1993/06/09	34.8299	53.3223	4.4	31.4	17:33:37	ISC
1993/06/30	35.2207	53.5641	4.3	48.4	23:05:38	ISC
1993/08/19	35.2108	52.152	4.27	59.6	10:04:34	ISC
1993/10/18	36.5472	53.7749	4.18	33	01:28:24	ISC
1994/11/21	36.0508	51.9133	3.7	43.9	18:55:18	ISC
1995/04/26	36.9793	49.4255	4.2	47.6	11:46:13	ISC
1995/06/03	35.9151	53.0864	3.91	49.9	20:08:35	ISC
1995/06/26	36.5973	51.1891	4.2	21.9	21:12:55	ISC
1995/11/23	36.0477	53.404	3.73	43.4	19:29:36	ISC
1996/01/14	36.5766	51.1422	3.55	33	20:05:24	ISC
1996/08/20	36.3878	53.1054	3.37	8.1	17:53:38	ISC
1996/08/25	36.0014	53.0204	3.91	37.4	14:17:09	ISC
1997/06/07	36.5102	50.3575	4.2	27.7	20:29:49	ISC
1997/06/23	35.5989	52.5273	3.55	33	15:06:03	ISC
1997/08/26	36.594	53.0551	3.4	42.8	00:44:51	ISC
1997/11/05	34.9405	51.3714	3.91	43.9	22:42:58	ISC
1998/01/02	36.5036	52.1954	3.6	9.7	00:03:12	ISC
1998/01/02	36.9035	52.3514	3.55	33	00:09:04	ISC
1998/01/09	36.4396	52.1901	4.4	44.6	19:06:15	ISC
1998/01/20	36.3903	52.1949	3.64	42.9	00:47:00	ISC
1998/01/24	35.9058	53.5744	4.3	28.2	22:51:56	ISC
1998/04/04	36.6127	49.5156	3.64	16.7	02:46:31	ISC
1998/04/20	36.8259	49.1512	3.1	33	02:50:00	ISC
1998/07/07	36.2212	52.0793	3.37	33	11:06:38	ISC
1998/08/30	36.0967	52.1254	3.37	33	15:12:55	ISC
1998/11/19	36.1874	53.9648	3.9	50.6	13:14:57	ISC
1998/12/03	36.0637	50.9724	3.6	46.2	13:13:35	ISC
1998/12/03	36.3028	51.1126	3.64	100	21:07:18	ISC
1998/12/19	36.9091	51.0433	3.5	10	04:54:00	ISC
1999/03/13	35.587	53.666	3.3	33	04:30:17	ISC
1999/03/26	36.636	50.223	3.64	33	12:06:53	ISC
1999/12/09	36.539	53.533	4.1	7.4	22:20:35	ISC
2001/03/04	35.052	53.156	3.37	7.2	11:45:56	ISC
2001/05/16	36.261	52.662	4.4	25.6	07:24:29	ISC

2001/06/24	35.838	52.184	3.37	4	07:05:18	ISC
2001/11/17	35.658	53.278	3.19	32.3	21:19:06	ISC
2001/11/23	34.106	49.856	3.46	15	19:30:48	ISC
2002/01/12	35.608	50.555	3.01	33	05:18:23	ISC
2002/02/14	36.78	49.464	3.4	45	20:06:23	ISC
2002/04/08	36.365	52.017	4.1	57.3	18:31:00	ISC
2002/04/19	36.523	49.774	4.6	38.8	13:46:51	ISC
2002/05/13	35.193	52.882	3.64	33	20:49:24	ISC
2002/05/21	36.292	51.547	3.3	12.2	10:48:35	ISC
2002/06/22	35.589	49.022	6.4	10	02:58:22	ISC
2002/06/22	35.594	49.009	4.09	56.9	03:32:02	ISC
2002/07/10	35.72	49.1	3.46	33	22:58:01	ISC
2002/08/23	35.502	49.324	3.37	33	13:05:04	ISC
2002/10/10	35.8235	52.249	5.6	14.9	12:13:41	ISC
2002/10/15	35.8384	52.2323	3.4	33	13:59:35	ISC
2002/10/15	35.8204	52.2318	3.5	10	16:56:08	ISC
2002/10/18	36.2833	52.4154	3.37	74.5	22:24:57	ISC
2003/06/21	35.6279	52.8586	3.6	23.9	15:00:05	ISC
2003/06/22	35.3616	52.6849	3.5	33	03:39:14	ISC
2003/09/30	36.4186	53.3713	3.64	33	15:33:03	ISC

7 – RESPONSE SPECTRA

Characteristics of ground motion, including the amplitude and frequency content of seismic waves, are changed as the waves travel from the earthquake source to the site under study. The shape of site-specific response spectrum is a function of a variety of parameters, including the earthquake magnitude, fault mechanism, site-to-source distance, fault rupture direction, and local soil condition.

The relationships between response spectral shape and the above mentioned parameters have been examined by Campbell and Bozorgnia (2003); Boore et al. (1997); Sadigh et al. (1997) and Abrahamson and Silva (1997). These four studies are currently used for determination of design earthquakes and response spectra in the entire western U.S., which is a very active seismic region. The design ground motion is the basis for seismic design of new facilities and seismic evaluation of existing structures. In other words, all structures in the western U.S., designed according to the International Building Code, are seismically designed based on the ground motion determined by these four ground motion relationships. Herein, these four ground motion relationships are used to derive the shape of the design spectra at the three sites of interest. As mentioned before, such smoothed spectra include site-specific characteristics such as style of faulting, and spectral shapes compatible with the potential magnitude, and local soil conditions.

7.1. Shape of Smoothed Response Spectra

As mentioned above the shape of smoothed response spectrum is a function of various parameters, including the earthquake magnitude, fault mechanism, site-to-source distance, fault rupture direction, and local soil condition. The actual values of spectral ordinates are also function of the return period of interest. Various deterministic and probabilistic values of spectral ordinates have been reported in Section 6.4.8. As presented in that section, three specific sites were selected as

examples to compare various spectral values. At a specific site, there are two options for the shape of the probabilistic spectra:

a) Uniform hazard spectra (UHS), i.e., spectral ordinates at various periods associated with a specific return period,
b) Simplified uniform hazard spectra, i.e., constructing UHS by using few spectral ordinates at few periods

Option (b) is used in the International building Code (IBC), where spectral ordinates at 0.2 and 1.0 sec are used to construct the simplified UHS. In this case, the spectral ordinate at period 0.2 sec is used to determine the "flat" portion of the acceleration spectrum, and a (1/T) curve is passed through the spectral ordinate at 1.0 sec. Figures 7.1, 7.2, and 7.3 show such spectra for sites 1, 2, and 3, respectively, based on the results of this study.

The shape and amplitudes of design spectra for seismic design are usually determined by various committees responsible to draft the building code. The building code committees use the PSAH results, their judgment, and experience and propose a smooth spectrum for seismic design.

Assuming that the simplified UHS, option (b) as explained above, is chosen by the building code committees for seismic design, there are at least two more choices for the values of spectral ordinates, including, but not limited to:

1. Design spectral ordinates at period 0.2 and 1.0 sec are based in probabilistic results for 475 years return period,

2. Design spectral ordinates at period 0.2 and 1.0 sec are based in probabilistic results for 2475 years return period, divided by a factor 1.5.

The second choice is implicitly based on the assumptions that a rare event (with a return period of 2475) should not cause structural "collapse" (i.e., collapse prevention case), and that the structures have approximately a "safety margin" of 1.5 against collapse. An important conclusion of the PSHA results presented in Section 6.4, and shown in Figures 7.1, 7.2 and 7.3 of this section, is that the results based on option (2) are more conservative that the design spectra constructed based on

option (1). For example, for site (1) the mean spectral ordinates at period 0.2 sec are 0.834g, and 1.488g for return periods 475 and 2475 years. A design spectral ordinate at period 0.2 sec based on option (2) listed above, is 1.488/1.5 = 0.992g which is larger than value of 0.834g (for return period of 475 years).

The PSHA results presented in this study include various values of spectral ordinates, including those discussed above. These results can be used by various building code committees to determine the appropriate level of conservatism for seismic design.

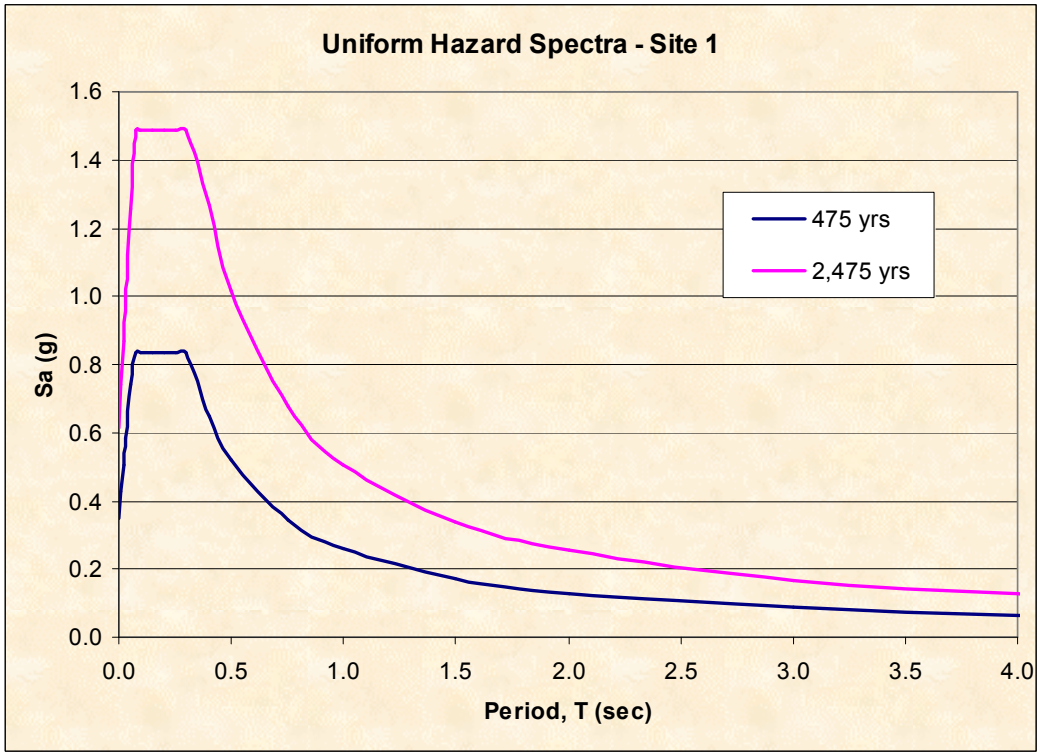

Figure 7.1: Simplified uniform hazard spectra for site 1 for return periods 475 and 2475 years

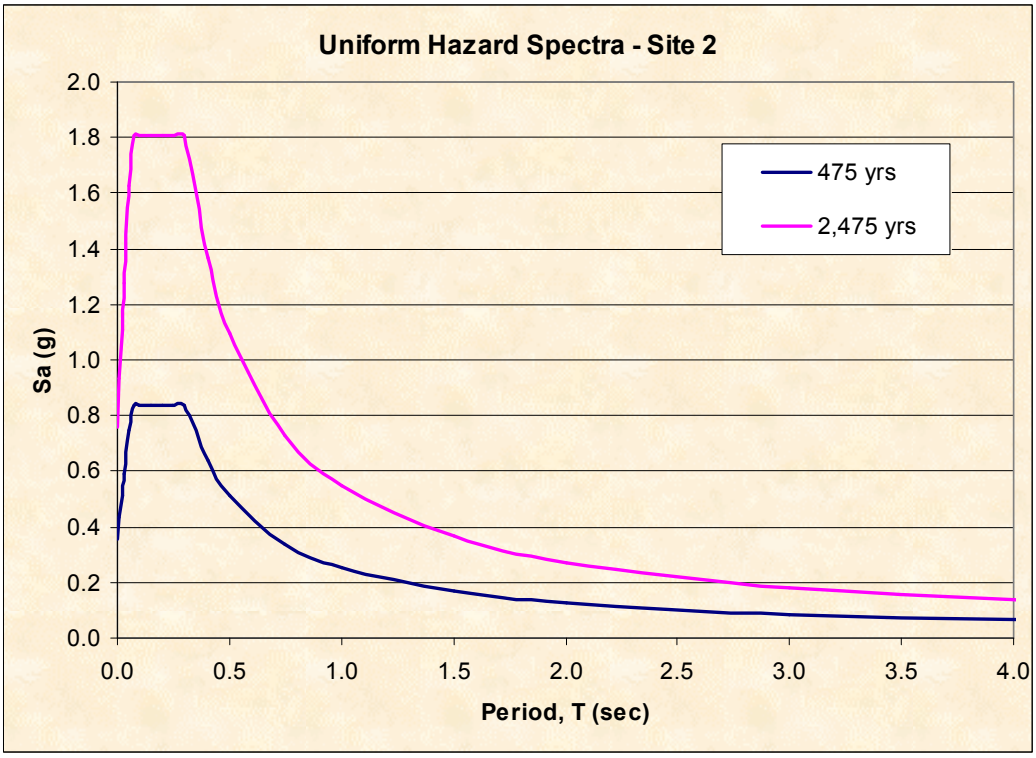

Figure 7.2: Simplified uniform hazard spectra for site 2 for return periods 475 and 2475 years

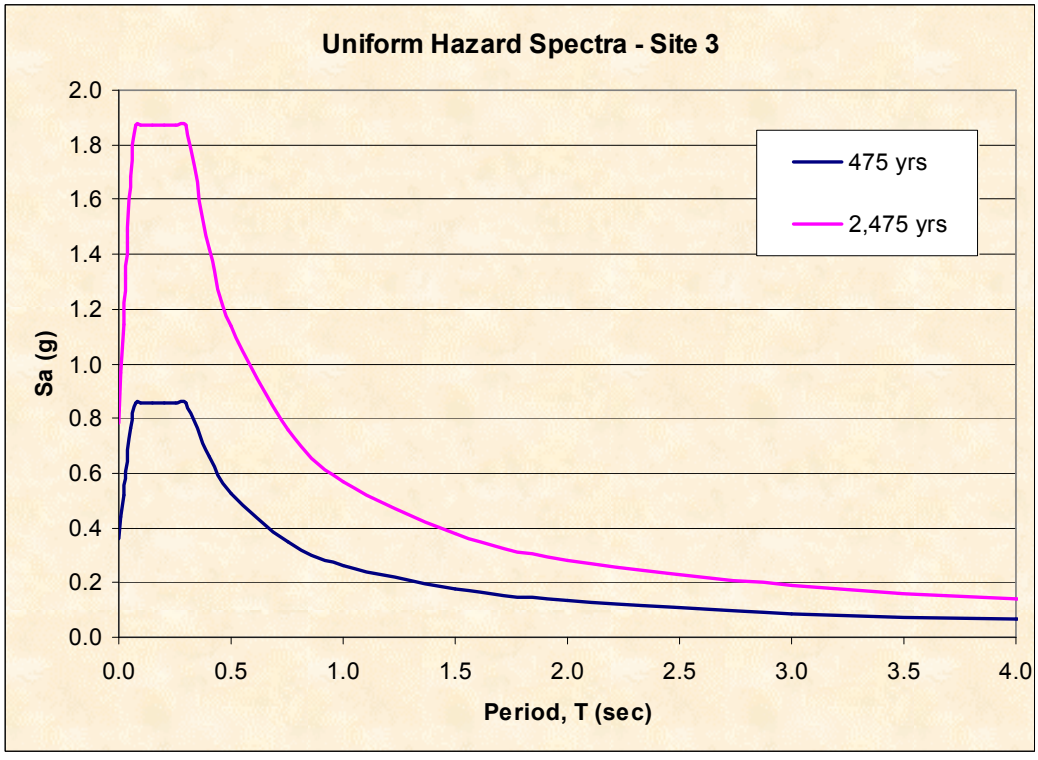

Figure 7.3: Simplified uniform hazard spectra for site 3 for return periods 475 and 2475 years

8. REFERENCES

Abbassi, M.R., 2004. The motion along the N-S faults in the Tehran piedmont since Late Quaternary. *Pazhuheshnameh, IIEES,* Tehran (http://www.iiees.ac.ir/publication/pajooheshnameh/ab_abbasi_atwun_83.html).

Abbassi, M.R., and Shabanian B.-, E., 1999. Evolution of the stress field in Tehran region during the Quaternary. *Proc. 3rd Int. Conf. Seism. Earthq. Enging. IIEES,* 67-77, Ma7 17-19, Tehran.

Abbassi, M.R., and Shabanian B.-, E., 2006. Determination of stress state and direction by inversion of fault-slip data in the southern flank of Central Alborz. *Geosciences, Geol. Surv. Iran,* **57**(12), 2-17 (in Persian with English abstract).

Abe, K., 1981. Magnitudes of large shallow earthquakes from 1904-1980. *Phys. Earth Planet. Inter.,* **27**, 72-92.

Abe, K., 1984. Complements to magnitudes of large shallow earthquakes from 1904 to 1980. *Physics. Earth Planet. Int.,* **34**, 17-23.

Abercrombie, R., 1994. Regional bias in estimates of earthquakes M_s due to surface-wave path effects. *Bull. Seism. Soc. Am.,* **84**, 377-382.

Adams, R., 1977. Survey of practice in determining magnitudes; Europe, Asia, Africa, Australasia, and Pacific. *World Data Center A,* Report **SE-8**, Washington, D.C.

Akasheh, B., and Berckemer, H., 1983. Focal mechanisms of earthquakes in Iran with special emphasis to small shocks in the Tehran region. *Geol. Surv. Iran,* **51**, 437-449.

Akasheh, B., and Berckemer, H., 1984. Focal mechanisms of earthquakes in Iran with special emphasis to small shocks in the Tehran region. Neues Jahrb. Paleontol. Abh., **168**, 244-255.

Akasheh, B., Eshghi, I., and Soltanian, R., 1976. The Iranian Long Period Array (ILPA). *J. Geophys.,* **42**, 159-162.

Alavi, M., 1996. Tectonostratigraphic synthesis and structural style of the Alborz Mountain system in northern Iran. *Geodynamic,* **21** (1), 1-33.

Alishan, L.M., 1882. Nachrichten uber erdbeben und vulkanologische phanomene. In: H. Abich, *Geologische Forschungen in den Kaukasischen Landern*, V.2, Vienna.

Allen, C.R., 1968. The tectonic environments of seismically active and inactive areas along the San Andeas fault system. *Proc. Conf. Geologic Problems San Andeas Fault System; W.R. Dickenson & A. Grantz (Eds.), Stanford University Press,* Standord, CA, 70-82.

Allen, C.R., Amand, P., Richter, C.F., and Nordquist, J.M., 1965. Relationship between seismicity and geologic structure in the southern California region. *Bull. Seism. Soc. Am.,* **55**, 753-797.

Allen, M.B., Ghassemi, M.R., Shahrabi, M., and Qorashi, M., 2003. Accomodation of late Cenozoic oblique shortening in the Alborz range, northern Iran. *J. Struct. Geol.* **25**, 659-672.

Alsinawi, S.A., 1988. The historical seismicity of the Arab countries. In: A.A.F. Al-Furaih (Ed.), *Proc. 3rd Arab Symp. Earthq. Seism., Geophysical-Seismological Observatory, King Saud Univ., Riyadth,* 8-10, 1986, 11-33.

Alsinawi, S., and Ghalib, H., 1975. Historical seismicity of Iraq. *Bull. Seism. Soc. Am.,* **65**, 541-547.

Alsinawi, S., and Issa, A.S., 1985. On the historical seismicity of Iraq. In: Historical seismograms and Earthquakes of the World. *Proc. IASPEI Wymp.,* August 27- 28, Tokyo, 85-92.

Ambraseys, N.N., 1978. The relocation of earthquakes in Iran. *Geophys. J.R. Astr. Soc.,* **53**, 117-121.

Ambraseys, N.N., 2001. Reassessment of earthquakes, 1900-1999, in the Eastern Mediterranean and the Middle East. *Geophy. J. Int.,* **145**, 471-485.

Ambraseys, N.N., and Jackson, J.A., 1998. Faulting associated with historical and recent earthquakes in the eastern Mediterranean region. *Geophys. J. Int.,* **133**, 390-406.

Ambraseys, N.N., and Melville, C.P., 1982. A history of Persian Earthquakes. *Cambridge University Press,* Cambridge, 210p.

Ambraseys, N.N., and Sarma, S., 1999. The assessment of total seismic moment. *J. Earthq. Eng.,* **3**, 439-461.

Ambraseys, N.N., and Tchalenko, J.S., 1969. Dasht-e-Bayaz earthqtuake of 31 August 1968. *UNESCO*, **1214/BMS**, Paris.

Amini, B., and Emami, M.H., 1992. Geological map of Tehran, 1:100,000. Geol Surv. Iran.
Anderson, J.G., Wesnousky, S.G., and Stirling, M.W., 1996. Earthquake size as a function of fault slip rate. *Bull. Seism. Soc. Am.,* **86** (3), 683-690.

Ashoori, E., 1994. Geomorphology of the north of Central Iran, Tehran. Ph.D. Thesis (in Persian).

Ashoori, E., 2002. Effective fault on seismology of Garmsar region. *Dept. Civil Engineer, Eq. Engineer. Faculty, Semnan University,* Sermnan, Iran, manuscript, 15p.

Ashtari, M., Hatzfeld, D., and Kamalian, N., 2005. Microseismicity in the region of Tehran. *Tectonophysics,* **395**, 193-208. doi:10.1016/j.tecto.2004.09.011.

Assereto, R., 1966. Geological map of upper Djadjerud and Lar valleys (Central Elburz, Iran). *Inst. Geol. Univ. Milano*, Serie G, Publ. N. **232**, 86p.

Babayan, T.H., 2006. Atlas of Strong Earthquakes of the Republic of Armenia, Artsakh, and Adjacent Territories From Ancient Times Through 2003. *Tigran Mets Publishing House,* Gyumri, Armenia, 139p.

Baharfirouzi, Kh., Nadim, H., and Shafeh, A.R., (n.d.; ca. 2004-2006). Geological map of Ramsar, Scale 1:100,000. *Geol. Surv. Iran,* **6163.**

Berberian, M., 1976- First seismotectonic map of Iran, 1:2,500,000. *Geol. Surv. Iran*, **39**.

Berberian, M., 1976- Contribution to the seismotectonics of Iran (part II). *Geol. Surv. Iran*, **39**, 518p.

Berberian, M., 1977- Contribution to the seismotectonics of Iran (part III). *Geol. Min. Surv*. Iran, **40**, 300p.

Berberian, M., 1979- Discussion of the paper A.A. Nowroozi, 1976 'Seismotectonic provinces of Iran.' *Bull. Seism. Soc. Am*., **69**(1), 293-297.

Berberian, M., 1979- Tabas-e-Golshan (Iran) catastrophic earthquake of September 16, 1978; a preliminary field report. *Disaster*, **2**(4), 207-219.

Berberian, M., 1979- Evaluation of the instrumental and relocated epicentres of Iranian earthquakes. *Geophys. J. Roy. Astr. Soc*. London, **58**, 625-630.

Berberian, M., 1979- Earthquake faulting and bedding thrust associated with the Tabas-e-Golshan (Iran) earthquake of September 16, 1978. *Bull. Seism. Soc. Am*., **69**(6), 1861-1887.

Berberian, M., 1981- Active faulting and tectonics of Iran. In H.K. Gupta and F.M. Delany (eds.), Zagros-Hindu Kush-Himalaya Geodynamic Evolution, *Am.Geophys. Union,* Geodynamics Series, Volume **3**, 33-69, *Am. Geophys. Union*.

Berberian, M., 1982- Aftershock tectoics of the 1978 Tabas-e-Golshan (Iran) earthquake sequence: a documented active 'thin-and thick-skinned tectonic' case. *Geophys. J.R. Astr. Soc*. London, **68**, 499-530.

Berberian, M., 1982- Discussion on the paper A. Mohajer-Ashjai and A.A. Nowroozi, 'The Tabas Earthquake of September 16, 1978 in East-Central Iran. *Geophysical Res. Lett.*, **9**(3), 193-194.

Berberian, M., 1983- The Southern Caspian: A compressional depression floored by a trapped, modified oceanic crust. *Can. J. Earth Sci*., **20**(2), 163-183.

Berberian, M., 1983 (distributed in 1984)- Continental deformation in the Iranian Plteau (contribution to the seismotectonics of Iran, part IV). *Geol. Surv. Iran*, **52**, 625p. (in English plus 74p. (in Persian).

Berberian, M., 1983 (distributed in 1984)- Generalized Tectonic Map of Iran, 1:1,500,000. *Geol. Surv. Iran*, **52**.

Berberian, M., 1984- Structural evolution and tectonics of the Iranian plateau: a plate tectonic approach. *27th International Geological Congress*, Moscow, Section 07, Tectonics of Continental Fold Belts, (Abstract) p.140.

Berberian, M., 1984 - Active tectonics of Iran. *27th International Geological Congress*, Moscow, Proc. Volume IV, Section 08, Geophysics: Seismicity (Abstract) p.38.

Berberian, M., Qorashi, M., Arzhangravesh, B., and Mohajer-Ashjai, A., 1985- Recent tectonics, seismotectonics, and earthquake-fault hazard study of the Greater Tehran region. *Geol. Surv. Iran*, **56**, 316p. (in Persian).

Berberian, M., 1989- Tectonics Evolution of Iranian mountain belts. *28th International Geological Congress, Washington, D.C.*, July 9-19, Abstract, Volume 1 of 3, 1-129-130.

Berberian, M., 1995a- Natural Hazards and the First Earthquake Catalogue of Iran. Volume 1: Historical Hazards in Iran Prior to 1900. A *UNESCO/IIEES* Publication during UN/IDNDR, 649 p., IIEES, Tehran.

Berberian, M., 1995b- Master 'Blind' thrust faults hidden under the Zagros folds: active basement tectonics and surface morphotectonics. *Tectonophysics*, **241**, 193-224.
Berberian, M., 1996- The Historical Record of Earthquakes in Persia. *Encyclopaedia Iranica, VII (F.6): Drugs-Ebn al-Atir, Mazda Publishers, Costa Mesa, California*, 635-640, U.S.A.

Berberian, M., 1997- Seismic sources of the Transcaucasian historical earthquakes. In: Historical and Prehistorical Earthquakes in the Caucasus (D. Giardini and S. Balassanian, eds.), NATO ASI Series, 2. Environment- Vol. **28**, 233-311, *Kluwer Academic Press*, the Netherlands.

Berberian, M., 2005. The 2003 Bam urban earthquake: A predictable seismotectonic pattern along the western margin of the rigid lut Block, southeastern Iran. *Earthquake Spectra,* **21**(S1), S35-S99.

Berberian, M., Asudeh, I., Bilham, R.G., Scholz, C.H., and Soufleris, C., 1979- Mechanism of the main shock and the aftershock study of the Tabas-e-Golshan (Iran) earthquake of September 16, 1978; a preliminary report. *Bull. Seism. Soc. Am*., **69**(6), 1851-1859.

Berberian, F., and Berberian M., 1981- Tectono-plutonic episodes in Iran. In: H.K. Gupta and F.M. Delany (eds.), Zagros-Hindu Kush-Himalaya Geodynamic Evolution, *Am. Geophys. Union,* Geodynamics Series, Volume **3**, 5-32,.

Berberian, M., Jackcon, J., Ghorashi, M., and Kadjar, M.H., 1984- Field and teleseismic observations of the 1981 Golbaf-Sirch earthquakes in SE Iran. *Geophys. J. R. Astr. Soc.* London, **77**, 809-838.
Berberian, M., Jackson J. A., Qorashi, M., Khatib, M.M., Priestley, K., Talebian, M., and Ghafuri-Ashtiani, M., 1999- The 1997 May 10 Zirkuh (Qa'enat) earthquake (Mw 7.2): faulting along the Sistan suture zone of eastern Iran. *Geophys. J. Int.*, **136** (3) , 671-694.

Berberian, M., Jackson, J.A., Qorashi, M., Talebian, M., Khatib, M., and Priestley, K., 2000- The Sefidabeh earthquakes in eastern Iran: Blind thrusting and bedding-plane slip on a growing anticline, and active tectonics of the Sistan suture zone. *Geophys. J. Int.*, **142**, 283-299.

Berberian, M., and King, G.C.P., 1981- Towards a paleogeography and tectonic evolution of Iran. *Can. J. Earth Sci.*, **18**(2), 210-265.

Berberian, M., and King, G.C.P., 1981- Towards a paleogeography and tectonic evolution of Iran; reply. *Can. J. Earth Sci*., **18**(11), 1764-1766.

Berberian, F., Muir, I.D., Pankhurst, R.J., and Berberian, M., 1982- Late Cretaceous and early Miocene Andean-type plutonic activity in northern Makran and Central Iran. *J. Geol. Soc.* London, **139**(5), 605-614.

Berberian, M., Qorashi, M., Mohajer-Ashjai, A., and Arzhangravesh, B., 1986- Towards a microzonation of the Tehran-Qazvin region (Iran). In: Proceedings of the National Algerian Conference on Seismic Microzonation, Ech-Cheliff, October 10-12, 1984, Algeria*, Organisme de Controle Technique de la Construction, Algeria*, 235-282.

Berberian, M., Qorashi, M., Jackson, J.A., Priestley, K., and Wallace, T., 1992- The Rudbar-Tarom earthquake of June 20, 1990 in NW Persia: preliminary field and seismological observations, and its tectonic significance. *Bull. Seism. Soc. Am*., **82**(4), 1726-1755.

Berberian, M., and Qorashi, M., 1994- Coseismic fault-related folding during the South Golbaf earthquake of November 20, 1989, in southeast Iran. *Geology,* **22**, 531-534.

Berberian, M., Ghorashi, M., Talebian, M., and Shoja-Taheri, J., 1996- Seismotectonic and earthquake-fault hazard investigations in the Semnan region (Contribution to the Seismotectonics of Iran, Part VII). *Geol. Surv. Iran*, No. **63**, 266p.

Berberian, M., and Yeats, R.S., 1999- Patterns of historical rupture in the Iranian Plateau. *Bull. Seism. Soc. Am.,* **89** (1), 120-139.

Berberian, m., and Yeats, R., 2000- Recurrence intervals of several 29th-century earthquakes in the Iranian Plateau based on archaeological evidence. *31st International Geological Congress*, August 2000, Rio de Janeiro, Brazil.

Berberian, M., and Yeats, R.S., 2001- Contribution of archaeological data to studies of earthquake history in the Iranian Plateau. *J. Struct. Geol*., Paul Hancock Memorial Issue, *J. Struct. Geol.,***23**, 536-584.

Berberian, M., Jackson, J.A., Fielding, E., Parsons, B.E., Priestly, K., Qorashi, M., Talebian, M., Walker, R., Wright, T.J., and Baker, E., 2001- The 1998 March 14 Fandoqa earthquake (M_w6.6) in Kerman, southeast Iran: Re-rupture of the 1981 Sirch earthquake fault, triggering of slip on adjacent thrusts, and the active tectonics of the Gowk fault zone. *Geophys. J. Int.,* 146 (2), 371-398.

BCIS. Bureau Central International de Seismologie, 5 rue Rene Descartes, F-67084 Strasbourg Cedex, France.

BGS. British Geological Survey, Global Seismology Unit, Murchison House, West Mains Road, Edinburgh, EH9 3LA, UK. http://www.earthquakes.bgs.ac.uk/.

BJI. Beijing, Institute of Geophysics, China Earthquake Administration, p.O. Box 8116, Beijing 100081, China.

Bolt, B.A., 1960. The revision of earthquake epicenters, focal depths and origin times using a high-speed computer. *Geophys. J. R. Astr. Soc.,* **3**, 433-440.

Bolurchi, M.J., 1997. Palaeoseismological study of the South Eshtehard fault. *M.Sc. Thesis, Azad Eslami Univ., Tehran*, Northern Branch (in Persian with English abstract).

Bonilla, M.G., Mark, R.K., and Lienkaemper, J.J., 1984. Statistical relations among earthquake magnitude, surface rupture length, and surface fault displacement. *USGS Open-File Report 84-256.*46p.

Bullen, K.E., and Bolt, B.A., 1985. An Introduction to the Theory of Seismology. *Cambridge University Press,* 4th Ed., 498p.

California Geological Survey, 1996. Probabilistic seismic hazard assessment for the State of California. California Department of Consevation, Division of Mines and Geology, Open-File Report96-08. U.S. Department of the Interior, U.S. Geological Survey, Open-File Report 96-706. http://www.consrv.ca.gov/cgs/rghm/psha/ofr9608/index.htm.

California Geological Survey, 2002. California fault parameters. California Department of Consevation, Division of Mines and Geology. http://www.consrv.ca.gov/cgs/rghm/psha/fault_parameters/htm/index.htm.

Cao, T., Peterson, M.D., and Reichle, M.S., 1996. Seismic hazard estimation from background seismicity in southern California. *Bull. Seism. Soc. Am.,* **86**, 1372-1381.

CGG, 1965. Etude Geophysique par prospection electrique dans la region de Tehran. *Companie Generale de Geophysique,* Tehran.

CSEM. Centre seismologique Euro-Mediterraneen, c/o LDG, BP12, 91680 Bruyeres-le-Chatel, France. http://www.emsc-csem.org.

Davidson, J., Hassanzadeh, J., Berzins, R., Stockli, D.F., Bashukooh, B., Turrin, B., and Pandamuz, A., 2004. The geology of Damavand volcano, Alborz Mountains, northern Iran. *Geological Society of America Bulletin,* **116**, 16-29.

Dehghani, G.A., and Makris, J., 1983. The gravity field and crustal structure of Iran. *Geol. Surv. Iran,* **51**, 51-68.

De Martini, P.M., Hessami, K., Pantosti, D., Addezio, G.D., Alinaghi, H., and Ghafory-Ashtiani, 1998. A geologic contribution to the evaluation of the seismic potential of the Kahrizak fault (Tehran, Iran). *Tectonophysics,* **287**, 187-199.

DHMR. Dhamar National Sesmological Observatory Center, P.O. Box 87175, Dhamar, Yemen. http://www.ygsmrb.com/.

Dolan, J.F., Sieh, K., Rockwell, T.K., Yeats, R.S., Shaw, J., Suppe, J., Huftile, G.J., and Gath, E.M., 1995. Prospects for larger or more frequent earthquakes in the Los Angeles metropolitan region. *Science,* **267**, 199-205.

Doloei, J., and Roberts, R., 2003. Crust and uppermost mantle structure of Tehran region from analysis of teleseismic P-waveform receiver function. *Tectonophysics,* **364**, 115-133.

Duda, S., 1965. Secular seismic energy release in the circum-Pacific belt. *Tectonophysics,* **2**, 409.

DUSS. Damascus, Department of Geology, Faculty of Sciences, Damascus University, Damascus, Syria.

Dziewonski, A.M., and Woodhouse, J.H., 1983. Studies of the seismic source using normal-mode theory. In: H. Kanamori and E. Boschi, (Eds.), Earthquakes: Observation, Theory, and Interpretations; Notes from the International School of Physics 'Enrico Ferni' (1982; Varenna, Italy), *North-Holland Publ. Co.,* Amsterdam, The Netherlands, 45-137.

Dziewonski, A.M., Chou, T., and Woodhouse, J.H., 1981. Determination of earthquake source parameters from waveform data for studies of global and regional seismicity. *J. Geophys. Res.,* **86**, 2825-2852.

EHB. See Engdahl, van der Hilst and Buland, 1998.

Ehteshami Moinabadi, M., and Yassaghi, A., 2006. Geometry and kinematics of the Mosha fault, south central Alborz range, Iran: An example of basement involved thrusting. *J. Asian Earth Sciences,* doi:10.1016/j.jseaes,2006.07.002

EIDC. Experimental (GSETT3) International Data Center. Center for Monitoring Research, 1300 North 17th Street, Suite 1450, Arlington, VA 22209, USA. http://www.cmr.gov/.

EMSC. European-Mediterranean Seismological Centre.
Engalenc, M., 1968. Contribution a la geologie, geomorphologie, hydrogeology de la region de Teheran (Iran). *These, C.E.R.H., Montpellier,* France, 365p.

Engdahl, E.R., and Bergman, E.A., 2001. Validation and generation of reference events by cluster analysis. *23rd Seismic Research Review,* Jackson Hole. http://www.cmr.gov/srs/srs2001/Screen/02-09.pdf.

Engdahl, E.R., and Villasenor, A., 2002. Global seismicity: 1900-1999. In: International Handbook of Earthquake and Engineering Seismology, V.**81A**, *Elsevier Science Ltd.,* Amsterdam, the Netherlands, 665-690.

Engdahl, E.R., van der Hilst, R., and Buland, R., 1998. Global teleseismic earthquake relocation with improved travel times and procedures for depth determination. *Bull. Seism. Soc. Am.,* **88**, 722-743.

Engdahl, E.R., Jackson, J.A., Myers, S.C., Bergman, E.A., and Priestley, K., 2006. Relocation and assessment of seismicity in the Iran region. *Geophys. J. Int.* **167**, 761-778.

Feghhi, Kh., 1999. Affection of active faults on groundwater table in Tehran region. *Proc. 3rd Int. Conf. Seism. & Earthq. Engineer.,* May 17-19, 1999, *IIEES*, Tehran, 127-137.

Fookes, P.G., and Knill, J.L., 1969. The application of engineering geology in the regional development of northern and central Iran. *Eng. Geol.* **3**, 81-120.

Frankel, A.D., Petersen, M.D., Mueller, C.S., Haller, K.M., Wheeler, R.L., Leyendecker, E.V., Wesson, R.L., Harmsen, S.C., Cramer, C.H., Perkins, D.M., and Ruskstales, K.S., 2002. Documentation for the 2002 update of the national seismic hazard maps. *USGS Open File Report* **02-420**. 33p.

Gao, L., and Wallace, T.C., 1995. The 1990 Rudbar-Tarom Iranian sequence: evidence fpr slip partitioning. *J. Geophys. Res.,* **100**, 15137-15332.

Gasperini, P., Bernardini, F., Valensise, G., and Boschi, E., 1999. Defining seismogenic sources from earthquake felt report. *Bull. Seism. Soc. Am,* **89**, 94-110.

Geller, R.J., and Kanamori, H., 1977. Magnitudes of great shallow earthquakes from 1904 to 1952. *Bull. Seism. Soc. Am.,* **67**, 587-598.

Geol. Surv. Iran. Geological Quadrangle Maps of Iran on scale of 1:250,000: Qazvin; Amol; Sari; Saveh; Tehran; Semnan; Qom; Aran and Kuh-e-Gugerd. *Geological Survey of Iran,* Tehran, Iran.

Geol. Surv. Iran. Geological Maps of Iran on scale of 1:100,000 Series Sheet: Rasht; Lagerud; Jirandeh; Javaherdeh; Ramsar; Chalus; Naushahr; Nur; Babol; Sari; Takestan; Qazvin; Shakran; Marzanabad; Baladeh; Amol; Qa'emshahr; Pol-e-Sefid; Danesfahan (Khiaraj); Eshtehard; Hashtgerd; Tehran; Fasham; Damavand; Firuzkuh; Semnan; Nobaran; Saveh; Zaviyeh; Garmsar; Farmihan; Tafresh; Qom; Arak; Salafchegan; Kahak; Aran; Kuh-e-Yakhab; and Qaleh Sardareh. *Geological Survey of Iran,* Tehran, Iran.

Ghods, A., and Sobouti, F., 2005. Quality assessment of seismic recording: the Tehran Seismic Telemetry Network. *Journal Asian Earth Sci.,* **25**, 687-694.

Grunthal, G., and Wahlstrom, R., 2007. A unified database of large European earthquakes. *EOS, Trans, AGU,* **88**(6), 69-71.

GSHAP, 1999. Global Seismic Hazard Assessment Program. *Ann. Geofis.,* **42**, 115-201.

GSHAP, 2000. The GSHAP global Seismic map. See Shedlock et al., 2000.

Guidoboni, E., and Traina, G., 1995. A new catalogue of earthquakes in the historical Armenian area from antiquity to the 12th century. *Ann. si Geofis.,* **XXXVIII**(1), 85-147.

Gutenberg, B., 1954. Amplitudes of surface waves and magnitudes of shallow earthquakes. *Bull. Seism. Soc. Am.* **34**, 2-12.

Gutenberg, B., and Richter, C., 1954. Seismicity of the Earth and Associated Phenomena. *Princeton University Press,* New Jersey, 2nd Edition, 310p.

Haghshenas, E., 1998. Geotechnical aspects overview of the Manjil earthquake north of Iran (20 June 1990). *Proc. 1st Iran-Japan Workshop Recent Earthquakes in Iran & Japan,* May 16-18, 1998, Tehran, 171-183.

Haghshenas, E., 1998. Geotechnical aspects overview of the Manjil earthquake north of Iran (20 June 1990). *Proc. 1st Iran-Japan Workshop Recent Earthquakes in Iran & Japan,* May 16-18, 1998, Tehran, 171-183.

Hanks, T.C., and Kanamori, H., 1979. A moment-magnitude scale. *J. Geophys. Res.,* **84**, 2348-2350.

Hanks, T.C., and Wyss, M., 1972. The use of body-wave spectra in the determination os seismic-source parameters. *Bull. Seism. Soc. Am.,* **62**, 561-589.

Hanks, T.C., Hileman, J.A., and Thacher, W., 1975. Seismic moments of the larger earthquakes of the southern California. *Geol. Soc. Am. Bull.,* **86**, 1131-1139.

Hays, W.W., 1980. Procedures for estimating earthquake ground motions. *USGS Professional Paper* **1114**, 75p.

Hedayati, A., Brander, J.L., and Berberian, M., 1976- Microearthquake survey of Tehran region. *Bull. Seism. Soc. Am*., **66**(5), 1713-1725.

Hedin, S., 1892. Der Demavand nach eigener beobachtung. *Verhandlung der Ges. Fur Erdkd. Zu Berlin,* **19**, 303.

Herd, D.G., 1979. Neotectonic framework of central California and its implications to microzonation of the San Francisco Bay region. *USGS Circular,* **807**, 3-12.

HFS. Hagfors Observatory, The National Defence Research Institue, Stockholm, Sweden.
HRVD. Centroid moment tensor catalogue. Harvard University , Department of Geological Sciences, Cambridge, MA 02138, USA. http://www.seismology.harvard.edu/cmtsearch.html.

IAEA, 2002. Evaluation of seismic hazard for nuclear power plants. IAEA Safety Standards Series, Safety Guide No. **NS-G-3.3**. *International Atomic Energy Agency,* Vienna, Austria, 31p.

IDC. International Data Center, CTBTO Preparatory Commission, Vienna International Cntre, P.O. Box 1200, A-1400 Vienna, Ausatria. http://www.ctbto.org/.

IGIL. Instituto Geofisico do Infante D. Luiz, Universidade de Lisboa, R. Escola Politecnica, 58, 1269-102, Lisboa, Portugal. http://www.igidl.ul.pt/.

IIEES. International Institute of Earthquake Engineering and Seismology (IIEES), 26 Arghavan Ave., Dibaji Shomali, Farmaniyeh, Tehran, Iran. http://www.iiees.ac.ir/.

ISC. International Seismological Centre, Pipers Lane, Thatcham, Berkshire RG19-4NS, UK. http://www.isc.ac.uk.

Jackson, D.D., Aki, K., Cornell, C.A., Dietrich, J.H., Henyey, T.L., Mahdyiar, M., Schwartz, D., and Ward, S.N., 1995. Seismic hazards in Southern California: probable earthquakes, 1994-2024. *Bull. Seism. Soc. Am.,* **85**(2), 379-439.

Jackson, J.A., and McKenzie, D.P., 1984. Active tectonics of the Alpine-Himalayan belt between western Turkey and Pakistan. *Geophys. J.R. Astron. Soc.,* **77**, 185-264.

Jackson, J., Priestley, K., Allen, M., and Berberian, M., 2002- Active tectonics of the South Caspian Basin. *Geophys. J. Int.,* **148** (2), 214-245.

Jeffreys, H., and Bullen, K.E., 1940. Seismological Tables.*British Association of Advancement of Science,* London.

JICA, 2000. The study on seismic microzoning of the greater Tehran area in the Islamic Republic of Iran. Draft final report in 3 volumes. *Japan International Cooperation Agency (JICA) & Centre for Earthquake and Environmental Studies of Tehran (CEST) Tehran Municipality.* Pacific Consultants International (PCI) and OYO Corporation.

Kanamori, H., 1977. The energy release in great earthquakes. *J. Geophys.Res.* **82**, 2981-2987.

Kanamori, H., 1983. Magnitude scale and quantification of earthquakes. *Tectonophysics,* **93**, 185-199.

Kanamori, H., and Anderson, D.L., 1975. Theoretical basis of some empirical relations in seismology. *Bull. Seism. Soc. Am.,* **65**, 1073-1096.

Karnik, V., 1968. Seismicity of the European Area. *Academia Publishing House of the Czechoslovak Academy of Sciences,* Praha, V.I, 364p.

Karnik, V., 1968. Seismicity of the European Area. *Academia Publishing House of the Czechoslovak Academy of Sciences,* Praha, V.II, 218p.

Karnik, V., 1996. Seismicity of Europe and the Mediterranean. *Geophys. Inst. Acad. Sci. Czech Republic,* Prague, 28p., maps and catalogue.

Kennett, B.L.N., and Engdahl, E.R., 1991. Traveltimes for global earthtquakes location and phase identification. *Geophys. J. Int.,* **105**, 425-465.

Kennett, B.L.N., Engdahl, E.R., and Buland, R., 1995. Constraints on seismic velocities in the Earth from traveltimes. *Heophys. J. Int.,* **122**, 108-124.

Khabbaz-nia, A.R., and Sadeghi, A., 2003. Geological map of Sari, 1:100,000. *Geol. Surv. Iran,* Sheet **6663.**

Khalili-Araghi, M., 1988. Finding the causes of unplanned Tehran growth. *Tehran University Publication,* Tehran (in Persian).

KISR. Kuwait Institute for Scientific Research, P.O. Box 24885, Safa, 24885, Kuwait.

Kondorskaya, N.V., and Shebalin, N.V., (eds.), 1977.Novii Katalog Silnikh Zemletriasenii na Territori SSSR do 1975 g. *Izd. Acad. Nauk. SSSR,* Moscow.

Kondorskaya, N.V., and Shebalin, N.V., (eds.), 1982. New Catalog of Strong Earthquakes in the USSR From Ancient Times Through 1977. *World Data Center A For Solid Earth Geophysics,* Report **SE-31**, NOAA, EDIS, Boulder, CO, 608p

.

Knill, J.L., and Jones, K.S., 1968. Ground-water conditions in greater Tehran. *Quart. J. Engng. Geol.* **1**, 181-194.

Kramer, S.L., 1996. Geotechnical earthquake engineering. *Prentice Hall,* Upper Saddle River, NJ, 653p.

LAO. Large Aperture Seismic Array. Seismic Discrimination Group, Lincoln Laboratory, MIT, 42 Carleton Street, Cambridge, MA 02142, USA.

Lee, W.HK, Kanamori, H., Jennings, P.C., and Kisslinger, C., 2002. The International Handbook of Earthquake and Engineering Seismology, V.**81A**, *Academic Press,* 933p.

Lienkaemper, J.J., 1984. Comparison of two surface-wave magnitude scales- M of Gutenberg and Richter (1954) and M_s of 'preliminary determination of epicenters'. *Bull. Seism. Soc. Am.,* **74**, 2357-2378.

Lilwall, R.C., and Douglas, A., 1970. Estimation of P-wave travel times using the joint epicenter method. *Geophys. J. Roy. Astron. Soc.,* **19**, 165-181.

Mangino, S., and Priestley, K., 1998. The crustal structure of the southern Caspian region. *Geophys. J. Int.,* **133**, 630-648.

McCaffrey, R., and Nabelek, J., 1987. Earthquakes, gravity, and the origin of the Bali Basin: an example of a nascent continental fold-and-thrust belt. *J. Geophys. Res., **92**, 441-460.*

McKenzie, D.P., 1972. Active tectonics of the Mediterranean region. *Geophys. J.R. Astron. Soc.,* **30**, 109-185.

Melville, C.P., 1978. Arabic and Persian source material on the historical seismicity of Iran from 7th to the 17th centuries. *Ph.D. Thesis,* University of Cambridge.

Molnar, P., and Lyon-Caen, H., 1989. Fault plane solutions of the earthquakes and active tectonics of the Tibetan Plateau and its margin. *Geophys. J. Int.,* **99**, 123-153.

Moinfar, A., Mahdavian, A., and Maleki, E., 1994. Historical and Instrumental Earthquake Data Collection for Iran. *Mahab Ghodss, Tehran.*

Morelli, A., and Dziewonski, A.M., 1993. Body wave traveltimes and a spherically symmetric P- and S-wave velocity model. *Geophys. J. Int.,* **112**(2), 128-194.

MOS. Moscow, Geophysical Survey of Russian Academy of Sciences, 249020, Kaluga region, Obninsk, Lenin Str., 189, Russia. http://www.gsras.ru/.

Mushketoff, I.V., and Orloff, A., 1893. Katalog zemletriesenii Rossiskoi Imperii. St. Petersburg.

MWP, 1968. Underground water, final report of geophysical resistivity prospection in the Tehran plain. *Ministry of Water and Power,* Hydrology Section, Report **16**, 9p, Tehran.

Mushketov, I.V., and Orlov, A.P., 1893. Catalog of Earthquakes in the Russian Empire [Katalog Zemletryasenity Rossiyskoy Imperii]. *Notes, Russian Geog. Soc*., **26**, St. Petersburgh.

NAO. NORSAR, P.O. Box 53, N-2027 Kjeller, Norway. http://www.norsar.no/.

Nabavi, M.S., 1972. Seismicity of Iran. M. Phill. Thesis, *Imperial College, University of London,* 276p.

Nabavi, M.S., 1977. Aspects of the seismic behaviour of Iran- Especially the southern Zagros area. Ph.D. Thesis, *Department of Geology, University College, London,* 227p.

Nabelek, J., 1984. Determination of earthquake source parameters from inversion of body waves. *Ph.D. Thesis, MIT*, Cambridge, MA, USA.

Nazari, H., 2005. Seismotectonic Map of the Central Alborz (with contributions by Ritz, J.-F., Talebian, M., and Moosavi, A.). *Geol. Surv. Iran,* Seismotectonic Section, 1:250,000 color map.

Nazari, H., 2006. Analyse de la tectonique recente et active dans l'Alborz Central et la region de Tehran: Approche morphotectonique et paleotectonique. *Thesis, Universite Montpellier II,* 274p.

Nazari, H., and Salamati, R., 1998. Geological Map of Rudbar, 1:100,000. *Geol. Surv. Iran,* Sheet **5863**.

Nazari, H., Ritz, J.F., Balescu, S., Lamothe, M., Salamati, R., Ghassemi, A., Shafei, A., Ghorashi, M., and Saidi, A., 2007. Paleoseismological analysis along the North Tehran fault (central Alborz, Iran). *J. Geophys. Res*., submitted.

NEIC. National Earthquake Information Center. U.S. Geological Survey Stop 967, National Earthquake Information Center, DFC, Denver, CO 80225-0046, USA. http://neic.usgs.gov/.

NEIS. National Earthquake Information Service. U.S. Geological Survey Stop 967, National Earthquake Information Center, DFC, Denver, CO 80225-0046, USA.

Nilforoushan, F., Vernant, P., Masson, F., Vigny, C., Martinod, J., Abbasi, M., Nankali, H., Hatzfeld, D., Bayer, R., Tavakoli, F., Ashtiani, A., Doerflinger, E., Daignieres, M., Collard, P., and Chery, J., 2002. GPS networks monitors the Arabia-Eurasia collision deformation in Iran. *J. Geod.,* **77**, 411-422.

NNC. Kazakhstan National Data Center, IGR NNC RK, Chaikinoy Str., 4, 480020, Almatay, Kazakhstan. www.kndc.kz.

Nowroozi, A., 1971. Seismotectonics of the Persian plateau, eastern Turkey, Caucasus and Hindu-Kush regions. *Bull. Seism. Soc. Am.,* **61**, 317-341.

Nowrrozi, A.A., and Ahmadi, G., 1986. Analysis of earthquake risk in Iran based on seismotectonic provinces. *Tectonophysics,* **122**, 89-114.

Nuttli, O.W., 1973. Seismic wave attenuation relations for eastern North America. *J. Geophys. Res.***78**, 855-876.

Obermeier, S.F., and Pond, E.C., 1999. Issues in using liquefaction features for paleoseismic analysis. *Seism. Res. Lett.,* **70** (1), 34-58

Oveisi, B., (n.d.). Geological Map of Sureyan [Suriayan], 1:100,000. *Geol. Surv. Iran,* Sheet **6750**.
Panza, G.F., Duda, S.J., Cernobori, L., and Herak, M., 1989. Gutenberg's surface-wave magnitude calibrating function: theoretical basis from synthetic seismograms. *Tectonophysics,* **166**, 35-43.

PEK. Beijing Institute of Geophysics, China Earthquake Administration, P.O. Box 8116, Beijing 100081, China.

Peronaci, F., 1958. Sismicita dell'Iran. *Ann. di. Geofis.,* **11**, 55.

Peronaci, F., 1959.Contributo alla conoscenza della caratteristiche sismiche dell'Iran settentrionalle. *Ann. di. Geofis.,* **12**, 523.

Petersen, K.D., Cramer, C.H., Bryant, W.A., Reichle, M.S., and Toppozada, T.R., 1996. Preliminary seismic hazard assessment for Los Angeles, Ventura, and Orange Counties, California, afftected by the 17 January 1994 Northridge earthquake. *Bull. Seism. Soc. Am.,* **86**(1B), S247-S261.

Petersen, M.D., Cramer, C.H., Reichle, M.S., Frankel, A.D., and Hanks, T.C., 2000. Discrepancy between earthquake rates implied by historic earthquakes and a consensus geologic source model for California. *Bull. Seism. Soc. Am.,* **90**(5), 1117-1132.

Poirier, J.P., and Taher, M.A., 1980. Historical seismicity in the Near and Middle East, north Africa, and Spain from Arabic documents (VIIth-XVIII century). *Bull. Seism. Soc. Am.,* **70**(6), 2185-2201.

Priestley, K., Baker, C., and Jackson, J.A., 1994. Implications of earthquake focal mechanism data for the active tectonics of the south Caspian Basin and surrounding regions. *Geophys. J. Int.,* **118**, 111-141.

Purkermai, M., and Soleymani, Sh., 1998. Introducing the seismic fault of the Mahdasht-South Karaj as one of the main seismic sources of the west Tehran and south Karaj. *Proc. 2nd Irania Geological Association Conf.,* Ferdowsi Univ., Mashhad, Iran (in Persian).

Quittmeyer, R.C., and Jacob, K.H., 1979. Historical and modern seismicity of Pakistan, Afghanistan, northern India and southeastern Iran. *Bull. Seism. Soc. Am.,* **69**, 773-823.

Reid, H.F., 1910. The mechanics of the earthquake. On: A.C. Lawson (chmn.), The California Earthquake of April 18, 1906. *Carnegie Institute Washington Publication,* **87**(2), 192p.

Reid, H.F., 1911. The elastic-rebound theory of earthquakes. *Bull. Dep. Geol. Univ. Calif.,* **6**, 412-444.

Rezaeian, M., 1998. Interaction of faults on water table changes in Tehran plain. M.Sc. Thesis, *Shahid Beheshti Univ*., Tehran, 133p. (in Persian with English Abstract).

Rezaeian, M.,, 1999. Tehran's groundwater and its structural conditions. *Geol. Surv. Iran.,* Int. Rep., 19p. (in Persian).

Richter, C.F., 1958. Elementary Seismology. *W.H. Freeman,* San Francisco, CA, 768p.

Richter, V.G., 1961. Vertical movements of the earth's crust and fluctuation in the level of the Caspian. *Geogr. v. Shkole,* **2**, 16.

Ritz, J.-F., Balescu, S., Soleymani, S., Abbasi, M., Nazari, H., Feghhi, K., Shabanian, E., Tabassi, H., Farbod, Y., Lamothe, Y., Michelot, J-L., Massault, M., Chery, J., and Vernant, P., 2003. Determing the long-term slip rate along the Mosha fault, central Alborz, Iran: Implications in terms of seismic activity. *Proc. SEE4, IIEES,* p.20 Tehran. Also, Attachment "A" in Nazari, 2006, 5pp.

Ritz, J.-F., Nazari, H., Ghassemi, A., Salamati, R., Shafei, A., Solaymani, S., and Vernant, P., 2006. Active transtension inside central Alborz: A new insight into northern Iran-southern Caspian geodynamics. *Geology,***34**(6), 477-480.

Rothe, J., 1969. The Seismicity of the Earth 1953-1965. *Earth Sci. Series, UNESCO, Paris.* Rowshandel, B., 2006. Incorporating source rupture characteristics into ground-motion hazard analysis models. *Seism. Res. Lett.,* **77**(6), 708-722.

Safa'i, H., 1995. The seismic sources of the Garmsar earthquakes. *Geosciences, Geol. Surv. Iran,* **4**(14), 28-34 (in Persian, with English abstract).

SAGP, 1958. Water resources survey Tehran region. Sir Alexander Gibb and Partners, London, *Plan Organization of Iran,* Tehran.

Schwartz, D.P., and Coppersmith, K.J., 1984. Fault behavior and characteristic earthquakes: Examples from the Wasatch and San Andreas Faults. *J. Geophys. Res.* **89**, 5681-5698.

Schwartz, D.P., and Coppersmith, K.J., 1986. Seismic Hazards: New trends in analysis using geologic data. In: Active Tectonics, *National Academic Press,* Washington, D.C., 215-230.

Scholz, C.H. 1982. Scaling laws for large earthquakes: consequences for physical models. *Bull. Seism. Soc. Am.* **72**, 1-14.

Scholz, C.H., Aviles, C.A., and Wesnousky, S.G., 1986. Scaling differences between large interplate and intraplate earthquakes. *Bull. Seism. Soc. Am.* **76**, 65-70.

Seed, H.B., 1979. Soil liquefaction and cyclic mobility evaluation for level ground during earthquakes. *J. Geotech. Engin., ASCE,* **105/GT2**, 210-255.

Seed, H.B., and Idriss, I.M., 1982. Ground motion and soil lequefaction during earthquakes. *Earthquake Engineering Research Institute,* Berkeley, CA.

Seed, H.B., Tokimatsu, K., Harder, L.F., and Chung, 1985. The influence of SPT procedure in soil liquefaction resistance evaluation. . *J. Geotech. Engin., ASCE,* **111/12**, 1425-1445.

Shahidi, A.R., and Nazari, H., 1996. Geological Map of Harsien [Harsin], 1:100,000. *Geol. Surv. Iran,* Sheet **5558**.

Shaw, J.H., 1993. Active blind-thrust faulting and strike-slip folding in California. *Ph.D. Thesis, Princeton University,* Princeton, NJ, 216p.

Shaw, J.H., and Suppe, J., 1994a. Active faulting and growth faulting in the eastern Santa Barbara Channel, California. *Geol. Soc. Am. Bull.* **78**, 700-721.

Shaw, J.H., and Suppe, J., 1994b. Earthquake hazards of active blind-thrust faults under the central Los Angeles basin, California. *J. Geophys. Res.,***101**, 8623-8642.

Shedlock, K.M., Giardini, D., Grunthal, G., and Zhang, P., 2000. The GSHAP global seismic hazard map. *Seism. Res. Lett.,* **71**(6), 679-686.

Sheibani, Z., 1990. A renovation proposal plan for the Emamzadeh ‘Abdolah and ‘Abidolah dome of Damavand. *Athar,* **18, 19**, 128-158 (in Persian).

Sieberg, A., 1932. Erdebengeographie. In: B. Gutenberg, Hanbuch der Geophysik, **4**, Berlin.
Sieh, K., 1978. Slip along the San Andreas fault associated with the great 1857 earthtquake. *Seism Soc. Am. Bull.,* **68**, 1421-1428.

SNSN. Saudi Nationa Seismic Network, King Abdualaziz City for Science and Technology, P.O. Box 6086, Riyadh 11442, Kingom of Saudi Arabia.
Soleymani, Sh., and Zare, M., 1999. Morphotectonic and recent tectonic movement study in the Tehran-Karaj region. *Proc. 3rd Int. Conf. Seism. & Earthq. Engineer., IIEES,* 19-31, Tehran May 17-19, 1999 (in Persian).

Stein, R.S., and Yeats, R.S., 1989. Hidden earthquakes. *Scientific Anerican,* **260**(6), 48-57.

Stirling, M.W., and Wesnousky, S.G., 1997. Do historical rates of seismicity in southern California require the occurrence of earthquake magnitudes greater than would be predicted from fault length? *Bull. Seism. Soc. Am.,* **87** (6), 166201666.

Stokoe, K.H., II, Roesset, J.M., Bierschwale, J.G., and Aoouad, M., 1988. Liquefaction potential of sands from shear wave velocity. *Proc. 9th World Conf. Earthq. Engin.,* Tokyo, Japan, **3**, 213-218.

Suppe, J., 1983. Geometry and kinematics of fault-bend folding. *Am. J. Sci.* **283**, 648-721.

Suppe, J., Chou, G.T., and Hook, S.C., 1992. Rates of folding and faulting determined from growth strata. In: Thrust Tectonics, K.R. McKlay (ed.), *Unwin Hyaman,* 105-121.

Tatar, M., 2001. Etude sismotectonique de deux zones de collision continentale: le Zagros Central et l'Alborz (Iran). *These de l'Universite de Grenoble,* France.

Tatar, M., Jackson, J., Hatzfeld, D., and Bergman, E., 2007. The 28 May 2004 Baladeh earthquake (M_w 6.2) in the Alborz, Iran: implications for the geology of the South Caspian Basin margin and for the seismic hazard of Tehran. *Geophys. J. Int.,* submitted.

Taymaz, T., Eyidogan, H., and Jackson, J., 1991. Source parameters of large earthquakes in the East Anatilian fault zone (Turkey). *Geophys. J. Int.,* **106**, 537-550.

Taymaz, T., Jackson, J., and McKenzie, D., 1991. Active tectonics of the north and central Agean Sea. *Geophys. J. Int.* **106**, 433-490.

Tchalenko, J.S., and Ambraseys, N.N., 1973. Earthquake destruction of adobe villages in Iran. *Ann di Geifis.,* **26**(2-3), 357-389.

Tchalenko, J.S., Berberian, M., Iranmanesh, H., Bailly, M., and Arsovsky, M., 1974. Tectonic framework of the Tehran region. *Geol. Surv. Iran,* **29**, 7-46

TEH. Institute of Geophysics, Tehran University (IGTU), Tehran. http://irsc.ut.ac.it/.

THR, Tehran, International Institute of Earthquake Engineering and Seismology (IIEES), 26 Arghavan Ave., Dibaji Shomali, Farmaniyeh, Tehran, Iran. http://www.iiees.ac.ir/.

Triep, R.G., Aberts, G.A., Lerner-Lam, A.L., Mishatkin, V., Zacharchenko, N., and Starovit, O., 1995. Active thrust front of the Greater Caucasus: the April 29, 1991, Racha earthquake sequence and its tectonic implications. *J. Geophys. Res.,* **100**, 4011-4033.

UPAR, 1992. Demographic statistics on Iranian cities (1956-1991). *Urban Planning and Architecture Research Centre,* Tehran.

Utsu, T., 2002. Relatioships between magnitude scales. In: W.H.K. Lee, H. Kanamori, Paul C. Jennings, and C.K. Kisslinger (eds.), International Handbook of Earthquake and Engineering Seismology. *Academic Press,* 733-746.

Vahdati Daneshmand, F., (compiler), 2005. Geological map of Pol-e-Sefid, 1:100,000. *Geol. Surv. Iran,* **6662**.
Vahdati Daneshmand, F., Karimi, H.R., Mosaffa, H.R., (Western half of the sheet); Ajdari, A., Gharib, F., Sadeghi, A., and Sai'di, A. (eastern half of the sheet), 2005. Geological map of Pol-e-Sefid, 1:100,000. *Geol. Surv. Iran,* **6662**.

Vernant, Ph., Nilforoushan, F., Hatzfeld, D., Abbasi, M., Vingy, C., Mason, F., Nankali, Martinod, J., Ashtiani, A., Bayer, R., Tavakoli, F., and Chery, J., 2004a. Contemporary crustal deformation and plate kinematics in the Middle East constrained by GPS measurements in Iran and northern Oman. *Geophys. J. Int.,* **157**, 381-398.

Vernant, Ph., Nilforoushan, F., Chery, J., Bayer, R., Djamour, Y., Mason, F., Nankali, H., Ritz, J.-F., Sedighi, M., and Tavakoli, F., 2004b. Deciphering oblique shortening of central Alborz in Iran using geodetic data. *Earth and Planetary Science Letters,* **223**, 177-185.

Villasenor, A., Bergman, E.A., Boyd, T.M., Engdahl, E.R., Frazer, D.W., Harden, M.M., Orth, J.L., Parks, R.L., and Shedlock, K.M., 1997. Towards a comprehensive catalog of global seismicity. *EOS Trans., AGU,* **78**, 581-588.

Ward, S.N., 1997. More on M_{max}. *Bull. Seism. Soc. Am,* **87** (5), 1199-1208.

Wells, D., and Coppersmith, K., 1994. New empirical relationships among magnitude, rupture length, rupture width, rupture area, and surface displacement. *Bull. Seism. Soc. Am.,* **84**, 974-1002.

Wesnousky, S.G., 1994. The Gutenberg-Richter or Charaacteristic earthquake distribution, which is it? *Bull. Seism. Soc. Am.,* **84** (6), 1940-1959.

Wesnousky, S.G., 2000. Crustal deformation process, seismicity, and the Gutenberg-Richter distribution; Annual Report, 2000. *University of Nevada,* 5p.

Wesnousky, S.G., Scholz, C.H., Shimazaki, K., and Matsuda, T., 1983. Earthquake frequency distribution and the mechanics of faulting. *J. Geophys. Res.,* **88** (B11), 9331-9340.

Willis, K.G., and Asgary, A., 1997. The impact of earthquake risk on housing markets: Evidence from Tehran real estate agents. *J. Housing Res.,* **8**(1), 125-136.

Wilson, A., 1930. Earthquakes in Persian. *Bull. Sch. Orient. Study, London Inst*., **6**(1), 103-131.
Yeats, R.S., Sieh, K., Allen, C.R., 1997. The Geology of Earthquakes. *Oxford University Press,* 568p.

Yegian, M.K., and Ghahraman, V.G., 1990. The Manji, Iran, earthquake of June 21, 1990. *EERI Newsletter,* **24**(12), 12-13.

Yegian, K.K., Ghahraman, V.G., Nogole-Sadat, M.A.A., and Daraie, H., 1995a. Liquefaction during the 1990 Manjil, Iran, earthquake, I: Case history data. *Bull. Seism. Soc. Am.,* **85**(1), 66-82.

Zur-RMT. Zurich moment tensors. Swiss Seismological Service, ETH-Honggerberg, CH-8093 Zurich, Switzerland. http://seismo.ethz.ch/info/mt.html.

References –Ground Motions

Abrahamson, N.A. (2000). "Effects of rupture directivity on probabilistic seismic hazard analysis," Proceedings of 6th International Conference on Seismic Zonation, Palm Springs.

Somerville, P.G., et al (1997). "Modification of Empirical Strong Ground Motion Attenuation Relations to Include the Amplitude and Duration Effects of Rupture Directivity,", Seismological Research Letters, Volume 68, Number 1, pp. 199.

Stewart, J.P. et al (2001). "Ground Motion Evaluation Procedures for Performance-Based Design," Pacific Earthquake Engineering Research Center, Ch. 4, http://nisee.berkeley.edu/library/PEER-200109/.

Abrahamson, N. A., and Silva, W. J., 1997. Empirical response spectral attenuation relations for shallow crustal earthquakes, *Seism. Res. Lett.* **68**, 94–127.
Abrahamson, N. A., *et al*., 2008. Comparisons of the NGA Ground-motion relations. *Journal of Earthquake Spectra*, 2008

Boore, D. M., and G. M. Atkinson. (2007). *Boore-Atkinson NGA ground motion relations for the geometric mean horizontal component of peak and spectral ground motion parameters.* PEER Report 2007/01. Berkeley, Calif.: Pacific Earthquake Engineering Research Center, University of California.

Boore, D. M., J. B. Joyner, and T. E. Fumal (1997). Equations for estimating horizontal response spectra and peak acceleration from western North American earthquakes: a summary of recent work. *Seism. Res. Lett.* 68**:** 128–53.

Boore, D. M., J. Watson-Lamprey, and N. Abrahamson. (2006). Orientation-independent measures of ground motion. *Bull. Seism. Soc. Am.* 96**:** 1502–11.

Bozorgnia, Y., and Campbell, K. W.,2007. Discussion of "Attenuation Relationship for Iran,", by Amiri, Mahdavian, and Dana, Journal of Earthquake Engineering, Vol. 11, 1031–1035.

Campbell, K. W., and Bozorgnia, Y., 2003. Updated near-source ground motion (attenuation) relations for the horizontal and vertical components of peak ground acceleration and acceleration response spectra, *Bull. Seism. Soc. Am.* **93**, 314–331.

Campbell, K. W., and Bozorgnia, Y., 2007. *Campbell-Bozorgnia NGA ground motion relations for the geometric mean horizontal component of peak and spectral ground motion parameters*, PEER Report No. 2007/02, Pacific Earthquake Engineering Research Center, University of California, Berkeley, 238 pp.

Campbell, K. W., and Bozorgnia, Y., 2008. NGA Ground motion model for the geometric mean horizontal component of PGA, PGV, PGD and 5% damped linear elastic response spectra for periods ranging from 0.01 to 10 s. *Journal of Earthquake Spectra*, 2008

Chiou, B. S.-J., R. R. Youngs. (2007). *Chiou-Youngs NGA ground motion relations for the geometric mean horizontal component of peak and spectral ground motion parameters.* (forthcoming) PEER Report. Berkeley, Calif.: Pacific Earthquake Engineering Research Center, University of California.

Power, M., *et al.*, 2008. An overview of NGA project. *Journal of Earthquake Spectra*, 2008

Sadigh, K., C. Y. Chang, J. A. Egan, F. Makdisi, and R. R. Youngs. (1997). Attenuation relationships for shallow crustal earthquakes based on California strong motion data. *Seism. Res. Lett.* 68**:** 180–89.

Shoja-Taheri, J., et al., 2007. *Comparison of Recorded Ground Motions in Iran and NGA Models*. Mashad University, 2007.

References – Section 6.5 – Geological Survey of Iran

Antoine , P., Bahain, J-J., Berillon, G., and Asgari-Khaneghah A., 2006. Tuf calcaire et alluviale en contexte tectonique actif: la formation de Baliran (province Mazandaran, Iran), Quaternaire, 17, (4), p. 321-331

Berberian M., M. Ghorashi, Arjhang-Ravesh, B.,Mohajer A., 1985. Seismotectonic and earthquake-fault hazard investigations in greater Tehran, (Contribution to the Seismotectonics of Iran, Part V). Geol. Surv. Iran, No. 56, 315p (in Persian).

Berberian M., Ghorashi M., Arjhang-Ravesh, B.,Mohajer A., 1992. Seismotectonic and earthquake-fault hazard investigations in the greater Qazvin region (Contribution to the Seismotectonics of Iran, Part VI). Geol. Surv. Iran, No. 61, 197p (in Persian), 1993.

Berberian M., M. Ghorashi, M. Talebian and J. Shoja-Taheri, 1996. Seismotectonic and earthquake - fault hazard investigations in the Semnan region (Contribution to the Seismotectonics of Iran, Part VII). Geol. Surv. Iran, No. 63, 266p (in Persian).

Berberian M., 1994. Natural hazard and the earthquake catalogue of Iran, Vol. 1: Historical Hazard in Iran Prior to 1900, Int. Inst. of Earthquake Engineering and Seismology, Tehran, Iran.

Berillon, G., Asgari Khaneghah, A., Antoine, P., Bahain, J.-J.,Chevrier, B., Zeitoun, V., Aminzadeh, N., Beheshti, M.,Ebadollahi Chanzanagh, H., Nochadi, S., 2007. Discovery of new open-air Paleolithic localities in Central Alborz, Northern Iran,V:52(4), 380-87.

Gardner, J.K., and L. Knopoff , 1974. Is the sequence of earthquakes in southern California with aftershocks removed Poissonian?, Bull. Seism. Soc. Am.64, 1363- 1367.

Gutenberg, B. and Richter, C. F., 1944. Frequency of earthquakes in California, Bull. Seis. Soc. Am., 34, 185-188.

Kijko A. and Sellevoll M. A., 1989. Estimation of earthquake hazard parameters from incomplete data files. Part I. Utilization of extreme and complete catalogs with different threshold magnitudes Bull. Seism. Soc. Am.79(3): 645 - 654.

Kijko A. and Sellevoll M. A. 1992. Estimation of earthquake hazard parameters from incomplete data files. Part II. Incorporation of magnitude heterogeneity, Bull. Seism. Soc. Am.82(1): 120 - 134.

Masson, F., Ch´ery, J., Martinod, J., Hatzfeld, D., Vernant, P., Tavakoli, F. & Ashtiani, A., 2005. Seismic versus aseismic deformation in Iran inferred from GPS and seismicity dat, Geophys. J. Int., **160,** 217–226.

Masson, F., Djamour, Y., Vangorp, S., Ch´ery, J., Tavakoli, F., Tatar M. & Nankali, H., 2006. Extension in NW Iran inferred from GPS enlightens the behavior of the south Caspian basin, EPSL, **252,** 180–188.

Nazari, H., 2006. Analyse de la tectonique recente et active dans l'Alborz Central et la region de Teheran:Approche morphotectonique et paleoseismologique, PhD thesis, Montpellier II, Montpellier.

Nazari, H., Ritz,J-F,Talebian,M.,Moosavi,A., Seismotectonic map of the Central Alborz, Goeological Survey of Iran, Tehran, 2005.

Ritz , J.-F., Nazari, H.,Ghassemi,A.,Salamatj,R.,Shafei ,A., Solaymani,S.,Vernant,P., 2006. Active transtention inside Central Alborz: A new insight into the Northern Iran-Southern Caspian geodynamics, Geology, 34 (6), 477-480.

Tatar, M., Jackson, J., Hatzfeld, J., and Bergman, E., 2007. The 2004 May 28 Baladeh earthquake (Mw 6.2) in the Alborz, Iran: overthrusting the South Caspian Basin margin, partitioning of oblique convergence and the seismic hazard of Tehran, Geophys. J. Int., doi: 10.1111/j.1365-246X.2007.03386.x

Vernant, P. *et al.*, 2004a. Contemporary crustal deformation and plate kinematics in Middle East constrained by GPS measurements in Iran and northern Oman, Geophys. J. Int., **157,** 381–398.

Vernant, P. *et al.*, 2004b. Deciphering oblique shortening of central Albors in Iran using geodetic data, Earth planet. Sci. Lett., **223,** 177–184.

9. APPENDIX A – EARTHQUAKE CATALOG